Universiteit Antwerpen

Faculty of Pharmaceutical, Biomedical and Veterinary Sciences

Exploring structural neuroplasticity in the zebra finch brain using *in vivo* MRI

Dissertation to obtain the degree of

Doctor in Biomedical Sciences

at the University of Antwerp, to be defended by

Julie HAMAIDE

Supervisors

Prof. Dr. Annemie Van der Linden

Prof. Dr. Marleen Verhoye

Antwerp, 2018

Exploring structural neuroplasticity in the zebra finch brain using *in vivo* MRI

***In vivo* MRI studie over structurele neuroplasticiteit in zebravinkhersenen**

Cover illustration

Front: Examples of structural MRI images of the zebra finch brain.

Top row: volume differences between the sensory and sensorimotor phase in male zebra finches (full description in Chapter 6).

Second row: 3-dimensional renders of the zebra finch brain (based on the population-based template described in Chapter 6)

Third row: *ex vivo* super-resolution reconstruction colour-coded track density maps of an adult male zebra finch brain (obtained from the 'test sample' described in Chapter 5)

Bottom row: sound spectrogram and oscillogram of a song bout of an adult male zebra finch (full description in Chapter 6 and 7).

Back: Perching adult male zebra finches - *Taeniopyiga guttata*

Design: Julie Hamaide and Natacha Hoevenaegel, Nieuwe Mediadienst, Universiteit Antwerpen.

This PhD project was funded by the Belgian Federal Science Policy Office: Interuniversity Attraction Poles ('PLASTOSCINE': P7/17) and an 'Uitvlaggingsmandaat' by the Department of Biomedical Sciences, University of Antwerp.

Members of the jury

Prof. Dr. Annemie Van der Linden – Promotor

Bio-Imaging Lab, Department of Biomedical Sciences, Faculty of Pharmaceutical, Biomedical and Veterinary Sciences, University of Antwerp, Belgium

Prof. Dr. Marleen Verhoye – Promotor

Bio-Imaging Lab, Department of Biomedical Sciences, Faculty of Pharmaceutical, Biomedical and Veterinary Sciences, University of Antwerp, Belgium

Prof. Dr. Michele Giugliano – Chair of the internal thesis committee

Lab of Theoretical Neurobiology and Neuroengineering, Department of Biomedical Sciences, Faculty of Pharmaceutical, Biomedical and Veterinary Sciences, University of Antwerp, Belgium

Prof. Dr. Jeroen Verhaeghe – Member of the internal thesis committee

Molecular Imaging Center Antwerp, Department of Molecular Imaging, Pathology, Radiotherapy and Oncology, Faculty of Medicine and Health Sciences, University of Antwerp, Belgium

Prof. Dr. Laura-Adela Harsan – Member of the external thesis jury

ICube Laboratory – Integrative Multimodal Imaging in Healthcare, Department of Biophysics and Nuclear Medicine, Faculty of Medicine, University of Strasbourg, France

Prof. Dr. Daniela Vallentin – Member of the external thesis jury

Animal Behavior & Neuroscience, Institute of Biology, Department of Biology, Chemistry and Pharmacy, Freie Universität Berlin, Germany

Dr. Dirk Smeets – Member of the external thesis jury

Chief Technology Officer, head of the research and development team (including IT), product manager of MS**metrix** and information security manager of ico**metrix**, Ico**metrix**–imaging biomarker experts, Leuven, Belgium

Table of contents

Summary

Proper understanding of the fundamental features in control of neuroplasticity are highly necessary to understand how the brain develops, how organisms are capable of learning and forming memories, how basic sensory but also higher cognitive skills develop in early life. A remarkable model to study developmental plasticity related to the acquisition of cognitive skills can be found in songbirds, more specifically in zebra finches. In contrast to vocalisations uttered by most vertebrate species, songbirds sing acoustically complex songs that are learned and can be modified based on the social context. This remarkable skill, shared by only few species, has been used extensively as a model for human speech learning. Despite intensive efforts in identifying the neural substrate in control of singing or implicated in auditory discrimination and perception, up to recently, research was mainly directed at the song control and auditory system, or areas directly related to the latter. Hence, **this thesis aimed at extending current views by (1) implementing *in vivo* MR-based imaging tools that allow to map structural neuroplastic events across the entire zebra finch brain while (2) birds learn to sing or (3) recover from brain trauma.**

We **first** implemented appropriate Magnetic Resonance-based Imaging (MRI) tools sensitive to capturing structural neuroplastic events of the entire brain at different spatial scales. We opted for Diffusion Tensor Imaging (DTI), a technique that infers microstructural tissue properties based on measuring the diffusion properties of water protons in tissues, and T2-weighted 3-dimensional (3D) anatomical scans that enable assessing overall gross neuroanatomy (shape and volume of areas). We probed the sensitivity of the optimised DTI protocol in a proof-of-principle study assessing known sex differences in brain structure. This experiment aligned with established findings, but also led to the discovery of additional sex differences in white matter structures surrounding or connecting brain areas implicated in song behaviour. To confirm the 'white matter nature' of the newly established sex differences, we performed additional super-resolution DTI and whole brain tractography on *post mortem* brain tissue in a male and a female zebra finch. The **second** goal of this thesis included mapping the structural development of the zebra finch brain from 20 to 200 days post hatching. As such, we traced alterations in local volume and intrinsic tissue properties that differed between both sexes or merely changed in function of age. Further, we analysed the songs sung by the juvenile male birds and quantified vocal performance by measuring song similarity to tutor song (based on the acoustical

properties of song). This uncovered four spatially confined areas where local tissue properties or volume correlated with song performance. The **third** goal of this thesis was to trace structural neuroplastic events in adult male zebra finches following neurotoxic lesioning of one component of the song control circuitry. Using whole-brain imaging, we observed structural neuroplastic adaptations affecting remote components of the song control system. The results corroborated with previous studies, and uncovered structural alterations in the lateral cerebellar nuclei. Moreover, we observed several links between song motif length and the microstructural properties of several brain areas linked to song control.

To conclude, this thesis initiates a potential novel framework able to assess structural neuroplastic events that characterise distinct stages of song learning in ontogeny as well as brain regeneration in adulthood using completely non-invasive MR-based *in vivo* imaging tools. In a broader context, the results of this thesis underscore the value of *in vivo* MR-based imaging in detecting structural neuroplastic events in an 'unbiased', data-driven way, and, as a result, providing clear spatial targets to further examine using more specific zoomed-in histological and molecular techniques.

Samenvatting

Inzicht in de fundamentele eigenschappen van neuroplasticiteit is zeer noodzakelijk om te begrijpen hoe de hersenen ontwikkelen, hoe men dingen kan leren en memoriseren, hoe bepaalde basis sensorische functies en complexe cognitieve vaardigheden verworven worden tijdens de eerste levensjaren. Een belangrijk model in de studie naar neuroplasticiteit gerelateerd met de acquisitie van cognitieve vaardigheden tijdens kindertijd en adolescentie, zijn zangvogels, meerbepaald zebravinken. In tegenstelling tot vocalisaties die geuit worden door de meeste gewervelde diersoorten, zingen zangvogels acoustisch complexe liedjes die aangeleerd zijn en aangepast kunnen worden op basis van de sociale context. Deze exceptionele eigenschap, die slechts teruggevonden wordt in een uiterst beperkt aantal species, werd reeds uitgebreid bestudeerd en gedocumenteerd als het best beschikbare model voor de studie naar bepaalde aspecten van spraakontwikkeling in kinderen. Ondanks de vele studies die het neurale substraat verantwoordelijk voor zang-gedrag en voor perceptie van en discriminatie tussen verschillende soorten zang zeer goed in kaart gebracht hebben, werd tot op heden het onderzoek altijd strikt gefocust op hersenregio's die voorheen in verband gebracht werden met zanggedrag, bijgevolg is er erg weinig geweten over de rest van de hersenen. Daarom zijn de doelen van dit doctoraatsonderzoek gefocust op (1) *in vivo* Magnetische Resonantie Beeldvormings-technieken (MRI) te implementeren in zebravink onderzoek, zodat we neuroplastische veranderingen in de structuur van de zebravink hersenen kunnen traceren wanneer (2) jonge vogels leren zingen, of wanneer (3) volwassen vinken recupereren van een hersen trauma.

Als eerste hebben we twee gepaste MRI protocols geselecteerd en geïmplementeerd om de zebravinkhersenen te onderzoeken. De eerste techniek, Diffusie Tensor Beeldvorming (DTI), meet de diffusie-eigenschappen van waterstof-protonen en leidt hieruit de intrinsieke micro-architectuur van het weefsel af. De tweede techniek, T2-gewogen 3-dimensionale (3D) hersenscans, laten toe om de grootte en de vorm van hersenregio's te evalueren. We testten de sensitiviteit van de nieuw-geïmplementeerde protocols door een validatiestudie uit te voeren die de gekende verschillen in hersenstructuur tussen mannelijke en vrouwelijke zebravinken succesvol detecteerde, maar ook nieuwe structuren in kaart bracht. Om meer inzicht te verkrijgen in de weefseleigenschappen die de nieuw opgemerkte structurele verschillen tusssen beide geslachten, hebben we super-resolutie DTI scans opgenomen van *post*

mortem hersenweefsel van een mannelijke en een vrouwelijke zebravink, en de data verwerkt met tractografie.

Ten tweede hebben we de gevalideerde protocols gebruikt om een spatio-temporele map te maken van de structurele ontwikkeling van de mannelijke en vrouwelijke zebravink hersenen tijdens de eerste 200 dagen van het leven. Op die manier hebben we veranderingen in volume (3D) en intrinsieke weefsel eigenschappen (DTI) gedetecteerd die uiteindelijk resulteren in structurele verschillen tussen de hersenen van mannelijke en vrouwelijke zebravinken of ontstaan ten gevolge van de leeftijd. Verder onderzochten we ook de zang van de jonge mannelijke zebravinken en quantificeerden de zangprestaties door te meten in welke mate de zang van de jonge zebravinken gelijkt op de zang van de tutor. Deze vergelijking leidde tot de detectie van vier hersenregio's waar de locale weefseleigenschappen, i.e. volume en/of intrinsieke eigenschappen, correleren met de zangprestatie.

Het derde doel van deze thesis was om structurele neuroplasticiteit te traceren in volwassen, mannelijke zebravinken tijdens het recuperatie-proces na hersentrauma aan één van de zangkernen van het hersencircuit dat zanggedrag controleert. Met behulp van de geïmplementeerde *in vivo* beeldvormingstechnieken ontdekten we structurele neuroplastische veranderingen in andere zangcontrole kernen van hetzelfde hersencircuit. Daarnaast ontdekten we ook structurele verandering in het cerebellum en observeerden we dat de structurele eigenschappen van verscheidene hersenregio's correleren met duur van de zang.

We concluderen dat de protocols ontwikkeld in deze thesis potentieel een nieuw kader vormen als niet-invasieve structurele beeldvormingsmethoden op maat van de zebravinkhersenen. In een ruimere context toont dit onderzoek de kracht van *in vivo* MRI aan in de detectie van structurele neuroplasticiteit in levende dieren of mensen, op een objectieve en data-gedreven manier. *In vivo* MRI laat toe om te bepalen welke hersenregio's op welke tijd veranderingen vertonen, ten gevolge van normale of ziekte-processen. Deze targets kunnen vervolgens verder in detail onderzocht worden door meer invasieve methoden zoals histologie en genetica.

List of Abbreviations

AChEI	acetyl choline esterase inhibitor
AD	axial diffusivity
ADC	apparent diffusion coefficient
AFP	anterior forebrain pathway
AIM-MRI	activity-induced manganese magnetic resonance imaging
AM	amplitude modulation
ANOVA	analysis of variance
ANTs	advanced normalisation tools
ASL	arterial spin labelling
Av	avalanche nucleus
b_0	non-diffusion weighted image
BBB	blood-brain barrier
BDNF	brain-derived neurotrophic factor
BOLD	blood-oxygen level dependent
BOS	birds' own song
BrdU	bromodeoxyuridine
CA	*commissura anterior* / anterior commissure
Ca^{2+}	calcium
CA1	cornu ammonis 1
CA3	cornu ammonis 3
CBF	cerebral blood flow
CBV	cerebral blood volume
CC-TD	color-coded track density (map)
CD11b	cluster of differentiation molecule 11b
CD68	cluster of differentiation molecule 68
ChABC	chondroitinase ABC
Cho	choline
CM	caudal mesopallium
CMM	*mesopallium caudomediale* / caudomedial mesopallium
$CMRO_2$	cerebral metabolic rate of oxygen
CNS	central nervous system
CLM	*mesopallium caudolaterale* / caudolateral mesopallium
CP	*commissura posterior* / posterior commissure
CSF	cerebrospinal fluid
CT	computed tomography
CV	coefficient of variation
DARPP-32	dopamine- and cAMP-regulated phosphoprotein
dv	divergence of velocity
DBM	deformation-based morphometry
DCM	dynamic causal modelling
DCX	doublecortin
DLM	*nucleus dorsolateralis anterior thalami pars medialis* / medial part of the dorsolateral nucleus of the anterior thalamus
DM	dorsomedial portion of the intercollicular nucleus
DMA	dorsomedial nucleus of the anterior thalamus

DMP	dorsomedial nucleus of the posterior thalamus
DTI	diffusion tensor imaging
dph	days post hatching
DW	diffusion-weighted
EEG	electroencephalography
EPI	echo planar imaging
FA	fractional anisotropy
FM	frequency modulation
fMRI	functional magnetic resonance imaging
fODF	fibre orientation distribution function
FOV	field-of-view
FPL	*fasciculus prosencephalis lateralis*
FWE	family wise error
FWHM	full width at half maximum
GABA	γ-aminobutyric acid
GAP43	growth-associated protein 43
GFAP	glial fibrillary acidic protein
Glu	glutamate
GRASE	gradient and spin echo
HARDI	high-angular resolution diffusion imaging
Hb	hemoglobine
HDACI	histon-deacetylase inhibitor
HSD	honest significant difference
HVC	high vocal centre (now used as proper name)
HRF	hemodynamic response function
ICA	independent component analysis
ICo	*nucleus intercollicularis* / intercollicular nucleus
IEG	immediate early gene
IGF-1	insuline-growth factor 1
IR	inversion Recovery
ISH	*in situ* hybridization
j	jacobian determinant
LaM	*lamina mesopallialis*
LCN	lateral cerebellar nuclei
LFS	lamina frontalis superior
LFF	low-frequency fluctuations
LMAN	*nucleus lateralis magnocellularis nidopallii anterioris* / lateral magnocellular nucleus of the anterior nidopallium
LPS	lipopolysaccharide(s)
LTD	long term depression
LTP	long term potentiation
λ_1, λ_2, λ_3	e*igenvalue* 1, 2 and 3
MALDI	matrix assisted laser desorption/ionisation
MD	mean diffusivity
MEG	magnetoencephalography
MEMRI	manganese-enhanced magnetic resonance imaging

MLd	*nucleus mesencephalicus lateralis pars dorsalis* / dorsal part of the lateral mesencephalic nucleus
Mn^{2+}	manganese
$MnCl_2$	manganese dichloride
MRI	magnetic resonance imaging
mRNA	messenger RNA
MRS	magnetic resonance spectroscopy
MTC	magnetisation transfer contrast
MWM	Morris water maze
NAA	N-acetyl aspartate
NCL	caudolateral nidopallium
NCM	*nidopallium caudomediale* / caudomedial nidopallium
NE	norepinephrine
NgR	nogo receptor
NIf	*nucleus interfacialis* / interfacial nucleus
NIRS	near-infrared spectroscopy
NMDA	N-methyl-D-aspartate
nXIIts	tracheosyringeal part of the nucleus of the XIIth cranial nerve
Otx2	Orthodenticle Homeobox 2 homeoprotein
Ov	*nucleus ovoidalis*
PD	proton density
PET	positron emission tomography
PFF	paradoxical functional facilitation
phMRI	pharmacological magnetic resonance imaging
PirB	paired-immuglobuline-like receptor B
PNN	perineuronal Nets
POA	pre-optic area
RA	*nucleus robustus arcopallii* / robust nucleus of the arcopallium
RARE	rapid-acquisition with relaxation enhancement
rCBV	relative cerebral blood volume
RA	*nucleus robustus arcopallialis* / robust nucleus of the arcopallium
RD	radial diffusivity
RF	radio-frequency
rmcorr	repeated-measures correlation
RNA	ribonucleic acid
ROI	region-of-interest
rsfMRI	resting state functional magnetic resonance imaging
SPA	sound analysis pro
SE	spin-echo
SE-EPI	spin-echo echo planar imaging
SNR	signal-to-noise ratio
SI_{max}	maximal signal intensity
SLR	serial longitudinal registration
SPECT	single-photon emission computed tomography
SPM	statistical parametric mapping
SRR-b_0	super-resolution reconstruction b_0
SRR-DTI	super-resolution reconstruction diffusion tensor imaging

SRR-FA	super-resolution reconstruction fractional anisotropy
SRR-MD	super-resolution reconstruction mean diffusion
SSRI	selective Serotonin Reuptake Inhibitors
Tau	taurine
TBI	traumatic brain injury
TBM	tensor-based morphometry
TD	track density (map)
TDI	track density imaging
TE	echo time
TeO	*tectum opticum*
tFA	*tractus fontro-arcopallialis*, fronto-arcopallial tract
TFM	*tractus thalamo-frontalis et frontalis thalamicus medialis*
TI	Inversion time
TMS	transcranial magnetic stimulation
tOM	*tractus occipitomesencephalicus*
TR	rRepetition time
TSM	*tractus septomesencephalicus*
TUNEL	terminal deoxynucleotidyl transferase dUTP nick end labeling
VBM	voxel-based morphometry
VMN	*nucleus ventromedialis hypothalami*
VP	ventral pallidum
ZENK	zif-268, egr-1, NGFI-A, Krox-24

Chapter 1

Songbirds in biomedical sciences: neuroplasticity, vocal learning and communication

1.1 NEUROPLASTICITY

One of the most crucial paradigm-shifts in the field of neurosciences of the 20th century was the notion that the adult brain is not fixed or immutable but can adapt structurally and functionally in response to experience or injury. Today, this phenomenon is defined as neuroplasticity and is regarded as a continuous interaction between innate genotype and environmental stimuli to ensure proper functioning of neural networks and to maintain homeostasis upon changing surroundings [1, 2]. Neuroplasticity relates to functional adaptations such as long-term potentiation (LTP) and depression (LTD) [3], over microscale structural alterations such as the formation of dendritic protrusions [4, 5], to the establishment of axonal projections, neurogenesis and macro-scale reorganization of functional and structural connectivity between distinct brain areas [6-9], etc. Insights into the fundamental properties of neuroplasticity are highly necessary to understand how the brain develops, processes information in advanced life stages, deals with changing internal and environmental stimuli, learns and memorises. These insights could guide us to design educational programs to expose children to proper environmental input during the ideal maturational time window, to understand what goes wrong in developmental disorders, to uncover possible ways in which we could up-regulate neuroplasticity to help the brain recover from traumata, stimulate life-long learning, etc. The ultimate goal of studying neuroplasticity would be to 'unlock the brain' [10] and restore levels of early neuroplasticity in adulthood as strategy to treat certain CNS disorders. Several attempts have been made [10-12], yet, further investigation is highly necessary and requires not only sensitive methods, but also effective research strategies and appropriate model systems. A prominent model in the study of neuroplasticity can be found in songbirds.

1.2 SONGBIRDS IN NEUROSCIENCE

Songbirds occupy an exclusive niche in neuroplasticity research by (1) their unique ability to communicate through complex socially-learned vocalisations, i.e. songs, and (2) the dramatic spontaneously-occurring seasonal neuroplasticity affecting the birds' behaviour as well as the functional, structural and biochemical properties of the brain. Vocal learning occurs in ontogeny and is most often studied in close-ended learners, i.e. birds that only learn a song during one period in early life. Seasonal neuroplasticity, on the other hand, mainly affects birds that live in temperate zones where the length of the day (photoperiod) varies over different seasons and

stipulates behaviour, e.g. at what time of the year birds should prepare to breed. Birds that display this extensive seasonal neuroplasticity are often termed open-ended learners as some of them manage to extend or adapt their song repertoire on a yearly basis [13-15].

1.2.1 Vocal learning in ontogeny

While most animals vocalise, only few species –humans, some bats [16], elephants [17], cetaceans (dolphins and whales), parrots, hummingbirds and songbirds [18]– go through an intense (vocal) learning period during which they modify the acoustic properties of their vocalisations by imitation of certain models. Of these few species, songbirds are most easily kept and investigated in a laboratory setting and, apart from human speech, bird song forms the one of the most elaborate and complex communication signals known to us from the animal kingdom [19]. Furthermore, ample evidence has been collected supporting songbirds as a valid model to study particular aspects of vocal learning and communication, displaying convincing parallels with e.g. human speech [20, 21]. For example, (1) song learning in songbirds relies strongly on audition and auditory feedback [22-24]. (2) It takes place in a well-defined time window during the first months of life, i.e. the critical period of vocal learning, and consists of an initial phase during which juvenile birds memorize species specific sounds and songs [25, 26] and a second phase where by trial-and-error the juvenile birds produce vocalizations trying to match their own sounds to the previously established song template [27, 28]. (3) Vocal imitation in ontogeny and vocal performance throughout life is context-dependent [29], and the context-dependence is probably driven by evolutionary conserved neural systems involved in motivation and reward [30]. (4) Interestingly, several studies have found cerebral asymmetries in the production, but especially the processing and perception of songs using different methodologies [31-36]. (5) Like speech, song informs on singer (speaker) identity, its population affiliation, territorial ownership, reproductive and emotional status, e.g. sings to court or to attack. This, however, is mainly encoded in the sound meta-info including tone, pitch and tempo (‘paralanguage’ [37]) and partly overlaps with certain non-learned vocalisations. (6) Several studies reported that similar genes are involved in bird song and human speech [38]. Most evidence coming from evolutionary biologists and genetic studies points towards convergent evolution of vocal communication in humans and songbirds [39]. Consequently, studying the critical period of vocal learning in juvenile birds or vocal communication (including perceptual processing) in adult songbirds will help to unravel the genetic and neural basis of

these particular behaviours and identify the mechanisms that enable or limit neuroplasticity and learning [40, 41].

1.2.2 Seasonal plasticity in adulthood

Besides vocal learning in ontogeny, several species of songbirds display extensive neuroplastic changes in adulthood that can be related to alterations in singing behaviour [42, 43], e.g. canaries (*Serinus canaria*) or European starlings (*Sturnus vulgaris*). In seasonal songbirds, the neural substrate that encodes singing behaviour, i.e. the song control system, displays substantial seasonal neuroplasticity as the volume and connectivity between different subcomponents of the song control system dramatically increases towards the breeding season preparing birds to sing [6, 44]. Indeed, photoperiod and/or hormonal factors initiate extensive morphological and functional neuroplasticity that include the recrudescence of several song control nuclei that is based on underlying phenomena such as dendrite branching, cell swelling, neurogenesis and neuronal recruitment, synaptogenesis, strengthening and weakening of fibre pathways that connect different components of the song control system, altered neuronal activity and response to particular stimuli, differential expression of peptide and neurotransmitter receptors etc. (for review: [42-46] and many others). Even though no direct translational parallels can be found with the human brain, studying hormone- and photoperiod-induced adult neuroplasticity in songbirds might lead to valuable insights into factors enabling spontaneously occurring neuroplasticity related to learning and memory in adulthood and inform on neural mechanisms that underlie specific biologically relevant behaviours.

1.2.3 Methods applied in songbird neurosciences

These exceptional phenomena –only rarely seen in other species– have been studied intensely and have led to important insights ranging from memory and perception related to vocal communication signals [47], over adult neurogenesis [48], the role of hormones in shaping brain and behaviour [49], to in-depth insights into genes important for speech and song learning such as FoxP2 [50]. Besides behavioural studies, most songbird neuroscience research engages histological, molecular, electrophysiological and/or functional magnetic resonance imaging (fMRI) techniques. Especially the first three methods, yield high sensitivity and (biological) specificity, unfortunately, they are extremely invasive and lack the brain-wide coverage present in brain-wide research methods such as (f)MRI. Consequently, so far mostly the song control and auditory systems have been targeted and are meanwhile quite well characterised, while

the remainder of the bird brain has been largely overlooked. Furthermore, the invasive nature of these methods strongly impedes with comprehensive longitudinal studies addressing neuroplastic events along, for example, brain development or song (reinforcement) learning within the same subject. Longitudinal studies enable drawing correlations between improvements in, e.g. song performance and potential functional and structural neuroplastic events occurring at certain locations in the brain. Even though correlation studies provide no direct and indisputable proof for causality, they do suggest some involvement of a particular brain region in the studied behaviour.

Relatively recently, and within the Bio-Imaging Lab, *in vivo* structural MR imaging tools, i.e. Diffusion Tensor Imaging (DTI), T_2-relaxometry and Manganese-enhanced MRI (MEMRI), have been applied to the European Starling brain to trace structural neuroplastic events occurring over different seasons [51]. DTI and T_2-relaxometry are two advanced *in vivo* structural imaging methods to non-invasively infer local tissue microstructure by measuring respectively the diffusion profile of water molecules [52], or by quantifying the relaxation time of brain tissue [53] in each voxel of the image (a voxel is a three-dimensional pixel). MEMRI relies on administration of exogenous contrast agents that allows to evaluate the volume of and connectivity between targeted brain structures. These (non-invasive) imaging studies have proven that seasonal plasticity does not exclusively affect the brain areas in control of singing behaviour, i.e. the song control and auditory system, but induce functional and structural changes in the olfactory [54] and visual system [6, 55] as well. Despite the successful application of structural imaging tools in seasonal songbirds, surprisingly few *in vivo* structural imaging studies have been reported in close-ended learners such as zebra finches. These methods include Manganese-enhanced MRI [56], and, a very recent study which uses conventional T_2-weighted anatomical scans to evaluate lesion size at several time points after neurotoxic trauma [57]. This lack of advanced structural MR-based methods is even more striking, considering that over the last decade functional MRI has been implemented successfully in songbirds, mostly in zebra finches (for review [58]). Furthermore, all previous structural and functional imaging experiments exclusively studied adult birds, hence, none of the *in vivo* imaging studies reported today have successfully targeted the brains of juvenile birds during the critical period for vocal learning. To conclude, given the great potential of *in vivo* non-invasive brain-wide structural imaging methods such as DTI to help extend the range of neurobiological investigations of the entire zebra finch brain, as was clearly demonstrated in

starlings, the major aim of this PhD project was to (1) implement a non-invasive translational brain-wide imaging tool to study the tiny brain of juvenile zebra finches *in vivo*, and (2) apply this method to characterise structural neuroplasticity during the critical period of vocal learning in juvenile birds, and (3) explore to what extent the zebra finch brain retains its neuroplastic capacity towards adulthood. By employing *in vivo* imaging tools in longitudinal study designs, alterations in vocal performance can be linked to structural differences in the brain, this way providing clear links between brain and behaviour.

The following sections will introduce zebra finches, the close-ended model species studied in this thesis. First several basic properties of song will be described, after which the neural substrate that encodes vocal control and communication i.e. the auditory and song control system, will be discussed, ending with a brief description of the critical period for vocal learning in ontogeny.

1.3 ZEBRA FINCHES AS A MODEL SPECIES FOR VOCAL LEARNING AND COMMUNICATION

Zebra finches or *Taeniopygia guttata* (Figure 1-1) are widely recognised as a valid model to study aspects of vocal learning and vocal communication, both in ontogeny and adulthood [20]. Unlike many other songbird species, zebra finches can be relatively easily bred in a laboratory, crucial if one aims to study the critical period for vocal learning that takes place during the first four months of *post*-hatch life. During the latter period, juvenile male zebra finches learn their song. When reaching adulthood, this song becomes fixed and remains –in normal circumstances– constant thereafter. Zebra finches do not show any yearly or seasonal cycle in song performance.

Song serves to coordinate behaviour. More specifically, while singing, birds anticipate a particular behavioural response of the audience [47]. For example, male zebra finches, as a non-territorial species, mainly use their song to attract a mate [59]. When male zebra finches sing to court a female they will optimise their vocal performance by increasing the number of introductory notes, singing faster and more stereotyped (less spectral variability) compared to undirected or solitary song [60]. Furthermore, besides singing, they will perform particular body gestures and beak movements (courtship dance) to convince the female of his fitness and suitability as a mating partner. Female zebra finches do not sing, but display a preference for

songs resembling the song of the father indicating that they do memorise a song model to some extent [61, 62]. Interestingly, this behavioural dimorphism is reflected in the neural substrate supporting singing behaviour as the volumes, connectivity and microstructural tissue properties of several song control nuclei differ greatly between male and female birds [63]. Interestingly, a cross-species comparison reveals that the extent of behavioural disparity is proportional to the morphological difference, for example in zebra finches where only males sing the difference in brain structure is much more pronounced compared to starlings, where both sexes do sing but to a different extent [64-67]. Even though in many species only male birds sing, both sexes must be able to perceive vocal patterns to enable a proper response. Consequently, less sex-differences are described in the auditory pathways. The auditory pathways of songbirds provide an excellent model system to further understanding into the mechanisms enabling or even driving the perception of social context-dependent communication signals [47]. Clear patterns of song selectivity have been shown to arise along the ascending auditory pathways.

Figure 1-1: Zebra finch family. Adult male zebra finches (left) can be recognised by the red beak, orange cheeks and white-dotted brown feathers on the sides. Adult female zebra finches (middle) have an orange beak and less colourful plumage compared to males. The clear sex-dependent phenotype only develops around 40 dph, before that age, both male and female juvenile birds have dark grey plumage with a black beak (right). The juvenile in this figure is around 40 dph as the beak is turning orange. Together with the absence of orange feathers near the cheeks or white-dotted brown features near the wings, the birds' appearance suggests it is a female juvenile zebra finch.

Not all vocalisations produced by birds are songs. The term 'song' is reserved for communication signals that meet the following criteria: socially-learned stereotyped sequences of complex acoustic sounds separated by silent intervals. Therefore, 'calls' produced by most vertebrates, are not (always) learned, are characterised by much simpler acoustical properties and a shorter duration (often mono-syllabic), are delivered in different contexts and are not accompanied by specific body gestures [19, 68]. Even though songbird 'calls' do not qualify as 'songs', they are valid communication signals. Compared to singing as a more 'formal affair' that is most often focussed on reproduction and territoriality, call behaviour is much more

opportunistic, less stereotyped and variable depending on the circumstances. Calls are used in widely diverse contexts, to name a few: (close-range) contact calls are produced to maintain coherence of the flock and allow birds to keep in touch with conspecifics while foraging food, flight calls aid in synchronisation and coordination of group movements, food-begging calls uttered by hatchlings draw parental attention and serve to request food, aggressive calls are exchanged during hostile interactions, alarm calls to signal danger and/or distress or inform on approaching predators etc. (for review [19]). Importantly, some calls are modifiable by learning, for example the 'loud', 'long' or 'contact calls' in zebra finches. Interestingly, only male, and not female, zebra finches are known to modify long calls illustrating that sex differences extend beyond singing behaviour [69, 70].

1.3.1 The song: terminology and structure

An easy and transparent way to visualise and quantify songs is the sound spectrogram. They are derived from oscillograms and visualise the time-frequency structure of sounds [71]. Oscillograms (time domain) present the amplitude and waveform of sounds in function of time, while the sound spectrogram (frequency domain) informs on the 'power' of frequencies sung at a particular window in time (Figure 1-2). The smallest unit of a song, defined as a continuous morphologically discrete trace on a song spectrogram, is the song 'element' or 'note' (indicated by the grey lines on top of the sound spectrogram in the inset of Figure 1-2). One or several notes can group together and form a 'syllable'. Different syllables are separated from one another by a silent interval of several ms. On average, three to five syllables comprise one song motif [60]. Syllables are considered to be the smallest unit of songs, as, in case birds are suddenly interrupted by a bursts of strobe light, they still finish the syllable before ceasing to sing [72]. The temporal and spectral profiles of syllables vary markedly within and between birds, but, the acoustical properties of each specific syllable within the song of a particular bird are strictly defined with only minor variability between renditions. Hence, bird identity and affiliation can be extracted by examining the sound spectrogram and/or spectro-temporal acoustics of individual motifs. Most often, zebra finches sing multiple renditions of the same song motif consecutively in a song 'bout'. A song bout is often preceded by a set of 'introductory notes'. The latter differ in number between renditions of songs, present no fixed inter-introductory note intervals, are quite similar across different birds and are present in 'isolate songs', i.e. crude songs sung by birds that have not been exposed to a proper song model during

the critical period for vocal learning [73]. Therefore, they are considered not to be part of the learned song. This makes that most often both introductory notes and calls are omitted from quantitative song analyses.

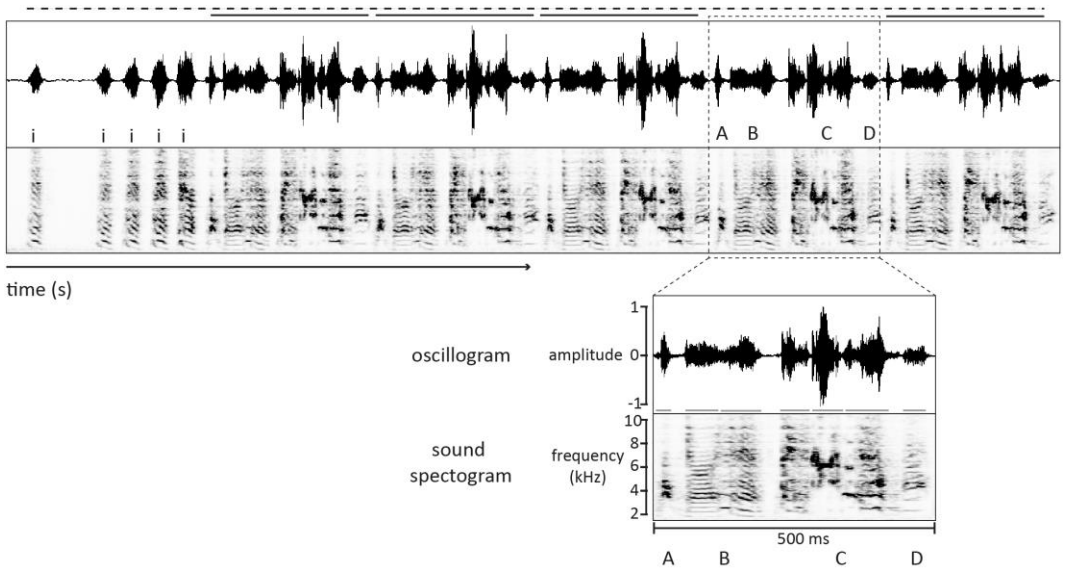

Figure 1-2: Oscillogram (amplitude) and sound spectrogram (frequency) of a song bout produced by an adult male zebra finch. The song bout (dashed line on top of the oscillogram) starts off with five introductory notes (i) followed by five song motifs (indicated by the solid black lines on top of the oscillogram). The different renditions of the motifs all appear highly similar in the sound spectrogram which is typical for crystallised song. The fourth song motif is enlarged in the inset. Different syllables are indicated by letters (A-D). A and D are syllables consisting of one note, while syllable B and C consist out of 2 and 3 notes (indicated by the grey lines on top of the sound spectrogram in the inset).

Like all sounds, song can be decomposed into a set of acoustical properties. Dedicated software programs have been developed that enable detailed quantitative analyses of the temporal (duration of song motif, syllables, inter-syllable intervals, song tempo) and spectral properties (pitch, Wiener entropy, frequency modulation) of song and to explore related measures such as the acoustic similarity between two songs [71]. This makes that by simply recording the songs, the precise stage of vocal learning or specific alterations to song properties resulting from training, treatment or lesion studies can be 'quantified'.

1.3.2 The neural substrate implicated in vocal control

The songbird brain is structured fundamentally different compared to the mammalian brain [74]. Instead of a laminar structure, i.e. cortical layers, grey matter is organized into nuclei. Each nucleus controls different functions and is interconnected to other nuclei via fibre tracts. This

way extensive circuitries are formed, of which the auditory and song control system respectively underlie audition and singing behaviour (Figure 1-3). The following sections will describe the generally accepted view of the major pathways and connections of the auditory and song control systems. Important to note is that the schematic representation of both systems is massively over-simplified: several parallel pathways and recurrent loops exist; synaptic connectivity follows a strict synaptic topology that is conserved along almost the entire circuitries; local micro-circuits within one anatomically defined or severalclose-by areas exist; the song control and auditory nuclei project to brain areas that are not included in the scheme but have been shown to be implicated in certain aspects of auditory or song control; even though only few interhemispheric connections exist (mostly limited to the thalamic and midbrain level [75]), they are not included in this scheme; etc. A full description of both systems, however, goes well beyond the scope of this thesis.

1.3.2.1 Song control system

The song control system consists of two major pathways that originate in two distinct cell populations of HVC (abbreviation used as a proper name) and send indirect or direct projections to nucleus *robustus arcopallialis* (RA), i.e. the anterior forebrain pathway or the caudal motor pathway respectively (Brenowitz et al., 1997). The anterior forebrain pathway is mostly important for song learning in ontogeny ([76, 77], for review: [78] and [79]) and song maintenance in adulthood [80-82]. It originates in HVC where it projects to Area X, *nucleus dorsolateralis anterior thalami pars medialis* (DLM), *nucleus lateralis magnocellularis nidopallii anterioris* (LMAN) and RA. In addition, LMAN projects 'recursively' to Area X. The caudal motor pathway sends direct projections from HVC to RA. From RA, the pathway continuous further to the dorsomedial portion (DM) of the *nucleus intercollicularis* (ICo) and next to (among others) the tracheosyringeal part of the nucleus of the XIIth cranial nerve (nXIIts). Finally, it arrives at the syrinx, which is the avian analogue of the larynx, and two respiratory nuclei. The caudal motor pathway is most extensively involved in the motor aspect of singing behaviour [83, 84] and encodes acoustic features of the long calls and learned vocalisations in male zebra finches [70]. Important to note is that specific sub-sets of muscles of the syrinx are responsible for producing the acoustical properties of song i.e. frequency and amplitude [85].

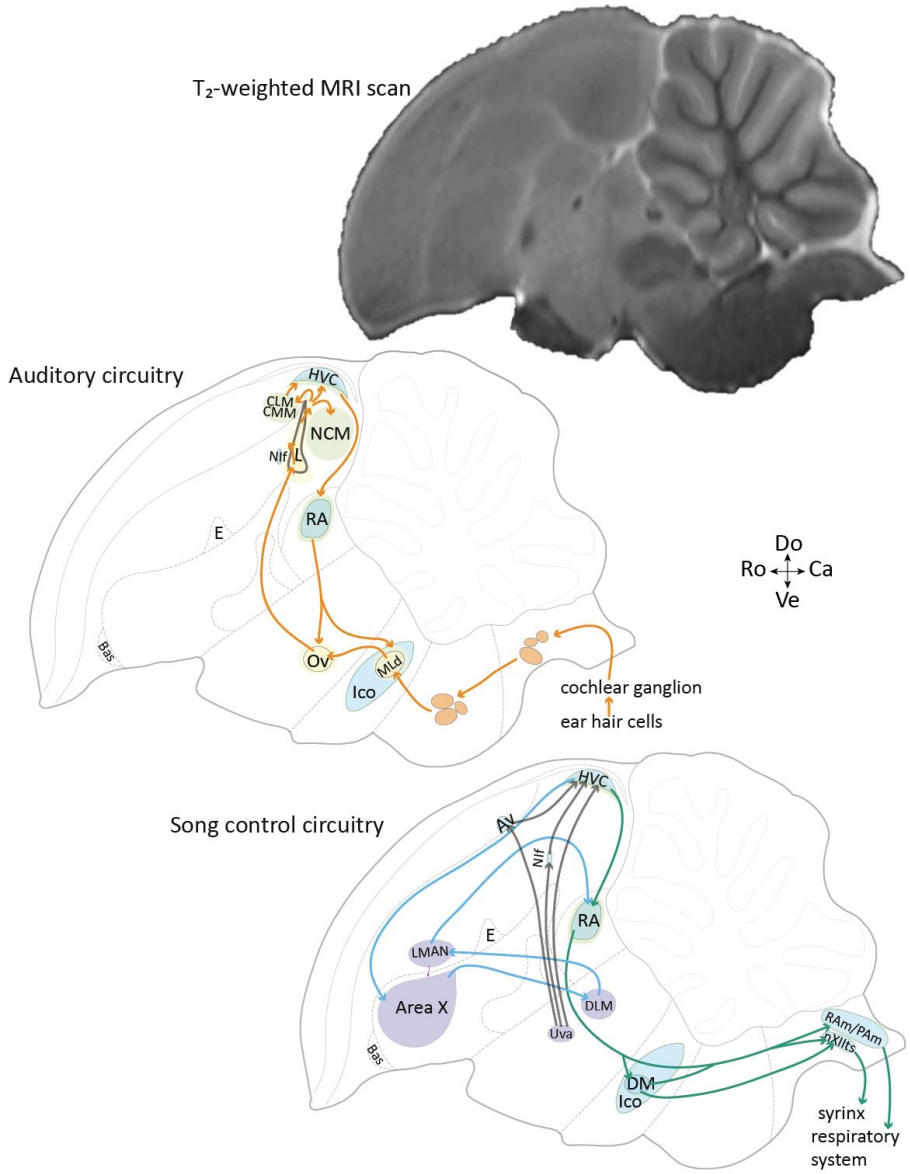

Figure 1-3: Schematic overview of the auditory and song control system in the songbird brain, derived from a T2-weighted magnetic resonance image. The colours of the nuclei refer to distinct groups or pathways, i.e. yellow refers to primary auditory nuclei, green to secondary or association auditory regions, orange to brainstem nuclei, blue to the caudal motor pathway, and purple to the anterior forebrain pathway. Several brain areas are encapsulated by a cup, shell or belt region that is indicated an additional (more transparent) shell surrounding the core region. Abbreviations of anatomical areas can be found in the text. Do: dorsal; Ve: ventral; Ro: rostral; Ca: caudal.

Each of these muscles receives afferent input from a particular subarea of nXIIts [86], this topographic organisation is preserved upstream to RA [87] and possibly even further to Area X, LMAN and DLM [88]. The topographic organisation of the song control system onto nXIIts

presents a mechanistic opportunity to the song control system to specifically 'control' downstream vocal musculature to produce particular acoustic features.

Singing behaviour is not only controlled by the song control circuitry: another set of interconnected nuclei, i.e. the social behaviour network, has been shown to influence the motivation to sing. Many components of the social behaviour network express various hormone receptors and affect singing behaviour depending on the social context [89-91].

1.3.2.2 Auditory system

The auditory system contains two major sets of projections termed the ascending and descending auditory pathways. The first originates in the inner ear and connects to the cochlear nuclei in the brainstem. Starting in the brainstem, a direct and indirect pathway travel by the auditory midbrain traversing *nucleus mesencephalicus lateralis pars dorsalis* (MLd; anatomically (and in many aspects also functionally) analogous to the mammalian *inferior colliculus*), *nucleus ovoidalis* (Ov, the avian auditory thalamus) and Field L. Field L is analogous to the mammalian primary auditory cortex and can be subdivided into regions L1, L2a, L2b, L3 and L, based differences in micro-architecture and connectivity. Sub-region Field L2 is the primary thalamorecipient zone, L1 and L3 also receive thalamic input but to a lesser extent. Next, Field L contacts several secondary and tertiary auditory telencephalic areas situated in the nido- and mesopallium, i.e. NCM, CMM, CLM [92-94]. The latter of which are known to be implicated in auditory perception to help shape vocal performance and display a varying selectivity for species-specific communication signals (for review e.g. [95, 96]). Because of its many afferent and efferent connections, Field L is often regarded as a relay station [97]. The second major pathway, i.e. descending auditory pathway, sends projections from Field L to CM, Nif and HVC (shelf) to RA (cup) [97-99] linking primary auditory centres to the song control system. Importantly however, similar to the latter, other loops and reciprocal connections exist which further complicate both circuitries[1].

[1] Several examples: Topographic organisation and parallel pathways in the song control system (Johnson et al., 1995 J Comp Neurol); Recurrent pathways in the anterior forebrain pathway (Hamaguchi and Mooney, 2012 J Neurosci); Connections between the song control and auditory system Vates et al., 1995 J Comp Neurol; Mello et al., 1998 J Comp Neurol); Topography and myotopographic organisation of the CMP and downstream nuclei (Iyengar et al., 1999 J Neurosci; Vicario et al., 1991 J Comp Neurol).

1.3.3 The critical period for song learning

Vocal learning can be defined as the ability to modify the acoustic and syntactic structure of vocalisations by imitation depending on social context, experience and auditory feedback, and serve as a means of communication [20, 100].

The critical period for vocal learning takes place during the first 120 days post hatching (dph) and consists of two partly-overlapping sub-phases, i.e. the sensory and the sensorimotor phase (for review e.g. [100] and [101]). During the sensory phase (appr. 20-45 dph), the juvenile birds memorize the song sung by an adult tutor bird. This phase is sometimes also referred to as the perceptual phase. During the sensorimotor phase (appr. 40-90 dph), the juvenile birds will start to vocalize, trying to match their own vocalizations to the previously memorized tutor song. After the sensorimotor phase, zebra finch males will evolve into the crystallization phase (appr. 90-120 dph), where the song will become fixed and, in normal circumstances, never change again. Importantly, the time at which proper experience is available should occur at the proper developmental window, if not, the skill will not be mastered as proficiently. This effect is illustrated by juvenile zebra finches raised in isolation of an adult male. They sing a 'crude' isolate song lacking proper structure, with noisy, broadband, monotonic prolonged syllables [62, 102]. Importantly, the isolated juvenile males can still learn zebra finch song when an adult male zebra finch is introduced after normal closure of the critical period of vocal learning, however, the resulting song will never match the quality of that sung by normally reared zebra finches [73, 102, 103]. Similar effects have been described in other close-ended songbird species [101, 104, 105].

During the sensorimotor learning process, simple vocalisations will evolve into complex structured vocal sound patterns that are strictly characterised by specific spectro-temporal acoustical properties. The song evolves from subsong (poorly structured, noisy and highly variable sounds [106], similar to babbling of human infants [107]), over plastic song (unstable, but already serial production of syllables in a tighter time frame) to crystallised song (remarkably stereotyped song). Consequently, vocal learning requires birds to master both characteristics by fine-tuning their neural apparatus based on trial-and-error (re)adjustment of their own vocalisations. This implies three processes: (1) being capable of introducing variability in vocalisations, (2) evaluation of own performance to a given template or model, and (3) retain only those elements (variability) that acoustically match with a given model to drive the motor

circuitry. The first has been appointed to the AFP, based on the effects of DLM lesion on variability of vocal babbling in juvenile birds [108], pharmacological inactivation of LMAN during singing in juvenile birds [109] and as it was found to induce both temporal and spectral variability in vocalisations [110]. The conversion or maybe even 'consolidation' of previously successful vocal explorations has been ascribed to distinct components. Ample evidence points towards HVC as 'time keeper', i.e. being responsible for the temporal characteristics of the motor program of song. For example, song tempo can be modified by altering the temperature of HVC [111, 112], multi-unit electrophysiological recordings showed that the activity of HVC neurons correlated with learning-induced alterations of the timing of particular song elements (during reinforcement learning by conditional auditory feedback). Importantly to note, however, HVC not only encodes timing but also takes part in song stereotypy (gradual change in balance of input into RA changing from LMAN to HVC towards song crystallisation [109].

REFERENCES

1. Butz, M., F. Wörgötter, and A. van Ooyen, *Activity-dependent structural plasticity.* Brain Research Reviews, 2009. **60**(2): p. 287-305.
2. Nagy, C. and G. Turecki, *Sensitive periods in epigenetics: bringing us closer to complex behavioral phenotypes.* Epigenomics, 2012. **4**(4): p. 445-457.
3. Malenka, R.C. and M.F. Bear, *LTP and LTD: An Embarrassment of Riches.* Neuron, 2004. **44**(1): p. 5-21.
4. Anthony, H. and S. Karel, *Experience-dependent structural synaptic plasticity in the mammalian brain.* Nature Reviews Neuroscience, 2009. **10**(10): p. 759-759.
5. Chen, C.-C., A. Bajnath, and J.C. Brumberg, *The Impact of Development and Sensory Deprivation on Dendritic Protrusions in the Mouse Barrel Cortex.* Cerebral Cortex, 2014.
6. De Groof, G., et al., *Seasonal rewiring of the songbird brain: an in vivo MRI study.* European Journal of Neuroscience, 2008. **28**(12): p. 2475-2485.
7. Oboti, L. and P. Peretto, *How neurogenesis finds its place in a hardwired sensory system.* Frontiers in Neuroscience, 2014. **8**.
8. Gheusi, G. and P.-M. Lledo, *Chapter 6 - Adult Neurogenesis in the Olfactory System Shapes Odor Memory and Perception*, in *Progress in Brain Research*, B. Edi and A.W. Donald, Editors. 2014, Elsevier. p. 157-175.
9. Barnes, S.J. and G.T. Finnerty, *Sensory Experience and Cortical Rewiring.* The Neuroscientist, 2010. **16**(2): p. 186-198.
10. Jon, J.B., *Neurodevelopment: unlocking the brain.* Nature, 2012. **487**(7405): p. 24-26.
11. Sale, A., et al., *GABAergic inhibition in visual cortical plasticity.* Frontiers in cellular neuroscience, 2010. **4**: p. 10.
12. Gervain, J., et al., *Valproate reopens critical-period learning of absolute pitch.* Frontiers in Systems Neuroscience, 2013. **7**.
13. Nottebohm, F., M.E. Nottebohm, and L. Crane, *Developmental and seasonal changes in canary song and their relation to changes in the anatomy of song-control nuclei.* Behavioral and Neural Biology, 1986. **46**(3): p. 445-471.

14. Brenowitz, E., et al., *Seasonal changes in avian song nuclei without seasonal changes in song repertoire.* The Journal of Neuroscience, 1991. **11**(5): p. 1367-1374.
15. Van Hout, A.J.M., et al., *Complex modulation of singing behavior by testosterone in an open-ended learner, the European Starling.* Hormones and Behavior, 2009. **56**(5): p. 564-573.
16. Vernes, S.C., *What bats have to say about speech and language.* Psychonomic Bulletin & Review, 2017. **24**(1): p. 111-117.
17. Poole, J.H., et al., *Animal behaviour: Elephants are capable of vocal learning.* Nature, 2005. **434**(7032): p. 455-456.
18. King, S.L. and P.K. McGregor, *Vocal matching: the what, the why and the how.* Biology Letters, 2016. **12**(10).
19. Marler, P., *Bird Calls: Their Potential for Behavioral Neurobiology.* Annals of the New York Academy of Sciences, 2004. **1016**(1): p. 31-44.
20. Brainard, M.S. and A.J. Doupe, *Translating Birdsong: Songbirds as a Model for Basic and Applied Medical Research.* Annual Review of Neuroscience, 2013. **36**(1): p. 489-517.
21. Konopka, G. and Todd F. Roberts, *Insights into the Neural and Genetic Basis of Vocal Communication.* Cell, 2016. **164**(6): p. 1269-1276.
22. Marler, P., *A comparative approach to vocal learning: song development in the white-crowned sparrow.* Journal Comparative Psychology, 1970. **71**(2): p. 1.
23. Brainard, M.S. and A.J. Doupe, *Auditory feedback in learning and maintenance of vocal behaviour.* Nat Rev Neurosci, 2000. **1**(1): p. 31-40.
24. Thorpe, W.H., *THE LEARNING OF SONG PATTERNS BY BIRDS, WITH ESPECIAL REFERENCE TO THE SONG OF THE CHAFFINCH FRINGILLA COELEBS.* Ibis, 1958. **100**(4): p. 535-570.
25. Marler, P. and S. Peters, *Sensitive Periods for Song Acquisition from Tape Recordings and Live Tutors in the Swamp Sparrow, Melospiza georgiana.* Ethology, 1988. **77**(1): p. 76-84.
26. Nelson, D.A., et al., *The timing of song memorization differs in males and females: a new assay for avian vocal learning.* Animal Behaviour, 1997. **54**(3): p. 587-597.
27. Immelmann, K., *{Song development in the zebra finch and other estrildid finches}.* Bird vocalizations (Hinde RA, ed), 1969: p. 61-74.
28. Marler, P. and S. Peters, *Developmental overproduction and selective attrition: New processes in the epigenesis of birdsong.* Developmental Psychobiology, 1982. **15**(4): p. 369-378.
29. Jarvis, E.D., et al., *For Whom The Bird Sings.* Neuron, 1998. **21**(4): p. 775-788.
30. Riters, L.V., *The role of motivation and reward neural systems in vocal communication in songbirds.* Frontiers in Neuroendocrinology, 2012. **33**(2): p. 194-209.
31. Moorman, S., et al., *Human-like brain hemispheric dominance in birdsong learning.* Proceedings of the National Academy of Sciences, 2012. **109**(31): p. 12782-12787.
32. George, I., et al., *Song perception in the European starling: hemispheric specialisation and individual variations.* Comptes Rendus Biologies, 2002. **325**(3): p. 197-204.
33. Poirier, C., et al., *Own-Song Recognition in the Songbird Auditory Pathway: Selectivity and Lateralization.* The Journal of Neuroscience, 2009. **29**(7): p. 2252-2258.
34. Voss, H.U., et al., *Functional MRI of the zebra finch brain during song stimulation suggests a lateralized response topography.* Proceedings of the National Academy of Sciences of the United States of America, 2007. **104**(25): p. 10667-10672.
35. Phan, M.L. and D.S. Vicario, *Hemispheric differences in processing of vocalizations depend on early experience.* Proceedings of the National Academy of Sciences of the United States of America, 2010. **107**(5): p. 2301-2306.
36. Nottebohm, F., T.M. Stokes, and C.M. Leonard, *Central control of song in the canary, Serinus canarius.* The Journal of Comparative Neurology, 1976. **165**(4): p. 457-486.
37. Wilbrecht, L. and F. Nottebohm, *Vocal learning in birds and humans.* Mental Retardation and Developmental Disabilities Research Reviews, 2003. **9**(3): p. 135-148.

38. Condro, M.C. and S.A. White, *Recent Advances in the Genetics of Vocal Learning.* Comparative cognition & behavior reviews, 2014. **9**: p. 75-98.
39. Pfenning, A.R., et al., *Convergent transcriptional specializations in the brains of humans and song-learning birds.* Science (New York, N.Y.), 2014. **346**(6215): p. 1256846-1256846.
40. Clayton, D.F., *Role of gene regulation in song circuit development and song learning.* Journal of Neurobiology, 1997. **33**(5): p. 549-571.
41. Warren, W.C., et al., *The genome of a songbird.* Nature, 2010. **464**(7289): p. 757-762.
42. Nottebohm, F., *A brain for all seasons: cyclical anatomical changes in song control nuclei of the canary brain.* Science, 1981. **214**(4527): p. 1368-1370.
43. Tramontin, A.D. and E.A. Brenowitz, *Seasonal plasticity in the adult brain.* Trends in Neurosciences, 2000. **23**(6): p. 251-258.
44. Brenowitz, E.A., *Plasticity of the Adult Avian Song Control System.* Annals of the New York Academy of Sciences, 2004. **1016**(1): p. 560-585.
45. Balthazart, J. and G.F. Ball, *Endocrine and social regulation of adult neurogenesis in songbirds.* Frontiers in Neuroendocrinology, 2016. **41**: p. 3-22.
46. Ball, G.F. and J. Balthazart, *Seasonal and hormonal modulation of neurotransmitter systems in the song control circuit.* Journal of Chemical Neuroanatomy, 2010. **39**(2): p. 82-95.
47. Knudsen, D. and T.Q. Gentner, *Mechanisms of Song Perception in Oscine Birds.* Brain and language, 2010. **115**(1): p. 59-68.
48. Barnea, A. and V. Pravosudov, *BIRDS AS A MODEL TO STUDY ADULT NEUROGENESIS: BRIDGING EVOLUTIONARY, COMPARATIVE AND NEUROETHOLOGICAL APPROCHES.* The European journal of neuroscience, 2011. **34**(6): p. 884-907.
49. Balthazart, J., et al., *Sex steroid-induced neuroplasticity and behavioral activation in birds.* The European journal of neuroscience, 2010. **32**(12): p. 2116-2132.
50. Wohlgemuth, S., I. Adam, and C. Scharff, *FoxP2 in songbirds.* Current Opinion in Neurobiology, 2014. **28**(Supplement C): p. 86-93.
51. De Groof, G. and A. Van der Linden, *Love songs, bird brains and diffusion tensor imaging.* NMR in Biomedicine, 2010. **23**(7): p. 873-883.
52. Mori, S. and J. Zhang, *Principles of Diffusion Tensor Imaging and Its Applications to Basic Neuroscience Research.* Neuron, 2006. **51**(5): p. 527-539.
53. Deoni, S.C.L., *Quantitative Relaxometry of the Brain.* Topics in Magnetic Resonance Imaging, 2010. **21**(2): p. 101-113 10.1097/RMR.0b013e31821e56d8.
54. De Groof, G., et al., *Neural Correlates of Behavioural Olfactory Sensitivity Changes Seasonally in European Starlings.* PLoS ONE, 2010. **5**(12): p. e14337.
55. De Groof, G., et al., *Structural Changes between Seasons in the Songbird Auditory Forebrain.* The Journal of Neuroscience, 2009. **29**(43): p. 13557-13565.
56. Tindemans, I., et al., *IR-SE and IR-MEMRI allow in vivo visualization of oscine neuroarchitecture including the main forebrain regions of the song control system.* NMR in Biomedicine, 2006. **19**(1): p. 18-29.
57. Lukacova, K., et al., *Imaging of striatal injury in a songbird brain.* General Physiology and Biophysics, 2017. **36**(1): p. 5.
58. Van Ruijssevelt, L., et al., *Current state-of-the-art of auditory functional MRI (fMRI) on zebra finches: Technique and scientific achievements.* Journal of Physiology-Paris, 2013. **107**(3): p. 156-169.
59. Kroodsma, D.E. and B.E. Byers, *The Function(s) of Bird Song.* American Zoologist, 1991. **31**(2): p. 318-328.
60. Sossinka, R. and J. Böhner, *Song Types in the Zebra Finch Poephila guttata castanotis1.* Zeitschrift für Tierpsychologie, 1980. **53**(2): p. 123-132.

61. Riebel, K., et al., *Sexual equality in zebra finch song preference: evidence for a dissociation between song recognition and production learning.* Proceedings of the Royal Society of London. Series B: Biological Sciences, 2002. **269**(1492): p. 729-733.
62. Williams, H., K. Kilander, and M.L. Sotanski, *Untutored song, reproductive success and song learning.* Animal Behaviour, 1993. **45**(4): p. 695-705.
63. Nottebohm, F. and A. Arnold, *Sexual dimorphism in vocal control areas of the songbird brain.* Science, 1976. **194**(4261): p. 211-213.
64. MacDougall-Shackleton, S.A. and G.F. Ball, *Comparative studies of sex differences in the song-control system of songbirds.* Trends in Neurosciences, 1999. **22**(10): p. 432-436.
65. Wade, J., *Genetic regulation of sex differences in songbirds and lizards.* Philosophical Transactions of the Royal Society B: Biological Sciences, 2016. **371**(1688): p. 20150112.
66. Wade, J. and A.P. Arnold, *Sexual Differentiation of the Zebra Finch Song System.* Annals of the New York Academy of Sciences, 2004. **1016**(1): p. 540-559.
67. Bernard, D.J., J.M. Casto, and G.F. Ball, *Sexual dimorphism in the volume of song control nuclei in European starlings: Assessment by a Nissl stain and autoradiography for muscarinic cholinergic receptors.* The Journal of Comparative Neurology, 1993. **334**(4): p. 559-570.
68. Konishi, M., *Birdsong: From Behavior to Neuron.* Annual Review of Neuroscience, 1985. **8**(1): p. 125-170.
69. Zann, R., *Ontogeny of the Zebra Finch Distance Call: I. Effects of Cross-fostering to Bengalese Finches.* Zeitschrift für Tierpsychologie, 1985. **68**(1): p. 1-23.
70. Simpson, H. and D. Vicario, *Brain pathways for learned and unlearned vocalizations differ in zebra finches.* The Journal of Neuroscience, 1990. **10**(5): p. 1541-1556.
71. Tchernichovski, O., et al., *A procedure for an automated measurement of song similarity.* Animal Behaviour, 2000. **59**(6): p. 1167-1176.
72. Cynx, J., *Experimental determination of a unit of song production in the zebra finch (Taeniopygia guttata).* Journal of Comparative Psychology, 1990. **104**(1): p. 3-10.
73. Eales, L.A., *Song learning in zebra finches: some effects of song model availability on what is learnt and when.* Animal Behaviour, 1985. **33**(4): p. 1293-1300.
74. Nottebohm, F., *Brain pathways for vocal learning in birds: a review of the first 10 years*, in *Progress in Psychobiology and Physiological Psychology*, J.M. Sprague and A.N. Epstein, Editors. 1980, Academic Press: New York. p. 85-214.
75. Vates, G.E., D.S. Vicario, and F. Nottebohm, *Reafferent thalamo-"cortical" loops in the song system of oscine songbirds.* The Journal of Comparative Neurology, 1997. **380**(2): p. 275-290.
76. Scharff, C. and F. Nottebohm, *A comparative study of the behavioral deficits following lesions of various parts of the zebra finch song system: implications for vocal learning.* The Journal of Neuroscience, 1991. **11**(9): p. 2896-2913.
77. Sohrabji, F., E.J. Nordeen, and K.W. Nordeen, *Selective impairment of song learning following lesions of a forebrain nucleus in the juvenile zebra finch.* Behavioral and Neural Biology, 1990. **53**(1): p. 51-63.
78. Bottjer, S.W. and F. Johnson, *Circuits, hormones, and learning: Vocal behavior in songbirds.* Journal of Neurobiology, 1997. **33**(5): p. 602-618.
79. Brainard, M.S., *Contributions of the Anterior Forebrain Pathway to Vocal Plasticity.* Annals of the New York Academy of Sciences, 2004. **1016**(1): p. 377-394.
80. Nordeen, K.W. and E.J. Nordeen, *Deafening-Induced Vocal Deterioration in Adult Songbirds Is Reversed by Disrupting a Basal Ganglia-Forebrain Circuit.* The Journal of Neuroscience, 2010. **30**(21): p. 7392-7400.
81. Hamaguchi, K. and R. Mooney, *Recurrent Interactions between the Input and Output of a Songbird Cortico-Basal Ganglia Pathway Are Implicated in Vocal Sequence Variability.* The Journal of Neuroscience, 2012. **32**(34): p. 11671-11687.

82. Perkel, D.J., *Origin of the Anterior Forebrain Pathway.* Annals of the New York Academy of Sciences, 2004. **1016**(1): p. 736-748.
83. Wild, J.M., *Descending projections of the songbird nucleus robustus archistriatalis.* The Journal of Comparative Neurology, 1993. **338**(2): p. 225-241.
84. Wild, J.M., *Neural pathways for the control of birdsong production.* Journal of Neurobiology, 1997. **33**(5): p. 653-670.
85. Goller, F. and R.A. Suthers, *Role of syringeal muscles in controlling the phonology of bird song.* Journal of Neurophysiology, 1996. **76**(1): p. 287-300.
86. Vicario, D.S. and F. Nottebohm, *Organization of the zebra finch song control system: I. Representation of syringeal muscles in the hypoglossal nucleus.* The Journal of Comparative Neurology, 1988. **271**(3): p. 346-354.
87. Vicario, D.S., *Organization of the zebra finch song control system: Functional organization of outputs from nucleus robustus archistriatalis.* The Journal of Comparative Neurology, 1991. **309**(4): p. 486-494.
88. Johnson, F., M.M. Sablan, and S.W. Bottjer, *Topographic organization of a forebrain pathway involved with vocal learning in zebra finches.* The Journal of Comparative Neurology, 1995. **358**(2): p. 260-278.
89. Goodson, J.L., *The Vertebrate Social Behavior Network: Evolutionary Themes and Variations.* Hormones and behavior, 2005. **48**(1): p. 11-22.
90. Heimovics, S.A. and L.V. Riters, *ZENK labeling within social behavior brain regions reveals breeding context-dependent patterns of neural activity associated with song in male European starlings (Sturnus vulgaris).* Behavioural Brain Research, 2007. **176**(2): p. 333-343.
91. Newman, S.W., *The Medial Extended Amygdala in Male Reproductive Behavior A Node in the Mammalian Social Behavior Network.* Annals of the New York Academy of Sciences, 1999. **877**(1): p. 242-257.
92. Wild, M.J., H.J. Karten, and B.J. Frost, *Connections of the auditory forebrain in the pigeon (columba livia).* The Journal of Comparative Neurology, 1993. **337**(1): p. 32-62.
93. Bauer, E.E., et al., *A Synaptic Basis for Auditory–Vocal Integration in the Songbird.* The Journal of Neuroscience, 2008. **28**(6): p. 1509-1522.
94. Shaevitz, S.S. and F.E. Theunissen, *Functional Connectivity Between Auditory Areas Field L and CLM and Song System Nucleus HVC in Anesthetized Zebra Finches.* Journal of Neurophysiology, 2007. **98**(5): p. 2747-2764.
95. Prather, J.F., *Auditory Signal Processing in Communication: Perception and Performance of Vocal Sounds.* Hearing research, 2013. **305**: p. 10.1016/j.heares.2013.06.007.
96. Mello, C.V., T.A.F. Velho, and R. Pinaud, *Song-Induced Gene Expression: A Window on Song Auditory Processing and Perception.* Annals of the New York Academy of Sciences, 2004. **1016**(1): p. 263-281.
97. Vates, G.E., et al., *Auditory pathways of caudal telencephalon and their relation to the song system of adult male zebra finches (Taenopygia guttata).* The Journal of Comparative Neurology, 1996. **366**(4): p. 613-642.
98. Kelley, D.B. and F. Nottebohm, *Projections of a telencephalic auditory nucleus– field L–in the canary.* The Journal of Comparative Neurology, 1979. **183**(3): p. 455-469.
99. Mello, C.V., et al., *Descending auditory pathways in the adult male zebra finch (Taeniopygia Guttata).* The Journal of Comparative Neurology, 1998. **395**(2): p. 137-160.
100. Doupe, A.J. and P.K. Kuhl, *BIRDSONG AND HUMAN SPEECH: Common Themes and Mechanisms.* Annual Review of Neuroscience, 1999. **22**(1): p. 567-631.
101. Marler, P. and S. Peters, *A Sensitive Period for Song Acquisition in the Song Sparrow, Melospiza melodia: A Case of Age-limited Learning.* Ethology, 1987. **76**(2): p. 89-100.
102. Feher, O., et al., *De novo establishment of wild-type song culture in the zebra finch.* Nature, 2009. **459**(7246): p. 564-568.

103. Morrison, R.G. and F. Nottebohm, *Role of a telencephalic nucleus in the delayed song learning of socially isolated zebra finches.* Journal of Neurobiology, 1993. **24**(8): p. 1045-1064.
104. Clayton, N.S., *Song Learning in Bengalese Finches: a Comparison with Zebra Finches.* Ethology, 1987. **76**(3): p. 247-255.
105. Marler, P. and M. Tamura, *Culturally Transmitted Patterns of Vocal Behavior in Sparrows.* Science, 1964. **146**(3650): p. 1483-1486.
106. Tchernichovski, O., et al., *Dynamics of the Vocal Imitation Process: How a Zebra Finch Learns Its Song.* Science, 2001. **291**(5513): p. 2564-2569.
107. Aronov, D., A.S. Andalman, and M.S. Fee, *A Specialized Forebrain Circuit for Vocal Babbling in the Juvenile Songbird.* Science, 2008. **320**(5876): p. 630-634.
108. Goldberg, J.H. and M.S. Fee, *Vocal babbling in songbirds requires the basal ganglia-recipient motor thalamus but not the basal ganglia.* Journal of Neurophysiology, 2011. **105**(6): p. 2729-2739.
109. Ölveczky, B.P., et al., *Changes in the neural control of a complex motor sequence during learning.* Journal of Neurophysiology, 2011. **106**(1): p. 386-397.
110. Ali, F., et al., *The basal ganglia is necessary for learning spectral, but not temporal features of birdsong.* Neuron, 2013. **80**(2): p. 494-506.
111. Aronov, D. and M.S. Fee, *Natural Changes in Brain Temperature Underlie Variations in Song Tempo during a Mating Behavior.* PLOS ONE, 2012. **7**(10): p. e47856.
112. Long, M.A. and M.S. Fee, *Using temperature to analyse temporal dynamics in the songbird motor pathway.* Nature, 2008. **456**(7219): p. 189-194.

Outline and scope of the thesis

Songbirds –especially zebra finches– can help us disentwine the complex brain-behaviour relationships as observed during socially-learned context-dependent vocal communication or the functional recovery of this behaviour after brain damage [1]. While ample functional imaging studies performed in adult zebra finches have been successful at exposing brain areas implicated in different aspects of song control and auditory processing of complex socially-relevant communication signals [2], surprisingly, *in vivo* imaging studies targeting structural tissue properties of the brain are completely lacking. Moreover, so far, no *in vivo* imaging studies have targeted the developing brain, when birds learn to sing. Therefore, **the aims of this PhD project** were to (1) implement an *in vivo* Magnetic Resonance-based Imaging (MRI) protocol that enables exploring the structural properties of the zebra finch brain, and use this protocol to establish a spatiotemporal map of structural neuroplastic changes (2) that characterise the different sub-phases of the critical period for vocal learning, and (3) that coincide with brain regeneration following neurotoxic lesioning of the striatal component of the song control circuitry. To reach these aims, we set out four objectives.

OBJECTIVE 1 - Literature review of MR-based imaging tools to study structural neuroplasticity *in vivo*.

The first four chapters of this thesis aim to provide a general framework supporting the hypotheses and objectives outlined below and the experimental data presented in Chapter 5, 6 and 7. Firstly, **Chapter 2** focusses on *in vivo* MRI as it has proven to be extremely valuable in the evaluation of functional, structural and biochemical properties of the living brain. This chapter emphasises on functional imaging techniques such as blood-oxygen-level-dependent (BOLD) fMRI, and structural imaging methods such as computational neuroanatomy including voxel-based morphometry, and diffusion tensor imaging (DTI), and only briefly introduces methods that rely on the administration of exogenous contrasts agents. Subsequently, **Chapter 3** explains how *in vivo* MRI has been applied successfully in the study of neuroplasticity in neuroscience research in general, in different species, and presents appropriate experimental designs and research strategies extremely relevant in the study of neuroplasticity. Furthermore,

it provides ample evidence how experience and activity, including skill training, are capable of shaping the brain not only in early life stages, but definitely also in adulthood and old age. Lastly, **Chapter 4** illustrates how several state-of-the-art MRI techniques have been employed successfully to study the functional and structural properties of the songbird brain. This chapter situates bird brain MRI at the Bio-Imaging lab from the early beginning up to the start of this thesis.

Inspired by the literature review covered in the first four chapters of this dissertation, we formulated objective 2, 3 and 4, that are described in Chapter 5, 6 and 7 respectively.

OBJECTIVE 2 - Optimise an *in vivo* DTI protocol that enables characterising the structural properties of the zebra finch brain.

Based on the literature reviews described in Chapter 3 and 4, we concluded that DTI is the most appropriate MRI technique to challenge our outstanding hypotheses. The optimised protocol should be robust enough to repeatedly obtain data in juvenile zebra finches as young as 20 dph (around fledging), when the critical period for vocal learning opens. Hence, the protocol needed to meet the following criteria: (1) sufficient spatial resolution, (2) sufficient angular resolution (i.e. ≥ 30 diffusion gradient directions are necessary for reliable estimation of the tensor [3], see. Chapter 2), and (3) reasonable acquisition time (i.e. < 2h). To test the sensitivity of the optimised protocol, we executed a proof-of-principle study aimed at detecting known structural sex differences in the adult zebra finch brain [4], using brain-wide data-driven voxel-wise statistical analyses. Furthermore, to clarify some of the observed sex differences identified by the *in vivo* proof-of-principle study, we implemented an *ex vivo* high-resolution DTI protocol that was processed to enable Super-Resolution Reconstruction Track Density Imaging (SRR TDI) and seed-based tractography in the zebra finch brain. These advanced DTI processing techniques mathematically estimate the spatial trajectory of fibre pathways in the brain. Given the modular instead of laminar organisation of the songbird brain, tractography methods were hypothesised to enable tracing fibre pathways connecting the different components of song control system. The results of the *in vivo* proof-of-principle study, *ex vivo* SRR TDI and tractography are outlined in **Chapter 5**.

OBJECTIVE 3 - Establish a spatio-temporal map of structural neuroplastic events occurring between 20 and 200 days post hatching.

As the *in vivo* DTI protocol proved to be sensitive enough to detect sex differences in adult zebra finch brains, we proceeded by using the same protocol to trace structural neuroplastic processes from young 'fledgling' to adult zebra finches. Furthermore, we refined a T_2-weighted 3D RARE MR pulse sequence which improved the anatomical contrast present in the 3D RARE images. This adaptation of the existing protocol enabled the implementation of automated morphometric analyses, including voxel-, tensor- or deformation-based morphometry (VBM, TBM or DBM; introduced in Chapter 2). Both methods rely on the analysis of spatial transformation parameters. The MR data processing pipelines for these methods are standardised for human [5-7] and, to some extent, rodent and primate MR images [8-11], but not for bird brain scans. Consequently, several challenges needed to be resolved, the most challenging being image segmentation. The full protocol is described in the methods section of **Chapter 6**. The resulting DBM data inform on localised relative volume changes in function of age, sex, treatment, performance, etc. By obtaining both DBM and DTI data, both macro- (volume) and micro-architectural tissue properties, respectively, could be characterised repeatedly in the same birds.

To explore potential changes in brain structure during and beyond the critical period for vocal learning, we designed a longitudinal study where we acquired DTI data and T_2-weighted 3-dimensional (3D) anatomical scans at several critical stages. More specifically, MRI data were obtained during the sensory phase (20 and 30 days post hatching (dph)), sensorimotor phase (40 and 65 dph), crystallisation phase (90 and 120 dph), and well past completion of song learning (200 dph). By comparing the structural properties of the brains of male and female birds, it is possible to distinguish between sensory- and sensorimotor-related aspects of vocal learning, as both male and female birds memorise the tutor song [12], but only males produce song. Furthermore, widespread effects that overlap between male and female birds are assumed to relate to general brain development that proceeds in parallel with vocal learning. Furthermore, by quantifying vocal output starting from the (advanced) sensorimotor phase, improvements in song performance could be measured and correlated with local volume changes or specific microstructural tissue properties. The latter comparisons might inform

whether vocal proficiency, e.g. quality and accuracy of tutor song copying, can be traced back to the neural substrate underlying singing, similar to training-induced neuroplasticity. The results are presented in **Chapter 6**.

OBJECTIVE 4 - Trace structural neuroplastic events evoked by neurotoxic lesioning of the striatal component of the song control circuitry in adult male zebra finches

Previous studies have describe extensive brain regeneration following neurotoxic lesioning of Area X that coincides with dramatic alterations in song performance, mainly affecting song tempo and, in some birds, marked stuttering-like behaviour [13]. To this end, we acquired DTI and T_2-weighted 3D scans before and at five time points, up to 4 months after neurotoxic lesioning of Area X. This enabled us to explore (1) whether targeted neurotoxic lesioning of one component of the song control system would affect the local volume and/or tissue micro-architectural properties of remote constituents of the same circuitry, and (2) whether relationships could be established between lesion-induced alterations to song performance and structural neuroplastic events. We hypothesised that structural neuroplastic events would mainly affect the local microarchitecture of immediate afferent and efferent brain regions, i.e. HVC, DLM and potentially LMAN, and would be less extensive than developmental plasticity traced in ontogeny (Chapter 6). Furthermore, we quantified alterations in song performance, reflected mainly in song tempo, and explored whether any change in song performance would correlate to alterations in local intrinsic tissue properties of the song control nuclei. The results are reported in **Chapter 7**.

Lastly, **Chapter 8** provides the general discussion and (potentially exciting) research questions that arose from the experimental data of this PhD project.

REFERENCES

1. Doupe, A.J. and P.K. Kuhl, *BIRDSONG AND HUMAN SPEECH: Common Themes and Mechanisms.* Annual Review of Neuroscience, 1999. **22**(1): p. 567-631.
2. Van Ruijssevelt, L., et al., *Current state-of-the-art of auditory functional MRI (fMRI) on zebra finches: Technique and scientific achievements.* Journal of Physiology-Paris, 2013. **107**(3): p. 156-169.
3. Jones, D.K., *The effect of gradient sampling schemes on measures derived from diffusion tensor MRI: A Monte Carlo study†.* Magnetic Resonance in Medicine, 2004. **51**(4): p. 807-815.
4. Nottebohm, F. and A. Arnold, *Sexual dimorphism in vocal control areas of the songbird brain.* Science, 1976. **194**(4261): p. 211-213.
5. Ashburner, J. and K.J. Friston, *Voxel-Based Morphometry—The Methods.* NeuroImage, 2000. **11**(6): p. 805-821.
6. Mechelli, A., et al., *Voxel-Based Morphometry of the Human Brain: Methods and Applications.* Current Medical Imaging Reviews, 2005: p. 105-113.
7. Ridgway, G.R., et al., *Ten simple rules for reporting voxel-based morphometry studies.* NeuroImage, 2008. **40**(4): p. 1429-1435.
8. Sawiak, S.J., J.-L. Picq, and M. Dhenain, *Voxel-based morphometry analyses of in-vivo MRI in the aging mouse lemur primate.* Frontiers in Aging Neuroscience, 2014. **6**.
9. Sawiak, S.J., et al., *Voxel-based morphometry with templates and validation in a mouse model of Huntington's disease.* Magnetic Resonance Imaging, 2013. **31**(9): p. 1522-1531.
10. Suzuki, H., et al., *Voxel-based morphometry and histological analysis for evaluating hippocampal damage in a rat model of cardiopulmonary resuscitation.* NeuroImage, 2013. **77**: p. 215-221.
11. Lau, J.C., et al., *Longitudinal neuroanatomical changes determined by deformation-based morphometry in a mouse model of Alzheimer's disease.* NeuroImage, 2008. **42**(1): p. 19-27.
12. Riebel, K., et al., *Sexual equality in zebra finch song preference: evidence for a dissociation between song recognition and production learning.* Proceedings of the Royal Society of London. Series B: Biological Sciences, 2002. **269**(1492): p. 729-733.
13. Kubikova, L., et al., *Basal ganglia function, stuttering, sequencing, and repair in adult songbirds.* Scientific Reports, 2014. **4**: p. 6590.

Chapter 2

The biological versatility of *in vivo* Magnetic Resonance Imaging

This chapter is based on the second part of a book chapter published as:

Hamaide J., Van Ruijssevelt L., Kara F., De Groof G., Van der Linden A. Exploring Plasticity and Cognitive Networks by in vivo MRI. Situated in 'Part VI: Special applications: chapter 31: Imaging in Neurology Research II' of the book Small Animal Imaging: Basic and Practical Guide; edited by Kiessling F., Pichler B., Hauff P. doi: 10.1007/978-3-319-42202-2.

2.1 INTRODUCTION

MRI is a commonly used (pre)clinical imaging modality to visualize soft tissues such as the brain. It is based on the principles of nuclear magnetic resonance, a spectroscopic technique to infer physical and chemical information of molecules. MRI relies on the detection of relaxation properties of the magnetic momentum (spin) of nuclei (most often hydrogen protons) after experiencing radio-frequency (RF) excitation (ordered in RF pulse sequences) when placed in an external magnetic field, i.e. MR scanner. Based on the relaxation signals captured by receiver coils, images or spectra –depending on the MR sequence– can be created. A variety of MRI pulse sequences with specific combinations of RF pulses and magnetic field gradients exist which exploit different characteristics hydrogen nuclei (protons) of water molecules in tissue. The most conventional and widely used MRI contrasts are found in T_1-, T_2-, T_2^*- and proton density (PD) weighted images. The resulting data sets provide superior anatomical contrast allowing a qualitative assessment of overall brain anatomy easily distinguishing grey and white matter. Slight adaptation of the basic T_1- and T_2-weighted MRI pulse sequences enables a quantitative evaluation of tissue properties reflecting tissue density, myelination etc. [3]. Besides anatomical assessment, specialized MRI techniques entail information on blood flow (Arterial Spin Labelling, Dynamic Susceptibility Contrast), vasculature (angiograms), diffusion properties (Diffusion-weighted Imaging, Diffusion Tensor Imaging, Diffusion Kurtosis Imaging), functional activation (Functional MRI, Resting State Functional MRI, Pharmacological MRI) and even the metabolic profile of tissues (Magnetic Resonance Spectroscopy, Chemical Exchange Saturation Transfer). Most of these imaging contrasts do not require the administration of exogenous contrast agents as opposed to, e.g. PET (radioactive tracers) and do not rely on hazardous ionizing radiation, e.g. CT, making MRI a truly non-invasive and safe imaging tool.

Most MR images present a field-of-view (FOV) that occupies the entire brain and includes high-resolution 3-dimensional information which can be viewed and virtually sliced along any possible plane. The non-invasive nature of this method allows performing dynamic longitudinal studies where functional, structural and metabolic brain changes can be followed up *in vivo* over time or upon treatment where each animal serves as its own reference. This essential feature makes MRI an exceptional tool to observe neuroplastic adaptations both acutely and in more extended time frames and to establish links between the observed MRI findings and behavioural data from the same animal. The spatial and temporal image resolution is

determined by the MRI modality of choice, the corresponding imaging pulse sequence, signal-to-noise ratio, acquisition time, and the available hardware. Temporal resolution primarily affects functional imaging modalities. Despite many efforts to speed up acquisition by, e.g. echo planar imaging (EPI) pulse sequences, multiband acquisition and parallel imaging, fMRI still relies on the detection of the intrinsic metabolic and hemodynamic response of neural tissue to a given stimulus which is markedly slower than the actual neural activity experienced by neurons, i.e. the hemodynamic response situated in the order of seconds, whereas neuronal activity goes well beyond this frequency [12, 13]. Besides its relatively low temporal resolution, fMRI provides an excellent 3-dimensional spatial resolution (0.2-1.0 mm for preclinical, small animal MR imaging) covering the entire brain and excluding the need for an *a priori* selection of brain regions involved. This strongly contrasts with other functional imaging techniques such as EEG, MEG, and NIRS, which in turn benefit from a substantially higher temporal resolution (sampling frequency: ms). In theory, the physical limitation of MR image voxel size is situated around 10 µm [9]. In practice however, achieving a reasonable signal-to-noise ratio coming from a (isotropic) resolution of 10-150 µm requires a large number of averages which results in a long acquisition time, merely confining such spatial precision to ex vivo experiments. On average, in vivo MRI experiments take up to 1-3h and are characterized by a spatial resolution of 100-200 µm (in plane).

A detailed description of physical and mathematical principles underlying MRI and the different MR contrasts, however, is far beyond the scope of this thesis. In general, this chapter focusses on the biological versatility of MRI techniques including most of the MR-based imaging tools used in neuroplasticity research (Chapter 3 and 4), therefore, more MR-based methods than those that have been actively used in the experimental work presented in this thesis are described in this chapter. More specifically, the following paragraphs will (1) start with a brief introduction, explaining the origin of the obtained tissue contrast in combination with its major advantages and disadvantages, and will (2) provide references to papers or reviews concerned with practical details on how to optimize experimental protocols –from animal procedures to MRI pulse sequences– and how to analyse and interpret the data.

2.2 FUNCTIONAL MRI

Since its introduction over 20 years ago [19, 20], functional magnetic resonance imaging (fMRI) has become one of the most popular techniques in the field of cognitive neurosciences for studying the localization, pattern and time course of brain activity in (pre)clinical and fundamental research (for reviews on the technique: [8, 21, 22]). To infer brain activity, fMRI measures activity driven changes in local cerebral blood flow (CBF), blood volume (CBV) and cerebral metabolic rate of oxygen ($CMRO_2$) consumption. This makes fMRI an indirect indicator of neuronal activity assessing what is commonly referred to as the hemodynamic response function (HRF). The complex interplay between CBF, CBV and $CMRO_2$ comprised in the HRF can be measured using Blood Oxygenation Level Dependent (BOLD) fMRI. BOLD is by far the most popular contrast used for fMRI and is based on the paramagnetic properties of deoxygenated haemoglobin. Figure 2-1 illustrates how neural activation can give rise to altered BOLD signals in fMRI (for review: [23-25]). In order to accurately sample the hemodynamic response to a specific task, MRI pulse sequences with a sufficient temporal resolution are required. Over recent years, numerous variations to the well-established EPI and gradient- and spin echo (GRASE) pulse sequences have been developed realizing a repetition time up to 0.5 s (for review of recently implemented fast and high-resolution fMRI sequences: [27]).

Besides the BOLD contrast, it is possible to specifically detect brain activity based on changes in CBF or CBV. For CBV-weighted fMRI, an exogenous intravascular contrast agent is administered to increase the sensitivity of the functional imaging protocol (for review: [28, 29]). Using Arterial Spin Labelling (ASL), a method in which blood protons in the brain feeding arteries are magnetically tagged to serve as endogenous tracer to measure brain perfusion, activity induced changes in CBF can be measured directly [30]. One can use fMRI to study neuronal activity in response to a certain task (activity induced fMRI), during rest (resting state fMRI, rsfMRI) or in response to acute drug challenges (pharmacological MRI, phMRI).

2.2.1 Activity-induced fMRI

The primary and most exploited use of fMRI is the inference of neural activity in response to a certain sensorimotor or cognitive task. Along with the choice of the right stimulus associated with the hypothesis, the way these stimuli are presented to the subject should be judiciously determined. The most commonly used stimulus presentation designs for fMRI experiments are

(i) a block design and (ii) an event-related design (for review on fMRI study designs: [11]). Most small animal fMRI studies are performed while animals are anesthetized.

This creates difficulties as anaesthetics often affect vasculature and/or neuronal signalling to different extents [31]. Therefore, depending on the animal model, the type of stimulus and the expected effect, different anaesthetics might be preferred [32-35]. In case of phMRI, when the stimulation paradigm is combined with or consists of a pharmacological challenge, not only the effect of the anaesthetic on the neuro-vascular coupling should be evaluated but also the impact of the anaesthesia on the targeted neurotransmitter system as well as the possible interactions between the anaesthetic and the drug of interest. Although the use of anaesthesia seems necessary to reduce motion and stress, efforts are being made to train animals including rats [36, 37], mice [38, 39] and even birds [40], to be scanned awake and to design adapted restraining setups [41]. The possibility of using awake animals in fMRI experiments extends the type of questions that can be addressed, but as the training is very time consuming, its implementation is not feasible for all fMRI studies. Finally, instabilities in physiological parameters can greatly influence the HRF [42-44]. During the experiment one should therefore strive to maximal physiological stability or at least allow to account for instabilities within the data analysis steps by monitoring parameters such as body temperature, breathing rate etc. closely while scanning.

To date, no consensus has been reached on the method of choice for fMRI data processing to extract activated brain regions from the fMRI time series. Typically, a voxel-based approach is opted. *Prior* to the voxel-based statistical modelling, some basic procedures are performed including (1) slice timing correction and realignment, (2) co-registration of functional and structural images and normalization to a standardized stereotactic space, and (3) smoothing. A clear overview of these processing steps can be found in, e.g. [11, 45, 46]. After pre-processing, the applied stimulation design (e.g. block design: box-car function) is convolved with a function which best describes how the BOLD signal evolves (e.g. HRF) in order to have a better estimation of the true design-related BOLD signal [47]. Finally, statistics can be performed via parametric or non-parametric methods resulting in statistical maps indicating areas of activation surviving a *pre*-set statistical threshold. These maps are first created on single subject level (first level analysis) after which they are used in second level analysis to perform group statistics. Besides maps indicating activated regions, alternative processing techniques are available, e.g. dynamic

causal modelling (DCM) which models interactions between activated regions to infer effective connectivity [48].

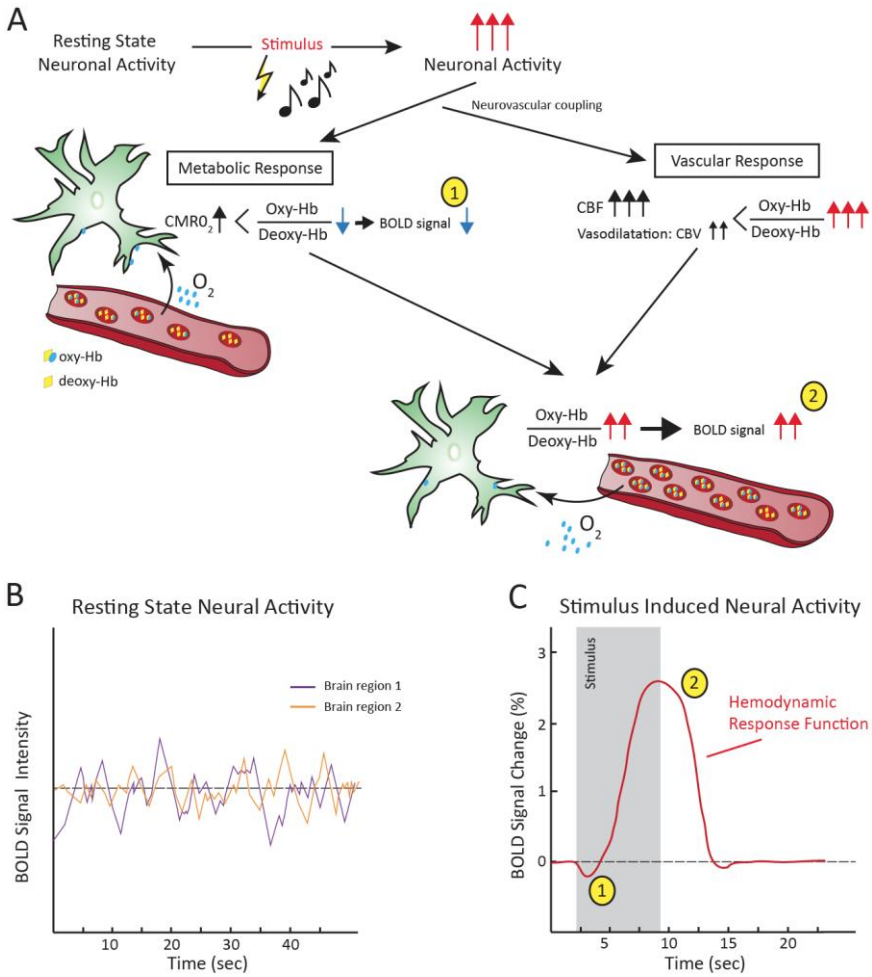

Figure 2-1: Schematic overview of the principle of BOLD fMRI. (**A**) When the brain is stimulated, local neural activity gives rise to a cascade of events which result in local changes in oxygen consumption and blood flow. This translation from neural to vascular signals is termed the 'neurovascular coupling'. First, the increased local metabolic activity (including cerebral metabolic rate of O_2 ($CMRO_2$) consumption) results in a decrease in the ratio between oxygenated (oxy-Hb) to deoxygenated hemoglobin (deoxy-Hb) in the blood. The paramagnetic properties of deoxy-Hb will induce an initial small dip in the BOLD signal reflected in changing T2(*) contrast (number 1 in panel A and C). Second, the initial, activity-induced oxygen consumption will be compensated by a massive increase in local blood flow (CBF) and vasodilatation resulting in an increased cerebral blood volume (CBV). The net increase in oxy-Hb/deoxy-Hb ratio will overcompensate the metabolic O_2 demand resulting in a large peak in the BOLD signal (number 2 in panel A and C). (**B**) Small fluctuations in the BOLD response are present when no stimulus is given. The time course of the BOLD signal measured in resting state fMRI (rsfMRI) experiments can be extracted from different brain regions and is used to study functional connectivity. (**C**) A typical time course of stimulus-induced BOLD signal changes. The percentage signal change compared to the rest condition is indicated. When temporal resolution allows it, the first small dip at the initiation of the stimulation followed by a peak in the BOLD signal can be picked up. The shape of the response follows the theoretical model of the hemodynamic response function.

2.2.2 Resting state fMRI

Brain activity continues even beyond participation to explicit tasks, as a result, activity-independent or spontaneous fluctuations of the BOLD signal can also be observed when the subject is at rest. Since brain regions with comparable fluctuation patterns are thought to be functionally connected [49], these spontaneous low frequency fluctuations of the BOLD signal (LFFs; typically ranging from 0.01-0.10 Hz) are used to investigate the functional architecture of the brain. Dedicated resting state fMRI sequences –most often gradient echo EPI– benefit from a higher temporal resolution and shorter scan times as compared to stimulus-induced fMRI. In recent years, rsfMRI has become a sensitive marker to study changes in brain circuitry beyond direct structural connections that are usually evaluated with anatomical techniques. For a more rigorous and detailed explanation of this method, we wish to refer to the many excellent text books and review articles available, e.g. [50, 51].

When performed in small animals, the subjects are usually anesthetized during acquisition with varying effects of the used compound on functional connectivity [34, 38, 52]. Therefore, similar to stimulus-induced fMRI, caution should be taken when choosing the type of anaesthetic for a particular study. Alternatively, the technique can also be performed in awake animals after habituation training [38, 53].

Pre-processing of resting state fMRI time series may include motion correction, slice timing correction, global signal regression, spatial normalisation, temporal filtering, and spatial smoothing. The benefit of using these pre-processing steps remains, however, a controversial topic [54-56]. For the post-processing of rsfMRI data, various software packages exist that support different processing strategies [26, 50]. The most widely used methods in the analysis of resting state data to infer functional connectivity are ROI-based [57], seed-based analyses and model-free, data-driven approaches such as independent component analysis (ICA) [58, 59] and graph-theory analysis (for methodological reviews: [26, 50]). Over the last years, graph analysis has gained substantial interest as rsfMRI data analysis approach (especially in combination with MRI contrasts sensitive to structural connectivity such as Diffusion Tensor Imaging [60]).

Functional connectivity assessed using rsfMRI is believed to reflect the basic and intrinsic organization of the resting brain. In humans and to some extend also in rodents, large scale ‘resting state networks’ can be detected including brain regions involved in, e.g. auditory

processing, motor function, visual processing, memory, executive functioning [61, 62] and the so-called default mode network which is active during rest and deactivated during goal-directed behaviour [63, 64]. These large-scale networks can be further divided in sub-regions reflecting network topology. By examining alterations in functional connectivity within or between these networks, rsfMRI is a powerful tool to study aspects of plasticity involving cortical reorganization, global network rearrangements and changes in region-to-region functional connectivity. As such, rsfMRI has emerged as a useful tool to study large-scale brain network maturation in infants and young children [65].

Reviews on fMRI techniques:

- *[2] Logothetis, N.K., What we can do and what we cannot do with fMRI. Nature, 2008. 453(7197): p. 869-78.*
- *[8] Di Salle, F., et al., Exploring brain function with magnetic resonance imaging. Eur J Radiol, 1999. 30(2): p. 84-94.*
- *[11] Amaro, E., Jr. and G.J. Barker, Study design in fMRI: basic principles. Brain Cogn, 2006. 60(3): p. 220-32.*
- *[15] Van der Linden, A., et al., MRI in small brains displaying extensive plasticity. Trends Neurosci, 2009. 32(5): p. 257-66.*
- *[18] van den Heuvel, M.P. and H.E. Hulshoff Pol, Exploring the brain network: a review on resting-state fMRI functional connectivity. Eur Neuropsychopharmacol, 2010. 20(8): p. 519-34.*
- *[26] Margulies, D.S., et al., Resting developments: a review of fMRI post-processing methodologies for spontaneous brain activity. MAGMA, 2010. 23(5-6): p. 289-307.*

2.3 STRUCTURAL MRI

The following paragraphs will discuss different MRI contrasts designed to evaluate brain volume and shape, intrinsic tissue properties and microarchitecture and overall structural connectivity.

2.3.1 Quantitative anatomy

2.3.1.1 Volumetry and morphometry

Conventional T_1-, T_2- and proton density weighted images provide qualitative information on overall (brain) anatomy, realizing a clear structural segmentation between grey and white matter and facilitating the localization of abnormalities, e.g. tumours or traumata. In case of sufficient image resolution, volumetric and morphometric analyses can be performed by very simple delineation of brain ROIs. In addition to manual delineation, several automated segmentation procedures exist which are perfectly suited for volumetric and morphometric analyses [66, 67]. The latter refers to voxel-based morphometry (VBM) which infers group

differences in grey and white matter concentration after discounting for individual differences in overall anatomy and position [68, 69]. A subset of different pre-processing steps needs to be fulfilled before a statistical map indicating structural differences is obtained (a clear overview of the different pre-processing steps can be found in [69, 70]). VBM is the most extensively used method for automated volumetry in human research, however, other similar procedures exist that use related measures and are not necessarily dependent on brain segmentation techniques to infer relative position or local volume differences within the brain, i.e. tensor- and deformation-based morphometry (respectively TBM and DBM). Even though VBM, DMB and TBM are closely related, the methods use different parameters extracted from the spatial normalisation procedure to infer local volume or shape differences [71, 72].

The success of automated morphometric analyses relies on the quality of the spatial normalisation procedure, i.e. how well distinct datasets can be transformed to spatially match with a reference image. The result of the spatial normalisation procedure is a normalised image, meaning that every voxel in image A corresponds to exactly the same anatomical structure in every other image of the study. The 'coordinate system' that is to be warped to the reference image is called the 'native space' and the reference image is defined by the 'template space'. The latter can be an (*ex vivo* acquired) high-resolution atlas, or a population-based template which is a mathematical 'average brain' calculated based on all datasets acquired in the study. The spatial transformation or 'normalisation' can be divided into linear (translation, rotation, scaling, shearing) and non-linear combinations. To obtain an accurate spatial registration of MRI data within one subject or patient (within-subject), one can achieve a good overlap with a linear transformation, while optimal voxel-wise correspondence of brain scans originating from different subjects (between-subject) requires non-linear normalisation procedures. Recent attempts at optimising between-subject image registration algorithms have resulted in refined image processing pipelines to detect localised (relative) volume changes in longitudinal MR image data, i.e. including repeated-measures [73]. This set of algorithms is combined in a publicly available software tool named 'serial longitudinal registration' (SLR) and is used in Chapter 6 and 7 of this dissertation.

One should bear in mind that when studying developing or injured brains, the overall brain architecture and intrinsic tissue properties undergo massive changes either due to maturation or recovery which directly affect T_1- and T_2-relaxation properties [74, 75]. Changing T_1- and T_2-

properties implies that the ideal pulse sequence settings e.g. repetition time (TR) and echo time (TE), evolve over ontogeny, which indicates that if a constant combination of TR and TE is applied over the entire development, this might lead to suboptimal image contrast thus interfering with accurate delineation of brain ROIs. Moreover, certain neuroplastic events might involve very subtle alterations in volume or shape that can easily be missed when merely considering volumes or shapes of tissue. Interestingly, since the longitudinal and transverse relaxation rates are intricately linked to tissue microstructure and biochemistry, quantitative analysis of the T_1- and T_2- relaxation times provides a wealth of information on neuroplastic changes associated with brain maturation, disease etc.

2.3.1.2 Quantitative relaxometry

Slight adaptation of specific parameters in basic T_1–weighted inversion recovery and T_2 –weighted spin echo pulse sequences allows quantitative assessment of T_1- and T_2-relaxation times which are intrinsically linked to ultrastructural tissue characteristics in terms of local tissue density, concentration of paramagnetic atoms, protein and lipid constitution and abundance of macromolecules [3]. Quantitative T_1- and T_2-mapping is often referred to as 'quantitative relaxometry' and is commonly used to follow up early brain development and aging as well as disease-related tissue alterations involving myelination-demyelination, inflammation-oedema, necrosis, iron accumulation, axonal growth, gyrification etc. (for methodological review: [3]).

In order to determine the T_1- or T_2-relaxation time of a specific brain region of interest, the same dataset needs to be acquired several times where each acquisition is performed with a different inversion time (TI) or TE, respectively. Then, for each voxel, the signal intensities are fitted to the inversion times (TI) or echo times (TE) with the proper exponential function. The resulting parameter estimates of T_1 or T_2 are then compiled in a T_1 or T_2 map where each voxel encodes the actual (absolute) relaxation time (T_1 or T_2). A more elaborate discussion of the acquisition and processing of T_1- and T_2-maps can be found in [76-79]. Besides the advantage of assessing quantitative parameters which directly relate to specific tissue characteristics, relaxometry is independent of the MR system or hardware used (but depending on the MR scanner magnet field strength), enabling to compare results obtained in different institutions.

Similar to the volumetric and morphometric analyses mentioned above, regions-of-interest can be delineated on the estimated T_1- and T_2-maps after which the mean quantitative indices (T_1-

or T_2-relaxation time) can be extracted and statistically analysed. In addition, also voxel-based approached have been introduced in this field [80]. Instead of using the actual transformation parameters, e.g. the deformation fields, the voxel intensities of spatially normalised datasets provide the necessary input for statistics. In other words, after successful spatial normalization, macroscopic shape and volume differences are discounted leaving only differences in voxel intensity –relaxation time– to be tested.

Several research groups have used quantitative relaxometry to follow up developmental brain changes in ontogeny in both healthy subjects and mice [75, 81, 82]. Kharatishvili and colleagues revealed that T_2-relaxation alterations could be linked to acute and long-term neurodegenerative changes resulting from epileptic seizures evoked by pilocarpine treatment [83] or traumatic brain injury (TBI) [84]. Myelination characteristic to brain maturation during ontogeny is regarded as one of the major critical period delineators since it structurally inhibits neuroplasticity. Besides T_2-relaxometry, several other methods exist which extend information on different aspects of myelin content and organization within the brain. Recently, multicomponent relaxometry has been introduced [85]. This method is used to determine the myelin water fraction or the water trapped in between myelin sheets as an indirect measure of myelin content [86]. For a technical review on water-based myelin imaging tools we refer to [87]. Besides relaxometry, alternative methods are available to monitor white matter changes, e.g. Magnetisation Transfer Imaging (MTC) and Diffusion Tensor Imaging (DTI).

Review on quantitative relaxometry techniques:

- *[3] Deoni, S.C.L., Quantitative Relaxometry of the Brain. Topics in Magnetic Resonance Imaging, 2010. 21(2): p. 101-113 10.1097/RMR.0b013e31821e56d8.*

2.3.1.3 Diffusion Tensor Imaging

Diffusion Tensor Imaging (DTI) was introduced in the 1990s [88]. As compared to conventional MRI, DTI provides a non-invasive means for characterizing tissue microstructure and macroscopic fibre orientation in, e.g. muscle [89] and nervous tissue [90], by measuring the random molecular Brownian motion (diffusion) of water molecules. Quantification of diffusion in tissues is achieved by supplementing a standard spin echo pulse sequence with bipolar diffusion encoding gradients [91]. Spin dephasing due to the translational motion of water molecules along the direction of the bipolar diffusion gradient results in a diffusion-dependent

signal loss. This forms the basis of quantifying the diffusion properties of tissue (detailed description in [9]).

By characterizing the overall 3-dimensional diffusion profile of water molecules within a voxel, inferences can be made concerning the tissue microarchitecture situated within that voxel. For example, cerebrospinal fluid imposes few hindrances to the movement of water molecules resulting in a direction-independent or *isotropic* diffusion profile. In contrast, white matter contains myelinated axons and cell membranes which force water molecules to move along fibres as compared to travelling perpendicular to them, this is referred to as an *anisotropic* diffusion profile [92]. Furthermore, grey matter presents many randomly oriented barriers which result in relatively isotropic but overall rather limited water diffusion. Then the question remains how to 'measure' the 3-dimensional diffusion profile.

The simplest diffusion-weighting experiment consists out of two acquisitions: firstly, a regular dataset without diffusion-weighting and secondly the same dataset with application of a diffusion gradient. This way an Apparent Diffusion Coefficient (ADC) map can be calculated where the intensity of each voxel is proportional to the extent of diffusion. ADC-maps are a valuable tool in the clinic to detect brain areas affected by, e.g. acute stroke [93]. The combination of the strength, duration and shape of the applied diffusion gradient defines the diffusion weighting and is represented by the 'b-value' (expressed in s/mm²). ADC-maps, however, only inform about the overall diffusion in a given voxel without deriving any information on the specific character of interactions between tissue and water molecules or on the 3-dimensional spatial diffusion profile. Moreover, the ADC contrast and thus diffusion measurement *per se* is highly dependent on the direction of the applied diffusion gradient: only water motion along the applied diffusion gradient axis can be detected. This observation led to the notion that the 3-dimensional diffusion profile of water molecules within one voxel can be estimated when at least six independent measurements are performed each applying a diffusion gradient along a different non-collinear direction [88]. This is exactly what is aimed for in DTI (for detailed information: [1, 5]).

Starting from the raw diffusion weighted data, the spatial diffusion profile of hydrogen protons in tissues is characterised by the (3x3) diffusion tensor of which several quantitative, rotationally invariant, indices can be extracted which inform on the estimated overall spatial diffusion profile of water molecules within one voxel. These include the three diffusion tensor

eigenvalues (λ_1, λ_2, λ_3) and derived metrics: mean diffusivity (MD), radial diffusivity (RD), axial diffusivity (AD) and fractional anisotropy (FA; for detailed overview of DTI (pre)processing pipeline: [14]). FA does not have a unit and is a continuous number ranging from 0 (perfectly isotropic diffusion e.g. CSF), to 1 (highly anisotropic diffusion). Figure 2-2 visualises the relationship between the brain structure and the eigenvalues. The DTI metrics are obtained via the following formula.

$$MD = \frac{\lambda_1 + \lambda_2 + \lambda_3}{3}$$

$$RD = \frac{\lambda_2 + \lambda_3}{2}$$

$$AD = \lambda_1$$

$$FA = \frac{\sqrt{3\,[(\lambda_1 - \lambda_2)^2 + (\lambda_2 - \lambda_3)^2 + (\lambda_3 - \lambda_1)^2]}}{\sqrt{2(\lambda_1^2 + \lambda_2^2 + \lambda_3^2)}}$$

In general, a diffusion gradient sampling scheme including at least 30 unique and evenly distributed diffusion gradient orientations is needed to robustly estimate FA, MD and the tensor orientation represented by the eigenvectors [94]. Again several basic processing techniques can be applied, i.e. histogram analysis, extraction of DTI parameters from manual or automatic delineation of ROIs or comparing DTI-parameter maps between groups on a voxel-wise level (for technical comparison between two most often used voxel-based DTI processing tools: [17]). The latter two techniques, ROI and voxel-based analyses, are in line with the previously described principles. Histogram distributional analysis on the other hand informs on global diffusion alterations enabling to detect subtle changes that affect the entire brain (after removal of CSF signal). An elaborate discussion on the different processing strategies in a group-versus-group study design can be found in Chapter 29 of [1]. In addition to these basic processing techniques also more advanced processing methods exist, e.g. tractography which aims at presenting a statistical visualisation of all white matter fibres [95]. Based on tractography, graph theory-based connectivity maps can be computed which describe different brain networks that reflect structural connectivity (especially interesting when performed together with functional MRI [96]). For these more advanced applications such as fibre tractography, it is recommended to acquire as many diffusion gradient directions (high angular resolution) as possible within the experimental time frame [94, 97]. The estimation of more

complex spatial diffusion profiles –in contrast to the DTI model which assumes that diffusion follows a Gaussian distribution– can be realized by alternative methods, e.g. HARDI (high-angular resolution diffusion imaging [98]), Q-ball imaging [99] etc. the latter method is expected to resolve subvoxel geometries such as multiple intra-voxel fibre orientations such as crossing, bending, twisting or fanning fibres.

A low signal-to-noise ratio (SNR) –due to diffusion weighting– and a long acquisition time are inherent to DTI. The first can be overcome by increasing the number of diffusion gradient directions within a given experiment, which then again results in a longer acquisition time. SNR should be closely evaluated since low SNR can cause underestimation of the diffusion anisotropy of the effective diffusion tensor [100]. Similar to quantitative relaxometry, DTI is highly sensitive, but unfortunately notoriously unspecific to a wide range of biological phenomena making the biological interpretation of the obtained results less straightforward [9, 101], especially since different microscopic tissue properties might result in a similar parameter readout. Consequently, in order to establish a profound knowledge of the underlying neuroplastic events additional measures need to be undertaken.

DTI has been thoroughly explored in the field of small animal MRI. Concha (2013) provides an extensive overview of how diffusion-MRI data can inform on biological tissue remodelling and white matter pathologies both in clinical and research environments [16]. Ample evidence of structural remodelling in response to motor and spatial maze learning has been published as well [102-105] and will be discussed in Chapter 3. Disregarding the often long acquisition times needed for acquiring high-resolution DTI datasets, several groups report on using *in vivo* DTI to study early ontogeny.

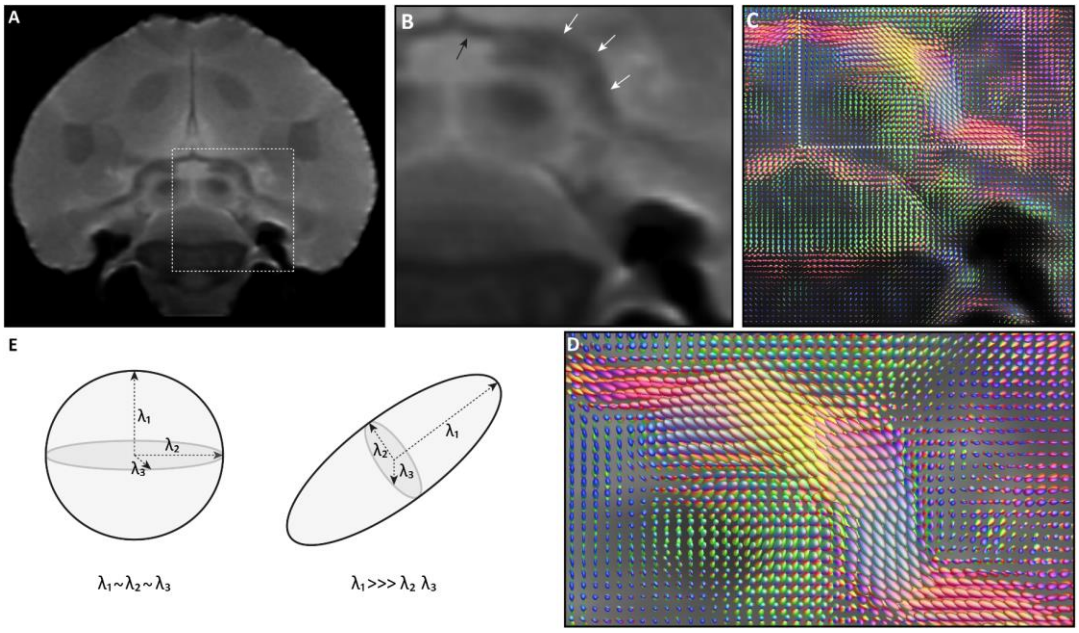

Figure 2-2: Relationship between brain anatomy and estimated diffusion profile. Panel A and B present a horizontal T_2-weighted slice of an adult male zebra finch brain, B is an enlargement of the inset in A. The arrows in B point to highly myelinated white matter structures (black arrow points to the anterior commissure, the white arrows to the occipitomesencephalic tract). Panel C, D and E present the spatial shape of the estimated diffusion profile for each voxel of the brain. Panel C covers the same anatomical area as B, while D zooms in on the inset delineated in C, focusing on the anterior commissure and occipitomesencephalic tract. Note that both fibre structures are clearly visible in D by the elongated ellipsoid diffusion shapes indicative of a highly anisotropic underlying microstructure. Panel E illustrates the link between the shape of the estimated diffusion profile and the eigenvalues (λ_1, λ_2 and λ_3). The ellipsoid (right) presents a highly anisotropic diffusion profile while the ball-shape illustrates an almost perfect isotropic diffusion profile. The figure is based on experimental data presented in Chapter 5 (*ex vivo* super-resolution reconstruction DTI data which have been processed for brain-wide tractography; spatial resolution of the reconstruction: (40x40x40)μm^3).

Reviews on DTI:

- *[1] Jones, D.K., Diffusion MRI: Theory, Methods, and Applications. 2010: Oxford University Press, USA.*
- *[6] Jones, D.K., T.R. Knösche, and R. Turner, White matter integrity, fiber count, and other fallacies: The do's and don'ts of diffusion MRI. NeuroImage, (2013).*
- *[9] Mori, S. and J. Zhang, Principles of Diffusion Tensor Imaging and Its Applications to Basic Neuroscience Research. Neuron, 2006. 51(5): p. 527-539.*
- *[17] Abe, O., et al., Voxel-based analysis of the diffusion tensor. Neuroradiology, 2010. 52(8): p. 699-710.*

2.4 CONTRAST-ENHANCED MRI

The intrinsic MR contrast attributable to differences in relaxation properties of water molecules in the tissues is not always sufficient to accurately differentiate brain architecture, moreover the MR signal is not always sensitive enough to pick up specific biological phenomena including activity-dependent neural connectivity, neurogenesis and cell migration. This highlights the need for exogenous specific contrast-enhancing agents.

In general two main groups of MR contrast agents can be distinguished based on contrast mechanisms on which they have a dominant effect. The first group of compounds directly reduce the T_1 relaxation of the tissue where they accumulate, resulting in hyper-intense (bright) signal on T_1-weighted images (positive MRI contrast, e.g. gadolinium or manganese). The latter contrast agents induce local magnetic field inhomogeneities which actively shorten T_2/T_2* relaxation time of protons in close vicinity of the administered contrast agent. This results in faster signal decay visible as a hypo-intense (dark) signal on conventional images (negative MRI contrast, e.g. iron oxide particles). The following sections will discuss specific applications of manganese-enhanced MRI (MEMRI) in detail. Even though very interesting, iron oxide particles fall beyond the scope of this thesis and will not be elaborated on.

2.4.1 MEMRI

Pautler and colleagues (1998) were the first to successfully visualize murine olfactory and visual pathways by using *in vivo* manganese-enhanced MRI (MEMRI) [106]. Manganese (Mn^{2+}) is an essential trace metal element [107] vital for controlling a number of different cellular reactions [108]. In the brain, it primarily functions as a cofactor for various enzymes [109]. Consequently, Mn^{2+} deficiency or toxicity can lead to various pathological phenotypes [107, 110, 111]. Interestingly, besides its many biological functions, Mn^{2+} also acts as a Ca^{2+} analogue. As a result, Mn^{2+} can be transported across the blood brain barrier (BBB), into excitable cells such as neurons and cardiac cells, upon activation of several types of Ca^{2+} channels [112, 113]. In addition to these passive and active transporters, Mn^{2+} is also able to enter the CNS through leaky vasculature at the circumventricular organs and the choroid plexus [114], and via the olfactory and retinal receptor neurons as well [115, 116]. Once inside glia cells and neurons, Mn^{2+} can follow axons by anterograde microtubule-dependent transport [117] and is it is able to cross synapses to neighbouring neurons [118].

Another remarkable physical feature of Mn^{2+} is that it is paramagnetic. Consequently, Mn^{2+} evokes positive contrast on T_1-weighted images by markedly reducing the T_1-relaxation of water molecules in the adjacent tissue (where it accumulates). The combination of both physical and biochemical properties makes Mn^{2+} an exceptionally suited MRI contrast agent (1) to study brain anatomy using the tissue-specific distribution of Mn^{2+} (similar to other contrast agents such as gadolinium), (2) to highlight brain regions activated upon certain task (activity-induced MEMRI or AIM-MRI) and (3) to assess neuronal connectivity (tract tracing [106]). The latter two characteristics rely on an activity-dependent accumulation of Mn^{2+} in cells (through voltage-gated Ca^{2+} channels). This implies that the signal intensity is a direct readout for neural activity, as opposed to fMRI which is an indirect measure for brain activation since it relies on the detection of the hemodynamic response of the brains' vasculature to a given stimulus. In addition, Mn^{2+} ($MnCl_2$) can be administered peripherally after which the animal is exposed to a certain stimulus during wakefulness, without the need for anaesthesia in contrast to most small-animal BOLD fMRI [119]. The disadvantage of AIM-MRI as compared to fMRI is that Mn^{2+} does not easily cross the BBB in non-physiological concentrations. Therefore it is often administered in combination with a BBB disrupting chemical such as mannitol. Interestingly, alternative routes of administration have been described when the auditory, visual, somatosensory and olfactory systems were topic of investigation [106, 119, 120]. The second main disadvantage of AIM-MEMRI is that only one stimulus can be assessed per imaging experiment. This is in contrast to fMRI where several different stimuli can be presented within the same imaging session. In addition, before applying a second stimulus the brain needs to be cleared from the previously applied Mn^{2+}, which entails that the second measurement cannot take place earlier than one week after the first.

Anatomical MEMRI has been used to visualize brain regions which otherwise appear indiscernible from their surrounding tissue, e.g. distinct cortical layers in rats and mice [121] and individual glomeruli in the olfactory bulb of rats [122]. Anatomical MEMRI has also been applied to visualize tissue remodelling at the cellular level acutely post status epilepticus in a rat model for temporal lobe epilepsy, where the difference in Mn^{2+}-signal in the dentate gyrus and CA3 subfield of the hippocampus corresponded to sites displaying mossy fiber sprouting, confirmed by *post mortem* histology [123]. The obtained anatomical contrast can also be used for volumetric assessments e. g. [124].

Interestingly, because of the ability of Mn^{2+} to travel transsynaptically to neighbouring neurons, Mn^{2+} can be used to investigate cortical projection fields of sensory neurons. This has been shown in several sensory systems such as the auditory (tonotopic mapping in inferior colliculus in mice [120]), visual (retinotopic mapping in superior colliculus [125]) and olfactory network (connectivity between olfactory bulb and downstream brain areas [126]). Also *in vivo* cortico-cortical and thalamocortical connectivity has been described in rodents [127]. They concluded that the timing of acquisition post injection is crucial to observe the expected effect. A more elaborate discussion of *in vivo* tract tracing experiment in mice, rats and nonhuman primates can be found in [128].

The same technique has been applied to visualize components of the brain circuitry in control of singing behaviour in starlings and canaries (for review [129]). A full description of the use of MEMRI bird brain imaging will be covered in Chapter 4.

Reviews on MEMRI:

- *[4] Silva, A.C., et al., Manganese-enhanced magnetic resonance imaging (MEMRI): methodological and practical considerations. NMR in Biomedicine, 2004. 17(8): p. 532-543.*
- *[7] Massaad, C. and R. Pautler, Manganese-Enhanced Magnetic Resonance Imaging (MEMRI), in Magnetic Resonance Neuroimaging, M. Modo and J.W.M. Bulte, Editors. 2011, Humana Press. p. 145-174.*
- *[10] Inoue, T., T. Majid, and G. Pautler Robia, Manganese enhanced MRI (MEMRI): neurophysiological applications, in Reviews in the Neurosciences. 2011. p. 675.*

2.5 CONCLUDING REMARKS

In vivo MRI represents a unique tool in plasticity and cognitive research given its power to capture functional, structural and biochemical (not discussed in this chapter) information from the entire brain on a relatively short time frame. In addition, its non-invasive nature allows repeated measures where the same animal can be followed up along, e.g. the course of development and aging, or over different training sessions. Importantly, this also enables to test for the existence of a causal relationship between the observed neuroplastic events and additional measures such as behavioural assessments or scores of cognitive tests. As compared to other whole-brain imaging methods, MRI does not rely on ionising or radioactive substances, which is of great importance as repeated exposure might provoke deleterious side effects obscuring the actual biologically relevant information. Still, one should not overlook the

possible effect of repeated anaesthesia –standard for all preclinical *in vivo* imaging methods except after habituation training– on the organisms' physiology or response to treatment.

Despite the 3-dimensional abundance of structural, functional and biochemical information, still relatively little information is given on the underlying biological nature of the observed effects. This lack of specificity can partly be overcome by combining different imaging modalities aimed at a multimodal imaging strategy [130], MR fingerprinting [131], or by co-registration to *ex vivo* modalities such as histology, MALDI and *in situ* hybridization. In addition, by using quantitative MRI contrasts, 'subvoxel' information on the underlying tissue properties such as water content, myelination, etc. can be deduced. So far, most structural and functional MRI contrasts have been widely explored in the field of plasticity and cognitive research. Yet, the versatility of MRS in neuroplasticity research is only beginning to be explored. Given the possibility to detect fluctuations in the balance of metabolites such as GABA and Glutamate, MRS will become a valuable tool to address future questions relating to both early and adult plasticity.

ACKNOWLEDGEMENTS

This work is supported by the Belgian Science Policy (Belspo; PLASTOSCINE P7/17), the Research Foundation – Flanders (FWO; G044311N; G.0302.13) and a grant by the Hercules Foundation (AUHA0012) to AVdL. GDG (postdoc), FK (postdoc) and LVR (PhD) are supported by FWO fellowships.

REFERENCES

1. Jones, D.K., *Diffusion MRI: Theory, Methods, and Applications*. 2010: Oxford University Press, USA.
2. Logothetis, N.K., *What we can do and what we cannot do with fMRI.* Nature, 2008. **453**(7197): p. 869-878.
3. Deoni, S.C.L., *Quantitative Relaxometry of the Brain.* Topics in Magnetic Resonance Imaging, 2010. **21**(2): p. 101-113 10.1097/RMR.0b013e31821e56d8.
4. Silva, A.C., et al., *Manganese-enhanced magnetic resonance imaging (MEMRI): methodological and practical considerations.* NMR in Biomedicine, 2004. **17**(8): p. 532-543.
5. Mori, S. and J. Tournier, *Introduction to Diffusion Tensor Imaging 2e: And Higher Order Models*. 2013: Elsevier Science & Technology Books.
6. Jones, D.K., T.R. Knösche, and R. Turner, *White matter integrity, fiber count, and other fallacies: The do's and don'ts of diffusion MRI.* NeuroImage, 2013. **73**: p. 239-254.
7. Massaad, C. and R. Pautler, *Manganese-Enhanced Magnetic Resonance Imaging (MEMRI)*, in *Magnetic Resonance Neuroimaging*, M. Modo and J.W.M. Bulte, Editors. 2011, Humana Press. p. 145-174.

8. Di Salle, F., et al., *Exploring brain function with magnetic resonance imaging.* Eur J Radiol, 1999. **30**(2): p. 84-94.
9. Mori, S. and J. Zhang, *Principles of Diffusion Tensor Imaging and Its Applications to Basic Neuroscience Research.* Neuron, 2006. **51**(5): p. 527-539.
10. Inoue, T., T. Majid, and G. Pautler Robia, *Manganese enhanced MRI (MEMRI): neurophysiological applications*, in *Reviews in the Neurosciences*. 2011. p. 675.
11. Amaro, E., Jr. and G.J. Barker, *Study design in fMRI: basic principles.* Brain Cogn, 2006. **60**(3): p. 220-32.
12. Logothetis, N.K. and B.A. Wandell, *Interpreting the BOLD Signal.* Annual Review of Physiology, 2004. **66**(1): p. 735-769.
13. Logothetis, N., et al., *Neurophysiological investigation of the basis of the fMRI signal.* Nature, 2001. **412**(6843): p. 150-157.
14. Soares, J., et al., *A hitchhiker's guide to Diffusion Tensor Imaging.* Frontiers in Neuroscience, 2013. **7**.
15. Amhaoul, H., et al., *Brain inflammation in a chronic epilepsy model: Evolving pattern of the translocator protein during epileptogenesis.* Neurobiology of Disease, 2015. **82**: p. 526-539.
16. Concha, L., *A macroscopic view of microstructure: Using diffusion-weighted images to infer damage, repair, and plasticity of white matter.* Neuroscience, 2014(0).
17. Abe, O., et al., *Voxel-based analysis of the diffusion tensor.* Neuroradiology, 2010. **52**(8): p. 699-710.
18. van den Heuvel, M.P. and H.E. Hulshoff Pol, *Exploring the brain network: A review on resting-state fMRI functional connectivity.* European Neuropsychopharmacology, 2010. **20**(8): p. 519-534.
19. Ogawa, S., et al., *Intrinsic signal changes accompanying sensory stimulation: functional brain mapping with magnetic resonance imaging.* Proc Natl Acad Sci U S A, 1992. **89**(13): p. 5951-5.
20. Kwong, K.K., et al., *Dynamic magnetic resonance imaging of human brain activity during primary sensory stimulation.* Proc Natl Acad Sci U S A, 1992. **89**(12): p. 5675-9.
21. Logothetis, N.K., *What we can do and what we cannot do with fMRI.* Nature, 2008. **453**(7197): p. 869-78.
22. Bandettini, P.A., *Twenty years of functional MRI: the science and the stories.* Neuroimage, 2012. **62**(2): p. 575-88.
23. Logothetis, N.K. and B.A. Wandell, *Interpreting the BOLD signal.* Annu Rev Physiol, 2004. **66**: p. 735-69.
24. Logothetis, N.K. and J. Pfeuffer, *On the nature of the BOLD fMRI contrast mechanism.* Magn Reson Imaging, 2004. **22**(10): p. 1517-31.
25. Malonek, D., et al., *Vascular imprints of neuronal activity: Relationships between the dynamics of cortical blood flow, oxygenation, and volume changes following sensorystimulation.* Proceedings of the National Academy of Sciences, 1997. **94**(26): p. 14826-14831.
26. Margulies, D.S., et al., *Resting developments: a review of fMRI post-processing methodologies for spontaneous brain activity.* MAGMA, 2010. **23**(5-6): p. 289-307.
27. Feinberg, D.A. and E. Yacoub, *The rapid development of high speed, resolution and precision in fMRI.* NeuroImage, 2012. **62**(2): p. 720-725.
28. Smirnakis, S.M., et al., *Spatial specificity of BOLD versus cerebral blood volume fMRI for mapping cortical organization.* J Cereb Blood Flow Metab, 2007. **27**(6): p. 1248-61.
29. Kim, S.G., et al., *Cerebral blood volume MRI with intravascular superparamagnetic iron oxide nanoparticles.* NMR Biomed, 2013. **26**(8): p. 949-62.
30. Detre, J.A. and J. Wang, *Technical aspects and utility of fMRI using BOLD and ASL.* Clin Neurophysiol, 2002. **113**(5): p. 621-34.

31. Masamoto, K. and I. Kanno, *Anesthesia and the quantitative evaluation of neurovascular coupling.* J Cereb Blood Flow Metab, 2012. **32**(7): p. 1233-47.
32. Schroeter, A., et al., *Specificity of stimulus-evoked fMRI responses in the mouse: the influence of systemic physiological changes associated with innocuous stimulation under four different anesthetics.* Neuroimage, 2014. **94**: p. 372-84.
33. Tsurugizawa, T., et al., *Effects of isoflurane and alpha-chloralose anesthesia on BOLD fMRI responses to ingested L-glutamate in rats.* Neuroscience, 2010. **165**(1): p. 244-51.
34. Williams, K.A., et al., *Comparison of alpha-chloralose, medetomidine and isoflurane anesthesia for functional connectivity mapping in the rat.* Magn Reson Imaging, 2010. **28**(7): p. 995-1003.
35. Boumans, T., et al., *Neural representation of spectral and temporal features of song in the auditory forebrain of zebra finches as revealed by functional MRI.* Eur J Neurosci, 2007. **26**(9): p. 2613-26.
36. King, J.A., et al., *Procedure for minimizing stress for fMRI studies in conscious rats.* J Neurosci Methods, 2005. **148**(2): p. 154-60.
37. Ferris, C.F., et al., *Functional magnetic resonance imaging in conscious animals: a new tool in behavioural neuroscience research.* J Neuroendocrinol, 2006. **18**(5): p. 307-18.
38. Jonckers, E., et al., *Different anesthesia regimes modulate the functional connectivity outcome in mice.* Magn Reson Med, 2013.
39. Desai, M., et al., *Mapping brain networks in awake mice using combined optical neural control and fMRI.* J Neurophysiol, 2011. **105**(3): p. 1393-405.
40. De Groof, G., et al., *Functional MRI and functional connectivity of the visual system of awake pigeons.* Behav Brain Res, 2013. **239**: p. 43-50.
41. Lahti, K.M., et al., *Imaging brain activity in conscious animals using functional MRI.* Journal of Neuroscience Methods, 1998. **82**(1): p. 75-83.
42. Birn, R.M., et al., *Separating respiratory-variation-related fluctuations from neuronal-activity-related fluctuations in fMRI.* NeuroImage, 2006. **31**(4): p. 1536-1548.
43. Kalisch, R., et al., *Blood Pressure Changes Induced by Arterial Blood Withdrawal Influence Bold Signal in Anesthesized Rats at 7 Tesla: Implications for Pharmacologic MRI.* NeuroImage, 2001. **14**(4): p. 891-898.
44. Wise, R.G., et al., *Resting fluctuations in arterial carbon dioxide induce significant low frequency variations in BOLD signal.* NeuroImage, 2004. **21**(4): p. 1652-1664.
45. Lindquist, M.A., *The Statistical Analysis of fMRI Data.* Statistical Science, 2008. **23**(4): p. 439-464.
46. James, J.S., et al., *fMRI paradigm designing and post-processing tools.* Indian J Radiol Imaging, 2014. **24**(1): p. 13-21.
47. Lindquist, M.A., et al., *Modeling the hemodynamic response function in fMRI: Efficiency, bias and mis-modeling.* Neuroimage, 2009. **45**(1): p. S187-S198.
48. Friston, K.J., L. Harrison, and W. Penny, *Dynamic causal modelling.* Neuroimage, 2003. **19**(4): p. 1273-302.
49. Lowe, M.J., et al., *Correlations in low-frequency BOLD fluctuations reflect cortico-cortical connections.* Neuroimage, 2000. **12**(5): p. 582-7.
50. van den Heuvel, M.P. and H.E. Hulshoff Pol, *Exploring the brain network: a review on resting-state fMRI functional connectivity.* Eur Neuropsychopharmacol, 2010. **20**(8): p. 519-34.
51. Kelly, C., et al., *Characterizing variation in the functional connectome: promise and pitfalls.* Trends in Cognitive Sciences, 2012. **16**(3): p. 181-188.
52. Peltier, S.J., et al., *Functional connectivity changes with concentration of sevoflurane anesthesia.* Neuroreport, 2005. **16**(3): p. 285-288.
53. Liang, Z., J. King, and N. Zhang, *Uncovering intrinsic connectional architecture of functional networks in awake rat brain.* J Neurosci, 2011. **31**(10): p. 3776-83.

54. Weissenbacher, A., et al., *Correlations and anticorrelations in resting-state functional connectivity MRI: a quantitative comparison of preprocessing strategies.* Neuroimage, 2009. **47**(4): p. 1408-16.
55. Gavrilescu, M., et al., *Functional connectivity estimation in fMRI data: influence of preprocessing and time course selection.* Hum Brain Mapp, 2008. **29**(9): p. 1040-52.
56. Chang, C. and G.H. Glover, *Effects of model-based physiological noise correction on default mode network anti-correlations and correlations.* Neuroimage, 2009. **47**(4): p. 1448-59.
57. Biswal, B., et al., *Functional Connectivity in the Motor Cortex of Resting Human Brain Using Echo-Planar Mri.* Magnetic Resonance in Medicine, 1995. **34**(4): p. 537-541.
58. Calhoun, V.D., et al., *A method for making group inferences from functional MRI data using independent component analysis.* Hum Brain Mapp, 2001. **14**(3): p. 140-51.
59. Beckmann, C.F., et al., *Investigations into resting-state connectivity using independent component analysis.* Philos Trans R Soc Lond B Biol Sci, 2005. **360**(1457): p. 1001-13.
60. Bullmore, E. and O. Sporns, *Complex brain networks: graph theoretical analysis of structural and functional systems.* Nat Rev Neurosci, 2009. **10**(3): p. 186-98.
61. Damoiseaux, J.S., et al., *Consistent resting-state networks across healthy subjects.* Proceedings of the National Academy of Sciences of the United States of America, 2006. **103**(37): p. 13848-13853.
62. Jonckers, E., et al., *Functional connectivity fMRI of the rodent brain: comparison of functional connectivity networks in rat and mouse.* PLoS One, 2011. **6**(4): p. e18876.
63. Lu, H., et al., *Rat brains also have a default mode network.* Proc Natl Acad Sci U S A, 2012. **109**(10): p. 3979-84.
64. Fransson, P., *Spontaneous low-frequency BOLD signal fluctuations: an fMRI investigation of the resting-state default mode of brain function hypothesis.* Hum Brain Mapp, 2005. **26**(1): p. 15-29.
65. Uddin, L.Q., K. Supekar, and V. Menon, *Typical and atypical development of functional human brain networks: insights from resting-state FMRI.* Front Syst Neurosci, 2010. **4**: p. 21.
66. Galinsky, V.L. and L.R. Frank, *Automated segmentation and shape characterization of volumetric data.* NeuroImage, 2014. **92**(0): p. 156-168.
67. Focke, N.K., et al., *Do manual and voxel-based morphometry measure the same? – A proof of concept study.* Frontiers in Psychiatry, 2014. **5**.
68. Ashburner, J. and K.J. Friston, *Voxel-Based Morphometry—The Methods.* NeuroImage, 2000. **11**(6): p. 805-821.
69. Whitwell, J.L., *Voxel-Based Morphometry: An Automated Technique for Assessing Structural Changes in the Brain.* The Journal of Neuroscience, 2009. **29**(31): p. 9661-9664.
70. Mechelli, A., et al., *Voxel-Based Morphometry of the Human Brain: Methods and Applications.* Current Medical Imaging Reviews, 2005: p. 105-113.
71. Chung, M.K., et al., *A Unified Statistical Approach to Deformation-Based Morphometry.* NeuroImage, 2001. **14**(3): p. 595-606.
72. Freeborough, P.A. and N.C. Fox, *Modeling Brain Deformations in Alzheimer Disease by Fluid Registration of Serial 3D MR Images.* Journal of Computer Assisted Tomography, 1998. **22**(5): p. 838-843.
73. Ashburner, J. and G.R. Ridgway, *Symmetric Diffeomorphic Modeling of Longitudinal Structural MRI.* Frontiers in Neuroscience, 2012. **6**: p. 197.
74. Paus, T., et al., *Maturation of white matter in the human brain: a review of magnetic resonance studies.* Brain Research Bulletin, 2001. **54**(3): p. 255-266.
75. Dubois, J., et al., *The early development of brain white matter: A review of imaging studies in fetuses, newborns and infants.* Neuroscience, (0).

76. Deoni, S.L., *Magnetic Resonance Relaxation and Quantitative Measurement in the Brain*, in *Magnetic Resonance Neuroimaging*, M. Modo and J.W.M. Bulte, Editors. 2011, Humana Press. p. 65-108.
77. Dula, A.N., D.F. Gochberg, and M.D. Does, *Optimal echo spacing for multi-echo imaging measurements of Bi-exponential T2 relaxation.* Journal of Magnetic Resonance, 2009. **196**(2): p. 149-156.
78. Crawley, A.P. and R.M. Henkelman, *Errors in T2 estimation using multislice multiple-echo imaging.* Magnetic Resonance in Medicine, 1987. **4**(1): p. 34-47.
79. Shrager, R.I., G.H. Weiss, and R.G.S. Spencer, *Optimal time spacings for T2 measurements: monoexponential and biexponential systems.* NMR in Biomedicine, 1998. **11**(6): p. 297-305.
80. Pell, G.S., et al., *Voxel-based relaxometry: a new approach for analysis of T2 relaxometry changes in epilepsy.* NeuroImage, 2004. **21**(2): p. 707-713.
81. Kara, F., et al., *In vivo measurement of transverse relaxation time in the mouse brain at 17.6 T.* Magnetic Resonance in Medicine, 2013. **70**(4): p. 985-993.
82. Ding, X.-Q., et al., *Normal Brain Maturation Characterized With Age-Related T2 Relaxation Times: An Attempt to Develop a Quantitative Imaging Measure for Clinical Use.* Investigative Radiology, 2004. **39**(12): p. 740-746.
83. Kharatishvili, I., et al., *MRI changes and complement activation correlate with epileptogenicity in a mouse model of temporal lobe epilepsy.* Brain Structure and Function, 2014. **219**(2): p. 683-706.
84. Kharatishvili, I., et al., *Quantitative T2 mapping as a potential marker for the initial assessment of the severity of damage after traumatic brain injury in rat.* Experimental Neurology, 2009. **217**(1): p. 154-164.
85. MacKay, A., et al., *In vivo visualization of myelin water in brain by magnetic resonance.* Magn Reson Med, 1994. **31**(6): p. 673-7.
86. MacKay, A., et al., *Insights into brain microstructure from the T2 distribution.* Magnetic Resonance Imaging, 2006. **24**(4): p. 515-525.
87. Alonso-Ortiz, E., I.R. Levesque, and G.B. Pike, *MRI-based myelin water imaging: A technical review.* Magnetic Resonance in Medicine, 2014: p. n/a-n/a.
88. Basser, P.J., J. Mattiello, and D. LeBihan, *MR diffusion tensor spectroscopy and imaging.* Biophysical Journal, 1994. **66**(1): p. 259-267.
89. Longwei, X., *Clinical application of diffusion tensor magnetic resonance imaging in skeletal muscle.* Muscles, Ligaments and Tendons Journal, 2012. **2**(1): p. 19-24.
90. Le Bihan, D., et al., *Diffusion tensor imaging: Concepts and applications.* Journal of Magnetic Resonance Imaging, 2001. **13**(4): p. 534-546.
91. Stejskal, E.O. and J.E. Tanner, *Spin Diffusion Measurements: Spin Echoes in the Presence of a Time-Dependent Field Gradient.* The Journal of Chemical Physics, 1965. **42**(1): p. 288-292.
92. Beaulieu, C., *The basis of anisotropic water diffusion in the nervous system – a technical review.* NMR in Biomedicine, 2002. **15**(7-8): p. 435-455.
93. Campbell, B.C.V. and I.M. Macrae, *Translational perspectives on perfusion–diffusion mismatch in ischemic stroke.* International Journal of Stroke, 2013: p. n/a-n/a.
94. Jones, D.K., *The effect of gradient sampling schemes on measures derived from diffusion tensor MRI: A Monte Carlo study†.* Magnetic Resonance in Medicine, 2004. **51**(4): p. 807-815.
95. Chung, H.-W., M.-C. Chou, and C.-Y. Chen, *Principles and Limitations of Computational Algorithms in Clinical Diffusion Tensor MR Tractography.* American Journal of Neuroradiology, 2011. **32**(1): p. 3-13.
96. Bullmore, E. and O. Sporns, *Complex brain networks: graph theoretical analysis of structural and functional systems.* Nat Rev Neurosci, 2009. **10**(3): p. 186-198.
97. Mangin, J.F., et al., *Toward global tractography.* NeuroImage, 2013. **80**(0): p. 290-296.

98. Tuch, D.S., et al., *High angular resolution diffusion imaging reveals intravoxel white matter fiber heterogeneity.* Magnetic Resonance in Medicine, 2002. **48**(4): p. 577-582.
99. Tuch, D.S., *Q-ball imaging.* Magnetic Resonance in Medicine, 2004. **52**(6): p. 1358-1372.
100. Jones, D.K. and P.J. Basser, *"Squashing peanuts and smashing pumpkins": How noise distorts diffusion-weighted MR data.* Magnetic Resonance in Medicine, 2004. **52**(5): p. 979-993.
101. Jones, D.K., T.R. Knösche, and R. Turner, *White matter integrity, fiber count, and other fallacies: The do's and don'ts of diffusion MRI.* NeuroImage, (0).
102. Sampaio-Baptista, C., et al., *Gray matter volume is associated with rate of subsequent skill learning after a long term training intervention.* NeuroImage, 2014. **96**(0): p. 158-166.
103. Sagi, Y., et al., *Learning in the Fast Lane: New Insights into Neuroplasticity.* Neuron, 2012. **73**(6): p. 1195-1203.
104. Hofstetter, S., et al., *Short-Term Learning Induces White Matter Plasticity in the Fornix.* The Journal of Neuroscience, 2013. **33**(31): p. 12844-12850.
105. Blumenfeld-Katzir, T., et al., *Diffusion MRI of Structural Brain Plasticity Induced by a Learning and Memory Task.* PLoS ONE, 2011. **6**(6): p. e20678.
106. Pautler, R.G., A.C. Silva, and A.P. Koretsky, *In vivo neuronal tract tracing using manganese-enhanced magnetic resonance imaging.* Magnetic Resonance in Medicine, 1998. **40**(5): p. 740-748.
107. Erikson, K.M., et al., *Interactions between excessive manganese exposures and dietary iron-deficiency in neurodegeneration.* Environmental Toxicology and Pharmacology, 2005. **19**(3): p. 415-421.
108. Erikson, K.M. and M. Aschner, *Manganese neurotoxicity and glutamate-GABA interaction.* Neurochemistry International, 2003. **43**(4–5): p. 475-480.
109. AB, S., *Manganese exposure, essentiality & toxicity.* Indian J Med Res, 2008. **128**(4): p. 16.
110. Avelino, M.A., et al., *Inherited manganism: The "cock-walk" gait and typical neuroimaging features.* Journal of the Neurological Sciences, 2014. **341**(1–2): p. 150-152.
111. Dobson, A.W., K.M. Erikson, and M. Aschner, *Manganese Neurotoxicity.* Annals of the New York Academy of Sciences, 2004. **1012**(1): p. 115-128.
112. Roth, J., S. Ponzoni, and M. Aschner, *Manganese Homeostasis and Transport*, in *Metallomics and the Cell*, L. Banci, Editor. 2013, Springer Netherlands. p. 169-201.
113. Gavin, C.E., K.K. Gunter, and T.E. Gunter, *Manganese and calcium efflux kinetics in brain mitochondria. Relevance to manganese toxicity*. Vol. 266. 1990. 329-34.
114. Aschner, M., *The transport of manganese across the blood–brain barrier.* NeuroToxicology, 2006. **27**(3): p. 311-314.
115. Tjälve, H., et al., *Uptake of Manganese and Cadmium from the Nasal Mucosa into the Central Nervous System via Olfactory Pathways in Rats *.* Pharmacology & Toxicology, 1996. **79**(6): p. 347-356.
116. Chan, K.C., et al., *In vivo evaluation of retinal and callosal projections in early postnatal development and plasticity using manganese-enhanced MRI and diffusion tensor imaging.* NeuroImage, 2012. **59**(3): p. 2274-2283.
117. Sloot, W.N. and J.-B.P. Gramsbergen, *Axonal transport of manganese and its relevance to selective neurotoxicity in the rat basal ganglia.* Brain Research, 1994. **657**(1–2): p. 124-132.
118. Takeda, A., et al., *Manganese Transport in the Neural Circuit of Rat CNS.* Brain Research Bulletin, 1998. **45**(2): p. 149-152.
119. Bissig, D. and B.A. Berkowitz, *Manganese-enhanced MRI of layer-specific activity in the visual cortex from awake and free-moving rats.* NeuroImage, 2009. **44**(3): p. 627-635.
120. Yu, X., et al., *In vivo auditory brain mapping in mice with Mn-enhanced MRI.* Nat Neurosci, 2005. **8**(7): p. 961-968.
121. Silva, A.C., et al., *Detection of cortical laminar architecture using manganese-enhanced MRI.* Journal of Neuroscience Methods, 2008. **167**(2): p. 246-257.

122. Chuang, K.-H., L. Belluscio, and A.P. Koretsky, *In vivo detection of individual glomeruli in the rodent olfactory bulb using manganese enhanced MRI.* NeuroImage, 2010. **49**(2): p. 1350-1356.
123. Nairismägi, J., et al., *Manganese-enhanced magnetic resonance imaging of mossy fiber plasticity in vivo.* NeuroImage, 2006. **30**(1): p. 130-135.
124. Golub, Y., et al., *Reduced hippocampus volume in the mouse model of Posttraumatic Stress Disorder.* Journal of Psychiatric Research, 2011. **45**(5): p. 650-659.
125. Chan, K.C., et al., *In vivo retinotopic mapping of superior colliculus using manganese-enhanced magnetic resonance imaging.* NeuroImage, 2011. **54**(1): p. 389-395.
126. Gutman, D., et al., *Mapping of the mouse olfactory system with manganese-enhanced magnetic resonance imaging and diffusion tensor imaging.* Brain Structure and Function, 2013. **218**(2): p. 527-537.
127. Tucciarone, J., et al., *Layer specific tracing of corticocortical and thalamocortical connectivity in the rodent using manganese enhanced MRI.* NeuroImage, 2009. **44**(3): p. 923-931.
128. Pautler, R.G., *In vivo, trans-synaptic tract-tracing utilizing manganese-enhanced magnetic resonance imaging (MEMRI).* NMR in Biomedicine, 2004. **17**(8): p. 595-601.
129. Van der Linden, A., et al., *Applications of manganese-enhanced magnetic resonance imaging (MEMRI) to image brain plasticity in song birds.* NMR in Biomedicine, 2004. **17**(8): p. 602-612.
130. Uludağ, K. and A. Roebroeck, *General overview on the merits of multimodal neuroimaging data fusion.* NeuroImage, (0).
131. Ma, D., et al., *Magnetic resonance fingerprinting.* Nature, 2013. **495**(7440): p. 187-192.

Chapter 3

MRI & Neuroplasticity: a perfect match

This chapter is based on:

Hamaide J., De Groof G., Van der Linden A. Neuroplasticity and MRI: a perfect match. NeuroImage. 2016 May 1; doi: 10.1016/j.neuroimage.2015.08.005; published in a special issue titled 'Effects of Physical and Cognitive activity on brain structure and function'.

3.1 INTRODUCTION

With the advent of neuroimaging tools designed to extract functional, structural and metabolic information of the brain in a non-invasive manner, the field of neuroscience has expanded widely. Numerous studies have described volume or shape changes of cortical brain areas upon specific motor or cognitive training programs [1], microstructural deficits related to cognitive decline in neurodegenerative disorders [2, 3], functional reallocation of specific brain areas after trauma [4], etc. Also the effects of stress [5, 6], hormones [7], (drug) addiction [8-12] and aging [13] on the brain have been evaluated thoroughly. Furthermore, convincing experimental and clinical evidence points toward the active role of experience and physical activity to partially unlock neuroplasticity in adult life and promote functional rehabilitation upon trauma [14]. An excellent review by Draganski and May (2008) compiles the state-of-the-art insights into the effect of motor training on brain morphometry and also highlights several 'flaws' in current understanding of training-induced brain adaptations: (i) the time-course of neuroplastic events is still relatively vague, (ii) the underlying biological mechanisms are far from clear and (iii) the relation between functional and structural neuroplastic adaptations is not yet understood [1]. In order to resolve these key questions, animal experiments are needed which can divulge the observed neuroplastic events up to the molecular level. Interestingly, several animal studies have already illustrated human-like plasticity in response to physical exercise, e.g. voluntary wheel running in mice [15] and rats [16], and cognitive training [17, 18] etc., indicating that most plasticity-related mechanisms are conserved among species.

Besides focusing on the effects of physical and cognitive exercising on brain structure and function, we aim to extend this literature review with exemplary high-impact studies which have led to major insights into mechanisms affecting or even directing neuroplasticity. We will start by exploring the effects of age and 'timing' on neuroplasticity after which we will discuss the effects of hormones on brain function and structure. Doing so, we intend to focus attention on how different MRI-based techniques have successfully captured neuroplastic events in different contexts but also on how MRI –besides conventional tools such as histology– might be of use in future experiments to study the effects of experience, training and skill acquisition on the brain.

3.2 NEUROPLASTICITY AND COGNITION, WHAT CAN WE LEARN FROM ANIMALS?

Most clinical studies describe effects observed with *in vivo* imaging tools often related to a specific behavioural phenotype, but fail to target the underlying biological mechanisms. Biomedical research, on the other hand, applies well-established translational models that mimic specific parts of disease or response upon experience. In addition, a laboratory setting allows to strictly control environmental input including diet, social interaction, rearing conditions, age, hormonal status etc., all of which are crucial determinants in experience-dependent or activity-induced neuroplasticity. Importantly, over the last decades genetically engineered animals –especially rodents– have become available and greatly help in elucidating mechanism underlying specific biological effects by knocking *in* or *down* specific genes translating molecular elements suspected to be involved. Moreover, animals with identical genetic backgrounds strongly reduce variance associated to differences in plasticity-related gene expression profiles, leaving the experimental intervention as single variable. Furthermore, the lifespan of most animals is markedly shorter and is characterized by an accelerated succession of developmental stages making it possible to study, e.g. disease ontogenesis up to more advanced stages or the age-dependency of neuroplastic processes within the same animal on relatively short timescales. Interestingly, several animal studies have already illustrated human-like plasticity in response to physical exercise, e.g. voluntary wheel running in mice [15] and rats [16], and cognitive training [17, 18] etc., indicating that most plasticity-related mechanisms are conserved among species.

Besides these advantages, several drawbacks should be mentioned as well. Despite the high conservation of biological processes amongst mammals and most vertebrates, important differences still exist which question the translational character of animal findings. Furthermore, studying genetically engineered animals sheds light onto very specific parts of disease or response upon a given experience, but still does not provide a clear understanding of the complete biological basis and how different systems interact to result in a specific behaviour. Although it broadens the variety of techniques and tests that can be applied, animal research narrows the range of biological questions that can be addressed. For example, information regarding higher cognitive skills such as reasoning and complex emotions, mathematics and planning etc., is in most cases impossible to extract from the animal brain.

Notwithstanding, several training procedures have been developed to assess human-like higher cognitive functionality in the animal brain, e.g. maze training for spatial learning and memory [19], conditioning paradigms [20, 21], etc.

MRI is a highly translational tool. Consequently, given its biological versatility, MRI has been used intensively in neuroplasticity research over the last decade to uncover brain loci affected by experience, activated upon stimulation etc. in various species [22-24]. This way several important determinants in setting boundaries on neuroplasticity have been uncovered. Age is the most well-known and strongest factor, but also hormones, physical workout, cognitive training programs etc. affect the brain at various levels. In the following sections, the above mentioned mechanisms along with appropriate models to assess the behavioural outcome will be introduced briefly and the involvement of MRI in tracing the resulting neuroplastic changes will be discussed. These findings have led to a deeper understanding of neuroplasticity in general, also related to the brains' response to physical and cognitive exercise in adulthood.

3.2.1 The impact of age on neuroplasticity

The susceptibility of the brain to undergo neuroplastic changes is strongly dependent on age. For example, children born blind due to, e.g. congenital cataract, or deaf should receive adequate medical treatment before respectively 6 weeks or 2 years of age to prevent impaired visual acuity [25] or altered auditory perception and language accuracy in adult life [26, 27]. This age-dependent variation in prognosis can be ascribed to the existence of sensitive and critical period, i.e. precisely delineated time windows in early life during which environmental stimuli most potently shape cortical brain circuitries responsible for the acquisition of various skills and abilities required in later life [28]. When reaching adulthood, previously established neural networks encoding acquired skills are consolidated, imposing strict boundaries on the brains' ability to adapt. Fortunately, neuroplasticity is never entirely down-regulated, allowing the adult organism to learn and retain memory at later life stages or for the adult brain to 'reshape' upon cognitive and physical training.

A very interesting study illustrating this age-dependent, differential sensitivity of the brain to motor learning was performed by Bengtsson and colleagues. They investigated the effects of piano practice on brain plasticity during distinct developmental periods, i.e. childhood, adolescence and adulthood. During childhood the largest number of brain areas displayed changes, whereas in older ages only a limited number of brain regions showed training-induced

adaptations. More specifically, the intensity of childhood piano practicing correlated with FA in the posterior limbs of the internal capsule (bilateral, containing corticospinal tracts), the corpus callosum (isthmus & upper splenium, body), and fibre tracts in the frontal lobe. Piano practicing intensity throughout adolescence and adulthood displayed significant correlations with FA in respectively the splenium and body of the corpus callosum, and in the left anterior limb of the internal capsule and a fibre bundle in the right temporo-parietal junction. Each of these white matter structures can be linked to functions vital for successful piano playing or –by extension– skilled motor performance [29]. Also in preclinical research has the age-dependency of neuroplastic events been observed. Blumenfeld-Katzir and colleagues (2011) found that 1, 4 and 12 month old rats showed a similar pattern of brain areas actively undergoing changes after 5 days of Morris Water Maze (MWM) training, however, the extent of the changes was different between the ages [30]. In addition, Van Praag et al. (2005) investigated the effects of voluntary wheel running in young versus old mice (3 versus 19 months of age), and found that spatial learning and hippocampal neurogenesis did not improve equally indicating that physical activity in mice exerts different effects on brain plasticity in early compared to older life stages [31]. Understanding age-dependent mechanisms posing 'temporal' boundaries on plasticity might help in finding possible targets implicated in enabling neuroplasticity following training in adulthood or old age.

Behaviour is affected by age as well. Indeed, Albani and colleagues (2015) detected dissimilar performances in the elevated plus maze –experimental setup to assess anxiety-related behaviour in rodents [32]– when testing rats at two successive maturational stages in early postnatal life, i.e. p17-19 versus p22-24, or when varying the illumination level of the environment, i.e. dim versus bright light. Interestingly, they also zoomed in on neuronal activation by investigating the expression of the immediate early gene Arc and found differential expression in the amygdala and visual cortex stipulated by age and surroundings (illumination). This study underlines important methodological considerations given that little differences in age (<1 week) or environment can have a major impact on the functional activation of the neural substrate encoding specific behaviours [33].

3.2.1.1 Childhood

Critical and sensitive periods of development

A clear distinction should be made between critical and sensitive periods. The first relates to basic functions of which proper experience must be present during the respective window of plasticity for the skill to develop properly, as after closure of the critical period the neural substrate encoding that particular skill will no longer be susceptible to change. For example filial imprinting [34, 35] and ocular dominance [36]. The latter, on the other hand, refers to skills or abilities of which the neural substrate displays maximum sensitivity to the input at a particular age, however, the sensitive period never closes entirely, leaving the organism still capable of learning or adjusting particular behaviours at later ages, for example language learning in humans [37]. Furthermore, the duration of the sensory or critical period depends on the skill, for example, imprinting takes merely a few hours, while speech and language learning last for several years.

Current insights into critical period plasticity have been extracted mainly from research devoted to the acquisition of sensory modalities such as the visual (ocular dominance theory [36, 38]), auditory (tonotopic mapping, pitch learning [27]) and somatosensory or tactile (whisker-barrel pathway [39]) systems in mammals. Based on these findings, Hensch (2004) outlines nine key principles that govern critical period plasticity. **(1)** Functional competition between inputs, this is clearly illustrated by ocular dominance studies, where the sensory deprived (enucleated or covered eye) will lose cortical territory to the dominant eye. **(2)** 'Electrical activity' reflected by action potentials used by neurons to transmit information receiving from and sending to neighbouring cells, including phenomena such as LTP, LTD. **(3)** Structural consolidation of previously established pathways, defined by increased expression of perineuronal nets and myelin that physically restrict neurons to make synaptic contacts to neighbouring cells and reduce molecular mobility (pose physical boundaries on cells). **(4)** A multitude of molecular mechanisms and elements, e.g. Brain-Derived Neurotrophic Factor (BDNF), Orthodenticle Homeobox 2 homeoprotein (Otx2), myelin-related Nogo Receptor (NgR), Insulin-like Growth Factor-1 (IGF-1), Paired immunoglobulin-like receptor B (PirB) etc. ([40-42]; for review: [41]). Recently, epigenetic mechanisms were proposed to be part of the interface between environmental stimuli experienced during early life critical periods and the sustained molecular, cellular and complex behavioural phenotypes [43]. **(5)** Experience is necessary to shape neural

circuits that ultimately result in a particular behaviour. **(6)** Unique timing and duration of critical periods across systems, following a hierarchical order similar to rostro-caudal gradients of brain maturation, where first basic abilities must develop before more complex skills can be acquired. **(7)** Delicate balance between excitation and inhibition, where GABA and glutamate are the primary modulators and take part of an intricate interplay with PNNs as they selectively accrue around PV-containing GABAergic interneurons. **(8)** The dependence on attention and motivation. **(9)** And, lastly, the possibility to re-induce periods heightened plasticity in adulthood.

Several attempts have been made to reopen plasticity in adulthood by pharmacological intervention, e.g. selective serotonin reuptake inhibitors (SSRI), histone deacetylase inhibitor (HDACI), chondroitinase ABC inhibitors (ChABCI), acetylcholine-esterase inhibitors (AChEI) etc. and altered environmental stimulation, e.g. deprivation by dark exposure or environmental enrichment [28, 42]. Nevertheless, still many questions remain as (1) what is the temporal succession of critical periods encoding distinct sensory skills; (2) to what extent can particular phenomena identified as setting boundaries on critical period plasticity, also limit plasticity related to the sensitive periods which often include the acquisition of complex multimodal or even higher cognitive skills such as speech and language learning; (3) can manipulation of these factor re-induce or 're-open' a critical period of neuroplasticity in adult life?

Bridging information from developmental studies in rodents, ferrets and cats, Olaverria and co-workers (2012) discuss the possibility of using Diffusion Tensor Imaging (DTI) as a reliable marker to evaluate the timing of critical periods in early brain development by mapping the effects of experience-dependent plasticity on cortico-cortical connectivity within the neural tissue encoding sensory skills such as the visual system [44]. A practical example in this context can be found in a study by Chan et al. (2012), who assessed the effects of early visual impairment, i.e. monocular enucleation and monocular deprivation –a popular model for critical period ocular dominance plasticity– in rodents by combining DTI and Manganese Enhanced MRI (MEMRI). They reported a reduced Fractional Anisotropy (FA) in the anterior and posterior retinal pathways in the monocular enucleated and deprived group compared to controls, indicative of respectively degeneration and immaturity of the tracts. Interestingly, the non-deprived eye was characterized by a higher FA compared to control rats [45]. Besides its use in probing structural connectivity, DTI is sensitive to microstructural rearrangements and

changing myelin content as well, both factors known to be implicated in limiting neuroplasticity. Remarkably, to our knowledge only a limited number of studies reported on targeting critical period plasticity with non-invasive imaging tools. Certain biological mechanisms setting boundaries on critical period plasticity, e.g. formation of PNNs, excitation-inhibition balance mediated through GABA etc. could possibly be targeted by *in vivo* MRI and are extremely likely to play a role in recovery from functional losses or several pathologies, e.g. impact of PNN abnormalities in Schizophrenia [46], in adulthood as well. Using MEMRI, Chan and colleagues were able to track axonal projections originating in the retinal ganglion cells and distinguish alterations to retinal and callosal projections resulting from early visual impairment. They succeeded in demarcating the contralateral cortical projection area and found a significantly increased volume in early blinded rats and mice compared to controls. The brains' response to monocular enucleation in early postnatal life has also been tackled by *in vivo* Magnetic Resonance Spectroscopy (MRS). Three weeks after surgery, Chow and colleagues (2011) found a significant reduction in the Taurine (Tau) and N-acetyl Aspartate (NAA) levels in the visual cortex contralateral to the enucleated eye indicative of neuronal loss and axonal damage [47]. Glutamate (Glu), Choline (Cho) and myo-Inositol concentrations were not affected. These observations are in line with previous histological studies [48, 49].

Interestingly, Ben-Ari and co-workers describe the role of GABA in directing cortical brain maturation by tightly controlling the excitation/inhibition balance and how dysregulation of GABA might give rise to neurodevelopmental disorders such as Autism Spectrum Disorder and epilepsy [50]. In addition, research on the visual system in rats describes GABA as a decisive determinant in imposing brakes on critical period plasticity [51]. Most of these findings, however, were discovered by invasive and highly localized molecular tools. MRS, on the other hand, can be regarded as an exceptional tool to evaluate critical period plasticity given its sensitivity to estimate the neurochemical signature of metabolites such as GABA in the living brain. Stagg (2014) nicely reviews how MRS can be applied in research aimed at tackling the role of GABA in cortical plasticity focused on the primary motor cortex. In addition, Stagg briefly touches upon the effects of acute neuromodulation of glutamate and GABA by non-invasive stimulation protocols such as Transcranial Magnetic Stimulation (TMS), and how this relates to the MRS GABA readout [52]. Besides focusing on GABA, also other MRS-detectable metabolites infer neuroplastic events possibly related to the establishment of higher cognitive learned skills. Based on a prior functional MRI (fMRI) study, Pugh et al. (2014) acquired MRS spectra in

children at two time points throughout the development of the neural circuitry involved in reading [53]. Focusing on NAA, Cho, Glu and GABA levels, they found inverse correlations between Cho and Glu levels and reading and linguistic performance in the occipital lobes. Fascinatingly, Glu levels at the first measurement were predictive of reading performance assessed during a behavioural follow up 24 months later [54].

A more unusual animal model displaying striking similarities to the process of human speech learning might shed light on the translational character of critical period determinants to higher cognitive functions. Indeed, similar to humans, songbirds –especially close-ended learners such as zebra finches– learn the song of their father (tutor) during two partly overlapping critical periods early in life (for review [55]). After closure of the critical periods for vocal learning, the song will be crystallized. Therefore, male birds sing only one stereotypic zebra finch song which –under normal circumstances– never changes again. A very interesting advantage of songbirds in neuroplasticity research is that their song directly reflects the specific stage of vocal learning. Moreover, songs can be easily recorded, quantified and related to the observed functional and structural changes. Of particular interest with regards to critical period plasticity, recently, the appearance of parvalbumin-positive interneurons and PNNs have been studied throughout the process of vocal learning [56]. Fascinatingly, song maturity correlated to the percentage of parvalbuminergic cells surrounded by PNNs in a brain area in control of song learning and production. Moreover, depriving juvenile male zebra finches of tutor song resulted in a decreased level of parvalbumine-positive interneurons and PNNs [56]. In line with observations from critical periods of sensory functions, if no proper stimulation, i.e. tutor song, is heard during the critical period for vocal learning, the deprived males will not be able to sing a typical zebra finch song in adult life [57]. In addition, another study by the same group showed that the distribution of perineuronal nets is highly sexually dimorphic in specific components of the song control circuitry, i.e. the brain circuitry in control of singing [58]. This was confirmed by others as well [59]. Interestingly, only male zebra finches sing, while both sexes memorize the tutor song. Consequently, the neural substrate in control of the motoric aspect of song production displays a differential density in PNNs in females as compared to males. Both findings strongly suggest that the sexually dimorphic and developmental evolution of expression of PNNs in the zebra finch brain might be correlated to critical period plasticity. In order to confirm or disprove these hypothetical presumptions a causal relationship between

behavioural changes, i.e. song output, and localized reorganization of the extracellular matrix needs to be established. Interestingly, in theory, it might be possible to track the formation of PNNs with *in vivo* imaging tools sensitive to microstructural rearrangements, e.g. DTI. Moreover, changing myelin contents and GABA levels can also be measured, making critical period plasticity highly fascinating to address with *in vivo* MRI.

Maladaptive critical period plasticity

Recent evidence suggests that the pathological basis of many neurodevelopmental disorders can be found in maladaptive critical period plasticity [60, 61]. Berger and colleagues hypothesize that the behavioural phenotype of autism spectrum disorder might result from a delicate interplay of genetic predisposition along with premature closing of the critical period for integration of sensory input, language and social skills [62]. Likewise, the pathological profile of several neurodevelopmental conditions, e.g. Down and Rett syndrome [63], schizophrenia [64, 65], epilepsy [66], fragile X syndrome [67] etc. have all been linked to improper critical period plasticity.

Regardless of genetic predisposition, early life rearing conditions are essential for proper brain development. Indeed, deprivation studies [39, 68] and rare case studies [69] show that if environmental stimuli are only experienced *prior* to or *post* opening or closure of the critical period encoding a specific skill, the skill will not be mastered as proficiently as in normal circumstances [70]. This implies that critical periods might be interpreted as 'windows of opportunity', i.e. the brain is only compliant to particular stimulation or environmental input at the respective maturational time frame. Another argument illustrating the vital importance of early life experiences can be found in adverse rearing conditions or early traumatic experiences. Bogart and colleagues (2014) investigated the consequences of different rearing conditions of brain morphology and found profound differences in global white-to-grey matter volume ratio, depth of cortical folds and grey matter thickness when comparing mother- and nursery-reared chimpanzees [71]. A similar study has been performed in the clinic, studying the effects of childhood emotional maltreatment on brain structure. The most striking differences were found in the medial prefrontal cortex, the brain area in control of cognitive and emotional (dys)functioning. Interestingly, both human [72] and animal evidence [73] suggests that the long-lasting consequences of early life stress and altered social experience might be mediated

through epigenetic mechanisms and, what is more, epigenetic mechanisms are believed to pass these effects on to the next generation.

3.2.1.2 Adulthood

Yin and Yuang review the existence of a balance between Hebbian and homeostatic plasticity in adult life [74]. Hebbian plasticity challenges existing functional and structural networks aimed at a constant refinement of current abilities and the corresponding neural substrate. Homeostatic plasticity, on the other hand, tries to preserve neuronal homeostasis and previously established connectivity by constraining network activity within physiological ranges. Several mechanisms in control of maintaining the balance between flexibility and stability of the brain have been identified (for review [74]), however, the tightly regulated interaction between these factors, the resulting large-scale effects on brain function and structure, and the corresponding behaviour remain obscure. Insights into this matter might be obtained from studies assessing the biological base of memory acquisition and retention, and recovery from trauma in adulthood. In addition, also the visual system has proven to be an interesting model in the context of studying adult neuroplasticity [75].

Learn and retain memory in adulthood

'*Cells that fire together, wire together*'. Donald Hebb was one of the first neuroscientists describing what we today refer to as the result of Long-Term Potentiation (LTP) [76, 77], often defined as the physiological basis or '*cellular consolidation*' of memory [78, 79]. LTP is a very clear example of experience-dependent plasticity since it mediates the reconfiguration of intrinsic homeostatic properties of individual neurons by sensitizing synapses, but also triggers large-scale network-wide adaptations based on environmental input. Indeed recently, parallel electrophysiological and fMRI recordings have targeted the acute effects of (artificial) induction of LTP on long-range global functional connectivity in adult rats [80]. This study was the first to reliably detect the rapid effects of LTP by fMRI, a technique that allows investigating widespread activation patterns of entire networks using a whole-brain approach. Remarkably, comparing BOLD activation maps while stimulating the perforant path between rats before (control) and after (potentiated) induction of LTP, they noted a significant enlargement of the activated network recruiting more distantly connected brain areas. In the potentiated condition, the cluster displaying voxels activated by stimulation encompassed the entire hippocampal formation, i.e. hippocampus proper, subiculum and entorhinal cortex, also

extending to the hippocampus of the contralateral hemisphere and involving extrahippocampal brain areas such as the perirhinal cortex, prefrontal cortex, nucleus accumbens and the anterior olfactory nucleus (ipsilateral hemisphere) [80]. Especially the latter observations uncovered an entire network of increased functional recruitment possibly reflecting intensified functional connectivity, extending beyond previously established areas of involvement known from electrophysiology and molecular studies. A follow up study revealed the effects of different stimulation paradigms and, using high-resolution functional imaging, they were able to specify the specific sub-locations of LTP-mediated effects in the hippocampus [81] (Figure 3-1).

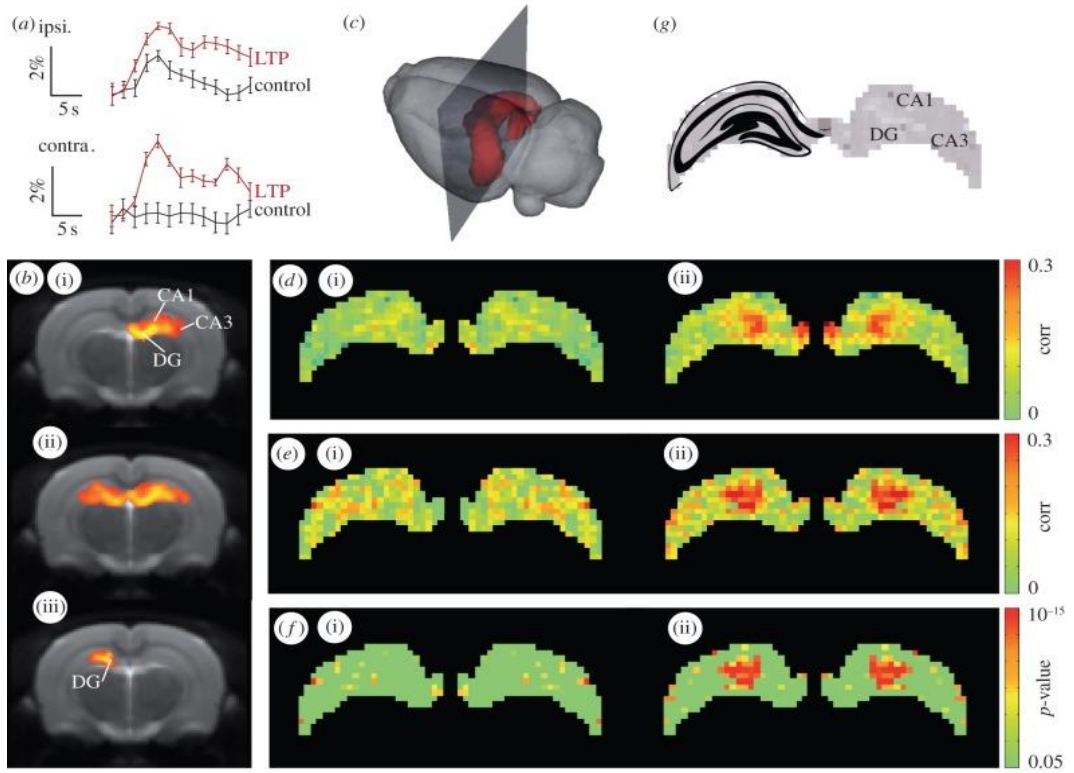

Figure 3-1: LTP elicits enhanced bilateral coupling detected by fMRI. (a) temporal evolution of the BOLD signal in the ipsi- and contralateral dorsal hippocampus before (black) and 3 h after induction of LTP (red). (b) Statistical maps illustrating voxels activated upon electrical stimulation pre (i) and post (ii) LTP induction (n=4, *p<0.001*). Statistical map highlighting the difference in activation when comparing fMRI maps before and after induction of LTP (*p<0.01*). Only the hippocampus is included in the analysis. (c) Three-dimensional reconstruction of the hippocampus and its relative position in the rat brain. (d) Group and (e) individual statistical maps indicating the cross-correlations of the BOLD-time courses before (i) and 3 h after (ii) induction of LTP. (f) Maps indicating significantly correlated voxels pre (i) and post (ii) induction of LTP. The colour code of the statistical significance and correlation coefficients can be found on the right. (g) Schematic legend of the hippocampal territories on a grey-scaled cross-correlation map. Reprinted from [81] with permission from The Philosophical Transactions of Royal Society of London, Series B Biological Sciences.

In addition to the functional repercussions of induction of LTP, also the local biochemical environment is affected. For example, LTP results in a modulation of pre- and post-synaptic strength mediated through neurotransmitters such as glutamate, and their receptors, e.g. NMDA-receptors. Moreover, a study in rats showed that LTP-like plasticity can only be successfully elicited after decreasing GABA levels in the motor cortex [82]. In theory, since both GABA and glutamate can be detected by *in vivo* spectroscopy, MRS might be able to detect LTP-mediated plasticity directly if it includes a sufficiently large brain area (partial volume effect).

Associative learning and conditioning

Besides tracing BOLD changes in response to LTP, fMRI has also been used intensively to visualize brain activation patterns over the course of associative learning, e.g. to expose the neural substrate tuned by eye-blink conditioning in rabbits [83]. The advantage of fMRI in this context is that it allows to evaluate the spatial location and possible hemispheric lateralization, magnitude and time course of BOLD activity across different stages. Evidence in favour of using small animals as a translational model to study mechanisms underlying associative learning is provided by a clinical study on human subjects where fMRI data was acquired while performing an associative memory training [84]. Interestingly, the observations could be replicated in mice [85]. Moreover, by studying CA3 NMDA receptor knock-out mice, Kent and colleagues could prove the involvement of NMDA receptors in the CA3 subregion of the hippocampus by showing an experience-dependent shift in hippocampal activity instigated by the learning task [85].

In addition to functional imaging, biochemical profiling has been used to study neuroplastic adaptations resulting from a learning task. Zhou and co-workers (2012) explored the use of MRS to assess acute and early effects of fear conditioning –model for post-traumatic stress disorder– on the brains of adult C57BL/6 mice. They reported a reduction in NAA, 1 day *post* conditioning in the hippocampus which persisted but slightly regressed throughout the first week *post* fear training. In addition, choline levels were lower the first day *post* conditioning, but this did not persist towards the 7 days' time point. In the cingulate cortex, only an acute reduction in NAA could be detected which did not last until one week *post* conditioning [86].

Motor and Spatial learning

Probably the most extensively investigated subtype of learning and memorization can be found in motor and spatial learning. In contrast to most conditioning paradigms, motor and spatial

learning are more difficult to assess by fMRI given the need for appropriate stimulation, the physical limitations of performing (complex) motor tasks in the MR scanner and the necessity to sedate animals during data acquisition (except for awake imaging after habituation training). Consequently, the impact of motor and/or spatial learning on microstructural remodelling of the brain has been studied extensively in both humans and animals [17, 30, 87-89], for review [90, 91]. In most cases, significant differences were found a few days or weeks after the motor training or learning paradigms had been completed. Indeed, most structural phenomena such as neurogenesis and network rearrangement are expected to be realized or at least detectable in the longer term. Sagi et al. (2012), however, succeeded in detecting acute experience-dependent microstructural remodelling of the hippocampus following spatial navigational learning [17]. Fascinatingly, they observed significant microstructural changes reflected in altered mean diffusivity (MD) values in human brains after only 2 hours of playing a virtual car race game and confirmed these observations in a rat study. Additional histological analyses of the hippocampal tissue of the rat brains displayed an upregulated synaptophysin immunoreactivity which is indicative of an increased number of synaptic vesicles, and revealed increased levels of BDNF. Since BDNF is commonly regarded as a marker for LTP [92], the authors hypothesized that changes in MD might be indicative of the neural substrate where LTP was triggered by the learning task. This was previously already proposed by [30] in a similar experimental setting, however, only combined MRI and electrophysiological measures can prove or disprove this statement [81]. BDNF and synaptic vesicles are expected to be responsible for only a minor contribution of the observed MD changes. The authors also found an increased GFAP immunoreactivity which suggests the active involvement of astrocytes. This might concern cell swelling and remodelling of glial processes that result in a change of volume of the intra- versus extracellular compartment. In addition, synaptogenesis, morphometric adaptations of axons, dendrites and glial processes, and alterations in cell body size are likely to take part in the biological correlate of the DTI parameter readout. Importantly, the magnitude of change in MD in the right parahippocampal tissue could be correlated to behavioural performance, i.e. task improvement is directly related to the change in tissue microarchitecture. Therefore, it leaves no surprise that intensive long-term training results in significant volume changes in these brain areas as previously observed by [93] and [94] in humans and rodents respectively. A related example investigating neuroplastic changes along the course of a single-food pellet reaching training in adult rats using *ex vivo* DTI, revealed

differences in FA and MD in several white matter fibre-containing structures, i.e. the cingulum, external capsule and parts of the corpus callosum in the hemisphere contralateral to the trained paw. The imaging findings were confirmed by *post mortem* histology testing for myelin. This paper was one of the first studies focusing on experience-dependent changes in white matter tracts instead of detecting alterations to volumes or microstructural reorganizations upon the acquisition of a particular motor task [95]. Another study aimed at finding rapid microstructural adaptations in response to a learning task was performed by the group of Wu (2013). Using voxel-based statistics, they found altered FA in the hippocampus, amygdala and cingulum as early as 1 hour and 1 day after fear conditioning [96]. These brain areas are known to be involved in processing of fearful experiences. Similar findings have been published in humans suffering post-traumatic stress disorder [97].

Also the acquisition of more advanced motor learning tasks has been examined thoroughly by *in vivo* imaging. Quallo and co-workers (2009) found that macaque monkeys displayed volume alterations in the superior temporal sulcus, the second somatosensory sulcus, intraparietal sulcus and lobule 5 of the cerebellar hemisphere (bilaterally) after learning to retrieve food rewards using a rake. Moreover, motor performance could be correlated to the extent of change observed on MRI in individual monkeys and the effects were more pronounced in the right hemisphere compared to the left [18]. A similar study was performed by Hihara et al. (2006) and described results of a tract tracing light microscopy analysis on the brains of adult monkeys after 3 weeks of tool-use training to retrieve food placed out of reach. Using anterograde tracers, they found differential connectivity originating from the temporo-parietal junction projecting to the intraparietal junction in trained monkeys compared to untrained controls, i.e. trained monkeys displayed a robust projection connecting both brain areas, whereas controls only showed a very weak connection. This observation involved the same brain areas as detected by *in vivo* voxel-based morphometry, suggesting that the tool-use training gave rise to strengthening of this sparse but existing pathway [98].

The inverse relationship between age and recovery from functional loss

The brains' ability to overcome injury is highest in childhood and adolescence but is not completely abolished towards adulthood [99]. Interesting in this context is the involvement of experience to promote rehabilitation, e.g. daily music listening to improve functional outcome after stroke [14, 100].

A remarkable feature characteristic to specific cases of brain or peripheral nervous system trauma can be found in paradoxical functional facilitation (PFF) when direct or indirect neural damage may result in the reinforcement of particular behavioural functions [101]. In general two main subtypes of PFF can be discerned, i.e. (i) restorative PFF, where after damage to an intact brain area improved or even normalized performance of a previously abnormal level of functioning can be found, e.g. the Sprague effect [102], and (ii) cross-modal plasticity, i.e. a coping mechanism of the brain where cortical circuitries previously encoding a particular skill or ability are re-assigned to process a new function after loss of the original one, e.g. after peripheral de-afferentiation or congenital blindness [103, 104]. Cross-modal plasticity has been thoroughly examined in blind subjects, where the onset of blindness, i.e. congenital, early or old age, strongly predicts the behavioural outcome (for review [104, 105]). Indeed, Voss (2013) discusses the existence of sensitive windows (similar to critical periods) during which compensatory changes might exert the largest effects, specifically focusing on insights obtained from investigations of impairments to the visual system [106]. Complementary to this review, Nahmani and Turrigiano, (2014) comprehensively list the similarities and dissimilarities in plasticity-related mechanisms in recovery from acute cortical trauma or ischemia in adulthood compared to neuroplasticity triggered by deprivation in early development. The authors explain that disinhibition is one of the primary mediators to release the brakes on cortical excitability and thus functional and structural plasticity, both in early as well as later life. They conclude that the capacity of the brain to '*functionally rewire*' is indeed strongly reliant on the maturational stage of the organism, and –in order to achieve a full understanding of the underlying neuroplastic mechanisms– combined multi-level assessments investigating both localized circuitry rewiring, expression of plasticity-related factors and behavioural tests assessing functional recovery need to be conducted. Especially since behavioural performance is the only reliable indicator of the functional success of the underlying neuroplastic adaptation [107].

Functional imaging techniques provide great advantage in evaluating the functional reallocation of cortical areas and cortical responsiveness to peripheral sensorimotor and/or cognitive stimulation. Indeed, Endo et al. (2007) showed a biphasic modulation of the BOLD response when comparing the acute versus long-term effects of complete thoracic spine transection in rats. The brain area activated upon stimulation partly invaded the adjacent sensory-deprived hind limb cortical territory (Figure 3-2). Moreover, the biphasic evolution of

the fMRI response to forelimb stimulation was echoed by enhanced gene expression of BDNF, NgR and LINGO-1, generally considered as neuroplasticity markers. When comparing their findings to previous reports, the authors concluded that the extent of cortical reorganization strongly depends on the type and severity of spinal cord injury [108]. However, since only adult animals were considered in this context, no assumptions on possible age-dependency could be made. In addition, fMRI upon visual stimulation has been used frequently to investigate population receptive field topographic maps both in humans [109] and animals [110].

Several other experimental models displaying cross-modal plasticity have been investigated using fMRI and resting state fMRI (rsfMRI) [111-114] or DTI to shed light on alterations in structural connectivity, e.g. [115, 116]. In addition, MEMRI is also an interesting tool to inspect cortical projection areas. Furthermore, the effects of stroke on the functional reorganization of the brain have been explored extensively [117]. Besides functional and structural imaging, the biochemical profile of cross-modal coping mechanisms following blindness have been researched exhaustively with MRS in both humans [118, 119] and animals [120].

The adaptive response of the brain to injury or trauma can be beneficial so that functionality can be (almost fully) regained, unfortunately however, in some cases neuroplasticity is maladaptive in that it triggers pathogenesis (for review we refer to the special issue of Neuroscience December 26, 2014 'Compensation Following Injury to the Adult Brain: Always for Good?'). Also in this field of research, MRI has proven to be a valuable non-invasive probe to trace the physiological fingerprint of pathology. A very well-known example in this context can be found in (acquired) epilepsy. Gröhn et al. (2011) reviews the use of combined MR measures to set up the pathological profile of disease ontogenesis and progression of epilepsy [121].

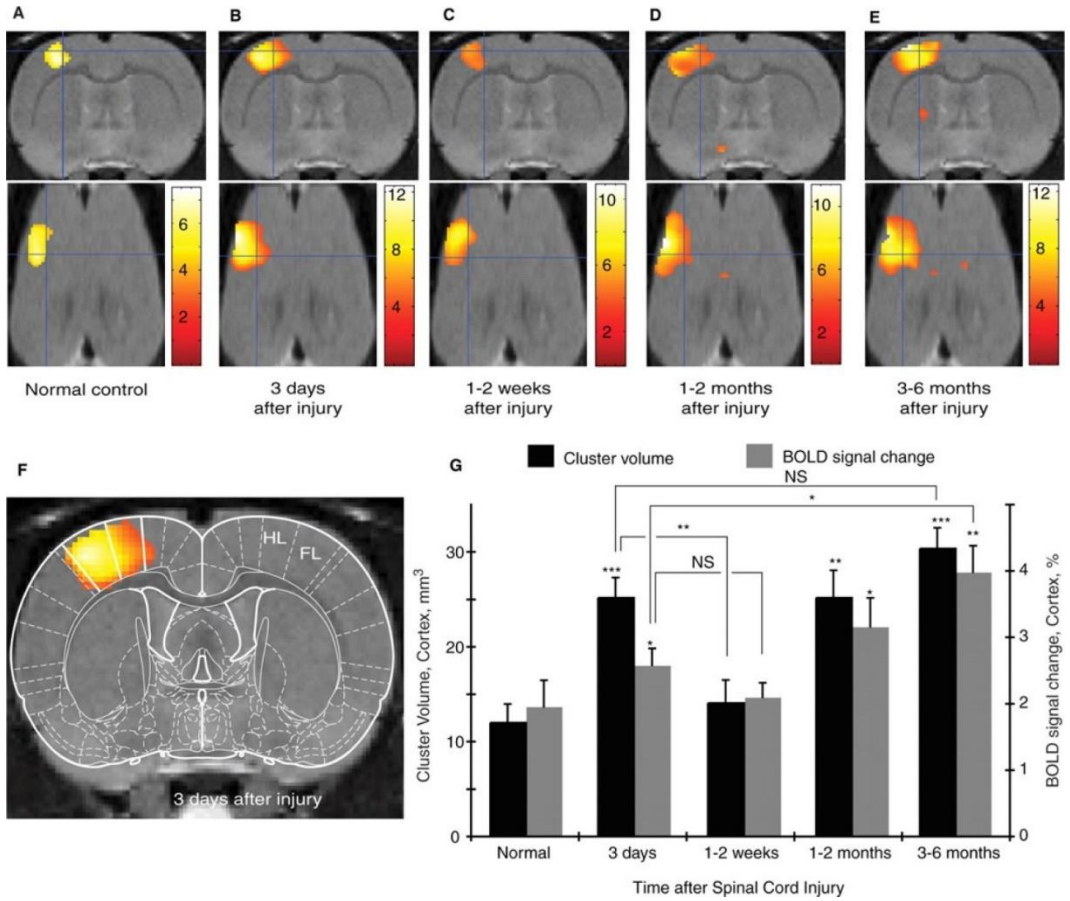

Figure 3-2: Temporal evolution of the fMRI activation of the primary sensory cortex upon contralateral forelimb stimulation after (complete) spinal cord transection. A: Cluster activated in control rats. B-E: Functional activation in injured animals at 3 days (B), 1-2 weeks (C), 1-2 months (D) and 3-6 months (E) post transection. The crosshair indicates exactly the same anatomical position in all panels. Interestingly, besides the 1-2 weeks post injury time point, all fMRI activation maps extend more caudal and medial compared to the control group. (F) Coronal slice illustrating the statistical map 3 days after spine transection overlaid on the Paxinos and Watson atlas indicating a medial but not lateral extension of the activated cluster. (HL: hind limb territory of primary somatosensory cortex; FL: forelimb territory) (G) Cluster volume and BOLD signal change (%) of activation in the primary somatosensory cortex at different time-points post transection compared to healthy controls (n = 12 rats per group). Data are represented as mean ± SEM, * $p < 0.05$; ** $p < 0.01$; *** $p < 0.001$; NS: non-significant. Reprinted from [108] with permission from Oxford University Press Journals.

For example, MEMRI hyper-intensities in the early stages after induction of *status epilepticus* have been correlated to mossy fibre sprouting in the dentate gyrus of the hippocampus [122], DTI revealed sites of axonal reorganization and myelin damage [123] where voxel-based processing of DTI datasets unveiled novel loci implicated in the pathogenic process [124], Arterial Spin Labelling (ASL) identified sites of hypo-/hyper-perfusion [125, 126], intravascular contrast agents shed light onto alterations in the vascular architecture [127] etc. Gröhn explains

that *in vivo* MRI has great potential in becoming a crucial tool for personalized medicine given its ability to infer disease ontogenesis and progression, which is of vital importance to evaluate individual rehabilitation programs and find novel targets for treatment [121].

3.2.2 Hormones are powerful modulators of brain structure and function

Hormones and brain plasticity are bi-directionally linked [128]. Mounting evidence can be found in favour of this statement. To name a few: (i) Hormones are indispensable during normal brain development and partly drive sexual differentiation; (ii) Neuroplasticity is dramatically down-regulated during adolescence towards adulthood, a period in life characterized by major fluctuations in hormonal homeostasis; (iii) Changing hormone levels during the menstrual cycle have been correlated to rapid structural [129, 130] and functional [131] neuroplastic adaptations (for review [132]); (iv) Animal studies have revealed the protective effect of oestrogens on age-associated cognitive decline related to neurodegeneration [133, 134]; and (v) The entire CNS is copiously sprinkled with hormone receptors and enzymes converting inactive pre-hormone molecules into their active counterpart, and vice versa.

Besides its well-known effects on behaviour, previous research on animals revealed sex hormone-mediated changes in gliagenesis, vasculature, neurogenesis and synaptic remodelling [135, 136]. Some of them occur very rapidly, e.g. a 32% decrease in synaptic density of hippocampal neurons 24 h after the onset of oestrus in rats [135], for a more recent review by the same lab we refer to [137]. Interestingly, voxel-based morphometry has been applied to explore the effects of hormones on the brains of menopausal women [138, 139] or the effect of the menstrual cycle on hippocampal morphology [140]. In addition, also the effects of altered testosterone [141] and thyroid [142] levels on the brain have been studied by *in vivo* imaging.

Not only mammals, but also songbirds have proven to be an extremely valuable model to study the effects of (sex) hormone treatments on structural brain anatomy and higher cognitive functioning, e.g. song-related contextual processing, both acutely and in the longer term, in ontogeny as well as more advanced life stages [143]. Songbirds are the living proof that the environment, hormonal status and behaviour can have a huge impact on the overall organization of the brain, both in terms of function and structure. This, however, will be reviewed in Chapter 4.

3.2.3 Physical activity and environmental complexity promote neuroplasticity

The intricate balance between Hebbian and homeostatic plasticity can be easily disrupted by activity or experience. Indeed, substantial clinical evidence illustrates the flexibility of the adult brain upon physical or cognitive challenges, or –by combining both– the enhancement of cognitive functioning upon physical exercise [144]. This not only relates to healthy subjects, patients suffering stroke or other neurotrauma and specific neurodegenerative disorders benefit significantly from physical workout and active participation to cognitive tasks [145]. Also in animal studies, the link between physical exercise and performance in spatial learning and memory tests has been demonstrated extensively both in health and disease [146] and has shown great resemblance in mechanistic pathways between animal and human plasticity [147]. A popular model used to mimic increased physical and cognitive challenges in a research environment is found in housing animals in an enriched environment, i.e. accommodate animals in large cages equipped with species-specific needs such as running wheels, labyrinths etc. of which the composition and arrangement within the cage is changed regularly [148]. Environmental enrichment promotes physical workout, provides more complexity as animals might need to overcome specific challenges to forage food or find its way back through the obstacles and encourages social interaction. Berardi and co-workers (2015) nicely review how environmental enrichment affects molecular plasticity-related (epi)genetic modulators, based on research dedicated mainly to the visual system [40].

3.2.3.1 Plasticity beyond critical periods: activity and experience are still able to shape the adult brain to a certain extent

In healthy animals, environmental enrichment and complex training paradigms have often been related to improved learning, memory and overall cognitive performance [149-151]. Interestingly, Sholz and colleagues (2015) used MEMRI –to improve anatomical contrast– to inspect macrostructural brain plasticity upon housing adult mice in an enriched environment. Previous studies reported that after around three weeks of enrichment neuroplastic adaptations are established and can be observed [149, 150]. Therefore, Scholz acquired manganese-enhanced anatomical datasets before, after three weeks of enriched housing conditions and after 4 weeks of enrichment combined with one week of Barnes maze training (to test spatial learning and memory). In addition, to evaluate whether a change of environment evokes acutely detectable brain changes, they performed high-resolution *ex vivo*

measurements of mouse brains which experienced 24h of enrichment (without application of $MnCl_2$). Using deformation-based morphometry, they found volumetric changes in the hippocampal formation and sensorimotor cortices after three weeks of enrichment and could observe a similar –but not significant– trend in the acute phase. The volumetric differences found in this study clearly show the malleability of the brain to experiencing a more complex and stimulating environment. The involvement of the hippocampus in learning and memory associated with navigation, exploration and locomotion, is in line with another study where Morris Water Maze training revealed differences in apparent diffusion coefficient of the hippocampus [30]. When relating housing conditions to performance in the Barnes maze, Scholz et al. confirmed that mice housed in a more stimulating environment learned the location of the escape box faster, but no differences in memory (during the probe trial) could be detected between the stimulated and control group [152]. Connected to this study, the same research group used high-resolution *ex vivo* 3-dimensional datasets and deformation-based morphometry to evaluate rapid structural modifications evoked by different maze learning procedures each mimicking a specific type of learning [94], and by rotarod training [153].

Biedermann and colleagues (2012) used high-resolution T_2-weighted datasets to inspect local volumetric alterations combined with MRS spectra including information on GABA and glutamate levels. Interestingly, they observed an inverse relationship between hippocampal volume (increase upon voluntary wheel running) and glutamate concentration (decrease) pointing towards the active involvement of the glutamatergic system in aerobic exercise-induced neuroplasticity [15] (Figure 3-3). This training-induced alteration in metabolic profile was also found in a previous study in humans where they detected acutely increased Glx (combined glutamate and glutamine signal) in the visual cortex after 10 min of vigorous exercise [154]. Other studies in humans used MRS to deduce metabolic changes resulting from endurance-training in middle-aged subjects [155], fast GABA level alterations were observed in the sensorimotor cortex due to motor-learning [156] and increased NAA (relative to creatine and choline) levels in the left posterior hippocampus related to rote learning [157], etc.

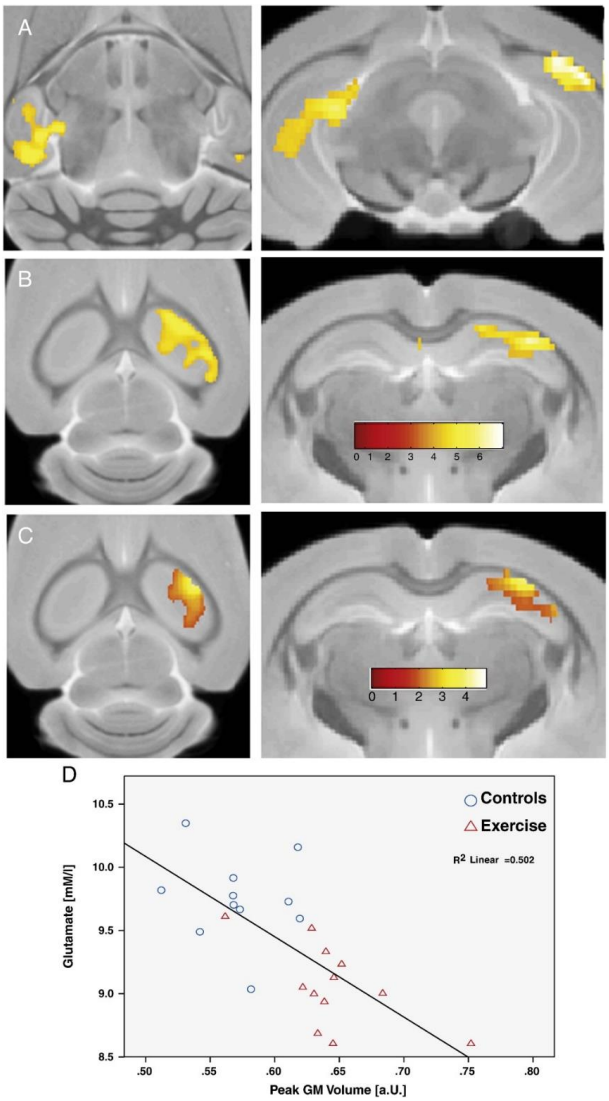

Figure 3-3: Results of voxel-based morphometric analysis comparing exercising and sedentary mice, and correlation of morphometric results to Glutamate levels as detected by MRS obtained from the right hippocampus. (A-B) Statistical map indicating clusters where increased grey matter was found co-localized with the left and right hippocampus ($p < 0.001$ uncorrected, 200 voxels cluster size). (C) Cluster in the hippocampus which is significantly negatively correlated with Glu levels. The colour-bars show the T-values of the statistical tests. (D) Glutamate levels represented in function of mean volume change in both sedentary and running mice. Reprinted from [15] with permission from Elsevier.

3.2.3.2 Activity-induced neuroplasticity to slow down disease progression or facilitate recovery

The beneficial effects of environmental enrichment on neurodegenerative disorders has been described in Huntington's [158, 159], Parkinson's [160], Alzheimer's [161] disease etc. Nithianantharajah and colleagues (2006) and Svensson et al. (2014) nicely review the effects of

physical exercise on disease progression, inflammation, behaviour etc. in neurodegenerative disorders, concluding to what extent preclinical research involving animal models can be translated to the human brain [149, 162]. A particularly interesting preclinical example can be found in a (preliminary) study by Little et al. (2012). Based on rsfMRI measures, they found an increased functional connectivity between CA1 and cortical areas when housing transgenic mice in environmental enriched conditions [163]. These findings could be linked to previously established results revealing increased hippocampal neurogenesis under similar experimental settings using a different transgenic mouse model for Alzheimer pathology [164]. Furthermore, Golub and co-workers (2011) showed that mice suffering post-traumatic stress disorder displayed a volume reduction of the left hippocampus and right amygdala. When the same stressor was applied in mice housed in a more stimulating environment, both a change in hippocampal volume and fear-related behaviour could be observed. The authors concluded that environmental enrichment counteracted the post-traumatic volume loss of the hippocampus and led to a decrease in contextual fear and arousal compared to traumatized mice kept in standard housing conditions.

Interestingly, the timing of enrichment, i.e. before, after or continuous, seemed to have similar effects on the behaviour, however, enrichment after foot shock appeared to be more effective in inhibiting hippocampal, but not amygdaloid, volume loss. In order to gain a more extensive understanding of the mechanisms resulting in the structural findings, Golub and colleagues performed *post mortem* ultramicroscopy to validate hippocampal volume changes, and Western Blotting tests to assess GAP43 (Growth Associated Protein 43) expression levels in the hippocampus and cerebellum. GAP43 is an axonal plasticity marker localized in the presynaptic terminal of axons and linked to neurite outgrowth. They found a reduction in hippocampal GAP43 expression after experiencing a foot shock and an increase in hippocampal GAP43 expression in mice housed in a stimulating environment greatly resembling the MRI findings. Interestingly, up-and down-regulation of GAP43 expression points to a respective pruning and strengthening of neuronal interconnectivity in response to traumatizing or complex stimulating experiences and is very likely part of the biological mechanisms responsible for the observed volume differences [165]. Likewise, Zhang (2014) and He (2014) found independently that treadmill pre-training reduced cerebral oedema in case of ischemic stroke. They hypothesized that it was probably partially instigated by improved mitochondrial function [166] and the

down-regulation of aquaporin 4 [167]. In addition, Jenks et al., (2013) reported improved spatial learning, memory performance and sociability in a rat model displaying severe malformations in cortical development, when the rat pups were raised in a maximally stimulating environment or allowed increased training time. Interestingly, after environmental enrichment, both control and cortical malformation groups outperformed the groups lacking a stimulating environment [168].

3.2.3.3 Role of the Vasculature

Aerobic exercise enhances blood flow. Consequently, the biological base responsible for the beneficial effects of physical exercise on neuroplasticity and cognition might be partially found in its effects on the vasculature. Indeed, Mariotti and co-workers (2014) tested the effect of forced mild physical training (treadmill running) in 25 month old mice. The old mice underwent imaging sessions before and after training during which multislice anatomical datasets, T_2 maps and contrast-enhanced relative Cerebral Blood Volume (rCBV) scans were acquired to test for resp. volumetry, microstructural rearrangements and the assessment of relative blood volume. They found a significant effect of training on rCBV in the old mice, but no differences in cortical thickness measured at the hippocampus and motor cortex, nor in relaxation properties reflecting water distribution, were detected. These observations suggest that mild aerobic exercise can induce regionally specific changes in perfusion (similar to [169]), without causing oedema or detectable volume changes in motor cortex and hippocampus. Interestingly, when testosterone was administered weekly during the entire motor training period, no additional differences were observed compared to the training group [170]. This finding excluded the additional effect of exogenous testosterone on activity-induced increases in cerebral perfusion as was first hypothesized. Likewise, a study in rhesus monkeys revealed an inverse relation between CBV and age and a positive correlation between CBV and memory performance in a delayed nonmatching-to-sample task. Interestingly, both effects were strictly confined to the dentate gyrus of the hippocampus. This indicates that non-neuronal factors that take part in neuroplasticity also behave differently in an age- and regionally specific manner.

To exclude biologically irrelevant observations due to age-related changes in biophysical properties of the vasculature which might obscure the actual biological effect, and to account for the fact that hemodynamic imaging only indirectly relates to brain function and metabolism, a parallel *in situ* hybridization (ISH) experiment was performed in rats. Arc –immediately early

gene that becomes upregulated in neurons that participate to a specific behaviour– RNA expression was evaluated in young, middle-aged and old rats after being briefly exposed to a novel environment (2 x 5 min). Interestingly, again a correlation between the number of Arc-positive cells (activated upon experiencing novel environment) and age could be observed exclusively in the dentate gyrus of the hippocampus. They concluded that the dentate gyrus is most significantly affected by aging and might be partially responsible for cognitive impairment related to advanced age [171]. Based on these observations, Blau and colleagues (2012) explored the presence of a link between age-related deficits in LTP and changes in vasculature in healthy rats, assessing both blood flow and blood-brain barrier (BBB) permeability.

Using a combination of *in vivo* MRI techniques, histology and flow cytometry of hippocampal tissue, they found a negative correlation between T_2 relaxation time, activated microglia expressing CD11b and CD68 mRNA and the ability to sustain LTP in the hippocampus, together with an age-related decrease in cerebral perfusion and increased BBB permeability. They hypothesized that reduced cerebral blood flow (and thus lowered tissue oxygenation) and impaired BBB permeability might destabilize local tissue homeostasis, which in combination with deregulated microglia may be a crucial determinant in sustaining neuro-inflammatory activity affecting synaptic functioning and the resulting cognitive decline [172].

3.2.3.4 Role of Neurogenesis

Numerous studies revealed an up-regulation or increased survival of newly generated neurons in response to physical exercise [31, 173], complex environmental stimulation [174, 175], and after mastering a learning task such as eye-blink conditioning [176], etc. Moreover, both in humans and rodents it has been shown that hormones, e.g. oestrogen and progestin [177, 178], promote neurogenesis and are linked to improved hippocampal-dependent learning and cognitive performance. A review by Jessberger and Gage (2014) discusses research dedicated to adult neurogenesis performed during the last few decades including the similarities and dissimilarities between animal-based research and clinical investigation, current methods to assess neurogenesis *in vivo* in the adult rodent and human brain, the interplay between neurogenesis and neuroplasticity, and the cellular and molecular mechanisms in control of adult neurogenesis [179].

In order to detect neurogenesis and especially the migration pattern of newly generated cells longitudinally in the living brain, the use of different non-invasive imaging tools have been

tested *including* bioluminescence, PET and MRI-based methods such as MRI reporter genes and iron oxide particles (for review: [180]). Most in vivo imaging tools label stem and/or progenitor cells derived from the subventricular zone and trace their travel along the rostral migration stream towards the olfactory bulb. In contrast, neural progenitor cells originating from the dentate gyrus migrate only a very short distance to the subgranular zone of the hippocampus. Unfortunately, this falls far beyond the accuracy of in vivo MRI or PET [181].

Direct labelling of stem and/or progenitor cells cannot be applied in all experimental designs which illustrates the need for indirect in vivo measures of neurogenesis. For *example,* Manganas et al. (2007) suggested the 1.28 ppm peak to be a biomarker for neurogenesis [182]. Follow up studies, however, found that the spectroscopic signal (1.28 ppm peak) correlated more to the presence of mobile lipids droplets within cells and apoptosis regardless of the cell type [183]. Therefore, the 1.28 ppm peak might reflect neurogenic niches rather than echoing neurogenesis per se [180]. Pereira et al. (2007) showed a positive link between neurogenesis and an increased cerebral blood volume (CBV) in the dentate gyrus of the hippocampus, the brain area most prone to activity-induced neurogenesis, and confirmed this finding by *post mortem* histology staining for BrdU (neurogenesis). Moreover they also found similar results in a parallel study on humans, where the increased CBV in the hippocampus could be correlated to both improved cardiopulmonary and cognitive function [169]. Other *post mortem* investigations confirmed neurogenesis as major factor underlying *in vivo* detected changes in grey matter volume in response to motor training [15]. Interestingly, Fuss and colleagues performed *in vivo* volumetric imaging and deduced the possible involvement of neurogenesis as underlying effect mediating hippocampal volume increases upon physical exercise by the experimental design, i.e. focal irradiation of the hippocampal formation blocks neurogenesis. Irradiated mice failed to show hippocampal volume increases due to physical exercise compared to non-irradiated control mice [184]. A different study by the same group evaluated the effects of voluntary wheel running on adult mice with and without focal irradiation of the hippocampus to interfere with local adult neurogenesis, and performed regressive analyses between volumetric MRI measurements and histological investigations testing for neurogenesis, proliferating and pynotic cells, blood vessel density and arborisation, glial cells, microglia, neuronal activation. They found that irradiated mice that had access to the running wheel did not show any differences in histological markers compared to the sedentary non-irradiated group. The sham-irradiated running group displayed higher grey matter volume

affecting the entire hippocampus compared to all other experimental groups. Interestingly, by utilizing a regression model testing for a relationship between whole hippocampal volume and the histological parameters, DCX-labelled new-born neurons correlated best and were most plausibly underlying the activity-dependent hippocampal volume increase [15].

However, one should note that indirect measures lack specificity and can only be held partially responsible for the underlying biology. For example, volumetric changes might be attributable by cell swelling and/or infiltration of glia cells, both of which are often more likely to occur. The location and time course of these changes can also be indicative of the observed changes, e.g. cell swelling can take place acutely, whereas neurogenesis and migration of newly generated cells can occupy days to weeks.

3.3 CONCLUSION

Using invasive methods, several mechanisms directing neuroplastic responses upon experience, training or treatment are unmasked which led to the identification of general principles (excitation/inhibition balance etc.), major factors (GABA, BDNF etc.) and genetic elements (Lynx-1, NogoR etc.). However, information is still relatively fragmented and generalization between different systems is suggested but still not fully proven. More in depth insights can only be realized by carefully designed animal experiments where *in vivo* imaging can guide in-depth *ex vivo* methods such as histology and genetic testing to decipher the involvement of and interaction between crucial mediators among different systems –ranging from basic sensorimotor to higher cognitive skills– and different species. Numerous histological methods and localized punching techniques combined with highly sensitive molecular assays allow to zoom in on the (epi-) genetic background driving the observed changes in highly localized brain niches. This strategy allows the establishment of cause-consequence relationships describing links between systems which might uncover targets to '*unlock the brain*' [28].

Still, this will be a challenging quest since many internal and external factors are able to influence the neuroplastic outcome. For example, the menstrual cycle affects the (micro-) structure of the brain, small differences in early age significantly interfere with the outcome of specific behavioural tests etc. This all stresses the need to carefully control the experimental conditions. Moreover, ample studies have illustrated that timing is crucial. This not only relates

to critical period plasticity in ontogeny, but also to the brain's adaptability following brain injury or to the effects of physical exercise on cognitive performance. Understanding the temporal profile of neuroplastic changes along the acquisition of specific skills over different training sessions or *post* trauma requires non-invasive translational imaging tools which allow to dynamically map functional, structural and metabolical events in the same subject. Indeed, a few exemplary studies have focused on the temporal progression of neuroplastic changes directly related to a specific training or learning paradigm [185-188], for review [189]. However, more research is still highly necessary and will lead to fundamental insights into the dynamics of learning and memory, but will also shed light on how to predict motor outcome or improvements in behavioural performance after a specific learning paradigm [54, 87] which is of crucial importance when, e.g. choosing specific rehabilitation strategies after brain injury [126]. Moreover, additional information on the behavioural outcome of this subject is the only reliable measure to 'quantify' the success of rehabilitation programs or learning paradigms. Fascinatingly, several imaging studies have been able to correlate the behavioural test scores to specific MRI parameter readouts. These findings illustrate the power of *in vivo* imaging to effectively uncover the neural substrate encoding specific skills responsible for specific behavioural functions. Many studies have already shown the added value of MRI in neuroplasticity research, however, still many opportunities and possibilities to investigate the brains' response upon change using MRI remain relatively unexplored. Combining several MRI contrasts might help in establishing a detailed profile of functional, structural and biochemical alterations which leads to a more complete picture of the underlying biology responsible for a specific behavioural readout. In addition, having this information, additional measures can be chosen more judiciously.

To conclude, with this review we hope to convince you that (small animal) MRI enables a powerful top-down imaging-guided research strategy in which a spatio-temporal profile of neuroplastic adaptations related to specific behavioural events can be targeted with more localized invasive methods which will lead to the disentanglement of the observed neuroplastic events up to the molecular level and will eventually deepen our understanding of human brain functioning.

ACKNOWLEDGMENTS

This research was supported by grants from the Research Foundation—Flanders (FWO, Project

No. G030213N and G044311N), the Hercules Foundation (Grant No. AUHA0012), Concerted Research Actions (GOA Funding) from the University of Antwerp and Interuniversity Attraction Poles (IAP) ('PLASTOCINE': P7/17) to AVdL. JH is a PhD student supported by the University of Antwerp. GDG is a Postdoctoral Fellow of the Research Foundation-Flanders (FWO).

REFERENCES

1. Draganski, B. and A. May, *Training-induced structural changes in the adult human brain.* Behavioural Brain Research, 2008. **192**(1): p. 137-142.
2. Niccolini, F. and M. Politis, *Neuroimaging in Huntington's disease.* World Journal of Radiology, 2014. **6**(6): p. 301-312.
3. McConathy, J. and Y.I. Sheline, *Imaging Biomarkers Associated With Cognitive Decline: A Review.* Biological Psychiatry, 2015. **77**(8): p. 685-692.
4. Frasnelli, J., et al., *Crossmodal plasticity in sensory loss*. Vol. 191. 2011. 233-49.
5. Dedovic, K., et al., *The Montreal Imaging Stress Task: using functional imaging to investigate the effects of perceiving and processing psychosocial stress in the human brain.* Journal of Psychiatry and Neuroscience, 2005. **30**(5): p. 319-325.
6. O'Doherty, D.C.M., et al., *A systematic review and meta-analysis of magnetic resonance imaging measurement of structural volumes in posttraumatic stress disorder.* Psychiatry Research: Neuroimaging.
7. Brabant, G., et al., *Visualizing hormone actions in the brain.* Trends in Endocrinology & Metabolism, 2011. **22**(5): p. 153-163.
8. Moulton, E.A., et al., *The cerebellum and addiction: insights gained from neuroimaging research.* Addiction Biology, 2014. **19**(3): p. 317-331.
9. Fowler, J.S., et al., *Imaging the Addicted Human Brain.* Science & Practice Perspectives, 2007. **3**(2): p. 4-16.
10. Parvaz, M.A., et al., *Neuroimaging for drug addiction and related behaviors.* Reviews in the neurosciences, 2011. **22**(6): p. 609-624.
11. Salo, R. and C. Fassbender, *Structural, Functional and Spectroscopic MRI Studies of Methamphetamine Addiction*, in *Brain Imaging in Behavioral Neuroscience*, C.S. Carter and J.W. Dalley, Editors. 2012, Springer Berlin Heidelberg. p. 321-364.
12. Viswanath, H., et al., *Alterations in Interhemispheric Functional and Anatomical Connectivity are Associated with Tobacco Smoking in Humans.* Frontiers in Human Neuroscience, 2015. **9**.
13. Lockhart, S. and C. DeCarli, *Structural Imaging Measures of Brain Aging.* Neuropsychology Review, 2014. **24**(3): p. 271-289.
14. Särkämö, T., et al., *Structural changes induced by daily music listening in the recovering brain after middle cerebral artery stroke: a voxel-based morphometry study.* Frontiers in Human Neuroscience, 2014. **8**.
15. Biedermann, S., et al., *In vivo voxel based morphometry: Detection of increased hippocampal volume and decreased glutamate levels in exercising mice.* NeuroImage, 2012. **61**(4): p. 1206-1212.
16. Sumiyoshi, A., et al., *Regional gray matter volume increases following 7 days of voluntary wheel running exercise: A longitudinal VBM study in rats.* NeuroImage, 2014. **98**(0): p. 82-90.
17. Sagi, Y., et al., *Learning in the Fast Lane: New Insights into Neuroplasticity.* Neuron, 2012. **73**(6): p. 1195-1203.

18. Quallo, M.M., et al., *Gray and white matter changes associated with tool-use learning in macaque monkeys.* Proceedings of the National Academy of Sciences, 2009. **106**(43): p. 18379-18384.
19. Vorhees, C.V. and M.T. Williams, *Assessing Spatial Learning and Memory in Rodents.* ILAR Journal, 2014. **55**(2): p. 310-332.
20. Aguado, L., *Neuroscience of Pavlovian Conditioning: A Brief Review.* The Spanish Journal of Psychology, 2003. **6**(02): p. 155-167.
21. Delgado, M.R., A. Olsson, and E.A. Phelps, *Extending animal models of fear conditioning to humans.* Biological Psychology, 2006. **73**(1): p. 39-48.
22. Van der Linden, A., et al., *Current status of functional MRI on small animals: application to physiology, pathophysiology, and cognition.* NMR in Biomedicine, 2007. **20**(5): p. 522-545.
23. Van der Linden, A., et al., *MRI in small brains displaying extensive plasticity.* Trends in Neurosciences, 2009. **32**(5): p. 257-266.
24. Pelled, G., *MRI of Neuronal Plasticity in Rodent Models*, in *Magnetic Resonance Neuroimaging*, M. Modo and J.W.M. Bulte, Editors. 2011, Humana Press. p. 567-578.
25. Fledelius, H.C., et al., *Human parallels to experimental myopia? A literature review on visual deprivation.* Acta Ophthalmologica, 2014: p. n/a-n/a.
26. Svirsky, M.A., S.W. Teoh, and H. Neuburger, *Development of Language and Speech Perception in Congenitally, Profoundly Deaf Children as a Function of Age at Cochlear Implantation.* Audiology and Neurotology, 2004. **9**(4): p. 224-233.
27. Kral, A., *Auditory critical periods: A review from system's perspective.* Neuroscience, 2013. **247**(0): p. 117-133.
28. Jon, J.B., *Neurodevelopment: unlocking the brain.* Nature, 2012. **487**(7405): p. 24-26.
29. Bengtsson, S.L., et al., *Extensive piano practicing has regionally specific effects on white matter development.* Nat Neurosci, 2005. **8**(9): p. 1148-1150.
30. Blumenfeld-Katzir, T., et al., *Diffusion MRI of Structural Brain Plasticity Induced by a Learning and Memory Task.* PLoS ONE, 2011. **6**(6): p. e20678.
31. van Praag, H., et al., *Exercise Enhances Learning and Hippocampal Neurogenesis in Aged Mice.* The Journal of Neuroscience, 2005. **25**(38): p. 8680-8685.
32. Walf, A.A. and C.A. Frye, *The use of the elevated plus maze as an assay of anxiety-related behavior in rodents.* Nature protocols, 2007. **2**(2): p. 322-328.
33. Albani, S.H., et al., *Behavior in the elevated plus maze is differentially affected by testing conditions in rats under and over three weeks of age.* Frontiers in Behavioral Neuroscience, 2015. **9**.
34. Bolhuis, J.J. and R.C. Honey, *Imprinting, learning and development: from behaviour to brain and back.* Trends in Neurosciences, 1998. **21**(7): p. 306-311.
35. McCabe, B.J., *Imprinting.* Wiley Interdisciplinary Reviews: Cognitive Science, 2013. **4**(4): p. 375-390.
36. Hensch, T.K., *CRITICAL PERIOD REGULATION.* Annual Review of Neuroscience, 2004. **27**(1): p. 549-579.
37. Knudsen, E.I., *Sensitive Periods in the Development of the Brain and Behavior.* Journal of Cognitive Neuroscience, 2004. **16**(8): p. 1412-1425.
38. Levelt, C.N. and M. Hübener, *Critical-Period Plasticity in the Visual Cortex.* Annual Review of Neuroscience, 2012. **35**(1): p. 309-330.
39. Erzurumlu, R.S. and P. Gaspar, *Development and critical period plasticity of the barrel cortex.* European Journal of Neuroscience, 2012. **35**(10): p. 1540-1553.
40. Berardi, N., A. Sale, and L. Maffei, *Brain structural and functional development: genetics and experience.* Developmental Medicine & Child Neurology, 2015. **57**: p. 4-9.

41. Tropea, D., A. Van Wart, and M. Sur, *Molecular mechanisms of experience-dependent plasticity in visual cortex.* Philosophical Transactions of the Royal Society B: Biological Sciences, 2009. **364**(1515): p. 341-355.
42. Nabel, E.M. and H. Morishita, *Regulating Critical Period Plasticity: Insight from the Visual System to Fear Circuitry for Therapeutic Interventions.* Frontiers in Psychiatry, 2013. **4**: p. 146.
43. Fagiolini, M., C.L. Jensen, and F.A. Champagne, *Epigenetic influences on brain development and plasticity.* Current Opinion in Neurobiology, 2009. **19**(2): p. 207-212.
44. Jaime, F.O., et al., *Deafferentation-Induced Plasticity of Visual Callosal Connections: Predicting Critical Periods and Analyzing Cortical Abnormalities Using Diffusion Tensor Imaging.* Neural Plasticity, 2012. **2012**.
45. Chan, K.C., et al., *In vivo evaluation of retinal and callosal projections in early postnatal development and plasticity using manganese-enhanced MRI and diffusion tensor imaging.* NeuroImage, 2012. **59**(3): p. 2274-2283.
46. Berretta, S., et al., *Losing the sugar coating: Potential impact of perineuronal net abnormalities on interneurons in schizophrenia.* Schizophrenia Research, 2015(0).
47. Chow, A.M., et al., *Metabolic changes in visual cortex of neonatal monocular enucleated rat: a proton magnetic resonance spectroscopy study.* International Journal of Developmental Neuroscience, 2011. **29**(1): p. 25-30.
48. Ribak, C.E. and R.T. Robertson, *Effects of neonatal monocular enucleation on the number of GAD-positive puncta in rat visual cortex.* Experimental Brain Research, 1986. **62**(1): p. 203-206.
49. Robertson, R.T., et al., *Neonatal enucleations reduce specific activity of acetylcholinesterase but not choline acetyltransferase in developing rat visual cortex.* Developmental Brain Research, 1988. **39**(2): p. 298-302.
50. Ben-Ari, Y., et al., *The GABA Excitatory/Inhibitory Shift in Brain Maturation and Neurological Disorders.* The Neuroscientist, 2012. **18**(5): p. 467-486.
51. Deidda, G., et al., *Early depolarizing GABA controls critical-period plasticity in the rat visual cortex.* Nat Neurosci, 2015. **18**(1): p. 87-96.
52. Stagg, C.J., *Magnetic Resonance Spectroscopy as a tool to study the role of GABA in motor-cortical plasticity.* NeuroImage, 2014. **86**(0): p. 19-27.
53. Pugh, K.R., et al., *The relationship between phonological and auditory processing and brain organization in beginning readers.* Brain and language, 2013. **125**(2): p. 173-183.
54. Pugh, K.R., et al., *Glutamate and Choline Levels Predict Individual Differences in Reading Ability in Emergent Readers.* The Journal of Neuroscience, 2014. **34**(11): p. 4082-4089.
55. Doupe, A.J. and P.K. Kuhl, *BIRDSONG AND HUMAN SPEECH: Common Themes and Mechanisms.* Annual Review of Neuroscience, 1999. **22**(1): p. 567-631.
56. Balmer, T.S., et al., *Modulation of Perineuronal Nets and Parvalbumin with Developmental Song Learning.* The Journal of Neuroscience, 2009. **29**(41): p. 12878-12885.
57. Feher, O., et al., *De novo establishment of wild-type song culture in the zebra finch.* Nature, 2009. **459**(7246): p. 564-568.
58. Meyer, C.E., E. Boroda, and T.A. Nick, *Sexually dimorphic perineuronal net expression in the songbird.* Basal Ganglia, 2014. **3**(4): p. 229-237.
59. Cornez, G., et al., *Anatomically Discrete Sex Differences in Neuroplasticity in Zebra Finches as Reflected by Perineuronal Nets.* PLoS ONE, 2015. **10**(4): p. e0123199.
60. Johnston, M.V., *Plasticity in the developing brain: Implications for rehabilitation.* Developmental Disabilities Research Reviews, 2009. **15**(2): p. 94-101.
61. Johnston, M.V., *Clinical disorders of brain plasticity.* Brain and Development, 2004. **26**(2): p. 73-80.

62. Berger, J.M., T.T. Rohn, and J.T. Oxford, *Autism as the Early Closure of a Neuroplastic Critical Period Normally Seen in Adolescence*. Vol. 1. 2013.
63. Fernandez, F. and C.C. Garner, *Over-inhibition: a model for developmental intellectual disability.* Trends in Neurosciences, 2007. **30**(10): p. 497-503.
64. Bitanihirwe, B.K.Y. and T.-U.W. Woo, *Perineuronal nets and schizophrenia: The importance of neuronal coatings.* Neuroscience & Biobehavioral Reviews, 2014. **45**(0): p. 85-99.
65. Morishita, H., et al., *Interneuron epigenomes during the critical period of cortical plasticity: Implications for schizophrenia.* Neurobiology of Learning and Memory, (0).
66. Coghlan, S., et al., *GABA system dysfunction in autism and related disorders: From synapse to symptoms.* Neuroscience & Biobehavioral Reviews, 2012. **36**(9): p. 2044-2055.
67. Kim, H., et al., *Impaired Critical Period Plasticity in Primary Auditory Cortex of Fragile X Model Mice.* The Journal of Neuroscience, 2013. **33**(40): p. 15686-15692.
68. Bengoetxea, H., et al., *Enriched and Deprived Sensory Experience Induces Structural Changes and Rewires Connectivity during the Postnatal Development of the Brain.* Neural Plasticity, 2012. **2012**: p. 305693.
69. Fromkin, V., et al., *The development of language in genie: a case of language acquisition beyond the "critical period".* Brain and Language, 1974. **1**(1): p. 81-107.
70. Berardi, N., T. Pizzorusso, and L. Maffei, *Critical periods during sensory development.* Current Opinion in Neurobiology, 2000. **10**(1): p. 138-145.
71. Bogart, S.L., et al., *Different early rearing experiences have long-term effects on cortical organization in captive chimpanzees (Pan troglodytes).* Developmental Science, 2014. **17**(2): p. 161-174.
72. Vaiserman, A.M., *Epigenetic programming by early-life stress: Evidence from human populations.* Developmental Dynamics, 2015. **244**(3): p. 254-265.
73. Gudsnuk, K. and F.A. Champagne, *Epigenetic Influence of Stress and the Social Environment.* ILAR Journal, 2012. **53**(3-4): p. 279-288.
74. Yin, J. and Q. Yuan, *Structural homeostasis in the nervous system: A balancing act for wiring plasticity and stability.* Frontiers in Cellular Neuroscience, 2015. **8**.
75. Wandell, B.A. and S.M. Smirnakis, *Plasticity and stability of visual field maps in adult primary visual cortex.* Nat Rev Neurosci, 2009. **10**(12): p. 873-884.
76. Hebb, D., *The Organization of Behavior: A Neuropsychological Theory*. 1949: Wiley.
77. Bliss, T.V.P. and T. Lømo, *Long-lasting potentiation of synaptic transmission in the dentate area of the anaesthetized rabbit following stimulation of the perforant path.* The Journal of Physiology, 1973. **232**(2): p. 331-356.
78. LYNCH, M.A., *Long-Term Potentiation and Memory*. Vol. 84. 2004. 87-136.
79. Mednick, S.C., et al., *An opportunistic theory of cellular and systems consolidation.* Trends in neurosciences, 2011. **34**(10): p. 504-514.
80. Canals, S., et al., *Functional MRI Evidence for LTP-Induced Neural Network Reorganization.* Current Biology, 2009. **19**(5): p. 398-403.
81. Alvarez-Salvado, E., et al., *Functional MRI of long-term potentiation: imaging network plasticity.* Philos Trans R Soc Lond B Biol Sci, 2014. **369**(1633): p. 20130152.
82. Trepel, C. and R.J. Racine, *GABAergic modulation of neocortical long-term potentiation in the freely moving rat.* Synapse, 2000. **35**(2): p. 120-128.
83. Miller, M.J., et al., *fMRI of the conscious rabbit during unilateral classical eyeblink conditioning reveals bilateral cerebellar activation.* J Neurosci, 2003. **23**(37): p. 11753-8.
84. Small, S.A., et al., *Circuit mechanisms underlying memory encoding and retrieval in the long axis of the hippocampal formation.* Nat Neurosci, 2001. **4**(4): p. 442-9.
85. Kent, K., et al., *CA3 NMDA receptors are required for experience-dependent shifts in hippocampal activity.* Hippocampus, 2007. **17**(10): p. 1003-11.

86. Zhou, I.Y., et al., *Magnetic resonance spectroscopy reveals N-acetylaspartate reduction in hippocampus and cingulate cortex after fear conditioning.* Psychiatry Research: Neuroimaging, 2012. **204**(2–3): p. 178-183.
87. Sampaio-Baptista, C., et al., *Gray matter volume is associated with rate of subsequent skill learning after a long term training intervention.* NeuroImage, 2014. **96**(0): p. 158-166.
88. Hofstetter, S., et al., *Short-Term Learning Induces White Matter Plasticity in the Fornix.* The Journal of Neuroscience, 2013. **33**(31): p. 12844-12850.
89. Imfeld, A., et al., *White matter plasticity in the corticospinal tract of musicians: A diffusion tensor imaging study.* NeuroImage, 2009. **46**(3): p. 600-607.
90. Dayan, E. and Leonardo G. Cohen, *Neuroplasticity Subserving Motor Skill Learning.* Neuron, 2011. **72**(3): p. 443-454.
91. Thomas, C. and C.I. Baker, *Teaching an adult brain new tricks: A critical review of evidence for training-dependent structural plasticity in humans.* NeuroImage, 2013. **73**(0): p. 225-236.
92. Lu, B., G. Nagappan, and Y. Lu, *BDNF and Synaptic Plasticity, Cognitive Function, and Dysfunction*, in *Neurotrophic Factors*, G.R. Lewin and B.D. Carter, Editors. 2014, Springer Berlin Heidelberg. p. 223-250.
93. Draganski, B., et al., *Neuroplasticity: Changes in grey matter induced by training.* Nature, 2004. **427**(6972): p. 311-312.
94. Lerch, J.P., et al., *Maze training in mice induces MRI-detectable brain shape changes specific to the type of learning.* NeuroImage, 2011. **54**(3): p. 2086-2095.
95. Sampaio-Baptista, C., et al., *Motor Skill Learning Induces Changes in White Matter Microstructure and Myelination.* The Journal of Neuroscience, 2013. **33**(50): p. 19499-19503.
96. Ding, A.Y., et al., *MR Diffusion Tensor Imaging Detects Rapid Microstructural Changes in Amygdala and Hippocampus Following Fear Conditioning in Mice.* PLoS ONE, 2013. **8**(1): p. e51704.
97. Van Boven, R.W., et al., *Advances in neuroimaging of traumatic brain injury and posttraumatic stress disorder.* Journal of rehabilitation research and development, 2009. **46**(6): p. 717-757.
98. Hihara, S., et al., *Extension of corticocortical afferents into the anterior bank of the intraparietal sulcus by tool-use training in adult monkeys.* Neuropsychologia, 2006. **44**(13): p. 2636-2646.
99. Nahmani, M. and G.G. Turrigiano, *Adult cortical plasticity following injury: Recapitulation of critical period mechanisms?* Neuroscience, (0).
100. Hannan, A.J., *Review: Environmental enrichment and brain repair: harnessing the therapeutic effects of cognitive stimulation and physical activity to enhance experience-dependent plasticity.* Neuropathology and Applied Neurobiology, 2014. **40**(1): p. 13-25.
101. Kapur, N., *Paradoxical functional facilitation in brain-behaviour research*. A critical review. Vol. 119. 1996. 1775-1790.
102. Sprague, J.M., *Interaction of cortex and superior colliculus in mediation of visually guided behavior in the cat.* Science, 1966. **153**(3743): p. 3.
103. Bavelier, D. and E. Hirshorn, *I see where you're hearing: how cross-modal plasticity may exploit homologous brain structures.* Nature Neuroscience, 2010. **13**(11): p. 1309-1311.
104. Urbanski, M., O.A. Coubard, and C. Bourlon, *Visualizing the blind brain: brain imaging of visual field defects from early recovery to rehabilitation techniques.* Frontiers in Integrative Neuroscience, 2014. **8**: p. 74.
105. Lazzouni, L. and F. Lepore, *Compensatory plasticity: time matters.* Frontiers in Human Neuroscience, 2014. **8**.
106. Voss, P., *Sensitive and critical periods in visual sensory deprivation.* Frontiers in Psychology, 2013. **4**: p. 664.

107. Nahmani, M. and G.G. Turrigiano, *Adult cortical plasticity following injury: Recapitulation of critical period mechanisms?* Neuroscience, 2014. **283**(0): p. 4-16.
108. Endo, T., et al., *Cortical sensory map rearrangement after spinal cord injury: fMRI responses linked to Nogo signalling.* Brain, 2007. **130**(Pt 11): p. 2951-61.
109. Papanikolaou, A., et al., *Population receptive field analysis of the primary visual cortex complements perimetry in patients with homonymous visual field defects.* Proceedings of the National Academy of Sciences, 2014. **111**(16): p. E1656-E1665.
110. Shao, Y., et al., *Visual cortex organisation in a macaque monkey with macular degeneration.* European Journal of Neuroscience, 2013. **38**(10): p. 3456-3464.
111. Pawela, C.P., et al., *Interhemispheric neuroplasticity following limb deafferentation detected by resting-state functional connectivity magnetic resonance imaging (fcMRI) and functional magnetic resonance imaging (fMRI).* NeuroImage, 2010. **49**(3): p. 2467-2478.
112. Pelled, G., et al., *Functional MRI detection of bilateral cortical reorganization in the rodent brain following peripheral nerve deafferentation.* NeuroImage, 2007. **37**(1): p. 262-273.
113. Yu, X., et al., *3D mapping of somatotopic reorganization with small animal functional MRI.* NeuroImage, 2010. **49**(2): p. 1667-1676.
114. Li, R., et al., *Cortical plasticity induced by different degrees of peripheral nerve injuries: a rat functional magnetic resonance imaging study under 9.4 Tesla.* Journal of Brachial Plexus and Peripheral Nerve Injury, 2013. **8**: p. 4-4.
115. Ramu, J., et al., *Brain fiber tract plasticity in experimental spinal cord injury: Diffusion tensor imaging.* Experimental Neurology, 2008. **212**(1): p. 100-107.
116. Wrigley, P.J., et al., *Anatomical Changes in Human Motor Cortex and Motor Pathways following Complete Thoracic Spinal Cord Injury.* Cerebral Cortex, 2009. **19**(1): p. 224-232.
117. Dijkhuizen, R., et al., *Functional MRI and Diffusion Tensor Imaging of Brain Reorganization After Experimental Stroke.* Translational Stroke Research, 2012. **3**(1): p. 36-43.
118. Weaver, K.E., et al., *Neurochemical changes within human early blind occipital cortex.* Neuroscience, 2013. **252**(0): p. 222-233.
119. Kupers, R. and M. Ptito, *Compensatory plasticity and cross-modal reorganization following early visual deprivation.* Neuroscience & Biobehavioral Reviews, 2014. **41**(0): p. 36-52.
120. Chan, K.C., M.M. Cheung, and E.X. Wu, *IN VIVO MULTIPARAMETRIC MAGNETIC RESONANCE IMAGING AND SPECTROSCOPY OF RODENT VISUAL SYSTEM.* Journal of Integrative Neuroscience, 2010. **09**(04): p. 477-508.
121. Gröhn, O., et al., *Multimodal MRI assessment of damage and plasticity caused by status epilepticus in the rat brain.* Epilepsia, 2011. **52**: p. 57-60.
122. Nairismägi, J., et al., *Manganese-enhanced magnetic resonance imaging of mossy fiber plasticity in vivo.* NeuroImage, 2006. **30**(1): p. 130-135.
123. Laitinen, T., et al., *Diffusion tensor MRI of axonal plasticity in the rat hippocampus.* NeuroImage, 2010. **51**(2): p. 521-530.
124. Sierra, A., et al., *Diffusion tensor MRI with tract-based spatial statistics and histology reveals undiscovered lesioned areas in kainate model of epilepsy in rat.* Brain Structure and Function, 2011. **216**(2): p. 123-135.
125. Choy, M., et al., *Cerebral blood flow changes during pilocarpine-induced status epilepticus activity in the rat hippocampus.* Experimental Neurology, 2010. **225**(1): p. 196-201.
126. Choy, M., et al., *Quantitative MRI predicts status epilepticus-induced hippocampal injury in the lithium–pilocarpine rat model.* Epilepsy Research, 2010. **88**(2–3): p. 221-230.
127. Hayward, N.M.E.A., et al., *Elevated cerebral blood flow and vascular density in the amygdala after status epilepticus in rats.* Neuroscience Letters, 2010. **484**(1): p. 39-42.
128. Institute, L.M.G.S.C.M.N.L.C., *Hormones and Brain Plasticity*. 2009: Oxford University Press, USA.

129. Hagemann, G., et al., *Changes in Brain Size during the Menstrual Cycle.* PLoS ONE, 2011. **6**(2): p. e14655.
130. Pletzer, B., et al., *Menstrual cycle and hormonal contraceptive use modulate human brain structure.* Brain Research, 2010. **1348**(0): p. 55-62.
131. Arelin, K., et al., *Progesterone mediates brain functional connectivity changes during the menstrual cycle - A pilot resting state MRI study.* Frontiers in Neuroscience, 2015. **9**.
132. Barth, C., A. Villringer, and J. Sacher, *Sex hormones affect neurotransmitters and shape the adult female brain during hormonal transition periods.* Frontiers in Neuroscience, 2015. **9**.
133. Lan, Y.-L., J. Zhao, and S. Li, *Update on the Neuroprotective Effect of Estrogen Receptor Alpha Against Alzheimer's Disease.* Journal of Alzheimer's Disease, 2015. **43**(4): p. 1137-1148.
134. Daniel, J.M., *Estrogens, estrogen receptors, and female cognitive aging: The impact of timing.* Hormones and Behavior, 2013. **63**(2): p. 231-237.
135. Woolley, C. and B. McEwen, *Estradiol mediates fluctuation in hippocampal synapse density during the estrous cycle in the adult rat [published erratum appears in J Neurosci 1992 Oct;12(10):following table of contents].* The Journal of Neuroscience, 1992. **12**(7): p. 2549-2554.
136. Yankova, M., S.A. Hart, and C.S. Woolley, *Estrogen increases synaptic connectivity between single presynaptic inputs and multiple postsynaptic CA1 pyramidal cells: A serial electron-microscopic study.* Proceedings of the National Academy of Sciences of the United States of America, 2001. **98**(6): p. 3525-3530.
137. Woolley, C.S., *Acute Effects of Estrogen on Neuronal Physiology.* Annual Review of Pharmacology and Toxicology, 2007. **47**(1): p. 657-680.
138. Wnuk, A., D.L. Korol, and K.I. Erickson, *Estrogens, hormone therapy, and hippocampal volume in postmenopausal women.* Maturitas, 2012. **73**(3): p. 186-190.
139. Boccardi, M., et al., *Effects of hormone therapy on brain morphology of healthy postmenopausal women: a Voxel-based morphometry study.* Menopause, 2006. **13**(4): p. 584-591.
140. Protopopescu, X., et al., *Hippocampal structural changes across the menstrual cycle.* Hippocampus, 2008. **18**(10): p. 985-988.
141. Höfer, P., R. Lanzenberger, and S. Kasper, *Testosterone in the brain: Neuroimaging findings and the potential role for neuropsychopharmacology.* European Neuropsychopharmacology, 2013. **23**(2): p. 79-88.
142. Cooke, G.E., et al., *Hippocampal Volume Is Decreased in Adults with Hypothyroidism.* Thyroid, 2013. **24**(3): p. 433-440.
143. Bottjer, S.W. and F. Johnson, *Circuits, hormones, and learning: Vocal behavior in songbirds.* Journal of Neurobiology, 1997. **33**(5): p. 602-618.
144. Hötting, K. and B. Röder, *Beneficial effects of physical exercise on neuroplasticity and cognition.* Neuroscience & Biobehavioral Reviews, 2013. **37**(9, Part B): p. 2243-2257.
145. Ahlskog, J.E., et al., *Physical Exercise as a Preventive or Disease-Modifying Treatment of Dementia and Brain Aging.* Mayo Clinic Proceedings, 2011. **86**(9): p. 876-884.
146. Johansson, B.B., *Functional and cellular effects of environmental enrichment after experimental brain infarcts.* Restorative Neurology and Neuroscience, 2004. **22**(3): p. 163-174.
147. Voss, M.W., et al., *Bridging animal and human models of exercise-induced brain plasticity.* Trends in Cognitive Sciences, 2013. **17**(10): p. 525-544.
148. Baumans, V., *Environmental Enrichment for Laboratory Rodents and Rabbits: Requirements of Rodents, Rabbits, and Research.* ILAR Journal, 2005. **46**(2): p. 162-170.
149. Nithianantharajah, J. and A.J. Hannan, *Enriched environments, experience-dependent plasticity and disorders of the nervous system.* Nat Rev Neurosci, 2006. **7**(9): p. 697-709.

150. van Praag, H., G. Kempermann, and F.H. Gage, *Neural consequences of enviromental enrichment.* Nat Rev Neurosci, 2000. **1**(3): p. 191-198.
151. Simpson, J. and J.P. Kelly, *The impact of environmental enrichment in laboratory rats—Behavioural and neurochemical aspects.* Behavioural Brain Research, 2011. **222**(1): p. 246-264.
152. Scholz, J., et al., *Environmental enrichment is associated with rapid volumetric brain changes in adult mice.* NeuroImage, 2015. **109**(0): p. 190-198.
153. Scholz, J., et al., *Rotarod training in mice is associated with changes in brain structure observable with multimodal MRI.* NeuroImage, 2015. **107**(0): p. 182-189.
154. Maddock, R.J., et al., *Vigorous exercise increases brain lactate and Glx (glutamate + glutamine): A dynamic 1H-MRS study.* NeuroImage, 2011. **57**(4): p. 1324-1330.
155. Gonzales, M., et al., *Aerobic Fitness and the Brain: Increased N-Acetyl-Aspartate and Choline Concentrations in Endurance-Trained Middle-Aged Adults.* Brain Topography, 2013. **26**(1): p. 126-134.
156. Floyer-Lea, A., et al., *Rapid Modulation of GABA Concentration in Human Sensorimotor Cortex During Motor Learning*. Vol. 95. 2006. 1639-1644.
157. Roche, R.A., et al., *Prolonged rote learning produces delayed memory facilitation and metabolic changes in the hippocampus of the ageing human brain*. 2009. p. 136.
158. van Dellen, A., et al., *Delaying the onset of Huntington's in mice.* Nature, 2000. **404**(6779): p. 721-722.
159. Lazic, S.E., et al., *Neurogenesis in the R6/1 transgenic mouse model of Huntington's disease: effects of environmental enrichment.* European Journal of Neuroscience, 2006. **23**(7): p. 1829-1838.
160. Faherty, C.J., et al., *Environmental enrichment in adulthood eliminates neuronal death in experimental Parkinsonism.* Molecular Brain Research, 2005. **134**(1): p. 170-179.
161. Görtz, N., et al., *Effects of environmental enrichment on exploration, anxiety, and memory in female TgCRND8 Alzheimer mice.* Behavioural Brain Research, 2008. **191**(1): p. 43-48.
162. Svensson, M., J. Lexell, and T. Deierborg, *Effects of Physical Exercise on Neuroinflammation, Neuroplasticity, Neurodegeneration, and Behavior: What We Can Learn From Animal Models in Clinical Settings.* Neurorehabilitation and Neural Repair, 2014.
163. Little, D.M., S. Foxely, and O. Lazarov, *A preliminary study targeting neuronal pathways activated following environmental enrichment by resting state functional magnetic resonance imaging.* J Alzheimers Dis, 2012. **32**(1): p. 101-7.
164. Herring, A., et al., *Environmental enrichment enhances cellular plasticity in transgenic mice with Alzheimer-like pathology.* Exp Neurol, 2009. **216**(1): p. 184-92.
165. Golub, Y., et al., *Reduced hippocampus volume in the mouse model of Posttraumatic Stress Disorder.* Journal of Psychiatric Research, 2011. **45**(5): p. 650-659.
166. Zhang, L., et al., *Exercise Pretreatment Promotes Mitochondrial Dynamic Protein OPA1 Expression after Cerebral Ischemia in Rats.* International Journal of Molecular Sciences, 2014. **15**(3): p. 4453-4463.
167. He, Z., et al., *Treadmill Pre-Training Ameliorates Brain Edema in Ischemic Stroke via Down-Regulation of Aquaporin-4: An MRI Study in Rats.* PLoS ONE, 2014. **9**(1): p. e84602.
168. Jenks, K.R., et al., *Enrichment and Training Improve Cognition in Rats with Cortical Malformations.* PLoS ONE, 2013. **8**(12): p. e84492.
169. Pereira, A.C., et al., *An in vivo correlate of exercise-induced neurogenesis in the adult dentate gyrus.* Proceedings of the National Academy of Sciences, 2007. **104**(13): p. 5638-5643.
170. Mariotti, R., et al., *Forced mild physical training improves blood volume in the motor and hippocampal cortex of old mice.* The journal of nutrition, health & aging, 2014. **18**(2): p. 178-183.

171. Small, S.A., et al., *Imaging correlates of brain function in monkeys and rats isolates a hippocampal subregion differentially vulnerable to aging.* Proceedings of the National Academy of Sciences of the United States of America, 2004. **101**(18): p. 7181-7186.
172. Blau, C.W., et al., *The age-related deficit in LTP is associated with changes in perfusion and blood-brain barrier permeability.* Neurobiology of Aging, 2012. **33**(5): p. 1005.e23-1005.e35.
173. van Praag, H., et al., *Running enhances neurogenesis, learning, and long-term potentiation in mice.* Proceedings of the National Academy of Sciences, 1999. **96**(23): p. 13427-13431.
174. Kempermann, G., H.G. Kuhn, and F.H. Gage, *More hippocampal neurons in adult mice living in an enriched environment.* Nature, 1997. **386**(6624): p. 493-495.
175. Olson, A.K., et al., *Environmental enrichment and voluntary exercise massively increase neurogenesis in the adult hippocampus via dissociable pathways.* Hippocampus, 2006. **16**(3): p. 250-260.
176. Curlik, I., Daniel Martin, G. DiFeo, and T.J. Shors, *Preparing for Adulthood: Thousands Upon Thousands of New Cells are Born in the Hippocampus During Puberty and Most Survive with Effortful Learning.* Frontiers in Neuroscience, 2014. **8**.
177. Luine, V., et al., *Estradiol enhances learning and memory in a spatial memory task and effects levels of monoaminergic neurotransmitters.* Hormones and behavior, 1998. **34**(2): p. 149.
178. McEwen, B.S., et al., *Ovarian steroids and the brain: Implications for cognition and aging.* Neurology, 1997. **48**(5 Suppl 7): p. 8S-15S.
179. Jessberger, S. and F.H. Gage, *Adult neurogenesis: bridging the gap between mice and humans.* Trends in Cell Biology, 2014. **24**(10): p. 558-563.
180. Couillard-Despres, S., et al., *In vivo monitoring of adult neurogenesis in health and disease.* Frontiers in Neuroscience, 2011. **5**.
181. Coquery, N., et al., *Intrahippocampal transplantation of mesenchymal stromal cells promotes neuroplasticity.* Cytotherapy, 2012. **14**(9): p. 1041-1053.
182. Manganas, L.N., et al., *Magnetic Resonance Spectroscopy Identifies Neural Progenitor Cells in the Live Human Brain.* Science, 2007. **318**(5852): p. 980-985.
183. Ramm, P., et al., *A Nuclear Magnetic Resonance Biomarker for Neural Progenitor Cells: Is It All Neurogenesis?* STEM CELLS, 2009. **27**(2): p. 420-423.
184. Fuss, J., et al., *Exercise boosts hippocampal volume by preventing early age-related gray matter loss.* Hippocampus, 2014. **24**(2): p. 131-134.
185. Hamzei, F., et al., *Dynamic gray matter changes within cortex and striatum after short motor skill training are associated with their increased functional interaction.* NeuroImage, 2012. **59**(4): p. 3364-3372.
186. Ma, L., et al., *Changes occur in resting state network of motor system during 4 weeks of motor skill learning.* NeuroImage, 2011. **58**(1): p. 226-233.
187. Taubert, M., et al., *Long-term effects of motor training on resting-state networks and underlying brain structure.* NeuroImage, 2011. **57**(4): p. 1492-1498.
188. Taubert, M., et al., *Dynamic Properties of Human Brain Structure: Learning-Related Changes in Cortical Areas and Associated Fiber Connections.* The Journal of Neuroscience, 2010. **30**(35): p. 11670-11677.
189. Taubert, M., A. Villringer, and P. Ragert, *Learning-Related Gray and White Matter Changes in Humans: An Update.* The Neuroscientist, 2012. **18**(4): p. 320-325.

Chapter 4

Two decades of bird brain MRI

This chapter is based on the second part of a book chapter that is currently under review: Hamaide J., Bigler A., Van der Linden A. MRI an ideal tool to explore the neural substrate of vocal communication in songbirds. Submitted to Elsevier B.V. for publication in 'Handbook of in vivo neural plasticity techniques: a systems neuroscience approach to the neural basis of memory and cognition', edited by Prof Dr Denise Manahan-Vaughan.

4.1 INTRODUCTION

Since its first application already 20 years ago [1], several MRI techniques have been used successfully in songbirds. The first *in vivo* studies showed that using conventional T_1- and T_2-weighted sequences no anatomical contrast of the song control system could be observed even at a very high spatial resolution [1, 2]. However, to visualize the song control and auditory system, other MRI methods have to be employed. The following paragraphs present an overview of how different MRI techniques have led to insights into the functional and structural (re-)organization of the songbird brain.

4.2 *IN VIVO* VISUALISATION OF THE SONG CONTROL NUCLEI

About the same time as Van der Linden and co-workers implemented MRI in songbirds, different research labs used manganese-enhanced MRI to investigate brain activation to e.g. somatosensory stimulation [3], or to perform *in vivo* tract tracing experiments [4]. Given the modular arrangement of the songbird brain, injection of $MnCl_2$ in one component of the song control system was hypothesized to enable a successful visualization of the entire song control circuitry.

To test this hypothesis, $MnCl_2$ was injected locally in HVC in adult European starlings [5]. HVC is situated on the caudo-dorsal surface of the telencephalon making it an ideal target for stereotactic injections, and sends afferent projections to area X and RA. Eight hours after injection, both RA and area X appeared clearly on the T_1-weighted images and their shape clearly matched previous descriptions (Figure 4-1). Furthermore, volumetric analysis of area X and RA confirmed the previously described disparity of these nuclei between both sexes [6].

The previously described study focused on area X and RA. However, as Mn^{2+} can be transported trans-synaptically, it should be possible to enhance entire circuitries. This was illustrated by Tindemans and colleagues in canaries [7]. After injection $MnCl_2$ in HVC and the contralateral MAN, they could discriminate the different (alternating) layers of the chiasma opticum, several laminae, distinct cell layers of the cerebellum and the deep cerebellar nuclei etc. This study literally highlighted and confirmed histological tract tracing studies that remote areas, often not directly associated with song control, clearly connect to the song control system. In contrast to previous studies, they used an inversion recovery sequence that required lower doses of Mn^{2+} but retained a sufficient contrast-to-noise ratio to trace different song control nuclei.

Moreover, while exploring the full potential of spin echo inversion recovery sequences in the songbird brain, they were able to achieve anatomical contrast of several song control nuclei even without administration of $MnCl_2$. This highly favourable finding was a first step towards truly non-invasive –without application of exogenous contrast agent– *in vivo* imaging of the songbird neuroanatomy.

4.3 FROM SEASONAL CHANGES TO SEX DIFFERENCES: UNCOVERING ALTERATIONS IN VOLUME, CONNECTIVITY AND MICROSTRUCTURAL TISSUE PROPERTIES OF THE BRAIN

After validation of the technique, MEMRI was applied to further disentangle the intricate relationships between behavioural, hormonal and neuroplastic changes observed in seasonal songbirds.

4.3.1 MEMRI reveals alterations in functional properties of distinct cell populations

Calcium signalling reflects neuronal activity [8], consequently, besides anatomical contrast enhancement, Mn^{2+} can serve as a highly sensitive and direct readout of neuronal activation [3]. This is nicely illustrated by Yu et al. who clearly showed the high-frequency tonotopic organization of the mouse inferior colliculus upon acoustic stimulation with particular frequency bands [9] and the effects of different rearing conditions on tonotopic map reorganization in juvenile mice [10]. Interestingly, in these experimental settings, the mice received $MnCl_2$ intraperitoneally and were exposed to the acoustic stimuli while being awake. This application of MEMRI is often termed activity-induced MEMRI or (AIM-MRI). Alternatively, the functional properties of particular cell groups can be evaluated as well. This is achieved by performing dynamic measurements where after injection of $MnCl_2$ in a specific brain region, the change in signal intensity to its projection area is monitored over time by acquiring the same T_1-weighted dataset at regular intervals and plot relative changes in signal intensity of specific ROIs as a function of time (Figure 4-1). The relative change in signal intensity can be modelled by a sigmoid function of which the kinetics are described by three parameters, i.e. the maximal signal intensity (SI_{max}), the time necessary to reach 50% of SI_{max} and the slope of the curve. Furthermore, based on the time after $MnCl_2$ injection and the time that the projection areas appear hyper-intense on the T_1-weighted images and the distance between two brain areas, it is possible to deduce the Mn^{2+} transport rate. Indeed, Van der Linden and

co-workers (2002) found that the HVC-area X and HVC-RA pathways convey Mn^{2+} (and thus Ca^{2+}) via fast axonal transport [5, 11].

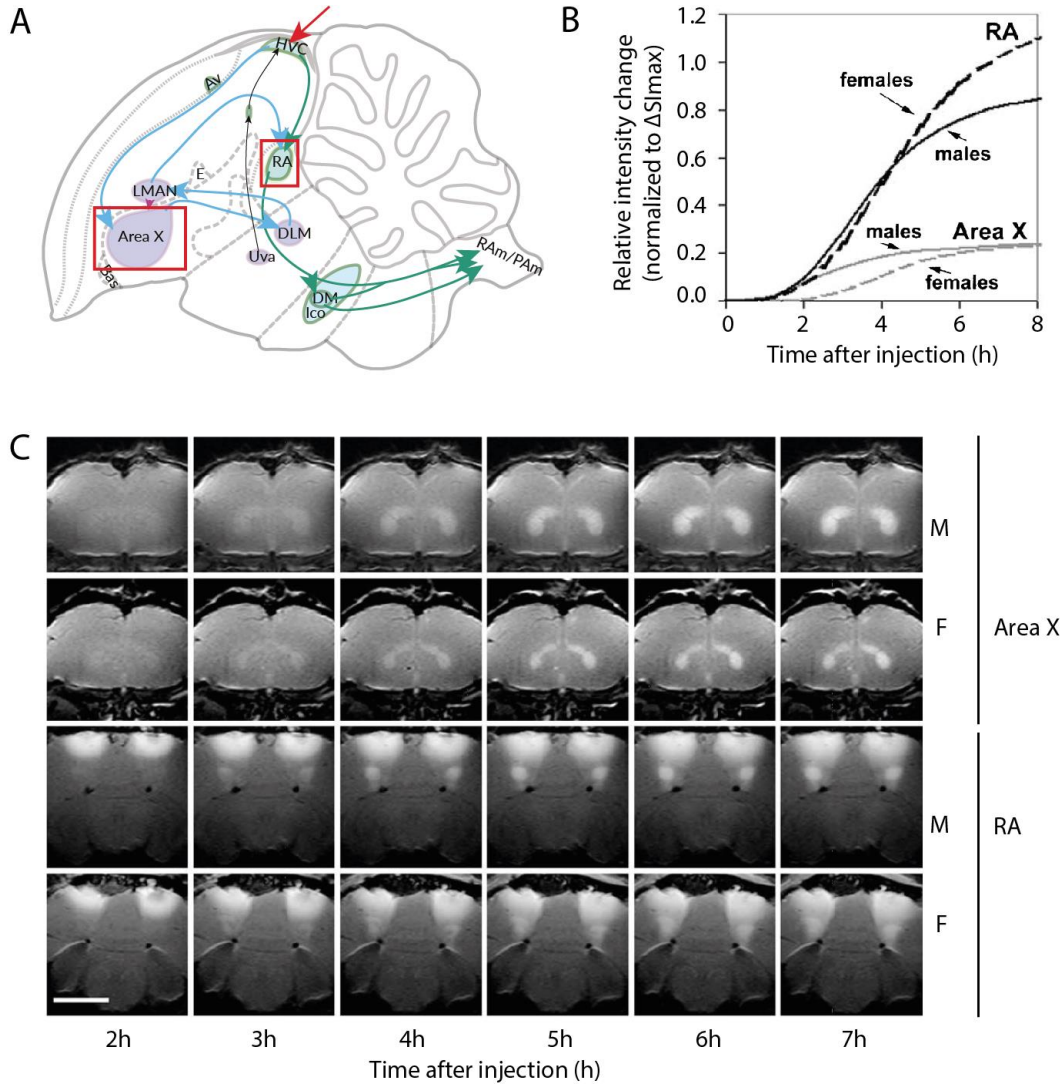

Figure 4-1: Dynamic MEMRI measurements in starlings. (A) Schematic overview of the songbird song control system. The red arrow indicates the injection site of manganese (into HVC). The red boxes indicate the projection areas where manganese is transported and measured, i.e. area X and RA. (B) Sigmoid curves describing the kinetics of manganese transport to area X and RA in adult male and female starlings. (C) Overview of manganese-enhanced images obtained at different times after injection. A clear difference in the size of area X (top rows) and RA (bottom rows) between male and female starlings can be observed. Modified from [5] with permission from Elsevier.

4.3.1.1 The functional properties of neurons can be tuned by (1) auditory stimulation

Several studies have shown that distinct HVC neuronal subpopulations respond in a selective manner to conspecific songs and birds' own song even in anesthetized conditions [12-14]. In the previously mentioned MEMRI experiments, the starlings were exposed to conspecific song playbacks during the entire time in between the stereotactic injection and MR data acquisition (± 30 min). Consequently, this might have affected the rate at which $MnCl_2$ was taken up and transported towards area X and RA. Therefore, another study was set up to explore whether the presence or absence of auditory stimulation would alter the dynamics of the Mn^{2+} transport in the song control circuitry [15]. To this end, adult male canaries underwent two imaging sessions several weeks apart with and without exposure to unfamiliar conspecific song. The ROI-based analysis informed that, after stimulation, the slope of the curve was increased in RA-projecting cells whereas in area X an increased SI_{max} could be observed, compared to the silent condition. This differential behaviour of distinct neuronal subpopulations within HVC suggests that unfamiliar conspecific song increased the activity of RA-projecting HVC neurons (increased slope, but similar SI_{max}), while the increased SI_{max} in area X implies that more area X-projecting neurons were activated by the stimulus and more projection neurons transported Mn^{2+} to area X (at the same rate) suggestive of 'functional recruitment'.

4.3.1.2 The functional properties of neurons can be tuned by (2) the sex of the birds

Dynamic MEMRI measurements tested for differences between male and female starlings near the end of the breeding season and revealed that the time to reach 50% of SI_{max} was significantly different between both sexes in RA and area X [5]. Furthermore, the slope of the curve indicating the rate of transport of area X (but not RA) was higher in female compared to male birds (Figure 4-1). These findings pointed to different kinetics of Mn^{2+} (and thus also Ca^{2+}) in male and female starlings and extended previously established sexual dimorphisms in the starlings' brain and behaviour [6, 16].

4.3.1.3 The functional properties of neurons can be tuned by (3) the hormonal status and photoperiod

Most song control nuclei contain hormone receptors which are crucial mediators connecting alterations in hormone levels to neuroplasticity [17]. Clear links between hormone production

and the photoperiod have been established in seasonal songbirds (for review [18]), however, still several major questions remain: Are neuroplastic changes causing alterations to song behaviour? Or do changes in song behaviour (or behavioural activity more broadly) elicit neuroplastic processes, similar to activity-induced neuroplasticity, and how/where do hormones act in this interplay? In order to gain insights into the mechanistic, causal relationships between and the exact contribution of different hormones to seasonal neuroplasticity and alterations in singing behaviour, ample researchers have investigated the effects of hormone treatments or manipulations of the photoperiod (ref e.g. [19, 20]).

Dynamic MEMRI measurements allow tracing structural and functional circuitry changes longitudinally in the same animal. Indeed, Van Meir and co-workers found a volume increase in RA and area X after a 6 weeks testosterone treatment in adult female starlings in the breeding season [21]. In control birds, the volumes of both nuclei reduced slightly towards the second measurement which indicates that the endogenous neuroplastic cycle continued and caused detectable volume changes even in a time span of several weeks. In addition, both the rate and total amount of Mn^{2+} transported to area X increased, following the testosterone treatment. A significant increase in the total amount of Mn^{2+} transported to RA could be observed in the second time point for the treated birds, however, this was mainly ascribed to the significant increase in volume of this nucleus and therefore does not imply altered functional connectivity or activity changes following testosterone treatment. These data point towards a cell- and pathway-specific effect of testosterone as two distinct cell populations within the same nucleus i.e. area X- and RA-projecting neurons in HVC, display differentially altered Mn^{2+} kinetics upon hormone treatment.

The same authors tested for possible relationships between song production and the size and functional properties of the song control nuclei in adult female starlings [22]. Interestingly, they observed that female starlings that sung at high song rate showed a higher Mn^{2+} accumulation in RA in both seasons compared to birds that sung less. This hints to an activity-dependent functional intensification of caudal motor pathway.

Another study in starlings revealed season-dependent changes in neuronal activity to olfactory stimulation. More specifically, De Groof and co-workers showed that during the breeding season the starlings showed a differential accumulation of Mn^{2+} in the olfactory bulb when they were exposed to milfoil –an aromatic herb that birds prefer to include in the nest material that

is considered to have an antiseptic function towards the offspring– compared to the non-stimulated condition [23]. In the summer (i.e. non-breeding season), however, no differences in Mn^{2+} accumulation could be observed. These findings suggest that only during the breeding season starlings are tuned to this transiently biologically relevant scent and seasonal plasticity goes beyond the song control system.

In conclusion, MEMRI can be used for several applications as it (1) realizes contrast enhancement of overall (neuro)anatomy, (2) enables studying structural and functional connectivity between brain areas and neural projection areas as it can be transported trans-synaptically and (3) provides a direct readout for neuronal activity with the additional bonus that it can be administered to awake, freely behaving animals as the imaging is often performed several hours after exposure to the stimulation. This allows to present animals with complex visual or context-dependent stimuli which are difficult or even impossible in the restricted environment of the scanner bore. However, the technique suffers several limitations e.g. dynamic MEMRI requires prolonged acquisition times and prolonged anaesthesia for up to 6-8 hours. In addition, only one stimulus can be presented at a time and at least 2 weeks should be in between two imaging sessions to ensure clearance of Mn^{2+} from the brain. Therefore, for future functional and structural imaging studies, alternative MRI techniques were considered.

4.3.2 DTI enables whole-brain assessment of structural connectivity and microstructural tissue characteristics

Targeted MEMRI permits volume quantification and the deduction of several properties related to functional connectivity between distinct brain areas. However, it does not inform on changes in structural connectivity or microstructural tissue properties. Nor could information beyond the song control nuclei be obtained if not targeted specifically with $MnCl_2$. DTI on the other hand, is known to be sensitive to anatomical and microstructural properties of the brain and, interestingly, several research groups had already implemented DTI protocols for small animal investigations (e.g. [24-26]. Hence, De Groof and co-workers developed a protocol to obtain DTI data in European starlings.

4.3.2.1 Seasonal changes in the connectivity and microstructural properties beyond the song control circuitry in adult starlings

The first DTI study in starlings convincingly showed that it enabled visualization of the entire song control system and provided additional anatomical contrast on several other important circuitries such as the auditory and visual system [27]. Importantly however, the anatomical contrast on several song control and auditory nuclei obtained by DTI was most evident on FA maps as it was mainly caused by the visualization of fibre capsules surrounding these nuclei. Follow-up studies researched whether neuroplastic changes between different seasons also occur outside of the song control system [28, 29]. To this end, nine male starlings were repeatedly imaged during the breeding and non-breeding season. Manual delineation of the ROIs resulted in two different outcomes, firstly, the volumes of the grey matter areas could be extracted and, secondly, the DTI parameters which inform on the intrinsic tissue properties were analysed. Five DTI parameters were evaluated, i.e. fractional anisotropy (FA), mean diffusivity (MD) and the three eigenvalues. MD represent the overall magnitude of water diffusion within a voxel, FA represents an arbitrary value ranging from 0 to 1 where 0 stands for a perfectly isotropic and 1 for a highly anisotropic diffusion profile of water protons within a voxel. For example, water protons in fibres and myelinated axons experience highly anisotropic diffusion as these water protons can only diffuse along and not perpendicular to the fibres, which makes that FA is extremely sensitive to detect alterations in highly structured (white matter) structures. The eigenvalues refer to the geometrical properties of the diffusion tensor (along three axes) estimated within a voxel. They are used to calculate MD and FA. Importantly however, even though less regularly described, the eigenvalues are valuable parameters to understand the origin of particular changes in MD and FA.

As the entire telencephalon showed a significant volume change between the two seasons, all volumetric analyses were performed using relative volumes (% relative to total telencephalon volume). RA, Area X and NCM showed a volume decrease towards the non-breeding season (summer) [29]. The first two are in line with previous reports and the MEMRI studies, the latter (i.e. NCM) was a novel finding. No direct correlations could be found between plasma testosterone levels and volume changes in these regions which suggests that additional factors, besides testosterone, are required to trigger this structural neuroplastic response. The volume decrease in area X was accompanied by a reduction in T_2 relaxation time which could be linked

to previous studies that showed a change in neuron size and spacing in adult male song sparrows between different seasons [30]. The volume decrease in NCM was mirrored by a significant reduction in FA and an increase in the third eigenvalue towards the summer. Interestingly, POA and VMN, two components of the social behaviour network, showed similar changes in FA and third eigenvalue, and, similar to NCM, are known to contain aromatase-positive cells. Aromatase-expressing cells show seasonal plasticity in canaries [31] and display highly complex branching patterns and large nuclei [32] which makes them a likely candidate to contribute to the alterations in microstructural tissue characteristics observed by DTI.

Several fibre tracts showed a reduction in FA towards the summer (non-breeding season), i.e. the HVC-RA tract, *tractus occipitomesencephalicus* (tOM), the LaM, LPS and the *commissura posterior* [28]. The reduction in FA in the HVC-RA tract and tOM were confirmed by a myelin stain. Furthermore, also the fibre capsules surrounding area X and RA displayed a lower FA in the summer compared to the spring. These wide-spread changes in connectivity provide additional proof that from season to season, the entire songbird brain undergoes dramatic structural remodelling. De Groof and co-workers managed to relate the changes observed by DTI to a decreased number of axonal projections possibly combined with demyelination by comparing the *in vivo* DTI to *ex vivo* myelin stained tissues. In addition, by relating their results to previously published histological findings, they were able to find parallels between changes in DTI parameters and neuronal density, some size, altered intra-and extracellular fluid and cell spacing.

Unfortunately, no songs were recorded consequently no relationships between singing performance and the underlying neural substrate (e.g. HVC-RA and tOM) could be tested. Such tests would inform on possible activity-dependent structural signatures as observed in many other use- or activity dependent structural imaging studies (for review [33]). However, based on the general findings, one could observe that most fibre tracts investigated in this study displayed a higher FA in the breeding season indicating that fibres are most tightly packed when birds sing most.

In conclusion, *in vivo* DTI in starlings revealed that seasonal neuroplasticity goes beyond the song control system, where the third eigenvalue was suggested to be marking altered aromatase activity (De Groof et al., 2008). The data in starlings showed that due to its natural composition, the songbird brain is an excellent model system to explore with DTI. In addition,

the songbird brain is relatively well characterized and can therefore be of use to further validate and fine-tune the possibilities of advanced DTI processing techniques to study neuroplasticity *in vivo*, helping to disentangle the biological underpinnings of complex DTI parameter readouts.

4.4 AUDITORY PROCESSING IN SONGBIRDS: FROM BASIC VALIDATION STUDIES, OVER SEASONAL CHANGES IN SONG DISCRIMINATION, TO LATERALISED BRAIN FUNCTION

Until several decades ago, most methods to investigate brain function relied on invasive methods. For example, electrophysiology had already been thoroughly explored in songbirds and allows one to investigate neural responses to biologically relevant stimuli, even in awake animals. This technique provides a direct readout for neural activity, but can only capture the response of one or a small group of neurons, which is not always representative to deduce how the brain processes information. Immediate early gene (IEG) expression studies have led to insights into brain regions that become activated upon certain stimuli [34], however, the detection of IEG expression relies on histological stainings, require sacrificing of the experimental subjects and consequently limit the number and nature of stimuli that can be presented and evaluated. *In vivo* functional MRI, on the other hand, provides a valid alternative to overcome the above-mentioned limitations. It would enable exploring the processing of different kinds of songs (even within one imaging session), modulation of song perception by hormone status, establishment of tutor and birds' own song in juvenile birds etc.

The technical implementation of the technique faced several challenges. The bones of birds are filled with air cavities that keep their weight minimal, which is necessary for efficient flight. This skeletal pneumaticity severely impacts bird brain imaging as the air cavities in the skull induce marked magnetic susceptibility artefacts that aggravate at higher field strengths. The first experiments included characterization and validations studies, where one slice containing functional information was obtained that was positioned on the primary and secondary auditory areas. Later optimizations allowed for multi-slice acquisition protocols where the FOV covered the entire brain.

4.4.1 Characterization of the BOLD response in European starlings

The songbird brain is structured fundamentally different compared to the mammalian brain. In addition, songbirds have a higher body temperature (40-41°C in normal conditions), and different neuronal densities and neuron-glia ratios in the brain [35] compared to mammals.

Consequently, the first tests on functional MRI in songbirds focused on finding out whether the hemodynamic response to a particular stimulation would be similar to what had been described previously in several mammalian species, including humans and primates [36, 37], rodents [38], etc.

The first study aimed to characterize the spatiotemporal properties of the BOLD response in the primary and secondary auditory regions of the adult starling brain during three different listening tasks [39]. The time course of the BOLD response showed a remarkable resemblance to evoked BOLD responses as seen in humans where a maximum signal strength was observed several seconds after the initiation of the stimulation, followed by a post-stimulus undershoot. In addition, differences in the presence and amplitude of the BOLD response were found between Field L and NCM, i.e. white noise, music and conspecific song elicited similar responses in Field L whereas NCM displayed no response to white noise, a low amplitude BOLD response to music and a clear BOLD response (though lower amplitude compared to Field L) to song playback. Importantly, these findings illustrate the emergence of song-selective brain responses along the ascending auditory pathway.

4.4.2 Implementation of BOLD fMRI in zebra finches: validation and song manipulation studies

Close-ended learners such as zebra finches form a 'simpler' model to investigate the neural substrate for processing of different stimuli compared to open-ended learners as from adulthood onwards vocal behaviour remains fixed. In addition, in close-ended learners, the experimental outcome is less likely to be affected by seasonal plasticity or altered hormone status. However, before zooming in on neural substrates, the functional imaging protocol established in starlings and transferred to zebra finches needed to be validated by established, golden standard methods.

4.4.2.1 BOLD fMRI 'versus' behavioural tests, immediate early genes and near-infrared spectroscopy

Two separate experiments compared BOLD fMRI findings to previously published immediate early gene (IEG) zenk expression to particular auditory stimuli [40, 41] and data obtained by *in vivo* near-infrared spectroscopy (NIRS) measurements [42].

The IEG expression by Vignal and co-workers (2004) and BOLD fMRI study by Boumans et al. (2008) presented adult male zebra finches with auditory stimuli where several levels of broadband noise were added to conspecific song. Both studies found a decreased expression of IEG and decreased BOLD response in NCM with increasing noise level. Interestingly, in contrast to IEG studies where never any IEG expression can be distinguished in Field L2 [43] and consequently no differences in activation of this structure can be assessed, BOLD fMRI showed a clear signal in this region. All stimuli resulted in similar BOLD profiles in Field L2 indicating that broadband noise did not alter neural activation in this primary auditory region. Furthermore, a behavioural experiment was set up to inspect whether the songs played in the magnet bore would evoke different responses (due to e.g. acoustic distortions induced by the magnetic field) compared to songs played in a normal environment e.g. sound box. No differences in the number of calls as a reaction to song recorded in the scanner or to normal songs could be detected indicating that birds perceive songs played in the scanner environment similar to 'normally' played songs.

NIRS is a non-invasive optical imaging technique that enables the detection of changing haemodynamics of the brain in response to stimulation [44]. Vignal et al. tested the sensitivity of ultrafast time-resolved NIRS and BOLD fMRI to detect hemodynamic changes in the zebra finch brain by comparing data obtained in normocapnic and hypercapnic conditions [42]. In mammals, the effects of hypercapnia on the vasculature of the brain have been well-described e.g. [45-47]. Interestingly, the local BOLD signal variation obtained by BOLD fMRI correlated well with the variations in total haemoglobin and oxygen saturation levels extracted from NIRS in adult zebra finches.

4.4.2.2 Stimulus-selectivity in the primary and secondary auditory areas in the processing of acoustic features of song

Uncovering mechanisms that relate sounds to neural activity, more specifically how neuronal tuning properties help discriminate between general non-specific and biologically-relevant natural sounds requires mechanisms that enable neurons to respond selectively to particular acoustic features of sounds [48, 49]. Consequently, evaluating which brain areas encode the acoustic features of bird song, e.g. temporal and spectral characteristics, is the first step towards exposing the neural substrates responsible for song discrimination. Interestingly, neuroimaging studies in other vertebrate species consistently revealed that specialized

responses to either temporal characteristics or intensity and spectral features of natural sounds occurs relatively early in the auditory pathways [50]. Based on these findings and electrophysiological data available in songbirds e.g. [51, 52], a study was performed to investigate how the auditory areas of the songbird brain process the acoustic features of conspecific song [53]. Adult male zebra finches were exposed to a variety of stimuli, including bird's own song (BOS), familiar conspecific songs and spectrally filtered or temporally filtered versions of these songs [53]. The auditory stimuli were presented in a commonly used on-off block stimulation paradigm (Figure 4-2). All stimuli evoked bilateral activation in the primary auditory region Field L. Interestingly, regional-specific differences in BOLD amplitude could be observed, i.e. the peak activation was observed in L2a, the primary target of the auditory thalamic nuclei, which attenuated towards the dorsal subareas, i.e. L1 and L2b, and ventral and ventro-medial surroundings of Field L (i.e. L3). Furthermore, the secondary auditory regions CMM, CLM and the main body of NCM was not activated in the majority of conditions, however based on signal strength a hierarchical organization between L2a, L2b and CMM was observed. In addition, no BOLD responses could be detected in song nucleus RA for any stimulus condition [53]. No lateralization was found, but it is possible that lateralization happens at the level of secondary auditory processing.

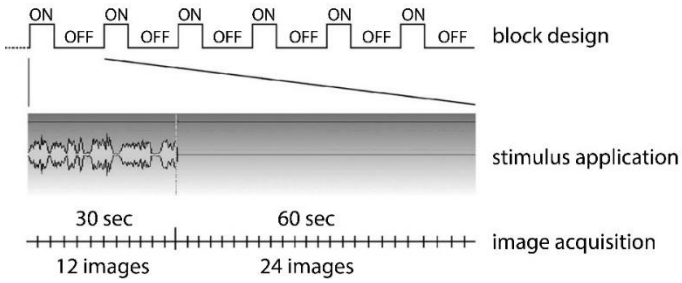

Figure 4-2: Example of a typical on-off stimulation block paradigm. In this example, periods of sound stimulation are alternated with periods of rest. In this representation of a trial course, each block (stimulus/rest) consists of 30 seconds of stimulation followed by 60 seconds of rest, during which 12 and 24 MR images are acquired, respectively. Boumans et al. (2008) used six different sound stimuli: BOS, reversed BOS, random BOS, familiar CON, BOS ripples and white noise versus rest. This figure is extracted from [54] with permission from Plos One.

Stimulus-specific testing revealed decreased responses in the ventral subdivisions of Field L to synthetic conspecific songs that lacked spectral or temporal structure. Importantly however, temporally filtered songs elicited overall higher BOLD responses compared to un-manipulated conspecific song. No difference between BOS and conspecific song could be detected in the

auditory areas [53], this was confirmed in a follow up study [54]. Identification of the neural substrate (selectively) responsive to BOS leads to greater understanding of the process for vocal learning where –during the sensorimotor phase– the juvenile bird tries to match his own, self-generated vocalizations to the previously memorized tutor song using a trial-and-error approach where auditory feedback is of crucial importance [55-57]. The authors suggested that the differentiation between BOS and conspecific song probably occurs at a higher level i.e. not in the primary auditory cortex analogues.

Another focus of the study by Boumans et al. (2007) was to evaluate the effect of three different anaesthetics on the neurovascular response to auditory stimulation, i.e. urethane, medetomidine and isoflurane [53]. They described that both extent (number of activated voxels) and strength of the activated area in the primary auditory regions are strongly affected by the anaesthetic. The effect of anaesthesia has been a major topic of investigation in other functional MRI studies as anaesthetics often affect neural activity and/or the vasculature upon stimulation e.g. [58, 59] or at rest e.g. [60, 61].

4.4.3 Brain-wide evaluation of song selectivity and hemispheric specialization in close-ended learners

The previously described optimization studies acquired only one slice of fMRI data which limited the field-of-view to the primary and secondary auditory brain regions. However, to explore whether other areas, previously not considered in IEG studies or difficult to access by electrophysiology, participate to the processing of auditory information, the field-of-view should encompass the entire brain. Consequently, additional optimizations were required and resulted in a multislice spin echo RARE –based imaging protocol as described by [62-64].

4.4.3.1 Song discrimination involves distinct song control and auditory areas

At approximately the same time as Poirier et al. (2009) reported whole-brain fMRI, another research group explored the spatial extent of song discrimination (i.e. BOLD response topography) between different categories of song in the adult male zebra finch brain [65]. Zebra finches were exposed to BOS, tutor's song, unfamiliar conspecific song and pure tones inside the fMRI scanner. All stimuli caused event-related BOLD signal increases in the auditory lobule (containing primary and secondary auditory areas), however familiar stimuli, i.e. BOS and tutor song, elicited a wider extent of significantly increased BOLD responses in secondary auditory areas NCM and CM compared to unfamiliar conspecific songs. Furthermore, they described a

higher BOLD amplitude in the right hemisphere suggestive of functional lateralization of mechanisms underlying song perception.

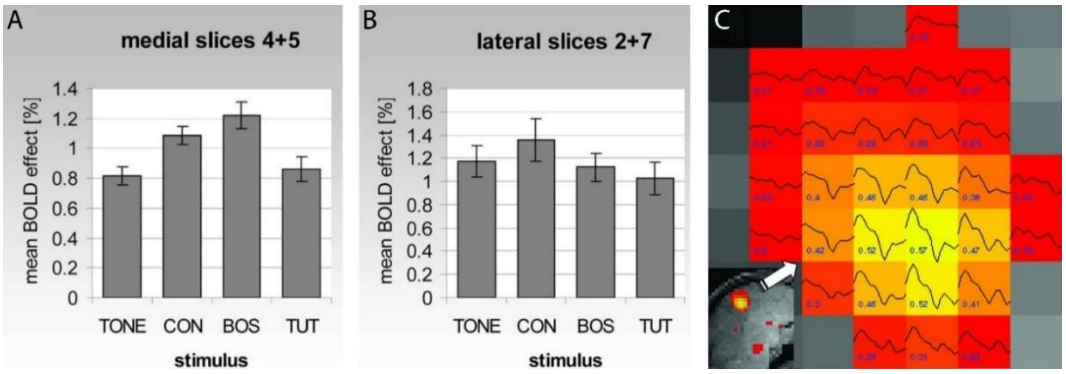

Figure 4-3: Time courses and location of BOLD responses in zebra finch to different categories of bird song. A. Mean BOLD response to BOS is significantly higher in medial slices, while responses to CON are located in lateral slices of the avian forebrain. **B-C**. Time course and location of main BOLD response. BOS activates voxels in the forebrain close to the sagittal midline of a male zebra finch. The colours and numbers represent the correlation coefficients of the response with the stimulation function. Shown are the averaged BOLD response time series with the characteristic shape as expected for this block design paradigm. This figure was obtained from [65] with permission from PNAS (Copyright (2007) National Academy of Sciences, U.S.A.).

In addition, the medial and lateral parts of the auditory forebrain displayed differential BOLD response amplitudes depending on the stimulus type presented (Figure 4-3). Interestingly, the medial parts of the brain (corresponding to the medial region of the auditory lobule) showed the biggest BOLD amplitude in response to BOS, the lateral slides, on the contrary, showed the strongest increase in BOLD signal to (unfamiliar) conspecific song.

In line with the study performed by Voss and co-workers (2007), Poirier et al. (2009) exposed adult male zebra finches to conspecific songs, BOS and heterospecific songs, i.e. canary and starling song, and used the benefit of 'whole-brain' fMRI to assess whether other brain areas beyond the primary and secondary auditory regions, were involved in the processing of different categories of song [66]. The fMRI outcome disclosed that selectivity emerges at the midbrain level, i.e. at MLd, early in the ascending auditory pathway. Surprisingly, the selectivity to BOS was lateralized to the right hemisphere, more specifically in right MLd, right HVC and right area X (Figure 4-4). This finding is reminiscent of own-voice recognition in humans [67].

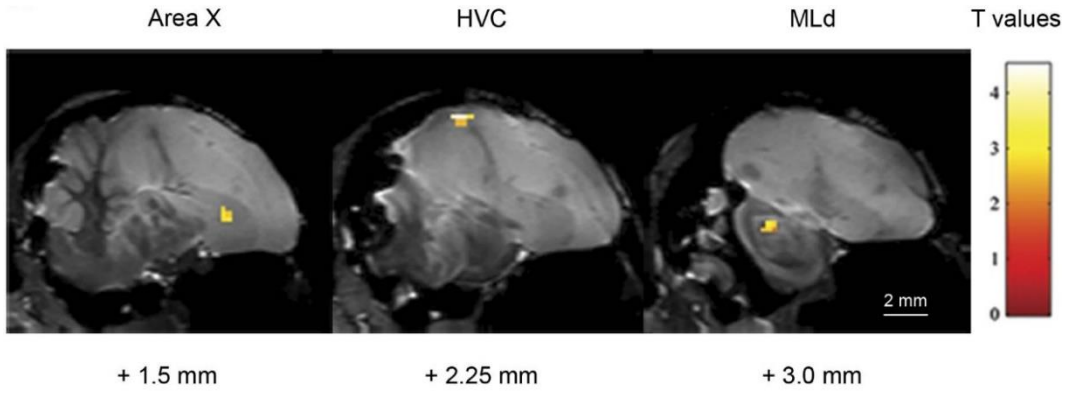

Figure 4-4: fMRI statistical maps displaying right hemispheric dominance when male zebra finches are exposed to own song. More specifically, right area x, right HVC and right MLd are involved. This figure was obtained from [66] with permission from the Society of Neurosciences.

Vocal learning occurs by imitation of an adult song model [68, 69]. Consequently, the BOS and the tutor song are acoustically highly similar and this led to the question as to whether neural selectivity for BOS and tutor song would involve similar brain areas. Consequently, a follow-up fMRI study was performed in adult zebra finches that were reared following a strictly controlled one-to-one tutoring paradigm, i.e. in the presence of only one adult male zebra finch [70]. When the juvenile zebra finches reached 100 days post hatching (approximate time of song crystallization when the critical period for vocal learning closes), they were group-housed together in large aviaries. Importantly, all tutors that participated to this study learnt their song via tape playback containing one of three song models. This implies that all birds in this study sung a copy of one of these three song models. Moreover, since after 100 dph, the juvenile finches were group housed prior to the fMRI measurements, and all auditory stimuli were composed of songs sung by birds in this study, all stimuli in this experiment contained familiar songs. During the fMRI measurements, the birds listened to three different stimuli containing either BOS, tutor song or familiar conspecific song. Importantly, the familiar conspecific song was based on recordings of a bird that was raised by a different tutor that had learnt the same song model as the tutor of the birds that underwent the fMRI scan. Consequently, all stimuli presented to the birds were –in terms of acoustical characteristics– highly similar. This was confirmed by statistical analysis as no significant difference in mean acoustic similarity could be observed between the different stimuli. Such a refined experimental paradigm enabled to challenge the discriminatory capabilities of the anaesthetized songbird brain to differentiate between the responses to acoustically close songs such as BOS and tutor song, while comparing

both categories of song to a third acoustically matched control stimulus, i.e. familiar conspecific song. The analysis showed that even though both left and right MLd were activated by the three stimuli, only the right MLd displayed a significantly higher BOLD response amplitude when hearing BOS and tutor song compared to familiar conspecific songs (Figure 4-5). This finding of BOS selectivity in right MLd corroborated the previous fMRI study [66]. In addition, positive correlations were observed between tutor song selectivity or BOS selectivity (compared to familiar conspecific stimulus) and learning accuracy in right MLd. Learning accuracy was quantified by the amount of song that experimental birds copied from the tutor. These findings suggest that the selective neural activation in MLd as reflected in the BOLD signal 'contrasts', does not solely rely on acoustic differences between the stimuli (controlled for by acoustic similarity of familiar conspecific song), but might point to an important role for MLd in song learning since learning accuracy correlated with the BOLD signal strength (normalized to conspecific song amplitude).

One of the major hurdles in investigating brain responses to particular stimuli is the need to anesthetize animals for successful data acquisition. Only few studies reported on using habituation training to enable awake imaging (e.g. in rodents [60], pigeon [71]). Importantly, functional lateralized responses measured by electrophysiology have been shown to be affected by anaesthesia [72], and possibly, the outcome of fMRI experiments might be obscured by applying specific pharmacological compounds. Moreover, the effects of the applied anaesthetic are considered to be region-specific. However, the previously mentioned studies reported (independently and) consistently on right-ward lateralized responses to similar categories of song stimuli which suggests robustness of the method.

Interestingly, another kind of 'robustness of auditory processing' has also been described in other songbird species such as the pin-tailed whydah that is known to be an obligate brood parasitic songbird, more specifically the rearing of juvenile birds relies on foster care of heterospecific songbird species. Consequently, juvenile pin-tailed whydahs are not or at least much less often exposed to conspecific song stimulation during the critical period for vocal learning. However, an fMRI study combined with behavioural tests showed that adult pin-tailed whydahs are able to discriminate hetero- and conspecific songs and, interestingly, they use the same neural substrate as non-parasitic songbirds [74].

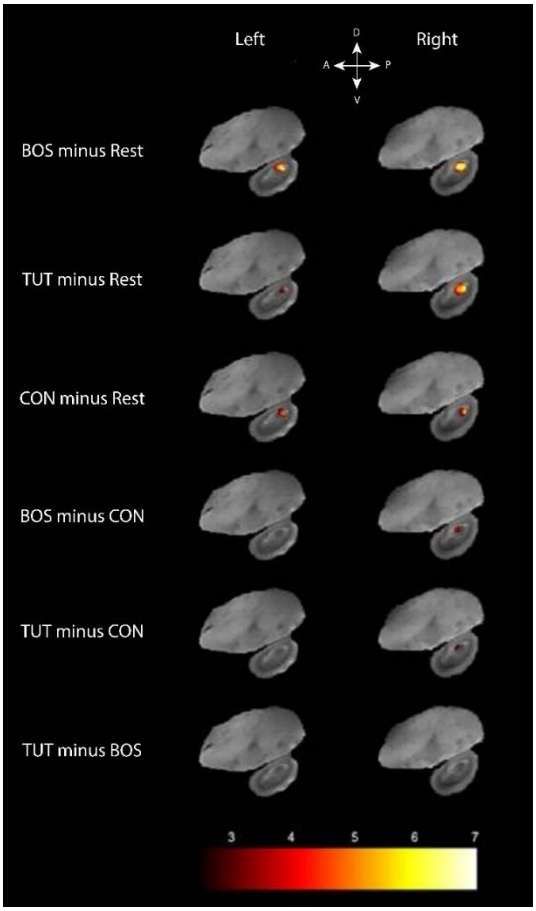

Figure 4-5: Statistical maps of BOLD activation elicited by the different stimuli. Statistical analysis shows that both left and right MLd were activated, but only the right auditory MLd displayed a significantly higher BOLD response to BOS and tutor song exposure compared to familiar conspecific songs, showing a selectivity to BOS and tutor song. This figure was obtained from [70] with permission form PlosOne.

The previously described fMRI studies investigated neural responses to normally reared and normally singing adult male songbirds. Interestingly, two 'manipulation' studies have been performed where (1) juvenile birds learnt song from an adult tutor that produced stuttering-like syllable repetitions in his song [75] and (2) the effect of social isolation to an adult tutor during the critical period for vocal learning [76]. Interestingly, in the latter study, also female zebra finches were investigated. The first study described attenuated BOLD response amplitude to the song of stuttering tutors compared to typical unfamiliar conspecific songs in Field L. This finding advocates for an innate neural preference for typical conspecific birdsong. Similar findings have been obtained in isolated female finches that have never been exposed to conspecific song (during the critical period for vocal learning) [76]. Male zebra finches, on the

other hand, only showed a typical conspecific neural response after exposure to tutor song during the critical period for vocal learning. This finding illustrates that besides sex differences in the structure of the song control system, also the functional properties of the zebra finch brain might be different between both sexes.

4.4.3.2 Alterations in song processing by pharmacological manipulation

Functional MRI can be combined with specific agonists or antagonists for a variety of relevant neurotransmitter systems and contribute in this way to unravel the involvement of specific neurotransmitter systems and its receptors in neuronal and behavioural responses. In the past, a dense noradrenergic innervation of the song control and auditory brain regions of songbirds has been identified [77-80]. Additionally norepinephrine (NE) has been shown to have high concentrations in the song control and auditory nuclei of songbirds (review [81]), and electrophysiological evidence indicates that NE can suppress BOS responsiveness in the avian song system [13, 82]. Poirier et al. (2011) used functional MRI to extend on these findings using DSP-4 injections (a specific noradrenergic toxin decreasing the level of NE), to unmasks own song selectivity in the dorsal part of NCM, a secondary auditory region [83]. In this fMRI experiment three types of song stimuli were used, namely BOS, familiar conspecific song and heterospecific song. BOS selectivity was measured by comparing activity during BOS versus conspecific song exposure (BOS minus CON). To investigate the effect of norepinephrine on BOS selectivity, they compared BOS minus conspecific song with DSP-4 injection versus BOS minus conspecific song with a control saline injection. Injection of DSP-4 resulted in higher BOS-selective responses compared to CON in the dorsal portion of NCM and increased BOLD responses in conspecific versus heterospecific stimuli in CMM.

4.4.4 Seasonal and hormone-induced neuromodulation of auditory processing in open-ended learners

De Groof et al. (2009) uncovered structural changes between breeding and non-breeding season in the NCM of European starlings. Interestingly, evidence collected from IEG and electrophysiology studies points towards an important role for NCM in the processing of conspecific song [43, 84]. Depending on the time of year, starlings reside in highly different social contexts during which the function of (conspecific) song changes markedly. For example, during the breeding season, starlings live in small groups and song is most important for mate recognition. While during the non-breeding season, starlings gather in large groups and use

song for group recognition [85]. Furthermore, recent research in canaries (*Serinus canaria*) showed altered neural activity in HVC to conspecific song depending on the seasonal status [86]. One major concern of this study was that in canaries the spectro-temporal characteristics of song change over the seasons. Consequently, no conclusions on song selectivity can be drawn as the different auditory responses might be ascribed to song selectivity or might be caused by a differential neural response to changes in the acoustic features of song. European starling song, on the other hand, displays no changes in song features over different seasons and can therefore provide a decisive answer.

De Groof and co-workers (2013) repeatedly scanned male European starlings during the breeding and non-breeding season while presenting them with pure tones (control stimulus to compare between different imaging sessions) and four types of starling song, i.e. species-specific whistles, individual whistles, species-specific warbling and individual warbling (for an in-depth description of starling song, we refer to [85]. Importantly, the song stimuli were based on song recordings of an unfamiliar starling to represent individual information or contained species-specific and group information (songs sung by all starlings). Voxel-based analyses showed that during the breeding season both dorso-rostral and caudal subareas of NCM showed a differential response when exposed to species-specific songs and songs conveying individual information. During the non-breeding season this selectivity was only observed in the dorso-rostral NCM. Importantly, the voxel-based outcome suggested that all effects were lateralized toward the right hemisphere. Consequently, a ROI-based test for lateralization confirmed that only the right dorso-rostral and/or caudal NCM activate differently to distinct types of conspecific communication signals depending on the seasonal status [87].

Besides exploring correlations between brain structure, function and hormonal status related to photoperiods, ample studies investigated how acute hormone treatments shape neural tuning which ultimately guides behaviour. Indeed, multiple evidence has been collected supporting the neuromodulatory role of oestrogens on brain and behaviour [88]. For example, a study in adult zebra finches showed that acute blockage of the local oestrogen production by administration of fadrozole (an aromatase inhibitor) in NCM disrupted song preference and altered auditory-evoked neural activity when comparing responses to tutor and birds' own song to conspecific song. Interestingly, local administration of estradiol boosted neural activity when the birds were presented with conspecific song or songs that contained elements of zebra finch

song. Importantly, the behavioural and electrophysiological data only differed when the fadrozole was administered in the left hemisphere [89]. Furthermore, the (rapid) behavioural response to estradiol treatment is dependent on the photoperiod, as observed in California mice [90] and song sparrows [91]. To inform whether it is possible to extrapolate the findings obtained in zebra finches to starlings and, if possible, to inform on the spatial extent of the area modulated by local oestrogens, auditory fMRI was performed during the breeding and non-breeding season, with and without (intraperitoneal) application of vorozole, another aromatase inhibitor [92]. Similar to zebra finches, a clear effect of treatment was observed in left NCM and left Field L, more specifically, the cluster included the rostral part of left NCM and the immediately adjacent left Field L and showed a higher BOLD amplitude reflecting stronger neural activity during control compared to vorozole condition. In addition, an interaction between photoperiod and treatment was observed in the caudal subdivision of left NCM. Post hoc tests revealed that in December, during the non-breeding season, vorozole treatment did not affect the stimulus-evoked BOLD responses. In March, vorozole treatment induced a rapid and significantly decreased BOLD amplitude in the rostral NCM-Field L complex to all stimuli. These results demonstrate that fMRI is an extremely powerful tool to evaluate the effectiveness of pharmacological compounds to modulate sensory processing/coding *in vivo*. Further descriptions of how functional MRI can be applied to inform on the neuromodulatory properties of particular pharmaca in small animal imaging can be found in [93].

4.5 CONCLUSION

Songbirds have been studied extensively with regards to critical period and adult neuroplasticity. Several MRI techniques have led to interesting insights into structural neuroplasticity, involving non-song control brain areas, and age- or photoperiod- or hormone-dependent auditory responses, where distinct areas of one anatomical brain region were shown to process different types of song. Functional imaging studies should judiciously consider the anaesthetic used for functional imaging as several studies, including fMRI but also electrophysiology etc., have shown differential neuro-vascular responses between awake and anesthetized conditions. Furthermore, when evaluating structural neuroplasticity or functional auditory processing in open-ended learning songbirds, hormone status and photoperiod should be carefully monitored to enable a correct interpretation of the experimental outcome. Moreover, additional measures, such as behavioural test, are required to disentangle the

intricate interplay of different mediators that act in concert on the brain. Importantly, the benefits of MRI clearly lie in its versatility as the MRI signal can be sensitized to a wide range of biological phenomena, its non-invasive nature, which allows repeated measures and correlation to additional metrics such as changing hormone levels and behavioural tests, and its ability to extract information from the entire brain at once.

ACKNOWLEDGEMENTS

This work is supported by the Belgian Science Policy (Belspo; PLASTOSCINE P7/17), the Research Foundation – Flanders (FWO; G044311N; G.0302.13) and a grant by the Hercules Foundation (AUHA0012) to AVdL.

REFERENCES

1. Van der Linden, A., et al., *Non invasive in vivo anatomical studies of the oscine brain by high resolution MRI microscopy.* Journal of Neuroscience Methods, 1998. **81**(1–2): p. 45-52.
2. Verhoye, M., et al., *Imaging birds in a bird cage: in-vivo FSE 3D MRI of bird brain.* Magnetic Resonance Materials in Physics, Biology and Medicine, 1998. **6**(1): p. 22-27.
3. Lin, Y.-J. and A.P. Koretsky, *Manganese ion enhances T1-weighted MRI during brain activation: An approach to direct imaging of brain function.* Magnetic Resonance in Medicine, 1997. **38**(3): p. 378-388.
4. Pautler, R.G., A.C. Silva, and A.P. Koretsky, *In vivo neuronal tract tracing using manganese-enhanced magnetic resonance imaging.* Magnetic Resonance in Medicine, 1998. **40**(5): p. 740-748.
5. Van der Linden, A., et al., *In vivo manganese-enhanced magnetic resonance imaging reveals connections and functional properties of the songbird vocal control system.* Neuroscience, 2002. **112**(2): p. 467-474.
6. Bernard, D.J., J.M. Casto, and G.F. Ball, *Sexual dimorphism in the volume of song control nuclei in European starlings: Assessment by a Nissl stain and autoradiography for muscarinic cholinergic receptors.* The Journal of Comparative Neurology, 1993. **334**(4): p. 559-570.
7. Tindemans, I., et al., *IR-SE and IR-MEMRI allow in vivo visualization of oscine neuroarchitecture including the main forebrain regions of the song control system.* NMR in Biomedicine, 2006. **19**(1): p. 18-29.
8. Brini, M., et al., *Neuronal calcium signaling: function and dysfunction.* Cellular and Molecular Life Sciences, 2014. **71**(15): p. 2787-2814.
9. Yu, X., et al., *In vivo auditory brain mapping in mice with Mn-enhanced MRI.* Nature neuroscience, 2005. **8**(7): p. 961-968.
10. Yu, X., et al., *Large-scale reorganization of the tonotopic map in mouse auditory midbrain revealed by MRI.* Proceedings of the National Academy of Sciences of the United States of America, 2007. **104**(29): p. 12193-12198.
11. Grafstein, B. and D.S. Forman, *Intracellular transport in neurons.* Physiological Reviews, 1980. **60**(4): p. 1167-1283.
12. Margoliash, D., *Preference for autogenous song by auditory neurons in a song system nucleus of the white-crowned sparrow.* The Journal of Neuroscience, 1986. **6**(6): p. 1643-1661.

13. Dave, A.S., A.C. Yu, and D. Margoliash, *Behavioral State Modulation of Auditory Activity in a Vocal Motor System.* Science, 1998. **282**(5397): p. 2250-2254.
14. Schmidt, M.F. and M. Konishi, *Gating of auditory responses in the vocal control system of awake songbirds.* Nat Neurosci, 1998. **1**(6): p. 513-518.
15. Tindemans, I., et al., *In vivo dynamic ME-MRI reveals differential functional responses of RA- and area X-projecting neurons in the HVC of canaries exposed to conspecific song.* European Journal of Neuroscience, 2003. **18**(12): p. 3352-3360.
16. Eens, M., *Understanding the Complex Song of the European Starling: An Integrated Ethological Approach*, in *Advances in the Study of Behavior*, J.S.R.C.T.S. Peter J.B. Slater and M. Manfred, Editors. 1997, Academic Press. p. 355-434.
17. Ball, G.F., et al., *Seasonal Plasticity in the Song Control System: Multiple Brain Sites of Steroid Hormone Action and the Importance of Variation in Song Behavior.* Annals of the New York Academy of Sciences, 2004. **1016**(1): p. 586-610.
18. Dawson, A., et al., *Photoperiodic Control of Seasonality in Birds.* Journal of Biological Rhythms, 2001. **16**(4): p. 365-380.
19. Smith, G.T., E.A. Brenowitz, and J.C. Wingfield, *Roles of photoperiod and testosterone in seasonal plasticity of the avian song control system.* Journal of Neurobiology, 1997. **32**(4): p. 426-442.
20. Rouse, M.L.J., et al., *Reproductive state modulates testosterone-induced singing in adult female European starlings (Sturnus vulgaris).* Hormones and Behavior, 2015. **72**: p. 78-87.
21. Van Meir, V., et al., *Differential effects of testosterone on neuronal populations and their connections in a sensorimotor brain nucleus controlling song production in songbirds: a manganese enhanced-magnetic resonance imaging study.* NeuroImage, 2004. **21**(3): p. 914-923.
22. Van Meir, V., et al., *In vivo MR imaging of the seasonal volumetric and functional plasticity of song control nuclei in relation to song output in a female songbird.* NeuroImage, 2006. **31**(3): p. 981-992.
23. De Groof, G., et al., *Neural Correlates of Behavioural Olfactory Sensitivity Changes Seasonally in European Starlings.* PLoS ONE, 2010. **5**(12): p. e14337.
24. Xue, R., et al., *In vivo three-dimensional reconstruction of rat brain axonal projections by diffusion tensor imaging.* Magnetic Resonance in Medicine, 1999. **42**(6): p. 1123-1127.
25. Lin, C.-P., et al., *Validation of Diffusion Tensor Magnetic Resonance Axonal Fiber Imaging with Registered Manganese-Enhanced Optic Tracts.* NeuroImage, 2001. **14**(5): p. 1035-1047.
26. Kim, D.-S., et al., *In vivo mapping of functional domains and axonal connectivity in cat visual cortex using magnetic resonance imaging.* Magnetic Resonance Imaging, 2003. **21**(10): p. 1131-1140.
27. De Groof, G., et al., *In vivo diffusion tensor imaging (DTI) of brain subdivisions and vocal pathways in songbirds.* NeuroImage, 2006. **29**(3): p. 754-763.
28. De Groof, G., et al., *Seasonal rewiring of the songbird brain: an in vivo MRI study.* European Journal of Neuroscience, 2008. **28**(12): p. 2475-2485.
29. De Groof, G., et al., *Structural Changes between Seasons in the Songbird Auditory Forebrain.* The Journal of Neuroscience, 2009. **29**(43): p. 13557-13565.
30. Thompson, C.K. and E.A. Brenowitz, *Seasonal change in neuron size and spacing but not neuronal recruitment in a basal ganglia nucleus in the avian song control system.* The Journal of Comparative Neurology, 2005. **481**(3): p. 276-283.
31. Fusani, L., et al., *Seasonal expression of androgen receptors, estrogen receptors, and aromatase in the canary brain in relation to circulating androgens and estrogens.* Journal of Neurobiology, 2000. **43**(3): p. 254-268.

32. Saldanha, C.J., et al., *Distribution and regulation of telencephalic aromatase expression in the zebra finch revealed with a specific antibody.* The Journal of Comparative Neurology, 2000. **423**(4): p. 619-630.
33. Johansen-Berg, H. and E. Duzel, *Neuroplasticity: Effects of Physical and Cognitive activity on brain structure and function.* NeuroImage, 2016. **131**: p. 1-3.
34. Mello, C.V., T.A.F. Velho, and R. Pinaud, *Song-Induced Gene Expression: A Window on Song Auditory Processing and Perception.* Annals of the New York Academy of Sciences, 2004. **1016**(1): p. 263-281.
35. Olkowicz, S., et al., *Birds have primate-like numbers of neurons in the forebrain.* Proceedings of the National Academy of Sciences, 2016. **113**(26): p. 7255-7260.
36. Logothetis, N.K., *The neural basis of the blood–oxygen–level–dependent functional magnetic resonance imaging signal.* Philosophical Transactions of the Royal Society of London. Series B: Biological Sciences, 2002. **357**(1424): p. 1003-1037.
37. Logothetis, N.K., *The Underpinnings of the BOLD Functional Magnetic Resonance Imaging Signal.* The Journal of Neuroscience, 2003. **23**(10): p. 3963-3971.
38. Van der Linden, A., et al., *Current status of functional MRI on small animals: application to physiology, pathophysiology, and cognition.* NMR in Biomedicine, 2007. **20**(5): p. 522-545.
39. Van Meir, V., et al., *Spatiotemporal properties of the BOLD response in the songbirds' auditory circuit during a variety of listening tasks.* NeuroImage, 2005. **25**(4): p. 1242-1255.
40. Vignal, C., et al., *Background noise does not modify song-induced genic activation in the bird brain.* Behavioural Brain Research, 2004. **153**(1): p. 241-248.
41. Boumans, T., et al., *Functional Magnetic Resonance Imaging in Zebra Finch Discerns the Neural Substrate Involved in Segregation of Conspecific Song From Background Noise.* Journal of Neurophysiology, 2008. **99**(2): p. 931-938.
42. Vignal, C., et al., *Measuring brain hemodynamic changes in a songbird: responses to hypercapnia measured with functional MRI and near-infrared spectroscopy.* Physics in Medicine and Biology, 2008. **53**(10): p. 2457.
43. Mello, C.V., D.S. Vicario, and D.F. Clayton, *Song presentation induces gene expression in the songbird forebrain.* Proceedings of the National Academy of Sciences of the United States of America, 1992. **89**(15): p. 6818-6822.
44. Boas, D.A., et al., *Twenty years of functional near-infrared spectroscopy: introduction for the special issue.* NeuroImage, 2014. **85, Part 1**: p. 1-5.
45. Duong, T.Q., C. Iadecola, and S.-G. Kim, *Effect of hyperoxia, hypercapnia, and hypoxia on cerebral interstitial oxygen tension and cerebral blood flow.* Magnetic Resonance in Medicine, 2001. **45**(1): p. 61-70.
46. Ito, H., et al., *Changes in Human Cerebral Blood Flow and Cerebral Blood Volume during Hypercapnia and Hypocapnia Measured by Positron Emission Tomography.* Journal of Cerebral Blood Flow & Metabolism, 2003. **23**(6): p. 665-670.
47. Martin, C., et al., *Haemodynamic and neural responses to hypercapnia in the awake rat.* European Journal of Neuroscience, 2006. **24**(9): p. 2601-2610.
48. Eggermont, J.J., *Between sound and perception: reviewing the search for a neural code.* Hearing Research, 2001. **157**(1–2): p. 1-42.
49. Gaucher, Q., et al., *How do auditory cortex neurons represent communication sounds?* Hearing Research, 2013. **305**: p. 102-112.
50. Kanwal, J.S. and J.P. Rauschecker, *Auditory cortex of bats and primates: managing species-specific calls for social communication.* Frontiers in bioscience : a journal and virtual library, 2007. **12**: p. 4621-4640.
51. Theunissen, F.E., K. Sen, and A.J. Doupe, *Spectral-Temporal Receptive Fields of Nonlinear Auditory Neurons Obtained Using Natural Sounds.* The Journal of Neuroscience, 2000. **20**(6): p. 2315-2331.

52. Sen, K., F.E. Theunissen, and A.J. Doupe, *Feature Analysis of Natural Sounds in the Songbird Auditory Forebrain.* Journal of Neurophysiology, 2001. **86**(3): p. 1445-1458.
53. Boumans, T., et al., *Neural representation of spectral and temporal features of song in the auditory forebrain of zebra finches as revealed by functional MRI.* The European Journal of Neuroscience, 2007. **26**(9): p. 2613-2626.
54. Boumans, T., et al., *Functional MRI of Auditory Responses in the Zebra Finch Forebrain Reveals a Hierarchical Organisation Based on Signal Strength but Not Selectivity.* PLoS ONE, 2008. **3**(9): p. e3184.
55. Konishi, M., *The Role of Auditory Feedback in the Control of Vocalization in the White-Crowned Sparrow1.* Zeitschrift für Tierpsychologie, 1965. **22**(7): p. 770-783.
56. Konishi, M., *The Role of Auditory Feedback in Birdsong.* Annals of the New York Academy of Sciences, 2004. **1016**(1): p. 463-475.
57. Tschida, K. and R. Mooney, *The role of auditory feedback in vocal learning and maintenance.* Current Opinion in Neurobiology, 2012. **22**(2): p. 320-327.
58. Masamoto, K. and I. Kanno, *Anesthesia and the quantitative evaluation of neurovascular coupling.* Journal of Cerebral Blood Flow & Metabolism, 2012. **32**(7): p. 1233-1247.
59. Schroeter, A., et al., *Specificity of stimulus-evoked fMRI responses in the mouse: The influence of systemic physiological changes associated with innocuous stimulation under four different anesthetics.* NeuroImage, 2014. **94**: p. 372-384.
60. Jonckers, E., et al., *Different anesthesia regimes modulate the functional connectivity outcome in mice.* Magnetic Resonance in Medicine, 2014. **72**(4): p. 1103-1112.
61. Grandjean, J., et al., *Optimization of anesthesia protocol for resting-state fMRI in mice based on differential effects of anesthetics on functional connectivity patterns.* NeuroImage, 2014. **102, Part 2**: p. 838-847.
62. Poirier, C., et al., *Implementation of spin-echo blood oxygen level-dependent (BOLD) functional MRI in birds.* NMR in Biomedicine, 2010. **23**(9): p. 1027-1032.
63. Poirier, C. and A.-M. Van der Linden, *Spin Echo BOLD fMRI on Songbirds*, in *In vivo NMR Imaging: Methods and Protocols*, L. Schröder and C. Faber, Editors. 2011, Humana Press: Totowa, NJ. p. 569-576.
64. Van Ruijssevelt, L., et al., *Functional Magnetic Resonance Imaging (fMRI) with Auditory Stimulation in Songbirds.* Journal of Visualized Experiments : JoVE, 2013(76): p. 4369.
65. Voss, H.U., et al., *Functional MRI of the zebra finch brain during song stimulation suggests a lateralized response topography.* Proceedings of the National Academy of Sciences of the United States of America, 2007. **104**(25): p. 10667-10672.
66. Poirier, C., et al., *Own-Song Recognition in the Songbird Auditory Pathway: Selectivity and Lateralization.* The Journal of Neuroscience, 2009. **29**(7): p. 2252-2258.
67. Rosa, C., et al., *Investigations of hemispheric specialization of self-voice recognition.* Brain and Cognition, 2008. **68**(2): p. 204-214.
68. Doupe, A.J. and P.K. Kuhl, *BIRDSONG AND HUMAN SPEECH: Common Themes and Mechanisms.* Annual Review of Neuroscience, 1999. **22**(1): p. 567-631.
69. Bolhuis, J.J., K. Okanoya, and C. Scharff, *Twitter evolution: converging mechanisms in birdsong and human speech.* Nat Rev Neurosci, 2010. **11**(11): p. 747-759.
70. van der Kant, A., et al., *Representation of Early Sensory Experience in the Adult Auditory Midbrain: Implications for Vocal Learning.* PLoS ONE, 2013. **8**(4): p. e61764.
71. De Groof, G., et al., *Functional MRI and functional connectivity of the visual system of awake pigeons.* Behavioural Brain Research, 2013. **239**(0): p. 43-50.
72. George, I., et al., *State-dependent hemispheric specialization in the songbird brain.* The Journal of Comparative Neurology, 2005. **488**(1): p. 48-60.
74. Louder, M.I.M., et al., *Shared neural substrates for song discrimination in parental and parasitic songbirds.* Neuroscience Letters, 2016. **622**: p. 49-54.

75. Voss, H.U., D. Salgado-Commissariat, and S.A. Helekar, *Altered Auditory BOLD Response to Conspecific Birdsong in Zebra Finches with Stuttered Syllables.* PLoS ONE, 2010. **5**(12): p. e14415.
76. Maul, K.K., et al., *The development of stimulus-specific auditory responses requires song exposure in male but not female zebra finches.* Developmental neurobiology, 2010. **70**(1): p. 28-40.
77. Sockman, K.W. and K.G. Salvante, *The integration of song environment by catecholaminergic systems innervating the auditory telencephalon of adult female European starlings.* Developmental Neurobiology, 2008. **68**(5): p. 656-668.
78. Barclay, S.R. and C.F. Harding, *Androstenedione modulation of monoamine levels and turnover in hypothalamic and vocal control nuclei in the male zebra finch: steroid effects on brain monoamines.* Brain Research, 1988. **459**(2): p. 333-343.
79. Harding, C.F., S.R. Barclay, and S.A. Waterman, *Changes in catecholamine levels and turnover rates in hypothalamic, vocal control, and auditory nuclei in male zebra finches during development.* Journal of Neurobiology, 1998. **34**(4): p. 329-346.
80. Mello, C., R. Pinaud, and S. Ribeiro, *Noradrenergic system of the zebra finch brain: Immunocytochemical study of dopamine-ß-hydroxylase.* The Journal of Comparative Neurology, 1998. **400**(2): p. 207-228.
81. Castelino, C.B. and M.F. Schmidt, *What birdsong can teach us about the central noradrenergic system.* Journal of Chemical Neuroanatomy, 2010. **39**(2): p. 96-111.
82. Cardin, J.A. and M.F. Schmidt, *Noradrenergic Inputs Mediate State Dependence of Auditory Responses in the Avian Song System.* The Journal of Neuroscience, 2004. **24**(35): p. 7745-7753.
83. Poirier, C., et al., *Own Song Selectivity in the Songbird Auditory Pathway: Suppression by Norepinephrine.* PLoS ONE, 2011. **6**(5): p. e20131.
84. Chew, S.J., D.S. Vicario, and F. Nottebohm, *A large-capacity memory system that recognizes the calls and songs of individual birds.* Proceedings of the National Academy of Sciences of the United States of America, 1996. **93**(5): p. 1950-1955.
85. Hausberger, M., *Social influences on song acquisition and sharing in the European starling (Sturnus vulgaris)*, in *Social Influences on Vocal Development*, C.T. Snowdon and M. Hausberger, Editors. 1997, Cambridge University Press: Cambridge. p. 128-156.
86. Alliende, J., K. Lehongre, and C. Del Negro, *A species-specific view of song representation in a sensorimotor nucleus.* Journal of Physiology-Paris, 2013. **107**(3): p. 193-202.
87. De Groof, G., et al., *Functional changes between seasons in the male songbird auditory forebrain.* Frontiers in Behavioral Neuroscience, 2013. **7**: p. 196.
88. Remage-Healey, L., S.D. Jeon, and N.R. Joshi, *Recent evidence for rapid synthesis and action of estrogens during auditory processing in a songbird.* Journal of neuroendocrinology, 2013. **25**(11): p. 1024-1031.
89. Remage-Healey, L., et al., *Brain estrogens rapidly strengthen auditory encoding and guide song preference in a songbird.* Proceedings of the National Academy of Sciences of the United States of America, 2010. **107**(8): p. 3852-3857.
90. Trainor, B.C., M.S. Finy, and R.J. Nelson, *Rapid effects of estradiol on male aggression depend on photoperiod in reproductively non-responsive mice.* Hormones and behavior, 2008. **53**(1): p. 192-199.
91. Heimovics, S.A., J.K. Ferris, and K.K. Soma, *Non-invasive administration of 17ß-estradiol rapidly increases aggressive behavior in non-breeding, but not breeding, male song sparrows.* Hormones and Behavior, 2015. **69**: p. 31-38.
92. De Groof, G., et al., *Topography and Lateralized Effect of Acute Aromatase Inhibition on Auditory Processing in a Seasonal Songbird.* The Journal of Neuroscience, 2017.

93. Jonckers, E., et al., *Imaging tools to study pharmacology: functional MRI on small rodents.* Frontiers in Pharmacology, 2015. **6**.

Chapter 5

Exploring sex differences in the adult zebra finch brain: *in vivo* diffusion tensor imaging and *ex vivo* super-resolution track density imaging

This chapter is based on:

Hamaide J, De Groof G, Van Steenkiste G, Jeurissen B, Van Audekerke J, Naeyaert M, Van Ruijssevelt L, Cornil C, Sijbers J, Verhoye M, Van der Linden A. *Exploring sex differences in the adult zebra finch brain: In vivo diffusion tensor imaging and ex vivo super-resolution track density imaging.* Neuroimage. 2017 Feb 1; doi: 10.1016/j.neuroimage.2016.09.067.

ABSTRACT

Zebra finches are an excellent model to study the process of vocal learning, a complex socially-learned tool of communication that forms the basis of spoken human language. So far, structural investigation of the zebra finch brain has been performed ex vivo using invasive methods such as histology. These methods are highly specific, however, they strongly interfere with performing whole-brain analyses and exclude longitudinal studies aimed at establishing causal correlations between neuroplastic events and specific behavioural performances. Therefore, the aim of the current study was to implement an in vivo Diffusion Tensor Imaging (DTI) protocol sensitive enough to detect structural sex differences in the adult zebra finch brain. Voxel-wise comparison of male and female DTI parameter maps shows clear differences in several components of the song control system (i.e. Area X surroundings, the high vocal centre (HVC) and the lateral magnocellular nucleus of the anterior nidopallium (LMAN)), which corroborate previous findings and are in line with the clear behavioural difference as only males sing. Furthermore, to obtain additional insights into the 3-dimensional organization of the zebra finch brain and clarify findings obtained by the in vivo study, ex vivo DTI data of the male and female brain were acquired as well, using a recently established super-resolution reconstruction (SRR) imaging strategy. Interestingly, the SRR-DTI approach led to a marked reduction in acquisition time without interfering with the (spatial and angular) resolution and SNR which enabled to acquire a data set characterized by a 78 µm isotropic resolution including 90 diffusion gradient directions within 44h of scanning time. Based on the reconstructed SRR-DTI maps, whole brain probabilistic Track Density Imaging (TDI) was performed for the purpose of super resolved track density imaging, further pushing the resolution up to 40 µm isotropic. The DTI and TDI maps realized atlas-quality anatomical maps that enable a clear delineation of most components of the song control and auditory systems. In conclusion, this study paves the way for longitudinal in vivo and high-resolution ex vivo experiments aimed at disentangling neuroplastic events that characterize the critical period for vocal learning in zebra finch ontogeny.

5.1 INTRODUCTION

Songbirds –zebra finches in particular– are currently regarded as the best animal model available to study specific aspects of the neurobiology of human speech learning [1, 2]. However, so far, no studies reported using non-invasive imaging methods to study the structural properties of the zebra finch brain *in vivo*. This strongly interferes with performing longitudinal studies aimed at tracing neuroplastic events along the process of vocal learning, establishing causal relationships between experience and brain plasticity and conducting whole-brain analyses. Previously, *in vivo* Diffusion Tensor Imaging (DTI) was successfully used in European starlings *(Sturnus vulgaris)* [3] where De Groof et al. showed seasonally recurring neuroplastic changes in living songbirds [4, 5]. These studies also showed that DTI is the MR method of choice to explore the anatomy of the songbird brain as conventional T1- and T2-weighted sequences do not yield anatomical contrast in the song control system [6, 7]. However, the protocol used to image adult starlings across seasons cannot be used to obtain data of the zebra finch brain as the total scanning time was 8 hours to scan one hemisphere. Such extended acquisition times might interfere with studying structural brain changes related to the process of vocal learning in juvenile songbirds in a longitudinal study design. In addition, obtaining data from one hemisphere hampers the investigation of possible lateralization of effects [8]. Fortunately, in recent years, faster sequences have become available. Consequently, the first aim of this study was to implement an *in vivo* imaging protocol to acquire DTI data of the zebra finch brain in a shorter time frame (< 2 hours).

The organization of the songbird brain is fundamentally different from the mammalian brain [2, 9, 10]. Instead of being organized in a multi-layered cortex as is the case in mammals, evolutionary similar pallium-derived structures are condensed in nuclei situated mainly in the forebrain [11]. Fibre tracts connect distinct nuclei to subsequent relay stations. This modular arrangement results in extensive circuitries and is morphologically comparable to more ventrally situated brain areas in the mammalian brain such as the thalamus and basal ganglia. Two main pathways, together termed as the ‘song control system’, characterize the neural substrate encoding singing behaviour (i.e. the anterior forebrain pathway and the caudal motor pathway). The first is most important in song learning [12-16] and consists of High Vocal Centre (HVC) that sends projections to Area X which in turn projects to the medial part of the dorsolateral nucleus of the anterior thalamus (DLM) that contacts the lateral magnocellular

nucleus of the nidopallium (LMAN) and finally reaches in the robust nucleus of the arcopallium (RA). The second pathway is responsible for the motor aspect of singing [17], encodes specific learned features of songs [18, 19], and contains a direct projection from HVC to RA and then projects further downstream to the vocal organ via several tracts among which the *tractus occipitomesencephalicus* (OM) [20]. Interestingly, only male zebra finches sing, consequently, the song control system is more enhanced in males. This sex difference in behaviour was first discovered by Nottebohm and Arnold (1976) who reported dramatic volume differences between both sexes in Area X, HVC and RA, in canaries and zebra finches [21]. From then onwards, several studies have explored the existence of sex differences in microstructural tissue properties describing differences in soma size [22], dendritic arborisation [23], distribution of perineuronal nets [24, 25], often affecting only specific components of the song control circuitry. As structural sexual dimorphisms in the songbird have been described extensively in literature [26], this provides the ideal question to test the sensitivity of the optimized *in vivo* DTI protocol. In addition, as sex differences in the songbird brain are well characterized by histology, specific biological properties might be linked to the DTI parameter readout.

Despite the clear sex differences, so far only atlases of the male zebra finch brain are available [27-29]. Hence, to obtain a high-resolution overview of the sex differences in the adult zebra finch brain, *ex vivo* imaging of a male and female brain was performed. To realize high-resolution DTI data within a shorter acquisition time, a recently developed super-resolution reconstruction (SRR) method [30] was combined with super-resolved track density imaging [31].

The aim of the current study was twofold: (1) to test a recently optimized *in vivo* DTI protocol to detect structural sex differences in the adult zebra finch brain, and (2) to perform *ex vivo* SRR-DTI scans on a male and female brain to obtain a clear, high-resolution view on the 3-dimensional organization of the adult zebra finch brain and to clarify specific findings detected in the *in vivo* data.

5.2 MATERIALS AND METHODS

5.2.1 Animals and Ethical statement

Adult male and female zebra finches (*Taeniopygia guttata*; n = 17 / sex) were purchased at a local supplier or bred in the animal facility (birds older than 200 days post hatching were considered adult). The birds were kept in indoor aviaries in non-breeding conditions with food and water available *ad libitum*. All experimental procedures were in accordance with the European Directive 2010/63/EU and approved by the Committee on Animal Care and Use at the University of Antwerp, Belgium (permit number 2012-43).

5.2.2 MRI data acquisition

5.2.2.1 In vivo DTI

The birds were anaesthetized with isoflurane (IsoFlo®, Abbott, Illinois, USA; induction: 2.5%; maintenance: 1.5-1.8%) in a mixture of N_2O (66%) and O_2 (33%). Throughout the entire imaging protocol, the physiological condition of the animals was continuously monitored by means of a pressure sensitive pad to detect the breathing rate, and a cloacal thermistor probe to measure body temperature (MR-compatible Small Animal Monitoring and Gating system, SA Instruments, Inc.). The latter was connected to a tightly controlled warm air feedback system to maintain the birds' body temperature within narrow physiological ranges (40.0 ± 0.2) °C. All zebra finches recovered perfectly within a few minutes after the experiment.

Images were acquired on a 7 T horizontal MR system (PharmaScan 70/16 US, Bruker BioSpin GmbH, Germany) equipped with standard Bruker setup (i.e. a quadrature transmit volume coil, a linear array receive coil designed for mice and a 400 mT/m gradient insert (Bruker BioSpin, Germany)). First, Turbo RARE T_2-weighted pilot scans along three orthogonal directions were acquired to assess the birds' position. Second, a field map was acquired to measure magnetic field inhomogeneities after which local shimming was performed. Next, coronal diffusion-weighted (DW) four shot SE-EPI images were acquired with 60 optimally distributed diffusion gradient directions [32]. Twenty-one non-DW b_0 data sets (b = 0 s/mm²; 7 b_0 per 20 DW images) were acquired. The image parameters were: FOV (20x15) mm², TE 22 ms, TR 7000 ms, acquisition matrix (105x79), in-plane resolution (0.19x0.19) mm², slice thickness 0.24 mm, b-value 670 s/mm², diffusion gradient duration (δ) 4 ms, diffusion gradient separation (Δ) 12 ms, scan duration approximately 1 h 20 min. For practical reasons, the Field-of-View (FOV) was

limited to the birds' telencephalon, cerebellum and the major dorsal parts of the mesencephalon and diencephalon, since these brain areas contain most relevant auditory and song control system nuclei. The entire DTI protocol was repeated twice to increase the SNR. Immediately after DTI, a 3-dimensional (3D) RARE scan positioned identical to the DTI data set was acquired for registration purposes. Over the course of the experiment two similar RARE sequences were used (imaging parameters $RARE^A$: TE 11 ms (TE_{eff} 44 ms), TR 3000 ms, RARE factor 8, FOV (16 x 14 x 14) mm^3, matrix (256 x 92 x 64), spatial resolution (0.06 x 0.15 x 0.22) mm^3 zero-filled to (0.06 x 0.05 x 0.05) mm^3, scan duration 35 min; or $RARE^B$: TE 11 ms (TE_{eff} 55 ms), TR 2500 ms, RARE factor 8, FOV (18 x 16 x 10) mm^3, matrix (265 x 92 x 64), spatial resolution (0.07 x 0.17 x 0.16) mm^3 zero-filled to (0.07 x 0.07 x 0.07) mm^3, scan duration 29 min). Each imaging session took approximately 2h 45min.

5.2.2.2 Ex vivo SRR-DTI

Two adult males and one adult female zebra finch that took part in the *in vivo* study, were euthanized by an intramuscular injection of pentobarbital (Nembutal, Ceva Sante Animale; 60 mg/kg) and transcardially perfused with ice-cold 4% paraformaldehyde (PFA) in a 0.1 M Phosphate Buffered Saline (PBS; pH 7.4) solution supplemented with gadolinium (1% Dotarem, 0.5 mmol gadoteric acid/ml; Guerbet, France). Next, the brains were post-fixed overnight with 4% PFA in 0.1 M PBS enriched with 1% Dotarem after which the tissue was transferred to 0.1 M PBS with 1% Dotarem and kept at 4°C for storage. The brains remained in the skull during the entire procedure so as to prevent mechanical damage throughout the different tissue processing and imaging steps.

Approximately eight hours prior to *ex vivo* imaging, the samples were removed from the refrigerator in order to acclimatize to the ambient bore temperature. The three zebra finch heads were imaged with a DW SE sequence on a horizontal 9.4 T MRI system (BioSpec, Bruker Biospin GmbH, Germany) with a circular polarized transmit resonator, quadrature receive surface coil and a 600 mT/m gradient insert (Bruker BioSpin, Germany). For one male and one female brain twelve low resolution data sets were acquired where each set was rotated around the phase-encoding direction at incremental steps of 15° for the purpose of super resolution reconstruction (Figure 5-1). Each of these sets consisted of 1 b_0 and 5 DW images (b = 2500 s/mm^2) with following acquisition parameters: FOV (15x15) mm^2, TE 26 ms, TR 10 000 ms, acquisition matrix (192 x 137) zero-filled to (192 x 192), in-plane resolution of (0.078 x 0.078)

mm², slice thickness 0.32 mm, 37 slices, δ 6 ms, Δ 14 ms, acquisition time 2h 40 min. The test male sample underwent a slightly different imaging protocol, where instead of 12 sets of low resolution images, 15 low resolution data sets were acquired rotated around the phase encoding axis at incremental steps of 12°. In addition, for each low resolution acquisition angle, 1 b_0 image together with 6 DW scans were acquired. All other imaging parameters remained identical. For each slice orientation, the diffusion gradient directions were uniformly sampled based on a method proposed by [33]. The in total 60 (male and female) or 90 (test male) diffusion gradient directions were selected and programmed in the absolute x-y-z coordinate system of the scanner. For details on the theory supporting the super-resolution reconstruction acquisition protocol we refer to [30]. Total acquisition time was approximately 44 hours (test sample) or 28 hours (one male, one female) per sample.

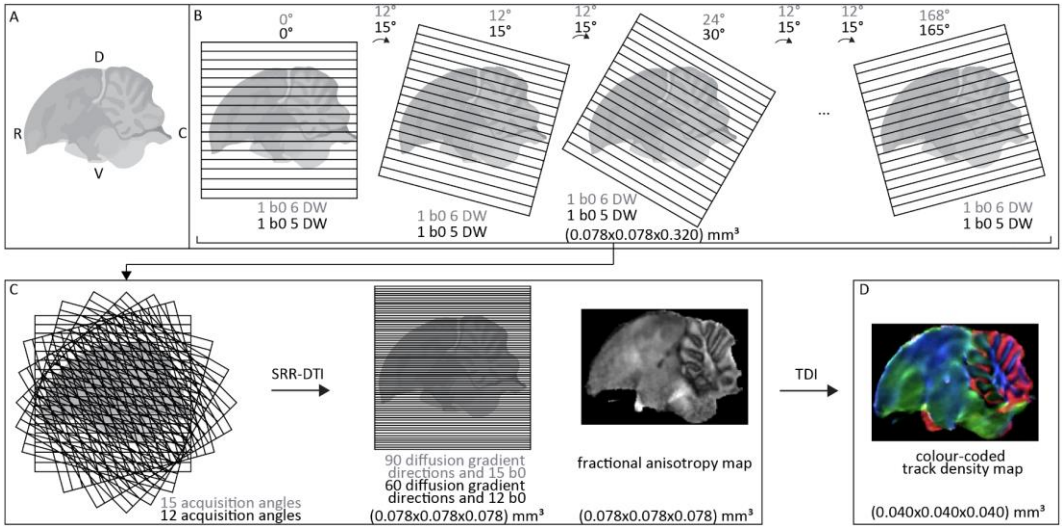

Figure 5-1: Schematic overview of the SRR-DTI data acquisition protocol. (A) Sagittal view of the zebra finch brain. (B-C-D) Chronological overview of the scanning procedure illustrating the different low resolution data sets that are rotated at incremental steps of either 15° (male and female brain, black font) or 12° (test male brain, grey font) around the phase-encoding axis. (C) All low-resolution data sets are reconstructed into a high-resolution grid along which the diffusion tensor is estimated and the DTI parameter maps are calculated. (D) Based on the reconstructed high-resolution SRR-DTI data, whole-brain fibre tractography was performed which resulted in track density images. Abbreviations: R: rostral; C: caudal; D: dorsal; V: ventral.

5.2.3 MRI data processing

5.2.3.1 In vivo DTI

First, the diffusion data were realigned to correct for subject motion using the Diffusion II toolbox in SPM8 (Statistical Parametric Mapping, http://www.fil.ion.ucl.ac.uk/spm/). First, a

rigid registration was performed between the b_0 images which was followed by an extended registration taking all DW images into account. The realigned DW-images of each subject were co-registered to the 3D RARE data set of the same imaging session using mutual information as the similarity metric. In parallel, the 3D RARE data set was spatially normalized to match the zebra finch atlas using a global 12-parameter affine transformation followed by nonlinear deformations. Next, the transformation matrix of the spatial normalization was applied to the realigned and co-registered DW images. Then, the diffusion tensor was estimated and DTI parameter maps were computed (i.e. fractional anisotropy (FA), mean diffusivity (MD), axial diffusivity (AD) and radial diffusivity (RD)). Finally, all DTI parameter maps were smoothed in plane using a Gaussian kernel (FWHM = 0.38 mm x 0.38 mm).

5.2.3.2 Ex vivo DTI

DTI with spatial super-resolution reconstruction (SRR-DTI)

From the acquired low resolution DW images, high resolution diffusion tensors were estimated on a (0.078x0.078x0.078) mm^3 grid, using SRR-DTI [30]. SRR-DTI combines the DTI estimation with super-resolution reconstruction, thereby enabling the direct estimation of high resolution diffusion tensors from a set of low resolution DW images. The motion parameters used by SRR-DTI were estimated using an iterative model-based motion correction scheme [34].

Super-resolved track density imaging (TDI)

In order to obtain fibre orientation distribution functions (fODFs) suitable for probabilistic fibre tracking, the following steps were performed. First, a dense set of predicted high resolution DW images were obtained from the high resolution diffusion tensor parameters estimated using SRR-DTI. Next, the white matter fibre response function was extracted from the high resolution DW data using the recursive calibration method described in [35]. Finally, fODFs were obtained by performing constrained spherical deconvolution [36], using the high resolution DW images and the single fibre response function created above, adopting the quadratic programming approach outlined in [37]. The spherical harmonic series describing the fODFs was terminated at order 8.

Probabilistic whole brain tractography was then performed using second order integration over the fODFs [38]. 10^8 streamlines were generated using the following parameters: fODF amplitude threshold of 0.1, step size of 0.08 mm, and a maximum angle between steps of 9°. From the resulting tractogram, track density maps were calculated at a super-resolution of (40

x 40 x 40) μm^3 [31]. In addition, probabilistic seed-based tractography was also performed in the male and female data set using the same parameters to visualize fibres encapsulating Area X. All steps were performed using MRtrix version 0.3 [39] (www.mrtrix.org).

5.2.4 Statistical analyses

A voxel-wise 2-sample t-test was used to test for differences between males and females for each DTI parameter map separately. To correct for multiple comparisons, a family-wise error (FWE) correction thresholded at $p<0.05$ was applied. Besides this very stringent correction, all statistical parameter maps were assessed uncorrected with an arbitrary threshold at $p<0.001$ in combination with a minimal cluster size of 3 voxels. The statistical maps were superimposed on the zebra finch atlas (displayed uncorrected $p<0.01$; minimum 16 voxels).

5.3 RESULTS

5.3.1 *In vivo* DTI

Independent voxel-wise two-sample t-tests comparing male and female DTI parameter maps revealed significant differences in several DTI parameters at various locations in the brain. As expected from a behavioural point of view (only males sing), most differences could be co-localized with the song control system nuclei. When investigating the statistical maps using an arbitrary threshold (no FWE correction), significant clusters complementary to the FWE findings could be observed. A detailed overview of the voxel-based results can be found in Table 5-1.

5.3.1.1 Fractional anisotropy

The strongest difference between adult male and female zebra finches was found bilaterally in the tissue surrounding Area X (Left: $p < 0.001$; Right $p = 0.023$; FWE corrected), a part of the anterior forebrain pathway involved in song learning. Within this cluster FA values are higher in males as compared to females. Close examination of the cluster suggests that it is situated mainly at the dorso-caudo-lateral edge almost entirely encapsulating Area X (Figure 5-2-A). In addition, a small part of the tOM rostral to nucleus DLM showed up as well (Left: $p = 0.0002$ (5 voxels); Right: $p = 0.0003$ (10 voxels); uncorrected; Figure 5-2-A).

FA values were higher in females as compared to males in two clusters at the location of HVC (Left: $p<0.004$; Right $p<0.004$; FWE corrected; Figure 5-2-B). When lowering the threshold for visualization of the statistical result to $p<0.01$, the clusters extend ventro-medially towards the dorsal part of NCM and Field L (Figure 5-2-B).

5.3.1.2 Mean diffusivity

A significantly increased MD in males compared to females was observed in left HVC ($p = 0.009$; FWE corrected). When exploring the data set without multiple comparison correction also right HVC ($p = 0.001$; uncorrected) and LMAN (Left: $p < 0.001$; Right: $p < 0.001$; uncorrected) were found to be different (Figure 5-2-C-D). The latter cluster can be visually confirmed on the *ex vivo* data sets as a hyper-intense spot covering LMAN in the male but not the female MD maps (inset Figure 5-2-C). There were no areas found which displayed a higher MD in females as compared to males.

5.3.1.3 Axial diffusivity

After multiple comparison correction, no clusters demonstrating a sex difference in AD could be found. When lowering the statistical threshold to $p<0.001$ uncorrected, left HVC and left LMAN were found to have higher AD in males ($p = 2.77*10^{-06}$; $p = 4.76*10^{-05}$ respectively). After exploring the statistical maps with $p<0.01$, both contralateral HVC and LMAN were found to be different as well. Moreover, two clusters with great resemblance to the Area X surroundings – similar to the voxel-wise difference in FA– were detected (Left and Right: $p = 0.001$). No other differences in AD have been observed.

5.3.1.4 Radial diffusivity

Both left LMAN and left HVC were found to have a significantly higher RD in males as compared to females ($p = 0.022$; $p = 0.004$; FWE corrected). Without multiple comparison correction the contralateral LMAN and HVC also displayed a clear disparity in RD ($p = 2.04*10^{-04}$; $p = 1.12*10^{-04}$, respectively), interestingly, a small cluster near right nucleus RA was detected as well ($p = 8.69*10^{-05}$ uncorrected).

5.3.2 *Ex vivo* SRR-DTI and TDI

The SRR-DTI protocol resulted in high quality diffusion MRI data, which were reconstructed into one data set characterized by an isotropic resolution of 78 µm. The different DTI parameter maps show a clear anatomical contrast. The implementation of the SRR technique to acquire DTI data resulted in a significant reduction of the total acquisition time (i.e. ±28h or ±44h for respectively 60 or 90 diffusion gradient directions). Other studies that use high-resolution *ex vivo* DTI, report on long acquisition durations, or reduce the angular and/or spatial resolution to obtain reasonable acquisition times. This marked reduction in scanning time also extends to T_2-weighted anatomical 3-dimensional data sets. If only the b_0 images would have been

acquired, the total acquisition time would be approximately 4.67h or 6.29h. This is in line with [40].

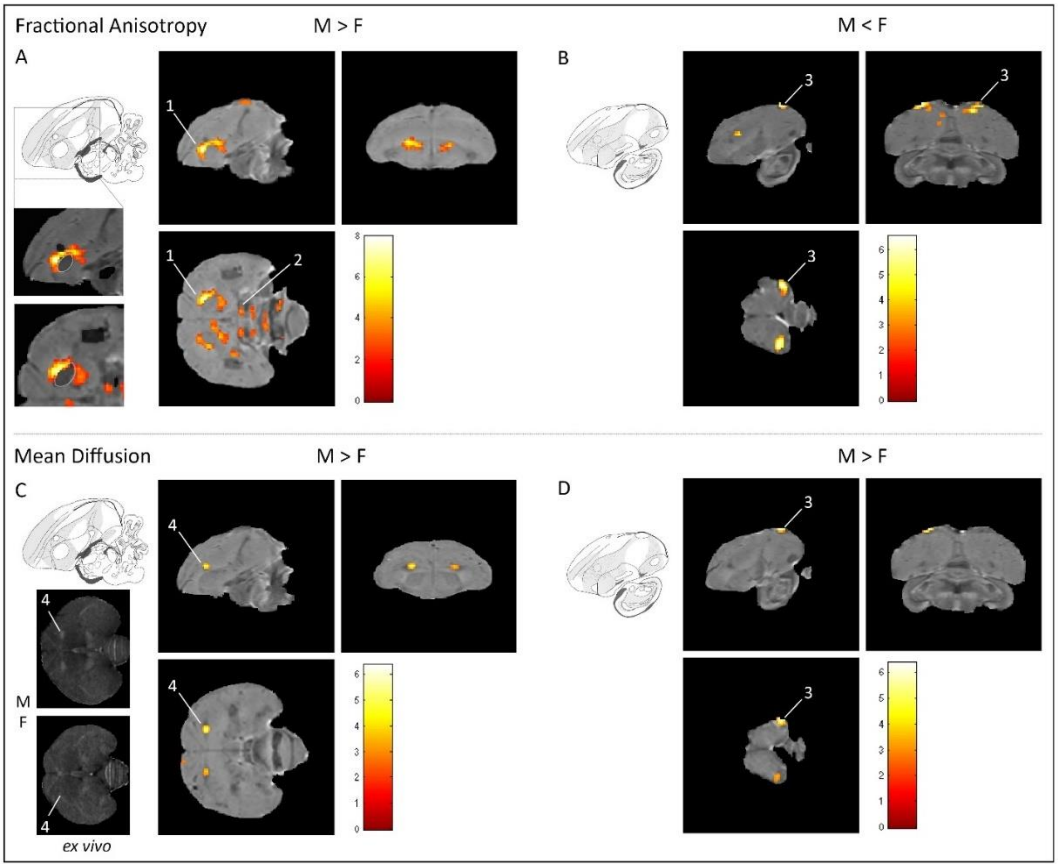

Figure 5-2: *In vivo* DTI confirms known sex differences. Statistical maps showing the voxels where (A) FA values are higher in males compared to females, (B) FA values are smaller in males compared to females, or (C-D) MD values are higher in males compared to female zebra finches. The statistical results are displayed uncorrected $p<0.01$ and overlaid onto the ZF atlas [29]. The t-values are colour coded according to the scales displayed on the right side of each panel. The numbers represent: (1) Area X surroundings, (2) part of the tOM, (3) HVC and (4) LMAN. The sagittal schematic atlas drawings are obtained from the zebra finch histological atlas browser [28], with permission of John Wiley and Sons. Both MRI inserts in panel A display a sagittal (top) and horizontal (bottom) slice of the ex vivo MRI atlas and illustrate that the cluster encapsulates Area X which is delineated by a white line. The two insets in panel C are the ex vivo SRR-MD maps of the male (top) and female (bottom) sample. LMAN (4) can be seen as hyper-intense spots on the male data set, whereas it cannot be discriminated from the surrounding tissue on the female data set.

Table 5-1: Summary of the results of the voxel-based analysis comparing male to female DTI parameter maps.

	M > F					M < F				
	brain area	hemisphere	cluster size **	*p*	*p**	brain area	hemisphere	cluster size**	*p*	*p**
FA	Area X surroundings	Left	215	<0.001	$<0.1*10^{-07}$	HVC	Left	28	0.004	$1.59*10^{-07}$
				0.009						
		Right	44	0.023	$<0.1*10^{-05}$		Right	29	0.004	$1.73*10^{-07}$
			26	0.043	$<0.1*10^{-04}$					
	part of tOM	Left	5		$1.97*10^{-04}$					
		Right	10		$2.63*10^{-04}$					
MD	HVC	Left	14	0.009	$1.88*10^{-07}$					
		Right	3		0.001					
	LMAN	Left	17		$2.47*10^{-06}$					
		Right	3		$4.17*10^{-04}$					
AD	HVC	Left	5		$2.77*10^{-06}$					
	LMAN	Left	8		$4.76*10^{-05}$					
RD	HVC	Left	19	0.004	$6.35*10^{-08}$					
		Right	8		$2.04*10^{-04}$					
	LMAN	Left	17	0.022	$1.21*10^{-06}$					
		Right	9		$1.12*10^{-04}$					
	RA	Right	6		$8.69*10^{-05}$					

* not corrected for multiple comparisons

** Cluster size: number of voxels in cluster when significance level is set uncorrected $p<0.001$.

p and *p**: *p*-value at peak level of the cluster.

5.3.2.1 Neuroanatomy

For all visualizations, the same reference frame as the *ex vivo* zebra finch atlas [29] was chosen (i.e. the symmetrical axis of the brain and a 10° clockwise rotation compared to the base of the brain in the midsagittal slice). This closely matches aligning the *commissura anterior* and *posterior* in a horizontal plane on the midsagittal slice. Figure 5-3 provides an overview of the different anatomical structures visible on the male SRR-b_0 data set. Many similarities can be found with the recently published schematic drawings by Karten and Mitra (www.brainarchitecture.org; [28]; Figure 5-3 B). Interestingly, several components of the song control circuitry (i.e. HVC, RA, LMAN, Area X and DLM), auditory system (i.e. MLd, *nucleus ovoidalis*, Field L), visual system (i.e. *entopallium* and *nucleus rotundus*) can be identified. In addition, many tracts that connect different brain areas can be localized as well. For example, the tOM which is a tract connecting the caudal motor pathway (HVC-RA) to the tracheosyringeal nucleus (nXIIts), and the *chiasma opticum* which contains the *tractus opticus* that relays information from the eyes to the *tectum opticum* can all be discerned.

The brain samples scanned for the SRR-b_0 and the *ex vivo* atlas [29] were processed identically (i.e. perfused with 4% PFA and 1% Dotarem), and both imaging protocols resulted in the same spatial resolution. Consequently, when comparing the SRR-b_0 images of the male zebra finch to the *ex vivo* zebra finch atlas [29], the resulting anatomical contrast is very similar. However, some differences can be observed (Figure 5-4). First, the SRR-b_0 images yield some additional contrast near the cerebellum enabling the identification of the different cerebellar layers (i.e. molecular and Purkinje-granule cell layers, the latter two cannot be distinguished on the SRR-b_0 data sets). Second, the boundaries of Area X are more clearly visible on the SRR-b_0 image compared to the *ex vivo* atlas. HVC, on the other hand, is more clearly visible on the *ex vivo* atlas. Lastly, the SRR-b_0 images more closely resemble the *in vivo* 3D RARE data (data not shown).

Visual inspection of the male and female SRR-b_0 data sets clearly shows the sex difference in Area X, RA and HVC (Figure 5-5). While in general smaller in females compared to males [21], HVC and RA cannot be differentiated from the surrounding tissue in the female SRR-b_0 data set. All other components of the song control circuitry (e.g. LMAN and DLM), and other systems, are clearly discernible in both sexes. Given that the SRR-b_0 of the male data set achieves the

same anatomical contrast as the *ex vivo* atlas, the female SRR-b_0 data set can serve as the first female zebra finch atlas.

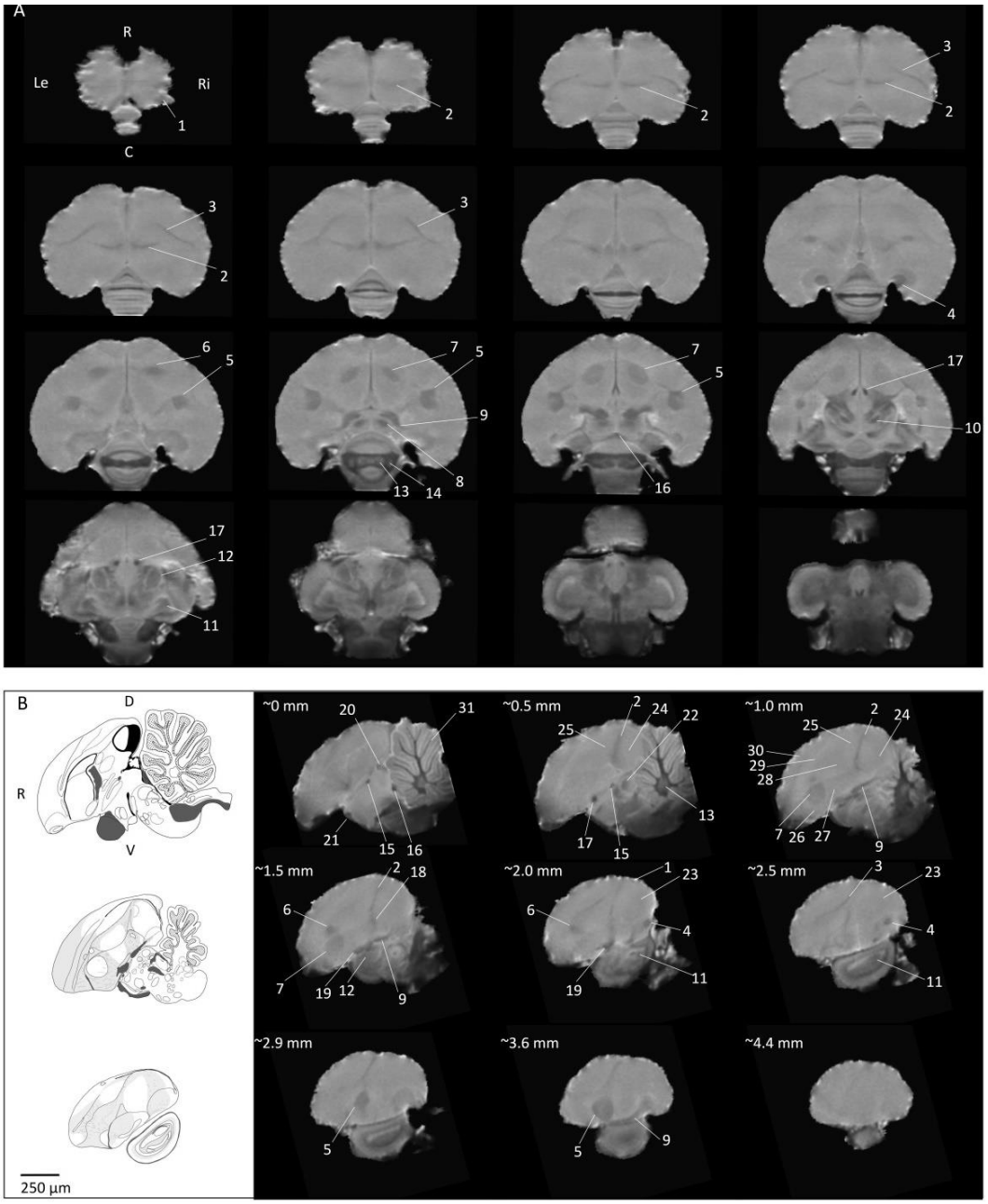

Figure 5-3: Overview of anatomical contrast provided by the male *ex vivo* SRR-DTI b_0 data set. Consecutive slices are ordered from left to right where the top left slice represents the most dorsal or medial and the bottom right slice the most ventral or lateral part of the zebra finch brain for respectively the horizontal or sagittal images. The schematic atlas drawings correspond to the adjacent sagittal MR image. For each sagittal slice the approximate distance from the midline is specified. The following structures can be identified: (1) HVC, (2) Field L, (3) lamina mesopallialis, (4) nucleus robustus arcopallialis, (5) entopallium, (6) LMAN, (7) Area X, (8) DLM, (9) tractus

occipitomesencephalicus, (10) nucleus ovoidalis, (11) MLd-DM-Ico (intercollicular nucleus) complex, (12) nucleus rotundus, (13) medial cerebellar nucleus, (14) lateral cerebellar nucleus, (15) commissura anterior, (16) commissura posterior, (17) tractus septomesencephalicus, (18) globus pallidus, (19) fasciculus prosencephalis lateralis (FPL), (20) plexus choroidalis, (21) chiasma opticum, (22) DMA, (23) NCL, (24) NCM, (25) CM, (26) striatum mediale, (27) striatum, (28) nidopallium, (29) mesopallium, (30) hyperpallium, (31) cerebellum. Abbreviations: (R) rostral, (C) caudal, (D) dorsal, (V) ventral, (Le) left, (Ri) right. The sagittal schematic atlas drawings are obtained from the zebra finch histological atlas browser [28], with permission of John Wiley and Sons.

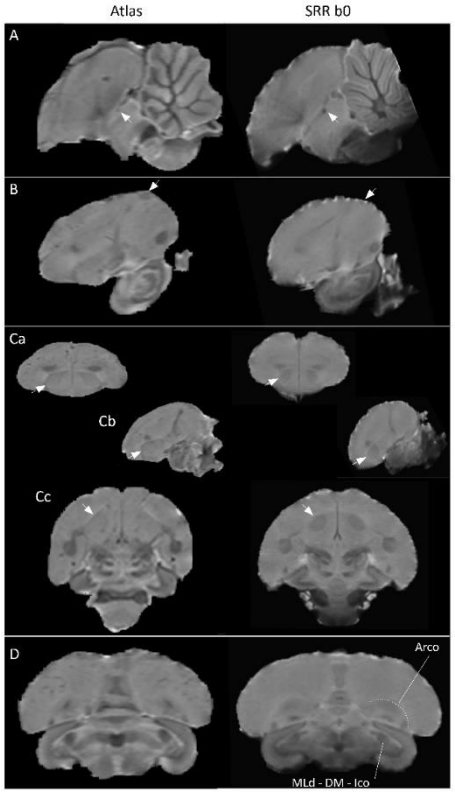

Figure 5-4: Comparison of the *ex vivo* zebra finch atlas by Poirier et al. (2008; left) and the *ex vivo* SRR-b_0 of a male zebra finch (right). In general, the same anatomical information can be extracted from both data sets. A few exceptions can be found. A: The commissura anterior (arrow) is more difficult to localize on the midsagittal slice on the ex vivo atlas compared to the SRR-b_0 image. Panel B shows that HVC is more clearly visible on the ex vivo atlas compared to the SRR-b_0. C: Area X is vaguely visible on the ex vivo atlas compared to the SRR-b_0, especially on the sagittal and horizontal slices (Cb and Cc respectively). Panel D illustrates that the SRR-b_0 image yields addition anatomical contrast near the arcopallium (Arco), MLd-DM-Ico complex.

5.3.2.1 Tractography

Overall, TDI and seed-based tractography markedly complement the T_2-weighted data set by providing 3-dimensional anatomical information on the macroscale structural connectivity of the songbird brain (Figure 5-6).

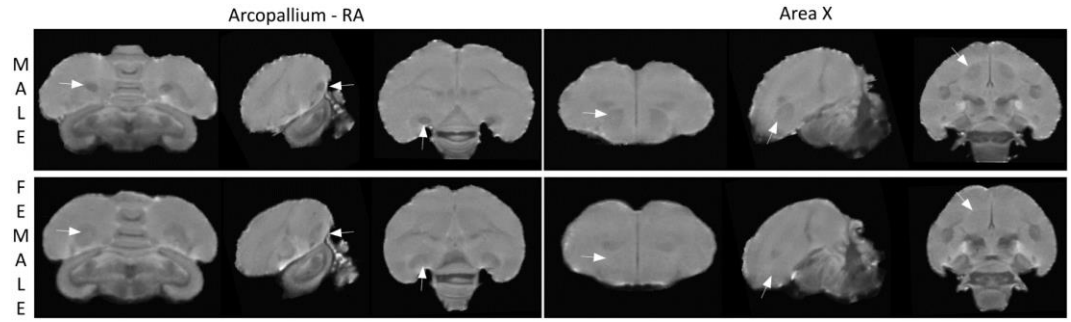

Figure 5-5: Sex difference near RA and Area X visualized by the *ex vivo* SRR-b_0. Male and female images can be found on the top and bottom row respectively. The left panel shows that nucleus RA can be clearly seen on the male data set, whereas it is not noticeable in the female brain. The same accounts for the right panel. Area X (arrow) can be demarcated clearly on the male images, whereas it cannot be identified in the female brain.

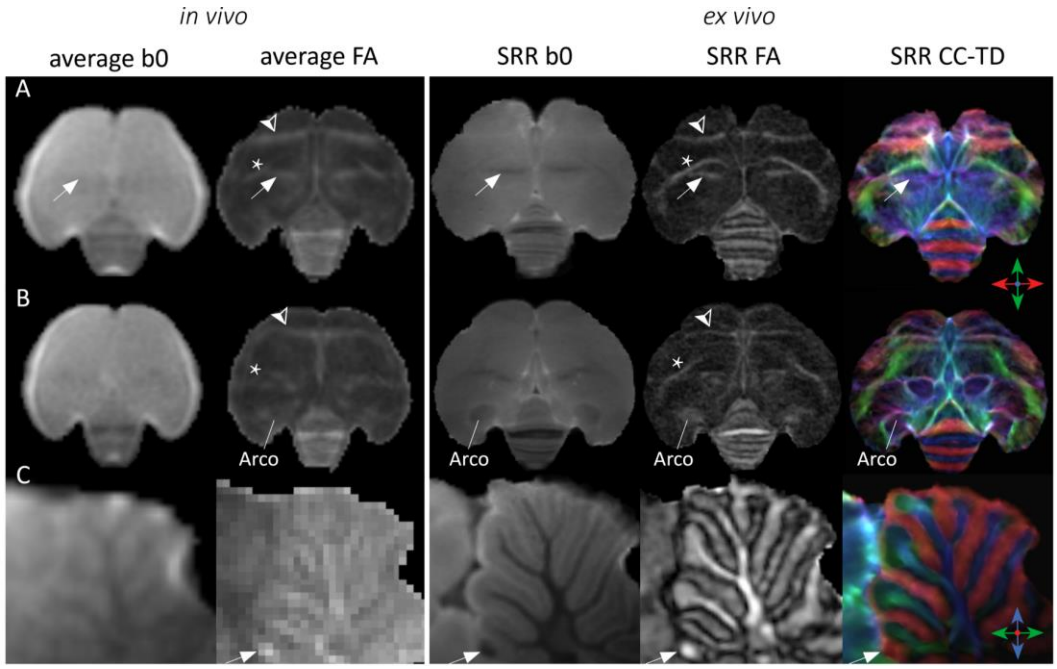

Figure 5-6: Visual comparison of the different modalities derived from the *in vivo* DTI and *ex vivo* SRR-DTI acquisition of the female brain. The three different modalities are presented in the different columns: average b0 image of 17 female birds (left image in vivo panel), average FA of 17 female birds (right image in vivo panel), SRR-b_0 (left image ex vivo panel), SRR-FA (middle image ex vivo panel) and SRR color-coded track density (CC-TD) maps (right image ex vivo panel). The three rows represent distinct locations in the brain: (A) horizontal slice through Field L (arrow), lamina mesopallialis (LaM, *) and lamina frontalis superior (LFS, arrow head), (B) horizontal slice through the arcopallium (Arco), LaM (*) and LFS (arrow head), (C) midsagittal slice focused on the cerebellum and commissura posterior (arrow).

TDI

TDI generated TD maps characterized by an additional increase in spatial resolution (40 x 40 x 40) µm³ by using a subvoxel fibre tracking procedure similar to [31]. The signal intensity and

colour-code of the TD maps informs on respectively the number and orientation of fibres estimated by the fibre tracking procedure. In contrast to FA, the resulting TD maps allow a very clear delineation of different brain areas (Figure 5-6, Figure 5-7, Figure 5-8) and provide clear anatomical contrast on general subdivisions of the brain (Figure 5-8).

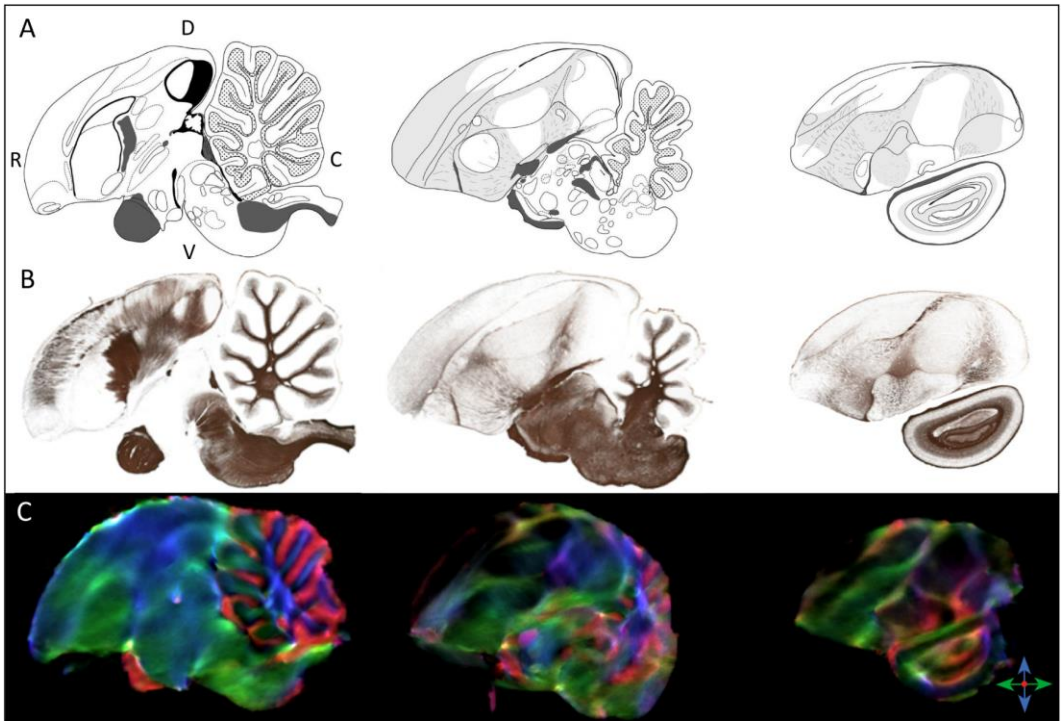

Figure 5-7: Comparison of the SRR CC-TD maps of the test male to the schematic atlas drawings and myelin-stained tissue sections. Panel A-B-C allows to compare the ex vivo TD maps of panel C (test male) to corresponding publicly available myelin stained brain sections (B) and schematic atlas drawings (A) [28], reprinted with permission of John Wiley and Sons.

Anatomical structures that show a similar signal intensity on FA maps or appear as one structure on myelin stained brain slices, can be further subdivided and specified on the color-coded TD maps. This is illustrated in Figure 5-6 A. For example, Field L and the LaM appear very similar on the FA map, whereas on the SRR CC-TD map they are represented in different colours that indicate the difference in directionality of both fibre-containing structures. This characteristic also helps to differentiate between distinct brain structures near the met-, mes- and diencephalon (Figure 5-7, Figure 5-8).

Seed-based tractography

The voxel-based comparison on the male and female FA maps shows a clear cup-shaped bilateral cluster encapsulating Area X (Figure 5-7; Figure 5-8). Based on the location and shape

of the cluster and based on the fact that only a difference in FA was found, it is very likely that the observed disparity originates from a difference in fibre density or fibre organization, rather than a volumetric difference that has been described extensively by histology [21]. To further explore the precise nature of this difference, seed-based fibre tractography was performed.

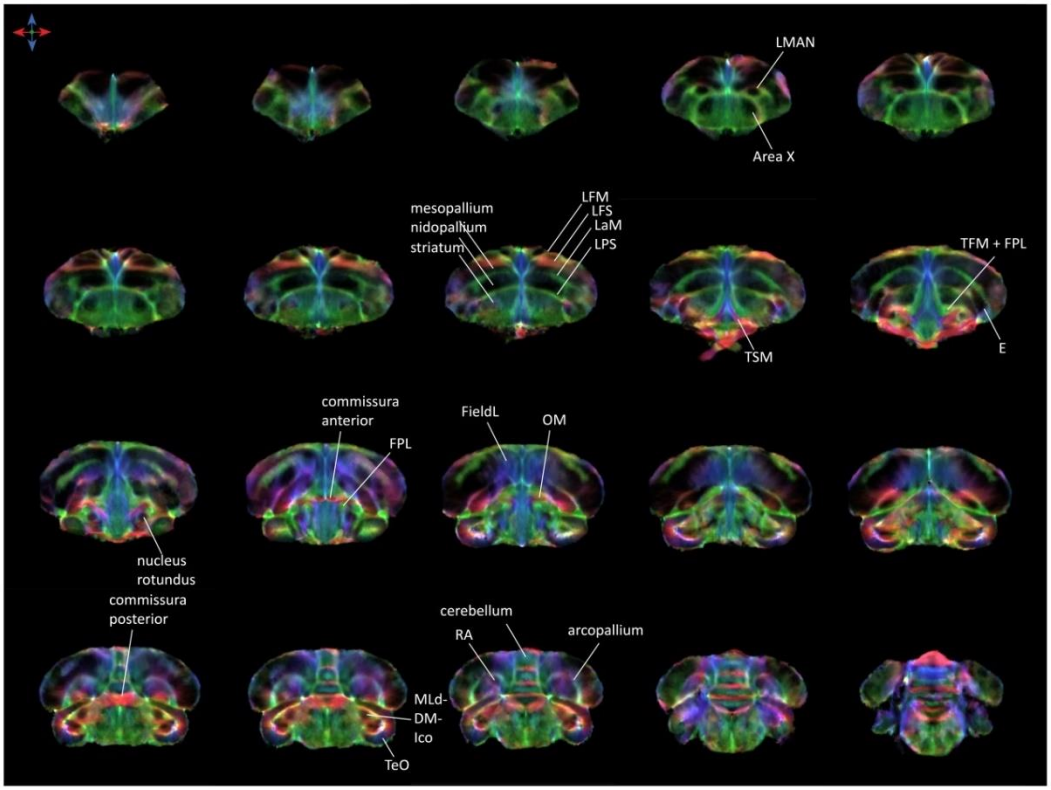

Figure 5-8: Coronal overview of the SRR CC-TD maps of the test male. The TD maps provide a complementary anatomical contrast to Figure 5-3. The TD maps allow to trace the connections between different components of e.g. the song control circuitry 3-dimensionally. In addition, several song control nuclei (e.g. LMAN and Area X) can be accurately demarcated based on the TD maps. Abbreviations can be found in the text, except for lamina pallio-subpallialis (LPS), tractus thalamo-frontalis and frontalis-thalamicus medialis (TFM), lamina frontalis suprema (LFM).

The result is shown in Figure 5-9. A unilateral seed was placed in the centre of Area X in the male brain and in the corresponding brain area in the striatum of the female brain. Even though both hemispheres were run separately, the resulting streamlines display a very symmetrical path both in the male and the female data set. The male data shows that the fibres run around a central 'void' of which the location and shape show convincing similarities to the anatomy of Area X (Figure 5-3, Figure 5-4, Figure 5-5, Figure 5-9). In contrast, the female data set demonstrates that the fibres originate and end very similar to the male, however, the streamlines appear to travel through instead of around Area X (or striatum). Besides Area X,

additional seeds were placed in other components of the song control and auditory system including LMAN, HVC, RA, MLd and Field L. The resulting streamlines show the immediate surroundings and the tract originating and/or arriving in the nuclei. It was not possible to visualize the entire song control circuitry, however, individual connections (e.g. X-DLM), were found. No left-right connectivity could be observed in any of the song control seeds tested. When placing a seed in *nucleus rotundus*, however, the estimated fibres ended up near the contralateral *nucleus rotundus* crossing the midline at the *commissura posterior* and, to a lesser extent, the *commissura anterior* (Figure 5-10 A-B).

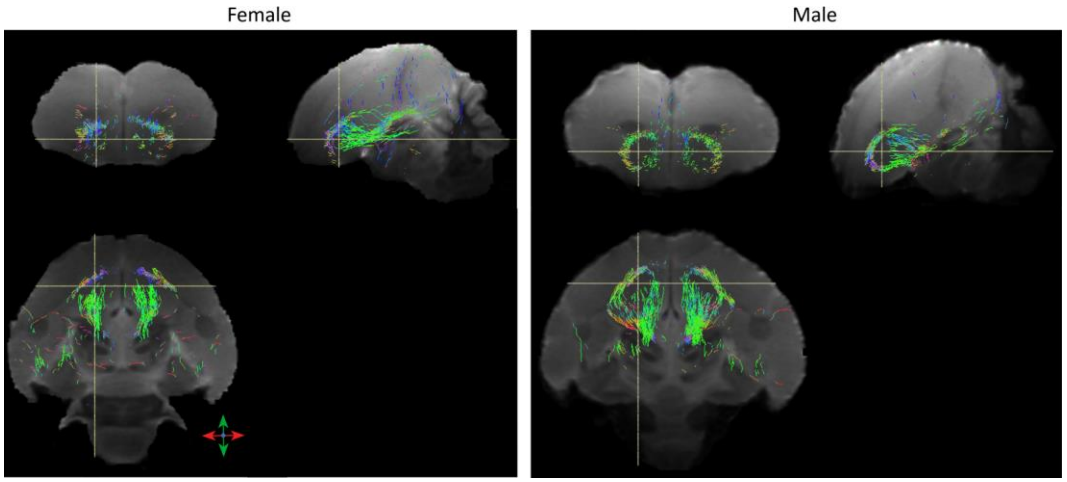

Figure 5-9: Tractography clarifies the sex difference of Area X surroundings. Seed-based fibre tractography performed in the male (right) and female (left) zebra finch brain in MRtrix using the following parameters (seed placed in the centre of Area X or corresponding coordinate in the medial striatum, sphere with radius of 1.0 mm, 500 tracks, angle 45°, minimum length 0.3124 mm, maximum length 150 mm, step size 0.04 mm). Both hemispheres were run separately and resulted in relatively symmetrical fibre populations (left versus right hemisphere). The cross-hair points to the approximate coordinates of the centre of Area X or the corresponding location in the female striatum (location of seed). In the male data set, no fibres were estimated near the point where cross-hairs meet. Instead, they appear to demarcate an Area X-shaped void. The different fibres appear to converge near the dorsoventral border of Area X where they extend towards DLM. In contrast, fibre tracking in the female data set shows no clear demarcation of Area X.

5.4 DISCUSSION

The present study demonstrates that (1) the *in vivo* DTI protocol is sensitive enough to detect structural disparities near Area X, HVC and LMAN, and extends current knowledge by showing a difference near the tOM, (2) the implementation of SRR-DTI in an *ex vivo* imaging protocol markedly reduced the acquisition time without interfering with spatial and angular resolution, (3) *ex vivo* SRR-DTI-based TDI provides an exquisite view on the structural connectivity of the

adult male ànd female zebra finch brain and clarifies the difference in FA near Area X observed by *in vivo* DTI.

5.4.1 *In vivo* detection of sex differences

In general, most differences appeared bilateral. Therefore, we conclude that there is no clear cerebral asymmetry of sex differences. This is in line with the work of Nixdorf-Bergweiler (1996) who did not find left-right differences in the volumes of LMAN, HVC, RA and Area X as defined based on Nissl stainings [41].

5.4.1.1 Macrostructural differences in fibre organisation

Area X surroundings

The strongest cluster detected in this *in vivo* study concerns a difference in FA in a cluster that encapsulates Area X. Interestingly, this observation matches previous reports: while being the largest song control nucleus in males (±1.5 mm^3), Area X cannot be discerned at all in females [42, 43]. To further clarify whether the observed cluster relates to a microstructural difference –Area X versus medial striatum in females– or reflects a marked contrast in fibre capsula surrounding Area X –similar to the RA cup, HVC shelf and entopallium belt regions– we performed *ex vivo* SRR-DTI and tractography (Figure 5-9 and Figure 5-10). In the male data set, the streamlines appear to delineate a structure of which the shape bears great resemblance to Area X. In females, on the other hand, the tracts run throughout the medial striatum. Interestingly however, both in the male and the female data set, the fibres appear to gather in the caudal part of the medial striatum to then travel caudally towards DLM, in the thalamus. This indicates that also in the female striatum –even in the absence of Area X– fibres gather and project in a manner similar to male zebra finches.

Apart from a clear anatomical difference visible on the *ex vivo* SRR- b_0 data sets, no differences in any other DTI parameter could be found in the tissue situated within Area X and the corresponding medial striatum in female birds. One could conclude that this *in vivo* DTI protocol is not sensitive enough to detect microstructural differences between Area X and the corresponding striatum in female birds. However, Person and colleagues (2008) described that even though there appears to be an extensive and highly specific topographic organization of neurons projecting from Area X and from the surrounding medial striatum to DLM, the morphology of the projecting cells is almost identical between both cell groups [44]. Reiner and

co-workers (2004) also report similarities in morphology of DLM projecting neurons whether they are located in Area X or in the surrounding striatum and describe them as having 'pallidal traits' [45]. Therefore, if only subtle morphological differences can be observed in cell populations within and outside of Area X in male birds, finding a difference between the medial striatum in female birds and Area X in males is, as a consequence, also less likely. Therefore, we conclude that the difference uncovered by *in vivo* DTI reflects a disparity in the (fibre) capsula surrounding Area X, which is absent in the female brain.

Parts of the tractus OM

We found an increased FA in males compared to females in the tOM rostral to DLM. This increase in FA in males might be indicative of a more densely organized or more robust tract in males compared to females. To our knowledge, this has never been reported before. This tract contains several fibre bundles that –among others– connect the caudal motor pathway (HVC-RA) to the syrinx, the avian analogue of the larynx [20]. In recent years, more research has focused on the effects of brain plasticity in healthy adults and how physical training and/or cognitive experience can affect brain grey and white matter. For review we refer to [46]. Even though the difference described here is not found after correlation of the DTI parameters to a specific behavioural performance or after comparison of pre- and post-training imaging sessions, the clear behavioural dimorphism '*males sing and females do not*', implies that vocal practicing might also have repercussion on this very specific subpart of the vocal motor pathway.

5.4.1.1 Microstructural tissue characteristics

HVC

Even though HVC cannot be discerned on the T2-weighted 3D RARE and as a consequence possible size differences between different birds cannot be corrected for during the normalisation procedure, the shape and location of the cluster suggests that the observed difference relates to a disparity in intrinsic cytoarchitectural properties rather than a macrostructural volume difference.

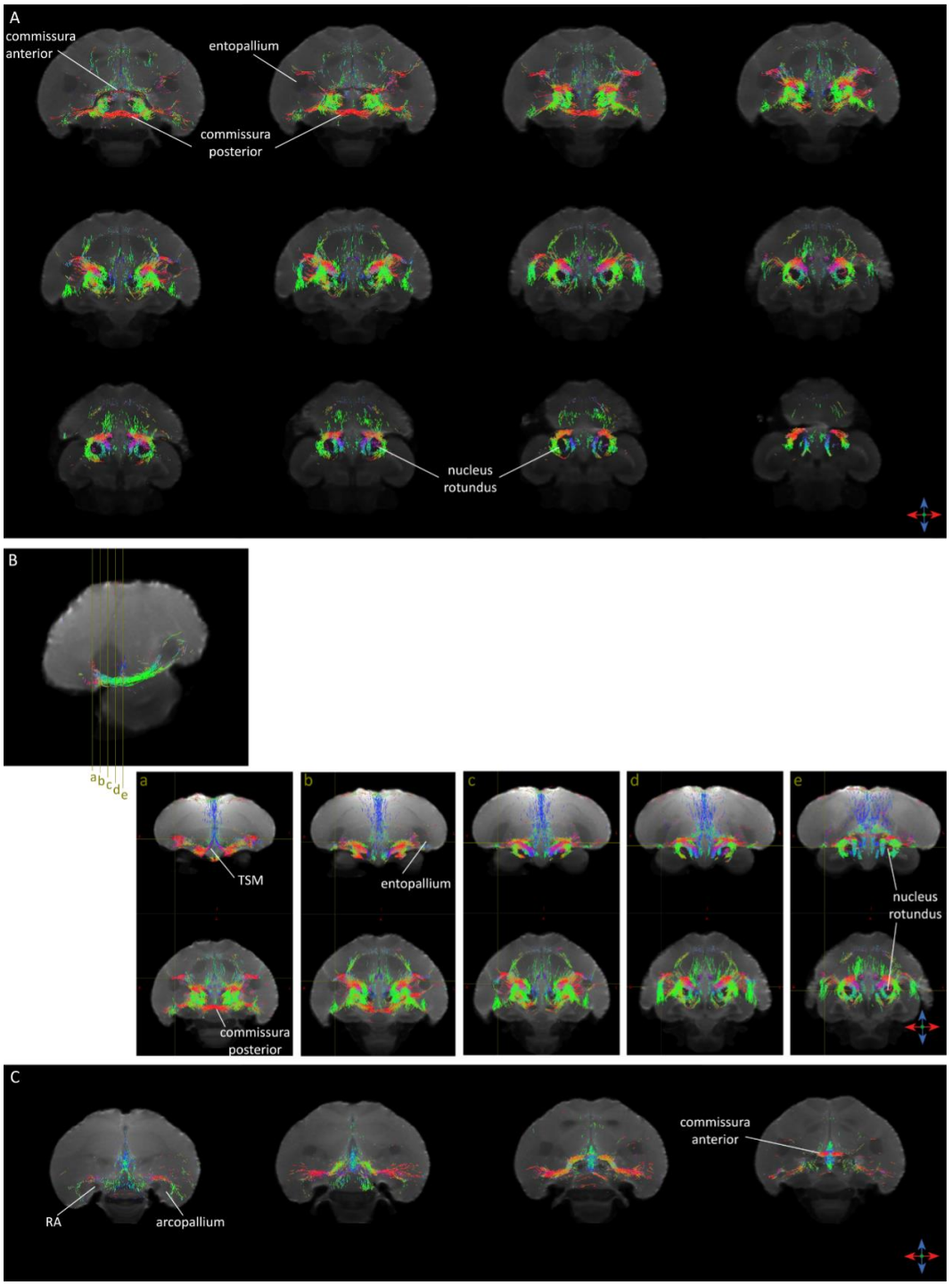

Figure 5-10: Seed-based tractography in the entopallium and the commissura anterior. Tractography in (A) nucleus rotundus (seed 1 and 2), (B) nucleus rotundus (seed 1 and 2) to entopallium (seed 3 and 4), and (C) commissura anterior (seed 1 midsagittal) to arcopallium. For each anatomical region, one seed was placed in the left and a second separate seed was placed in the right hemisphere except for the commissura anterior.

HVC was found to have a higher FA in females, compared to males. Interestingly, Nixdorf-Bergweiler and Von Bohlen und Halbach (2004) observed a strong male-biased (M>F) difference in the number of myelinated axonal profiles per unit area of tissue in adult zebra finches in HVC [47]. Intuitively, one would expect that a higher density of axonal profiles is linked to a higher FA, however, this assumption only holds up if the axonal fibres are coherently organized [48]. Furthermore, part of the axonal profiles that originate in HVC travel to RA. The tract connecting HVC and RA is termed the caudal motor pathway owing to its role in the motor aspect of singing [17]. Instead of being organized into a vast bundle of parallel fibres similar to the European starling [3], the zebra finches' caudal motor pathway consists of fibres that are almost individually projecting from HVC to RA [28]. Its relatively 'diffuse' nature combined with the partial volume effect inherent to DTI makes it impossible to visualize the tract or detect any differences along its path, even though this sex difference has been described extensively in the literature [49-51]. Despite observing differences along the path, the FA cluster co-localised with HVC might suggest detecting a difference in fibres exiting HVC. In male birds, more myelinated axons leave HVC, but in a less well organized manner compared to female birds. This might be partly responsible for a lower FA in males compared to females.

Differences in the number of axonal profiles and RA-projecting axons are not likely to be solely accountable for the disparity observed in FA. Another possible candidate are interneurons. By investigating zebra finches, Grisham and Arnold found a sex difference in GABA-like immunoreactivity in HVC and RA [52]. Two independent studies concluded that the GABA-like cells are likely to be local interneurons [53, 54]. As they form local networks by making synapses with neighbouring cells, interneurons increase complexity and might affect the local diffusion properties. Based on these properties and the assumption that HVC contains more interneurons in males compared to females, the interneurons might also contribute to a lower FA in male zebra finches as observed in the voxel-based analysis.

Gurney (1982) investigated the effects of early hormone treatment on sexual differentiation of the zebra finches' brain and behaviour. In normally reared female zebra finches, HVC and RA neurons are smaller and less well-separated compared to the large-bodied and spaciously spread neurons reported in males [55]. Combining findings obtained by Nixdorf-Bergweiler (1996) and Kirn and De Voogd (1989) suggests that in HVC and RA neuronal density is larger in female compared to male birds at 60 dph [41, 56]. These sex differences in soma size (M>F) and

cell density (M<F) were also confirmed by others [42, 57-61]. The surface/volume ratio of cells which is inherently coupled to cell size, is an important factor as the density and spatial organization of 'physical barriers' such as membranes greatly affect the overall diffusion properties of the tissue making diffusion MRI –especially MD– a highly sensitive probe to detect variation in cell size [62]. Therefore, the sex differences in cell density and soma size might be related to the observed difference in MD.

LMAN

In contrast to Area X, HVC and RA, LMAN shows anatomical contrast on the 3D RARE used for spatial normalization. Consequently, any differences in size or shape might be eliminated by the registration procedure leaving only differences in intrinsic tissue properties to be detected. This, however, does not affect the biological interpretation of the result as several independent studies have confirmed that the size of LMAN is similar between male and female birds [22, 41, 47]. In addition, no sex difference in myelination have been found in LMAN [47]. Interestingly, Nixdorf-Bergweiler (1996) performed detailed stereological analyses focused on LMAN and found that adult females displayed a higher neuronal density in LMAN (i.e. 91% more neurons per unit volume compared to male zebra finches [41]). Even though brain tissue is comprised of more than only neurons, these vast differences might contribute to the observed differences in MD.

In conclusion, even though only suggestions of the biological mechanisms underlying the observed differences can be made based on the DTI findings, the clusters detected with the voxel-based analysis clearly align with established findings. In addition, the voxel-based analysis yields detailed insight into the spatial extent of the sex differences. Therefore, we conclude that the optimized protocol is sensitive enough to detect known male-female differences in the adult zebra finch brain.

5.4.2 Implementation of DTI – methodological considerations

Fast sequences that are often used for DTI experiments in mammals cannot be readily adopted in songbirds because of certain physiological properties inherent to songbird neuroanatomy ([3]; for example, the air cavities in the skull). Using a four-shot EPI sequence [63], most severe image artefacts were overcome except for brain areas near the caudal parts of the songbird brain lateral to the cerebellum. This area corresponds to the arcopallium which contains RA. As the imaging artefacts are slightly different for each bird and no opposite phase encoding

polarity data were acquired [64, 65], the image distortions could not be corrected. In addition, the field maps were not used to unwarp the artefacts [66].

The 3D RARE suffers less susceptibility artefacts and yields more anatomical contrast compared to the DTI b_0. Consequently, the 3D RARE was used to improve spatial normalisation to the *ex vivo* zebra finch atlas [29]. However, the difference in susceptibility artefacts led to a suboptimal alignment of the DTI and 3D RARE scans near the arcopallium. Therefore, spatial normalisation might be imperfect in this region which might explain why only very weak voxel-based differences could be detected near RA.

5.4.3 *Ex vivo* SRR-DTI

The primary goal of this study was to implement an *in vivo* DTI protocol that allows to explore macro- and microstructural tissue characteristics of the zebra finch brain on a reasonable time frame. However, to further clarify observations detected *in vivo* and explore songbird neuroanatomy in greater detail, *ex vivo* DTI was opted.

Most *ex vivo* DTI protocols result in images with very high spatial resolution, however, often only 6-12 diffusion gradient directions are acquired. The most obvious reason for this are the often long acquisition times. To surpass the trade-off between acquisition time, spatial resolution and SNR inherent to DTI, we chose to employ a recently developed SRR method to acquire high-resolution DTI data [30].

5.4.3.1 Bypassing the trade-off

The *ex vivo* zebra finch atlas published by Poirier and co-workers (2008) was acquired in 54.6 hours [29]. The *ex vivo* data sets presented here were obtained within approximately 28 or 44 hours, while containing both T_2-weighted anatomical information (SRR-b_0) and DTI data which included 60 or 90 diffusion gradient directions, respectively. Visual comparison of the *ex vivo* atlas by Poirier and the SRR-b_0 images of the male bird showed that most brain areas can be identified in both data sets (Figure 5-4). In addition, the overall image contrast of the SRR-b_0 images relates more closely to the 3D RARE data sets acquired *in vivo* compared to the atlas (data not shown). Furthermore, as both the *ex vivo* atlas and the SRR-b_0 of the male sample provide similar information, the SRR-b_0 image of the female brain can serve as the first MRI-based atlas of the female zebra finch brain. If only the SRR-b_0 images had been acquired, the total acquisition time would be 6.29 or 4.67 hours to obtain a T2-weighted data set with

isotropic resolution of 80 µm. However, if the goal is to acquire high resolution T2-weighted data sets in a (relatively) short time span, then the number of acquisition angles (set of low resolution data sets) can be reduced even further. In this case (in plane resolution 0.078 mm, slice thickness 0.320 mm), the minimal number of low resolution data sets necessary to enable a reconstruction is 7 (based on anisotropy factor [30]), which corresponds to approximately 2.8 hours of scanning time, without using a fast imaging sequence. This is coming very close to high-resolution *in vivo* scanning times. This could be of great interest for 'high-throughput' studies investigating subtle changes in brain volume or shape following training or along the course of pathology.

Still, depending on the goal of the study, *in vivo* imaging might not provide sufficient anatomical contrast or detail. Lerch and colleagues (2012) nicely reviewed how to choose between *in* and *ex vivo* acquisition when investigating changes in neuroanatomy [67, 68]. Therefore, the method proposed by Van Steenkiste and colleagues can markedly increase efficiency.

5.4.3.2 Qualitative assessment of sex differences on the ex vivo SRR-b0's

The female SRR-b_0 data set shows similar contrast compared to the male data set, however, Area X, RA and HVC cannot be localized. Concerning Area X, this is in line with previous histological studies, where Nissl stained tissue sections also appear to lack this part of the song control system in female zebra finches. HVC and RA, on the other hand, are known to be smaller in females, however, they should be discernible on the *ex vivo* data set [41]. A possible explanation for this might be that HVC and RA in the female brain accumulate the gadolinium differently. The sex difference in cell density and cell spacing might lead to a differential accumulation of the contrast agent as gadoterate meglumine resides in the extracellular matrix [69, 70]. Partial volume effects are less likely to lay at the basis as several laminae and small brain areas such as the *nucleus ovoidalis* can be clearly found on both the male and female data sets (volume of *nucleus ovoidalis* appr. 0.07 mm^3 [29] compared to 0.07-0.10 mm^3 and 0.05-0.08 mm^3 for respectively female RA and female HVC [41, 71]).

5.4.3.3 Structural connectivity of the zebra finch brain

The TDI method proposed by Calamante and co-workers (2010) enables unravelling fibre complexity on a subvoxel level. Combined with the SRR-DTI technique, the resulting high-resolution data set (i.e. (40x40x40) μm^3), provides highly valuable information on the 3-

dimensional organisation of structural connectivity of the zebra finch brain almost up to the mesoscale level.

The TD maps illustrate that –due to its nuclear instead of laminar organization [11]– the songbird brain serves as an excellent model for DTI and tractography [72]. The song control, auditory and visual systems consist of sets of interconnected nuclei where each component appears to be surrounded by a fibre-containing capsula. The CC TD maps provide a clear view on the song control nuclei which cannot be distinguished on T2-weighted data sets without contrast enhancement (Figure 5-8; [6]). Furthermore, near the optical lobes (TeO) the TD maps clearly show a fibre organization reminiscent of the orientation of myelinated fibres in the mammalian cortex (perpendicular to the cortical surface). Interestingly, the radial organization of fibres in the optical lobes is in accordance with myelin-stained histological sections (Figure 5-7). Besides anatomical contrast on specific brain areas, the CC TD maps exhibit a clear view on the major subdivisions of the brain. Several laminae (i.e. lamina frontalis suprema and superior, lamina mesopallialis and *lamina palio-subpallialis*), split the songbird telencephalon in different subareas (i.e. hyperpallium, nidopallium, mesopallium, striatum (Figure 5-8) [27, 28]).

The results of the seed-based tractography provide highly symmetrical results, and, besides Area X, most results of tractography are similar between the male and female brain. As DTI-based tractography deduces axonal geometry from the diffusion properties of water molecules in tissues, anatomical accuracy can only be validated by parallel analysis of histological tracer studies [73-79].

Seed-based tractography of telencephalic brain areas produced streamlines that were strictly confined to the ipsilateral hemisphere. The only clear left-right connection at the level of the telencephalon detected in this study was found in the *commissura anterior* which could be clearly traced back to the arcopallium via the tOM. This ‘lack’ of left-right connectivity in the telencephalon has been demonstrated by neuroanatomists [17]. When seeding tracts in more ventrally positioned brain areas such as the *nucleus rotundus*, an important relay centre for processing of visual information, the resulting streamlines appear to travel to the contralateral hemisphere passing the *commissura posterior* and, to a lesser extent, the *commissura anterior* (Figure 5-10). This observation contrasts with previous findings. Even though *nucleus rotundus* receives input from the TeO of both the ipsi- and contralateral hemispheres [80, 81], no tracer

studies report on the existence of a connection between left and right *nucleus rotundus*. Furthermore, the streamlines seeded in *nucleus rotundus* do not reach the TeO, consequently the resulting trans-hemispheric connection appears misleading. This might be attributed to parameter settings or suboptimal placement of the seed [76]. Interestingly however, the estimated fibre profile appears to end near the rostral part of the entopallium. This projection might pertain to the tectofugal pathway, where after passing *nucleus rotundus* fibres travel to the entopallium via the FPL [82]**.**

Besides the Area X-DLM connection no other pathways that directly connect consecutive song control system nuclei could be traced. This might partly be explained as several pathways are (assumed to be) embedded in the laminae (e.g. the first part of the anterior forebrain pathway (HVC to Area X projection) partly resides in the LaM [3]). Consequently, the tracking algorithm needs to identify the appropriate subpart of the lamina that contains the fibres heading to the next relay centre of the circuitry. The HVC to RA tract, on the other hand, is too diffusely and randomly organized in zebra finches to detect by DTI [49-51]. In addition, the songbird brain is characterized by a highly topographical organization which might also be responsible for the difficulties in finding structural tracts connecting distinct brain areas, even at this resolution.

5.5 CONCLUSION

The observed differences in LMAN and HVC are in line with previous histological investigations. Interestingly, the disparities surrounding but not including Area X and the part of the tOM are complementary to previous histological findings. Consequently, we conclude that the *in vivo* DTI protocol is sensitive enough to detect known sex differences in the adult zebra finch brain. This *in vivo* protocol enables future longitudinal studies where microstructural rearrangements can be traced over time within the same subject, where differences in tissue microarchitecture or connectivity might be related to the precise stage of vocal learning or upon treatment. *Ex vivo* SRR-DTI and TDI provide an unprecedented 3-dimensional overview of the overall organization of the zebra finch brain –including the female brain– with clear anatomical contrast on the song control circuitry.

ACKNOWLEDGEMENTS

We would like to thank Professor Harvey Karten for providing access to the schematic atlas drawings of the zebra finch brain. This research was supported by grants from the Research

Foundation—Flanders (FWO, Project No. G030213N, G044311N and G037813N), the Hercules Foundation (Grant No. AUHA0012), Concerted Research Actions (GOA Funding) from the University of Antwerp and Interuniversity Attraction Poles (IAP) initiated by the Belgian Science Policy Office ('PLASTOCINE': P7/17 and P7/11) to AVdL, CAC and JS. JH, GVS and MN are PhD students supported by the University of Antwerp. LVR is a PhD student funded by the Research Foundation-Flanders (FWO). GDG and BJ are a Postdoctoral Fellows of the FWO. CAC is a Research Associate from Fonds de la Recherche National (F.R.S.-FNRS).

REFERENCES

1. Brainard, M.S. and A.J. Doupe, *Translating Birdsong: Songbirds as a Model for Basic and Applied Medical Research.* Annual Review of Neuroscience, 2013. **36**(1): p. 489-517.
2. Doupe, A.J. and P.K. Kuhl, *BIRDSONG AND HUMAN SPEECH: Common Themes and Mechanisms.* Annual Review of Neuroscience, 1999. **22**(1): p. 567-631.
3. De Groof, G., et al., *In vivo diffusion tensor imaging (DTI) of brain subdivisions and vocal pathways in songbirds.* NeuroImage, 2006. **29**(3): p. 754-763.
4. De Groof, G., et al., *Structural Changes between Seasons in the Songbird Auditory Forebrain.* The Journal of Neuroscience, 2009. **29**(43): p. 13557-13565.
5. De Groof, G., et al., *Seasonal rewiring of the songbird brain: an in vivo MRI study.* European Journal of Neuroscience, 2008. **28**(12): p. 2475-2485.
6. Van der Linden, A., et al., *Non invasive in vivo anatomical studies of the oscine brain by high resolution MRI microscopy.* Journal of Neuroscience Methods, 1998. **81**(1–2): p. 45-52.
7. Verhoye, M., et al., *Imaging birds in a bird cage: in-vivo FSE 3D MRI of bird brain.* Magnetic Resonance Materials in Physics, Biology and Medicine, 1998. **6**(1): p. 22-27.
8. Toga, A.W. and P.M. Thompson, *Mapping brain asymmetry.* Nat Rev Neurosci, 2003. **4**(1): p. 37-48.
9. Jarvis, E.D., et al., *Avian brains and a new understanding of vertebrate brain evolution.* Nat Rev Neurosci, 2005. **6**(2): p. 151-159.
10. Jarvis, E.D., *Learned Birdsong and the Neurobiology of Human Language.* Annals of the New York Academy of Sciences, 2004. **1016**(1): p. 749-777.
11. Karten, H.J. and T. Shimizu, *The Origins of Neocortex: Connections and Lamination as Distinct Events in Evolution.* Journal of Cognitive Neuroscience, 1989. **1**(4): p. 291-301.
12. Aronov, D., A.S. Andalman, and M.S. Fee, *A Specialized Forebrain Circuit for Vocal Babbling in the Juvenile Songbird.* Science, 2008. **320**(5876): p. 630-634.
13. Ölveczky, B.P., A.S. Andalman, and M.S. Fee, *Vocal Experimentation in the Juvenile Songbird Requires a Basal Ganglia Circuit.* PLoS Biology, 2005. **3**(5): p. e153.
14. Bottjer, S., E. Miesner, and A. Arnold, *Forebrain lesions disrupt development but not maintenance of song in passerine birds.* Science, 1984. **224**(4651): p. 901-903.
15. Scharff, C. and F. Nottebohm, *A comparative study of the behavioral deficits following lesions of various parts of the zebra finch song system: implications for vocal learning.* The Journal of Neuroscience, 1991. **11**(9): p. 2896-2913.
16. Brainard, M.S. and A.J. Doupe, *Interruption of a basal ganglia-forebrain circuit prevents plasticity of learned vocalizations.* Nature, 2000. **404**(6779): p. 762-766.
17. Wild, J.M., *Neural pathways for the control of birdsong production.* Journal of Neurobiology, 1997. **33**(5): p. 653-670.

18. Simpson, H. and D. Vicario, *Brain pathways for learned and unlearned vocalizations differ in zebra finches.* The Journal of Neuroscience, 1990. **10**(5): p. 1541-1556.
19. Yu, A.C. and D. Margoliash, *Temporal Hierarchical Control of Singing in Birds.* Science, 1996. **273**(5283): p. 1871-1875.
20. Wild, J.M., *Descending projections of the songbird nucleus robustus archistriatalis.* The Journal of Comparative Neurology, 1993. **338**(2): p. 225-241.
21. Nottebohm, F. and A. Arnold, *Sexual dimorphism in vocal control areas of the songbird brain.* Science, 1976. **194**(4261): p. 211-213.
22. Nixdorf-Bergweiler, B.E., *Lateral magnocellular nucleus of the anterior neostriatum (LMAN) in the zebra finch: Neuronal connectivity and the emergence of sex differences in cell morphology.* Microscopy Research and Technique, 2001. **54**(6): p. 335-353.
23. Gurney, M., *Hormonal control of cell form and number in the zebra finch song system.* The Journal of Neuroscience, 1981. **1**(6): p. 658-673.
24. Meyer, C.E., E. Boroda, and T.A. Nick, *Sexually dimorphic perineuronal net expression in the songbird.* Basal Ganglia, 2014. **3**(4): p. 229-237.
25. Cornez, G., et al., *Anatomically Discrete Sex Differences in Neuroplasticity in Zebra Finches as Reflected by Perineuronal Nets.* PLoS ONE, 2015. **10**(4): p. e0123199.
26. Ball, G.F. and S.A. Macdougall-Shackleton, *Sex differences in songbirds 25 years later: What have we learned and where do we go?* Microscopy Research and Technique, 2001. **54**(6): p. 327-334.
27. Nixdorf-Bergweiler, B. and H.-J. Bischof, *Atlas Of The Brain Of The Zebra Finch, Taeniopygia Guttata: With Special Emphasis On Telencephalic Visual And Song System Nuclei in Transverse and Sagittal Sections*, ed. N.C.f.B.I. (US). 2007.
28. Karten, H.J., et al., *Digital Atlas of the Zebra Finch (Taeniopygia guttata) Brain: a High Resolution Photo Atlas.* The Journal of comparative neurology, 2013. **521**(16): p. 3702-3715.
29. Poirier, C., et al., *A three-dimensional MRI atlas of the zebra finch brain in stereotaxic coordinates.* NeuroImage, 2008. **41**(1): p. 1-6.
30. Van Steenkiste, G., et al., *Super-resolution reconstruction of diffusion parameters from diffusion-weighted images with different slice orientations.* Magnetic Resonance in Medicine, 2016. **75**(1): p. 181-195.
31. Calamante, F., et al., *Track-density imaging (TDI): Super-resolution white matter imaging using whole-brain track-density mapping.* NeuroImage, 2010. **53**(4): p. 1233-1243.
32. Jones, D.K., M.A. Horsfield, and A. Simmons, *Optimal strategies for measuring diffusion in anisotropic systems by magnetic resonance imaging.* Magnetic Resonance in Medicine, 1999. **42**(3): p. 515-525.
33. Caruyer, E., et al., *Design of multishell sampling schemes with uniform coverage in diffusion MRI.* Magnetic Resonance in Medicine, 2013. **69**(6): p. 1534-1540.
34. Bai, Y. and D.C. Alexander. *Model-based registration to correct for motion between acquisitions in diffusion MR imaging*. in *Biomedical Imaging: From Nano to Macro, 2008. ISBI 2008. 5th IEEE International Symposium on*. 2008.
35. Tax, C.M.W., et al., *Recursive calibration of the fibre response function for spherical deconvolution of diffusion MRI data.* NeuroImage, 2014. **86**: p. 67-80.
36. Tournier, J.D., F. Calamante, and A. Connelly, *Robust determination of the fibre orientation distribution in diffusion MRI: Non-negativity constrained super-resolved spherical deconvolution.* NeuroImage, 2007. **35**(4): p. 1459-1472.
37. Jeurissen, B., et al., *Multi-tissue constrained spherical deconvolution for improved analysis of multi-shell diffusion MRI data.* NeuroImage, 2014. **103**: p. 411-426.
38. Tournier, J.C., F.; Connelly, A. *Improved probabilistic streamlines tractography by 2nd order integration over fibre orientation distributions*. in *International Society for Magnetic Resonance in Medicine (ISMRM)*. 2010. Stockholm.

39. Tournier, J.D., F. Calamante, and A. Connelly, *MRtrix: Diffusion tractography in crossing fibre regions.* International Journal of Imaging Systems and Technology, 2012. **22**(1): p. 53-66.
40. Poot, D.H.J., V. Van Meir, and J. Sijbers, *General and Efficient Super-Resolution Method for Multi-slice MRI*, in *Medical Image Computing and Computer-Assisted Intervention – MICCAI 2010*, T. Jiang, et al., Editors. 2010, Springer Berlin Heidelberg. p. 615-622.
41. Nixdorf-Bergweiler, B.E., *Divergent and parallel development in volume sizes of telencephalic song nuclei in and female zebra finches.* The Journal of Comparative Neurology, 1996. **375**(3): p. 445-456.
42. Nottebohm, F. and A.P. Arnold, *Sexual dimorphism in vocal control areas of the songbird brain.* Science (New York, N.Y.), 1976. **194**(4261): p. 211-213.
43. MacDougall-Shackleton, S.A. and G.F. Ball, *Comparative studies of sex differences in the song-control system of songbirds.* Trends in Neurosciences, 1999. **22**(10): p. 432-436.
44. Person, A.L., et al., *Organization of the songbird basal ganglia, including area X.* The Journal of Comparative Neurology, 2008. **508**(5): p. 840-866.
45. Reiner, A., et al., *An immunohistochemical and pathway tracing study of the striatopallidal organization of area X in the male zebra finch.* The Journal of Comparative Neurology, 2004. **469**(2): p. 239-261.
46. Zatorre, R.J., R.D. Fields, and H. Johansen-Berg, *Plasticity in Gray and White: Neuroimaging changes in brain structure during learning.* Nature neuroscience, 2012. **15**(4): p. 528-536.
47. Nixdorf-Bergweiler, B. and V. von Bohlen und Halbach, *Major sex differences in the development of myelination are prominent in song system nucleus HVC but not lMAN.* Animal Biology, 2004. **54**(1): p. 27-43.
48. Mori, S. and J. Zhang, *Principles of Diffusion Tensor Imaging and Its Applications to Basic Neuroscience Research.* Neuron, 2006. **51**(5): p. 527-539.
49. Konishi, M. and E. Akutagawa, *Neuronal growth, atrophy and death in a sexually dimorphic song nucleus in the zebra finch brain.* Nature, 1985. **315**(6015): p. 145-147.
50. Mooney, R. and M. Rao, *Waiting periods versus early innervation: the development of axonal connections in the zebra finch song system.* The Journal of Neuroscience, 1994. **14**(11): p. 6532-6543.
51. Wang, J., H. Sakaguchi, and M. Sokabe, *Sex differences in the vocal motor pathway of the zebra finch revealed by real-time optical imaging technique.* NeuroReport, 1999. **10**(12): p. 2487-2491.
52. Grisham, W. and A.P. Arnold, *Distribution of GABA-like immunoreactivity in the song system of the zebra finch.* Brain Research, 1994. **651**(1–2): p. 115-122.
53. Paton, J., B. O'Loughlin, and F. Nottebohm, *Cells born in adult canary forebrain are local interneurons.* The Journal of Neuroscience, 1985. **5**(11): p. 3088-3093.
54. Pinaud, R. and C.V. Mello, *GABA immunoreactivity in auditory and song control brain areas of zebra finches.* Journal of Chemical Neuroanatomy, 2007. **34**(1–2): p. 1-21.
55. Gurney, M.E., *Behavioral correlates of sexual differentiation in the zebra finch song system.* Brain Research, 1982. **231**(1): p. 153-172.
56. Kirn, J. and T. DeVoogd, *Genesis and death of vocal control neurons during sexual differentiation in the zebra finch.* The Journal of Neuroscience, 1989. **9**(9): p. 3176-3187.
57. Bottjer, S.W., E.A. Miesner, and A.P. Arnold, *Changes in neuronal number, density and size account for increases in volume of song-control nuclei during song development in zebra finches.* Neuroscience Letters, 1986. **67**(3): p. 263-268.
58. Grisham, W. and A.P. Arnold, *A direct comparison of the masculinizing effects of testosterone, androstenedione, estrogen, and progesterone on the development of the zebra finch song system.* Journal of Neurobiology, 1995. **26**(2): p. 163-170.

59. Bender, A.T. and S.L. Veney, *Treatment with the specific estrogen receptor antagonist ICI 182,780 demasculinizes neuron soma size in the developing zebra finch brain.* Brain Research, 2008. **1246**: p. 47-53.
60. Konishi, M. and E. Akutagawa, *A critical period for estrogen action on neurons of the song control system in the zebra finch.* Proceedings of the National Academy of Sciences of the United States of America, 1988. **85**(18): p. 7006-7007.
61. Wade, J. and A.P. Arnold, *Sexual Differentiation of the Zebra Finch Song System.* Annals of the New York Academy of Sciences, 2004. **1016**(1): p. 540-559.
62. Le Bihan, D., *The 'wet mind': water and functional neuroimaging.* Physics in Medicine and Biology, 2007. **52**(7): p. R57.
63. Porter, D.A. and R.M. Heidemann, *High resolution diffusion-weighted imaging using readout-segmented echo-planar imaging, parallel imaging and a two-dimensional navigator-based reacquisition.* Magnetic Resonance in Medicine, 2009. **62**(2): p. 468-475.
64. Holland, D., J.M. Kuperman, and A.M. Dale, *Efficient Correction of Inhomogeneous Static Magnetic Field-Induced Distortion in Echo Planar Imaging.* NeuroImage, 2010. **50**(1): p. 175.
65. Andersson, J.L.R., S. Skare, and J. Ashburner, *How to correct susceptibility distortions in spin-echo echo-planar images: application to diffusion tensor imaging.* NeuroImage, 2003. **20**(2): p. 870-888.
66. Chen, B., H. Guo, and A.W. Song, *Correction for direction-dependent distortions in diffusion tensor imaging using matched magnetic field maps.* NeuroImage, 2006. **30**(1): p. 121-129.
67. Lerch, J.P., et al., *Wanted Dead or Alive? The tradeoff between in-vivo versus ex-vivo MR brain imaging in the mouse.* Frontiers in Neuroinformatics, 2012. **6**.
68. Mackenzie-Graham, A., *In Vivo vs. Ex Vivo Magnetic Resonance Imaging in Mice.* Frontiers in Neuroinformatics, 2012. **6**.
69. Reisinger, C., et al., *Dynamic magnetic resonance angiography of the arteries of the hand. A comparison between an extracellular and an intravascular contrast agent.* European Radiology, 2008. **19**(2): p. 495-502.
70. Marty, B., et al., *Hindered diffusion of MRI contrast agents in rat brain extracellular micro-environment assessed by acquisition of dynamic T1 and T2 maps.* Contrast Media & Molecular Imaging, 2013. **8**(1): p. 12-19.
71. Bottjer, S., S. Glaessner, and A. Arnold, *Ontogeny of brain nuclei controlling song learning and behavior in zebra finches.* The Journal of Neuroscience, 1985. **5**(6): p. 1556-1562.
72. De Groof, G. and A. Van der Linden, *Love songs, bird brains and diffusion tensor imaging.* NMR in Biomedicine, 2010. **23**(7): p. 873-883.
73. Jbabdi, S. and H. Johansen-Berg, *Tractography - where do we go from here?* Brain connectivity, 2011. **1**(3): p. 169-183.
74. Aurobrata, G. and D. Rachid, *A survey of current trends in diffusion MRI for structural brain connectivity.* Journal of Neural Engineering, 2016. **13**(1): p. 011001.
75. Calabrese, E., et al., *A Diffusion MRI Tractography Connectome of the Mouse Brain and Comparison with Neuronal Tracer Data.* Cerebral Cortex, 2015.
76. Thomas, C., et al., *Anatomical accuracy of brain connections derived from diffusion MRI tractography is inherently limited.* Proceedings of the National Academy of Sciences, 2014. **111**(46): p. 16574-16579.
77. Dyrby, T.B., et al., *Validation of in vitro probabilistic tractography.* NeuroImage, 2007. **37**(4): p. 1267-1277.
78. Azadbakht, H., et al., *Validation of High-Resolution Tractography Against In Vivo Tracing in the Macaque Visual Cortex.* Cerebral Cortex, 2015.
79. Dauguet, J., et al., *Comparison of fibre tracts derived from in-vivo DTI tractography with 3D histological neural tract tracer reconstruction on a macaque brain.* NeuroImage, 2007. **37**(2): p. 530-538.

80. Schmidt, A. and H.-J. Bischof, *Integration of information from both eyes by single neurons of nucleus rotundus, ectostriatum and lateral neostriatum in the zebra finch (Taeniopygia guttata castanotis Gould).* Brain Research, 2001. **923**(1–2): p. 20-31.
81. Karten, H.J. and A.M. Revzin, *The afferent connections of the nucleus rotundus in the pigeon.* Brain Research, 1966. **2**(4): p. 368-377.
82. Karten, H.J. and W. Hodos, *Telencephalic projections of the nucleus rotundus in the pigeon (Columba livia).* The Journal of Comparative Neurology, 1970. **140**(1): p. 35-51.

Chapter 6

Longitudinal *in vivo* magnetic resonance imaging study maps structural plasticity in the brain of juvenile zebra finches during the first 200 days of post-hatch life

The results described in this chapter are currently in preparation for publication.

Hamaide J, De Groof G, Van Ruijssevelt L, Van Audekerke J, Verhoye M, Van der Linden A. *Volumetric development of the zebra finch brain throughout the first 200 days of post hatch life traced by* in vivo *MRI*, under review at NeuroImage.

Hamaide J, Lukacova K, Verhoye M, Van der Linden A. *Practice makes perfect:* in vivo *detection of structural neuroplasticity related to vocal imitation*, in preparation.

6.1 INTRODUCTION

Vocal learning can be defined as the ability to modify the acoustic structure of vocalisations by imitation. This exceptional skill is shared by only few species [1], is acquired during a sensitive period early in life, and relies on auditory feedback along with instructive social experiences [2, 3]. Intriguingly, remarkable parallels have been recognised between bird song and human speech learning [4]. Indeed, much like human infants learn to speak, juvenile zebra finches master their song in two partly overlapping sensitive periods [5]. First, during the sensory phase, juvenile birds memorise a specific song model sung by an adult male (tutor). Next, during the sensorimotor phase, they will try to match their own vocalisations to the previously memorised tutor model by trial-and-error practicing. Reaching the end of the sensorimotor phase, zebra finch song will 'crystallise' implying that their song will become 'fixed' and, in normal circumstances, will remain unchanged.

Prior studies aimed at characterising brain areas implicated in song acquisition and maintenance in respectively ontogeny and adulthood, have mainly used invasive methods including histology, electrophysiology and immediate early genes (IEGs). As such, a clear understanding has been established of (1) the importance of the auditory system in sensory learning of the tutor song model [6-8] and in relaying auditory feedback to guide sensorimotor learning and active song maintenance in adulthood [9, 10]; (2) the role of the anterior forebrain pathway in introducing vocal variability during sensorimotor vocal practicing [11]; and (3) the involvement of the caudal motor pathway in driving motor output [12, 13]. Despite these major advancements in the current understanding of mechanisms and brain areas implicated in vocal learning, surprisingly, no clear and comprehensive overview is available on the structural development of the songbird brain outside of the classical song control and auditory systems. Furthermore, even beyond crystallisation, adult songbirds retain some form of vocal motor practicing [14-17]. This post critical period song refinement implies continuing neuroplastic processes. Moreover, little is known about how song learning or vocal proficiency affects the structural properties of the brain and whether areas outside of the classical song control and auditory systems might be actively shaped by vocal practicing.

Accurate descriptions of brain maturation or brain-behaviour relationships requires tools that enable repeated measures. In humans, MRI emerged as a prominent tool to quantify adaptations to brain function and structure that arise over development, e.g. [18-21], or along

training or learning paradigms, e.g. [22, 23]. Some of these studies have been able to correlate microstructural remodelling –measured by *in vivo* DTI– to the rate of task improvement during the learning process, both in humans and rodents [24]. Recently, technical improvements have enabled the implementation of such MR-based structural imaging methods to small animals including songbirds, e.g. [25] and Chapter 5, and bring the research questions outlined above within the range of experimentation.

The aim of the present study was threefold. (1) Create a comprehensive overview of structural neuroplastic events characterising the first 200 days of post hatch life in both male and female zebra finches. (2) Building further on the data presented in Chapter 5, trace the establishment of sex differences in brain structure. (3) Search for possible brain-behaviour relationship by assessing whether improvements in vocal behaviour can be traced back to altered structural properties of the brain. To this end, we obtained T2-weighted 3-dimensional (3D) anatomical scans and DTI data at seven time points coinciding with developmental milestones relative to vocal learning in male and female zebra finches. Exploiting the advantages of *in vivo* MRI, we performed brain-wide voxel-wise statistical analyses to quantitatively explore gross anatomical differences in volume (3D) or in intrinsic tissue properties (DTI) that arise between both sexes or as a consequence of age. Furthermore, by quantifying vocal proficiency from advanced sensorimotor to fully crystallised song, improvements in vocal behaviour could be related to changes in the structural properties of the brain.

6.2 MATERIALS AND METHODS

6.2.1 Animals and Ethical statement

Male (n = 16) and female (n = 19) zebra finches (*Taeniopyiga guttata*) were bred in the local animal facility. Only birds with a grey phenotype were included in this study, as white plumage morphs have been shown to display functional alterations in the visual system [26]. The birds were housed in individual cages together with an adult male (tutor), an adult female and one or two other juvenile birds. Consequently, not all birds were raised by their biological parents (the hatchlings moved to a different nest between 5 and 12 days post hatching (dph), before the sex of the birds was known). Each cage was shielded from its neighbouring cages, this way the juvenile birds could interact (visual and auditory) with only one adult male bird, but could hear all other birds of the room (6-12 other tutors and many other juveniles). The ambient room

temperature and humidity was controlled, the light-dark cycle was kept constant at 12h-12h, and food and water was available *ad libitum* at all times. In addition, from the initiation of the breeding program until the juvenile birds reached the age of 30 dph egg food was provided as well. The Committee on Animal Care and Use at the University of Antwerp (Belgium) approved all experimental procedures (permit number 2012-43 and 2016-05) and all efforts were made to minimize animal suffering.

6.2.2 Study design

We collected *in vivo* MRI data at seven time-points during and after the critical period for vocal learning, i.e. during the sensory phase (20 and 30 dph), sensorimotor phase (40 and 65 dph), crystallisation phase (90 and 120) and past the critical period (200 dph). We strived for maximal accuracy of the age of acquisition (relative errors of age at acquisition are respectively: 1.39%, 0.73%, 1.15%; 0.97%, 0.84%, 0.78%, and 0.61%). During each imaging session, a 3-dimensional Rapid Acquisition with Relaxation Enhancement (3D RARE) and Diffusion Tensor Imaging (DTI) scan was acquired. Additionally, the songs of the male birds were recorded after each imaging session from 65 dph onwards. Prior to or at the end of the experiment, the songs of the corresponding tutors were recorded as well to enable song similarity scoring (tutor versus tutee).

6.2.3 MRI data acquisition

All MRI data were acquired on 7 T horizontal MR system (PharmaScan, 70/16 US, Bruker BioSpin GmbH, Germany) combined with a quadrature transmit volume coil, linear array receive coil designed for mice, and a gradient insert (maximal strength: 400 mT/m; Bruker BioSpin, Germany). The same imaging protocol was used as described in Chapter 5. In brief, the zebra finches were anaesthetised with isoflurane (IsoFlo®, Abbott, Illinois, USA; induction: 2.0-2.5%; maintenance: 1.4-1.6%). After collecting T_2-weighted Turbo RARE pilot scans to enable uniform slice positioning across imaging sessions, a fieldmap was acquired to assess field homogeneity and guide subsequent localised shimming. The latter was performed to correct possible magnetic field inhomogeneities in a pre-set rectangular volume-of-interest covering major parts of the telencephalon of the birds. Next, DTI data were obtained by using a four-shot spin echo (SE) echo planar imaging (EPI) pulse sequence with the following parameters: TE 22 ms, TR 7000 ms, FOV (20x15) mm^2, acquisition matrix (105x79), in-plane resolution (0.19x0.19) mm^2, slice thickness 0.24 mm, b-value 670 s/mm^2, diffusion gradient duration (δ) 4 ms, diffusion

gradient separation (Δ) 12 ms. A total number of 60 unique, non-collinear diffusion gradient directions [27], and 21 non-diffusion-weighted (b_0) volumes were sampled. The b0 and diffusion-weighted volumes were acquired interleaved, i.e. 7 b_0 images followed by 20 diffusion gradient directions and this was repeated three times. The entire DTI protocol was collected twice to increase the SNR (total DTI scanning duration: 72 min). The field-of-view covered the entire telencephalon and diencephalon which contain the auditory system and brain areas implicated in song control, the cerebellum and parts of the mesencephalon. Immediately following each set of DTI scans, a T_2-weigthed 3D RARE dataset was obtained with the following settings: TE 11 ms (TE_{eff} 55 ms), TR 2500 ms, RARE factor 8, FOV (18x16x10) mm^3, matrix (256x92x64) zero-filled to (256x228x142), spatial resolution (0.07x0.17x0.16) mm^3 zero-filled to (0.07 x 0.07 x 0.07) mm^3, scan duration 29 min. The FOV of the 3D RARE scan captured the entire zebra finch brain.

Throughout the entire imaging procedure, the birds' physiological condition was monitored closely by means of a pressure sensitive pad placed under the chest of the bird to detect the breathing rate, and a cloacal thermistor probe connected to a warm air feedback system to maintain the birds' body temperature within narrow physiological ranges (40.0 ± 0.2) °C (MR-compatible Small Animal Monitoring and Gating system, SA Instruments, Inc). All animals recovered uneventfully within a few minutes after discontinuation of the anaesthesia.

6.2.4 MRI data processing

The DTI and 3D RARE datasets were pre-processed to enable voxel-wise statistical testing using the following software packages: SPM12 (Statistical Parametric Mapping, r 6225, Wellcome Trust Centre for Neuroimaging, London, UK, http://www.fil.ion.ucl.ac.uk/spm/) supplemented with the Diffusion II toolbox (https://sourceforge.net/projects/diffusion.spmtools.p/) and DARTEL tools [28], Amira (v5.4.0, FEI; https://www.fei.com/software/amira-3d-for-life-sciences/), ANTs (Advanced Normalization tools; [29]; http://stnava.github.io/ANTs/) and FSL (FMRIB Software Library; [30]; https://fsl.fmrib.ox.ac.uk/fsl/fslwiki/FSL). Figure 6-1 presents an overview of the different processing steps.

6.2.4.1 Deformation-Based Morphometry

The following paragraph provides a chronological overview of the processing steps necessary to extract the normalised, modulated jacobian determinants that encode local changes in tissue volume existing between each individual 3D RARE scan and the population-based template.

Firstly, the individual 3D RARE scans were masked (Amira 5.4.0) so that the resulting images only contained the brain. This manual brain extraction appeared necessary as for the youngest ages (20, 30 and 40 dph), no clear boundaries could be established between the rostral parts of the brain, meninges and skull, leading to suboptimal subsequent image registration. Secondly, one average 'intra-subject' 3D dataset was created for each animal based on the seven individual, masked 3D RARE scans acquired at the different ages using the serial longitudinal registration (SLR) tool of SPM12 [31]. This tool incorporates an intensity non-uniformity (bias field) correction, followed by a rigid-body transformation and several nonlinear diffeomorphic registration steps [31]. The SLR generated an average 'intra-subject' 3D ('midpoint average'), jacobian determinant (j) maps, divergence of velocity (dv) maps and deformation fields. The latter three encode, respectively, relative volume changes (j and dv) and the spatial transformation parameters that define the transformation from the midpoint average to the individual masked 3D scans in native space. Next, the midpoint averages of all animals were inputted in the 'buildtemplateparallel' function of the Advanced Normalization Tools (ANTs; [29]). The resulting 'inter-subject' population-based 3D was used by the FMRIB Automated Segmentation Tool (FAST; [32]) embedded in FSL, to extract tissue probability maps reflecting mainly grey matter (c_1), white matter (c_2) and cerebrospinal fluid (c_3), using the default settings for T_2-weighted datasets (an example of the resulting segments can be found in Figure 6-4). The three probability maps created in this step were used as tissue class *priors* for segmenting the individual midpoint averages using the default settings of the (old)segment batch in SPM12. Then, the within-subject 3D segments were used to create a segment-based template in DARTEL [28, 33]. Next, the ANTs-based T_2-weighted template was warped via the 'DARTEL: existing template' batch to spatially match with the segment template. The resulting DARTEL-ANTs population-based template was used as reference space. The flow fields produced by DARTEL that encode the spatial transformation parameters to warp the midpoint average to the reference space, were applied to the jacobian determinant maps (with modulation to preserve relative volume differences existing between different subjects) and divergence of velocity (without modulation) that were previously produced during the SLR step. Lastly, the warped modulated jacobian determinant maps were smoothed in plane using a Gaussian kernel with FWHM (0.14x0.14) mm^2.

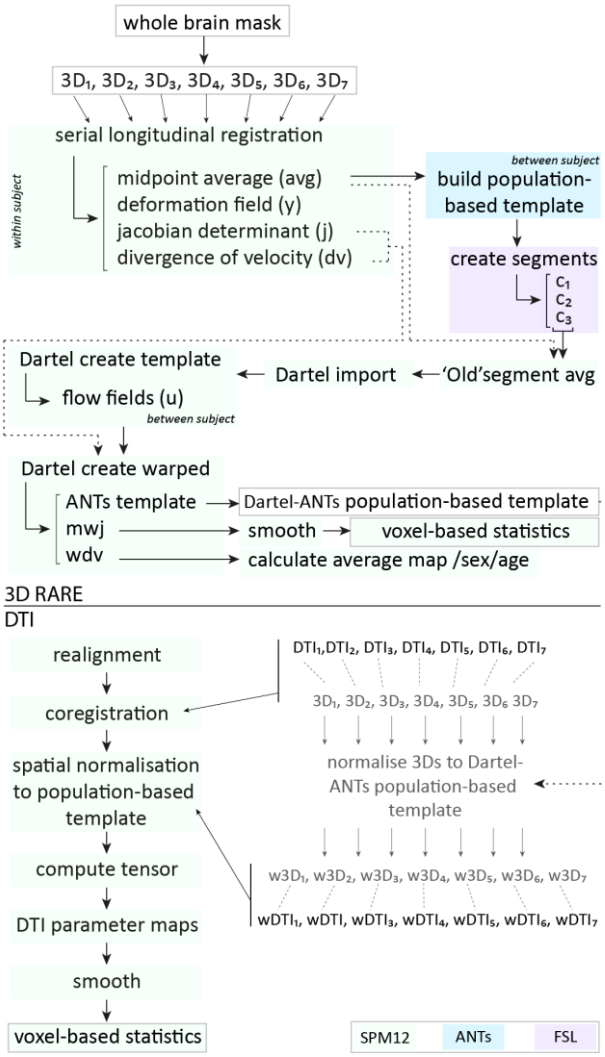

Figure 6-1: Schematic overview of the processing pipeline of the 3D RARE (top) and DTI (bottom) data. A detailed description can be found in section 6.2.4.1 and 6.2.4.2 respectively.

6.2.4.2 Diffusion Tensor Imaging

This paragraph provides a chronological overview of the processing steps necessary to calculate the diffusion tensor and DTI metrics after first spatially normalising the raw diffusion data.

All DTI analyses were performed in SPM12 equipped with the Diffusion II toolbox. Firstly, the DTI volumes were realigned to correct for possible subject motion. The realignment procedure consisted of two consecutive steps: an initial estimation on the b_0 images, followed by a linear registration including all (b_0 and diffusion-weighted) volumes. Secondly, the realigned DTI series were co-registered to the individual masked 3D dataset acquired at the same age. The co-registration utilised normalised mutual information as objective function for inter-modal

within-subject registration. In parallel, the individual masked 3D RARE datasets were bias corrected and spatially normalised to the DARTEL-ANTs population-based template using a 12-parameter affine global transformation followed by nonlinear deformations. These estimated spatial normalisation parameters were applied to the co-registered DTI volumes. This way the DTI data was transformed to the DARTEL-ANTs template space. Then, the diffusion tensor was estimated and the DTI parameter maps i.e. the Eigenvalues (λ_1, λ_2, λ_3), Fractional Anisotropy (FA), and Mean Diffusivity (MD) were calculated. Lastly, the DTI parameter maps were smoothed in plane using a Gaussian kernel with FWHM of (0.38x0.38) mm^2.

Several quality controls were performed throughout the DTI data processing procedures to evaluate data quality, including a visual inspection for ghosting, excessive movement, and spatial correspondence of registered images to the reference space (after co-registration and spatial normalisation procedures).

6.2.4.3 Volumetry

Whole brain, segment (c_1, c_2 and c_3) and cluster-based ROI volumes (extracted from voxel-wise statistical tests, see. section 6.2.6.1) were estimated by performing a back-transform of the template mask, segments and ROIs using the inverse spatial transformation parameters generated during the spatial normalisation. The volumes of the back-transformed masks were extracted via the 'get_totals' function in SPM12 (whole brain and segments) or using Matlab (version R2016b; MathWorks, Natwick, MA, USA).

6.2.5 Song recordings and analyses

The undirected songs sung by the juvenile and adult male zebra finches were recorded in custom-build sound attenuation chambers equipped with the automated song detection setup implemented in Sound Analysis Pro (SAP; [34]; http://soundanalysispro.com/). All song analyses were performed off-line. Calls and introductory notes were omitted from all analyses. As song tempo changes over the course of a day, we only used the first 20 song sung during the morning (starting from the initiation of the photophase). First, the motif length (ms) was measured after which each individual motif was segmented into its different syllables. The syllable segmentation was based on sharp changes in amplitude and frequency. The latter measure was chosen to avert inconsistent determination of the syllable ending caused by more silent singing towards the last part of the syllable. Second, several acoustic features that reflect the spectro-temporal structure of individual syllables were quantified, i.e. (1) pitch-related measures that

inform on the perceived tone of sounds (including pitch, mean frequency, peak frequency and goodness of pitch), (2) Wiener entropy is a measure for the width and uniformity of the power spectrum [34], it quantifies the tonality of sounds and is expressed on a logarithmic scale where white noise approaches '0' and pure tones are characterised by large, negative Wiener entropy values, (3) syllable and inter-syllable interval duration. Based on the latter two measures, estimates of song density were made (song density is defined by the duration of all syllables relative to the duration of the sum of all syllables and inter-syllable intervals of a motif, expressed in percentage). Furthermore, to evaluate syllable feature variability over the different ages, the standard deviation, as an estimate for vocal variability [11], was defined for each acoustic property. No corrections to the standard deviation for number of samples were made as for each bird and time point, always exactly 20 song motifs were analysed.

Next, similarity to tutor song was measured between song motifs using an automated procedure in SAP that quantifies the acoustic similarity between two songs based on pitch, FM, AM, goodness of pitch and Wiener entropy [34]. Song similarity was calculated using the default settings of SAP (asymmetric comparisons of mean values, minimum duration 10ms, 10x10 comparisons), and accuracy, % similarity and % sequential were used for statistical testing. Further, according to the method conceptualised by Scharff and Nottebohm, motif sequence stereotypy was computed, based on visual assessment of sequence consistency and linearity [11]. Sequence linearity reflects how consistent notes are ordered within the song motif by counting the different transition types of each syllable of the motif. Sequence consistency quantifies how often a particular syllable sequence occurs over different renditions of a specific motif. Song sequence stereotypy is defined as the average of sequence linearity and sequence consistency.

6.2.6 Statistical analyses

Even though the data were thoroughly checked at several stages in the pre-processing, an additional quality control was performed based on outlier detection. To this end, several ROIs were delineated on an average FA map and, next, the average DTI parameters were extracted for each ROI and each bird and time point separately. Only if several ROIs displayed outlying values for a specific DTI parameter (automated detection via Mahalanobis distances [35] performed in JMP® (Version 13, SAS Institute Inc., Cary, NC, 1989-2007)), a particular time-point of a specific bird was categorised as an outlier and excluded from subsequent analyses. This

strategy detected four outliers. Visual inspection of the raw data informed that two of the four animals displayed excessively large ventricles at the 20 dph time points and appeared normal thereafter. The other two animals showed an abnormal cerebellar folding pattern. Based on the outlier detection and visual confirmation of brain abnormalities (both of which could result in suboptimal image registration), these four animals were excluded from the DTI and 3D RARE analyses. In addition, one animal had one missing DTI scan, leaving 30 zebra finches (14 males, 16 females) for voxel-wise statistical testing of the DTI data and 31 birds (15 males, 16 females) for DBM.

6.2.6.1 Voxel-based analysis

Interactions and main effects

All voxel-wise statistical tests were executed in SPM12. Firstly, repeated-measures ANOVA's were performed on each set of smoothed DTI parameter and smoothed, modulated jacobian determinant maps, including 'subject' as random factor, and 'sex' and 'age' as fixed factors. Only for the DMB analysis, a covariate describing the whole brain volume was included in the flexible factorial design. This design allowed for testing within-subject effects including interactions (age*sex) and main effects (age). Secondly, a separate voxel-wise ANOVA (full factorial design; including 'age' and 'sex' as fixed effects) was set up to explore sex differences in datasets obtained at 65, 90, 120 and 200 dph. The latter time points were chosen as Nixdorf-Bergweiler (1996) reported that in normal rearing conditions, sex differences are fully established around 60 dph [36]. Lastly, 2-sample T-tests were performed on the MRI parameter maps pooled from 120 and 200 dph to explore sex differences that only arise towards adulthood and might be missed by the interaction.

To further clarify when in time most extensive neuroplastic changes occur, hypothesis-driven F-tests comparing consecutive time points or successive subphases of vocal learning were executed. Unless explicitly stated, only clusters that survived a family-wise error (FWE) correction thresholded at $p_{FWE}<0.05$ (or stricter) combined with a minimal cluster size (k_E) of at least 5 or 20 voxels respectively for DTI and DBM analyses, were considered significant. All statistical maps are displayed overlaid onto the population-based template. Appendix 6-A provides an overview of the anatomical structures detectable on sagittal and horizontal slices.

Multiple regression between song features and MRI parameter maps

Structural properties of the brain are tuned by learning and behavioural performance [22]. To explore potential relationships between robust measures of song performance and the structural properties of the songbird brain, voxel-wise multiple regressions were set up between the smoothed MRI parameter maps and % similarity, song density and sequence stereotypy. For DBM analyses, the normalised jacobian determinant maps were log-transformed [37] and total brain volume was added to the statistical design as additional covariate. All statistical parametric maps (SPMs) were assessed at $p_{FWE}<0.05$ and $k_E \geq 5$voxels or 20 voxels for respectively DTI and DBM analyses, and displayed overlaid onto the population-based template.

Post hoc testing of clusters detected by voxel-based analyses

Clusters detected by the voxel-based analysis that displayed a significant interaction between age*sex, changes over time or between both sexes were converted to ROIs ('cluster-based ROIs') of which the mean DTI metrics, modulated jacobian determinant, or (relative) volume were extracted for *post hoc* statistical testing in JMP® software (Version 13, SAS Institute Inc., Cary, NC, 1989-2007). First, a linear mixed model was selected to confirm the presence of an interaction or main effect ('subject': random variable, 'age' and 'sex': fixed variables). Next, *post hoc* tests using Tukey's HSD (Honest Significant Difference) were used to situate which time points differed significantly, or at what age sex differences arise.

The voxel-wise multiple regression in SPM does not allow including a random effect for bird identity. Consequently, by inserting repeated-measures data we violate the assumption of independency of measures. To correct for this potential confound, we extracted the mean DTI metrics or log-transformed jacobian determinants of the voxel-based clusters and performed an additional repeated-measures correlation analysis [38] in Rstudio (version 1.1.383, Rstudio®, Boston, MA, USA; http://www.rstudio.com/) as this function is not available in JMP® software. This latter test informs on the existence of possible within-subject correlations between the structural properties of the brain and the song scores. Lastly, Spearman's ρ was calculated to illustrate the nature of possible overall associations between MRI parameter maps and song scores at a specific age, without taking subject identity into account.

6.2.6.2 Song features

Songs were analysed on two levels i.e. on the motif and on the syllable level. A linear mixed model was set up including age as fixed effect, subject as random effect, and subject*age as random slope and –only for the syllable level– syllable identity as random effect nested within subject. If a significant main effect could be observed for any of the song features examined, *post hoc* tests were performed to situate when in time actual changes occur using Tukey's HSD (Honest Significant Difference). In addition, a similar linear mixed model tested whether the variability of the acoustic properties changed over time. Furthermore, to determine whether certain motif feature scores, i.e. song similarity, song stereotypy or song density, were dependent on the tutor by which the birds were raised, a mixed model was performed with 'tutor' as fixed effect and 'subject' as random effect.

6.3 RESULTS

6.3.1 The establishment of sex differences in brain structure

Two different strategies were employed to situate when in time structural differences between both sexes arise in the zebra finch brain. First, we tested for an interaction between age and sex to unveil clusters that display a sex-dependent developmental trajectory of local volumes or diffusion properties. Second, we searched for possible main effects of sex when sex differences should be fully established [36]. The latter included statistical tests based on data obtained at 65-90-120-200 dph or 120-200 dph, to increase the sensitivity to detect subtle sex differences that only arise towards or in adulthood.

6.3.1.1 Sex differences in local tissue volume

The results of the statistical tests exploring sex differences in local volume are summarised in Figure 6-2 and Table 6-1. Appendix 6-B includes graphs to situate how the modulated jacobian determinant and relative volume extracted from the cluster-based ROIs change over time.

Distinct brain areas display a sex-dependent trajectory in relative volume changes over time

The voxel-wise repeated-measures ANOVA of the smoothed, modulated jacobian determinant maps identified an interaction between age and sex at several clusters in various locations in the brain. The most significant cluster was localised near the occipitomesencephalic tract (tOM) at the level of the thalamus and more ventrally near the intercollicular nucleus (ICo) and the dorsal part of the lateral mesencephalic nucleus (MLd). At an exploratory statistical threshold

($p_{uncorrected}$<0.001; k_E≥100 voxels), the latter cluster extends towards the di- and mesencephalon (specifically to ICo) and more caudally towards the cerebellum. When exploring the spatial extent of the cluster even more *liberally* ($p_{uncorrected}$<0.01; k_E≥100 voxels), the ventral tOM cluster connects to the cluster covering the tOM near the thalamus (data not shown). Furthermore, three song control nuclei i.e. HVC and RA of the right hemisphere and area X of the left hemisphere, were found to display a sex-dependent volumetric development over time as well. No clusters could be observed co-localised with the left RA, left HVC and right Area X, when testing for an interaction between age and sex.

Localised volume differences between male and female zebra finches at 65, 90, 120 and 200 dph

Males are characterised by significantly larger modulated jacobian determinants (reflecting larger volumes) compared to females in several parts of the tOM (left and right, near the thalamus and more ventrally towards the Ico-DM-MLd complex), and a ventral part of Field L (right) that potentially overlaps with the interfacial nucleus (NIf), at p_{FWE}<0.05 k_E≥20 voxels. At an exploratory threshold ($p_{uncorrected}$<0.001; k_E≥20 voxels), additional clusters were detected near HVC (left, right), the arcopallium including RA (right), and LMAN (left, right) and the contralateral ventral Field L-NIf cluster (left). No supra-threshold clusters were found displaying larger volumes in females compared to males. Lastly, a 2-sample T-test including data obtained at 120 and 200 dph, replicated the SPM of the full factorial testing for sex differences at 65-90-120-200 dph. The results of the voxel-wise statistical tests are summarised in Table 6-1.

Table 6-1: Clusters displaying an interaction or a sex difference in local tissue volume, obtained by the voxel-wise repeated-measures ANOVA performed on the smoothed, modulated jacobian determinant maps.

Statistical test	Cluster - ROI		Cluster level		Peak level	
			p_{FWE}	k_E	p_{FWE}	*F*
Interaction age*sex	tOM near thalamus	Left	<0.001	183	<0.001	17.22
		Right	<0.001	79	<0.001	13.09
Main effect sex		Left	0.001	94	0.001	6.24
		Right	0.001	103	0.003	5.93
Interaction age*sex	HVC	Left	.	.	.	.
		right	<0.001	109	<0.001	12.00
Main effect sex		Left	.	.	.	.
		right	0.009	25	0.005	5.78
Interaction age*sex	tOM near ICo	Left	<0.001	220	<0.001	10.63
		Right	<0.001	212	<0.001	11.66
Main effect sex		Left	0.004	42	0.002	6.00
		right	(subpart of large fragmented cluster)			
Interaction age*sex	Area X	Left	<0.001	396	0.001	9.69
		Right	.	.	.	.
	RA	Left	.	.	.	.
		Right	0.002	43	0.003	9.15
Main effect sex	Ventral part of Field L	Left	0.338	.	0.026	5.36
		Right	0.002	64	0.001	6.24
	LMAN	Left	0.896	.	0.131	4.92
		Right	0.966	.	0.051	5.19
	RA-arcopallium	Left	.	.	.	.
		Right	<0.001	.	0.054	5.17

'Interaction age*sex' was performed in a flexible factorial design and serves to unveil brain regions that display a sex-dependent trajectory, while the 'Main effect of sex' is extracted from a full factorial statistical test and informs on areas that display absolute volume differences between both sexes.
The 'Cluster level' and 'Peak level' columns refer to respectively the *p*-value (after 'Family Wise Error' correction for multiple comparisons) of the clusters and cluster extent (k_E), and *p*- and *F*-values of the peak voxel of the clusters respectively, provided by SPM. The '.' indicates that no cluster or no significant differences could be observed in this region. Abbreviations: tOM: occipitomesencephalic tract; RA: robust nucleus of the arcopallium; HVC: abbreviation used as proper name.

The clusters that displayed an interaction and/or a sex difference in the voxel-wise analysis were converted to ROIs, of which the average modulated jacobian determinant value was extracted and subjected to *post hoc* statistical testing (Tukey's HSD) to situate when in time the actual difference occurs. For all ROIs, except for the cluster co-localised with the ventral portion of Field L possibly including NIf, the significant interaction between age and sex was confirmed by a linear mixed model (HVC right: p=0.0020 $F_{(6,186.0)}$=3.6358; RA right: p=0.0005 $F_{(6,186.0)}$=4.2766; Area X left p=0.0003 $F_{(6,186.0)}$=4.4707; part of the tOM near the thalamus left p<0.0001 $F_{(6,186.0)}$=18.1338; part of the tOM near the thalamus right p<0.0001 $F_{(6,186.0)}$=9.6597;

ventral part of the tOM cluster left $p<0.0001$ $F_{(6,186.0)}=14.4741$; ventral part of the tOM cluster right $p<0.0001$ $F_{(6,186.0)}=14.6646$; ventral portion of Field L or Nif right: $p=0.1202$ $F_{(6,186.0)}=1.7125$; left: $p=0.7961$ $F_{(6,186.0)}=0.7961$). Importantly however, the clusters near the ventral portion of Field L displayed a clear sex difference in volume (main effect of sex: right: $p=0.0119$ $F_{(1,31.0)}=7.1427$; left: $p=0.0182$ $F_{(1,31.0)}=6.2189$). Further, the cluster-based ROIs were back-transformed from the population-based template to the native space for volume extraction. Figure 6-17 in Appendix 6-B provides details on nature of the interaction between age and sex, main effect of sex extracted from the cluster-based ROIs and the relative volume of the cluster-based ROIs in native space.

6.3.1.1 Sex differences in micro-architectural tissue properties

A voxel-wise repeated-measures ANOVA was performed on the smoothed DTI parameter maps, only clusters surviving $p_{FWE}<0.05$ and $k_E\geq5$ voxels were used for further statistical testing. An interaction between age and sex was detected bilateral at the Area X surroundings (FA), arcopallium (FA), and HVC (λ_3). In addition, 2-sample T-tests were performed to explore sex differences at 120 and 200 dph, with $p_{FWE}<0.05$ $k_E\geq5$ voxels. This analysis complemented previous results with clusters in left LMAN (MD, M>F), left RA (MD, M>F) and left HVC (MD, M>F). Interestingly, when using an exploratory statistical threshold ($p_{uncorrected}<0.001$; $k_E\geq10$ voxels), clusters covering right RA and right HVC could be detected as well. The full factorial design testing male-female differences at 65-90-120-200 dph did not uncover any additional clusters. Table 6-2 and Figure 6-3 summarise the voxel-wise statistical outcome.

Table 6-2: Clusters displaying a sex difference in local tissue microstructural properties.

DTI parameter	Statistical test	Cluster - ROI		Cluster level		Peak level	
				p_{FWE}	k_E	p_{FWE}	*F* or *T*
FA	Interaction age*sex	Arcopallium	Left	<0.001	21	<0.001	16.49
			Right	<0.001	28	<0.001	25.39
		Rostro-lateral Area X surroundings	Left	<0.001	34	<0.001	10.33
			Right	0.001	20	0.002	8.76
		Caudal Area X surroundings	Left	<0.001	11	<0.001	9.62
			Right	<0.001	16	0.001	9.08
λ_3		HVC	Left	<0.001	15	<0.001	9.98
			Right	0.002	5	0.007	8.13
MD	M>F (2-sample T-test)		Left	0.006	9	0.020	4.77
			Right	0.428	37	0.036	5.03
		LMAN	Left	0.010	6	0.001	6.00
			Right	.	.	.	.
		RA	Left	0.010	6	0.003	5.74
			Right	0.880	10	0.034	5.05
		Area X	Left	0.665	22	0.347	4.23
			Right	.	.	.	.

The statistical maps were assessed at $p_{FWE}<0.05$ and $k_E \geq 5$voxels (grey values reflect clusters found at an exploratory threshold of $p_{uncorrected}<0.001$ and $k_E \geq 10$voxels). 'Interaction age*sex' was performed in a flexible factorial design and serves to unveil brain regions that display a sex-dependent trajectory, while the 'Main effect of sex' is extracted from a 2-sample T-test performed on data obtained at 120 and 200 dph and informs on areas that display absolute differences in intrinsic tissue properties between both sexes. The 'Cluster level' and 'Peak level' columns refer to respectively the *p*-value (after 'Family Wise Error' correction for multiple comparisons) of the clusters and cluster extent (k_E), and *p*- and *F*-values of the peak voxel of the clusters respectively, provided by SPM. The '.' indicates that no cluster or no significant differences could be observed. Abbreviations: RA: robust nucleus of the arcopallium; LMAN: magnocellular nucleus of the anterior nidopallium.

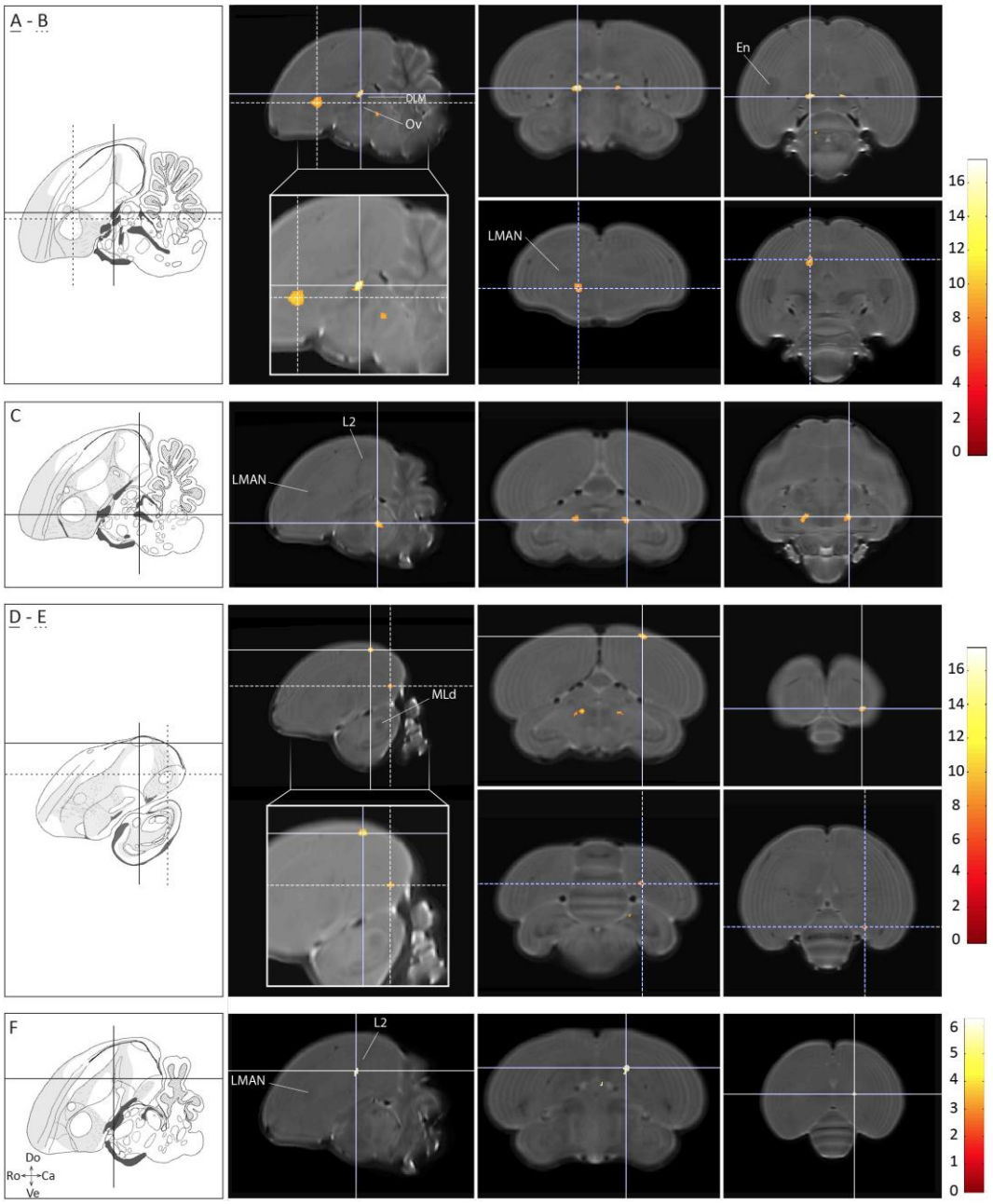

Figure 6-2: Relative volume differences between both sexes. Statistical Parametric Maps illustrating the spatial extent of the clusters observed by the interaction between age*sex (A-E) or a main effect of sex (F). The crosshairs converge on (A) tOM near the thalamus, (B) left Area X, (C) tOM near ICo, (D) right HVC, (E) right RA, and (F) the ventral portion of Field L potentially co-localised with Nif. The results are displayed $p_{FWE}<0.05$; $k_E \geq 20$ voxels, overlaid on the population-based template, and colour-coded according to the scales on the right (F-values). The schematic atlas drawings, obtained from [39], present sagittal slices at approximately the same anatomical level as the MR images (exception: En (instead of 'E') refers to the Entopallium). Abbreviations: Do: dorsal; Ve: ventral; Ro: rostral; Ca: caudal.

Next, the clusters described above were converted to ROIs for in depth *post hoc* statistical testing, the results of which can be found in the graphs in Appendix 6-C.

These statistical tests corroborate the *in vivo* proof-of-principle study described in Chapter 5, as now we are able to trace when in time sex differences become apparent (Appendix 6-C). The rostro-lateral and caudal Area X surrounding clusters show a difference in FA between both sexes from 30 dph onwards (FA M>F). The sex difference in FA in the arcopallium becomes detectable at 40 dph (FA M>F), whereas HVC only shows a sex-difference in λ_3 from 65 dph onwards (λ_3 M>F mirrored by FA M<F). Interestingly, the differences in FA observed in the interaction between age and sex are driven by different parameter profiles ($\lambda_{1,2,3}$). This suggests that different biological mechanisms might be driving the observed changes. For example, the sex difference in FA detected in the arcopallium reflects an increase in FA values for male birds, while in female birds FA increases slightly from 20 to 30 dph but remains stable thereafter. This effect is paralleled by steadily increasing differences in λ_1 and λ_3 between male and female juveniles (λ_1 M>F; λ_3 M<F), both masked by a main age-effect visible as a decrease of both parameters towards 200 dph. No significant differences were observed in λ_2 or MD in the arcopallium, the latter of which suggests that the increase and decrease in respectively λ_1 and λ_3 change proportionally. Furthermore, the significant differences in FA near the rostro-lateral Area X surroundings are mainly driven by changes in λ_3 that become significant from 40 dph onwards (10 days later compared to differences in FA). The caudal surroundings on the other hand, do not show a significant change in any of the λ's between males and females over time.

The cluster near HVC detected by the interaction between age and sex in λ_3, and the 2-sample t-test comparing MD in males and females at 120 and 200 dph, are not fully coextensive. This might be explained by the topographical complexity of HVC. More specifically, different portions of HVC (including HVC_{shelf}) might present different microstructural tissue characteristics leading to distinct DTI parameter readouts. However, we cannot fully guarantee that both clusters described above relate to similar topographic areas in both male and female birds, based on the following three reasons. (1) HVC cannot be distinguished from surrounding tissues on the T_2-weighted 3D scans used to spatially normalise the DTI data. (2) There is no anatomical contrast of HVC embedded in the DTI parameter maps (in line with observations in starlings [40]). (3) There exists a clear sex difference in volume exists between both sexes ([36]

and in part suggested by the DBM data above (right HVC)). Hence, alternatively, the DTI parameter readout might also suggest a macrostructural difference in local volume.

The disparities in MD between both sexes observed in LMAN, RA and Area X originated late and early, respectively at 120, 120 and 20 dph, and were driven by respectively alterations in λ_1-λ_2-λ_3, λ_2-λ_3, and λ_2-λ_3. Interestingly, the unilateral sex difference in Area X appears to dissolve towards later ages.

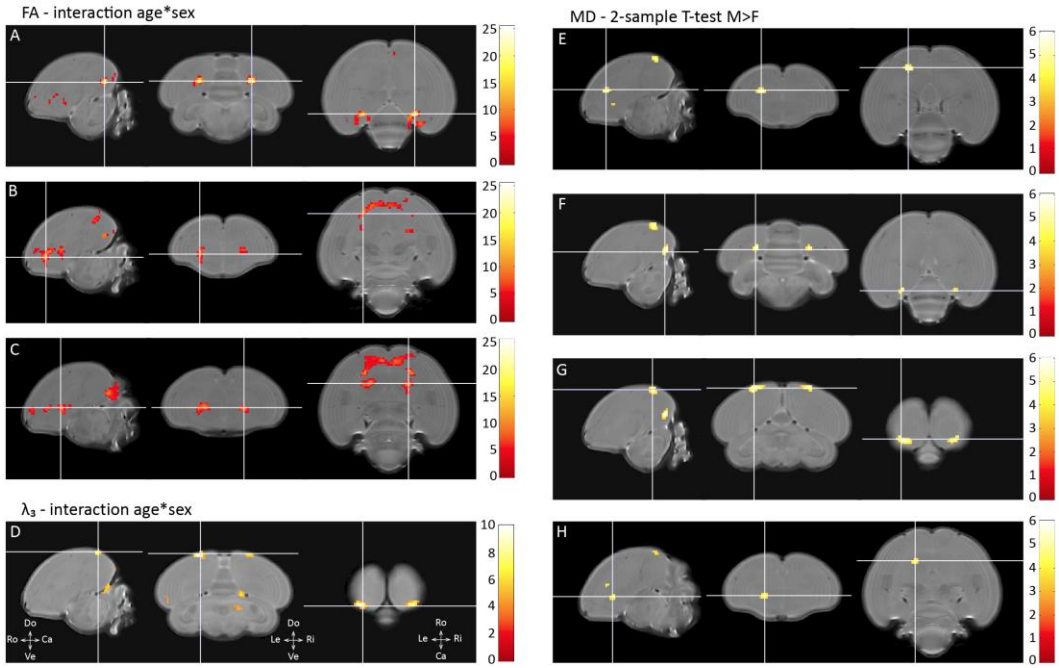

Figure 6-3: Sex differences detected by in vivo DTI. Statistical parametric maps highlighting voxels that display an interaction between age*sex (A-D) or a main effect of sex of data obtained at 120 and 200 dph (M>F; E-H) for FA (A-C), λ_3 (D) or MD (E-H). The crosshairs converge at RA (A), rostro-lateral Area X surroundings (B), caudal Area X surroundings (C), HVC (D), LMAN (E), RA (F), HVC (G) and Area X (H). The maps are thresholded at $p_{uncorrected}<0.001$; $k_E \geq 30$voxels (A-D) or $p_{uncorrected}<0.001$; $k_E \geq 10$voxels (E-H) and scaled according to the colour-code immediately right of each set of slices (interaction: F-values; 2-sample T-test: T-values). Abbreviations: Do: dorsal; Ve: ventral; Ro: rostral; Ca: caudal.

6.3.2 Mapping developmental neuroplasticity: volumetric and micro-architectural changes from fledging to adulthood

The previous analyses clearly show that several regions related to the auditory and song control system display sex differences, consequently, testing for effects over time was performed for each sex separately.

6.3.2.1 Brain-wide and localised volume changes

Segmenting modular instead of laminar brains

Even though the bird brain differs fundamentally from the mammalian brain, the FAST tool of FSL managed to discriminate three different tissue classes on the population-based template built in ANTs, i.e. c_1 containing mostly grey matter areas, c_2 including the majority of white matter structures and c_3 encompassing mostly CSF. Figure 6-4 illustrates the resulting tissue probability maps. These maps were used as tissue *priors* to segment the mid-point averages outputted by the SLR in the 'Old segment' batch in SPM. Next, these maps were used in two ways: (1) to create the final population-based template in DARTEL, and (2) to extract tissue compartment volumes in native space.

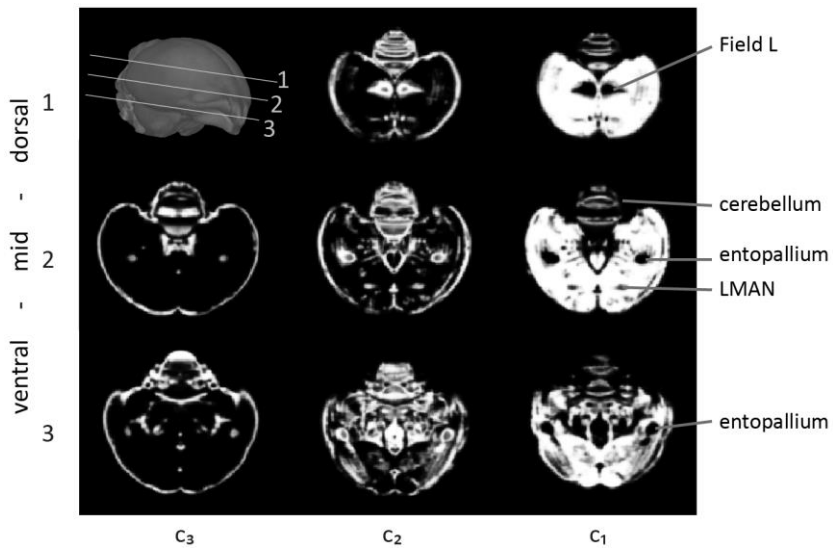

Figure 6-4: Overview of the tissue segments. The top left corner presents a 3D-rendered view of the population-based template that indicates the location at which the three different horizontal slices were obtained (1, 2 and 3).

Volumes of brain compartments

The total brain volume and volume of the tissue compartments were determined by back-projecting the 'whole brain mask' from the template and the segments made on the average 3D produced during the SLR step to the individual datasets in native space and extracting the volumes of the back-projected masks using the 'get_totals' function of SPM. Alternatively, the whole brain volume can be computed by summing the different segments. This, however, often leads to an overestimation of the total brain volume. Next, the relative segment volumes were calculated by dividing the absolute segment volume by the 'sum of the segments' of the

corresponding time point, and multiplying by 100. The linear mixed model identified an interaction between age*sex for the whole brain volume ($F_{(6,186.0)}$= 5.6735; p<0.0001), but not for relative c_1, c_2, and c_3 volumes ($F_{(6,186.0)}$= 0.5597; p=0.7620; $F_{(6,186.0)}$= 0.8598; p=0.5265; $F_{(6,186.0)}$= 1.589; p=0.1589 respectively). The three segments did show a significant main effect of time (c_1: $F_{(6,192.0)}$= 119.5394 p<0.0001; c_2: $F_{(1,192.0)}$= 139.0462 p<0.0001; c_3: $F_{(6,192.0)}$= 67.7312 p<0.0001), and a weak main effect of sex was observed for c_2 and c_3 (c_1: $F_{(1,31.0)}$= 0.0238 p=0.8785; c_2: $F_{(1,31.0)}$= 4.3850 p=0.0445 M>F; c_3: $F_{(1,31.0)}$= 4.5859 p=0.0402 M<F). The results of the *post hoc* tests (Tukey HSD) are summarised in Figure 6-5.

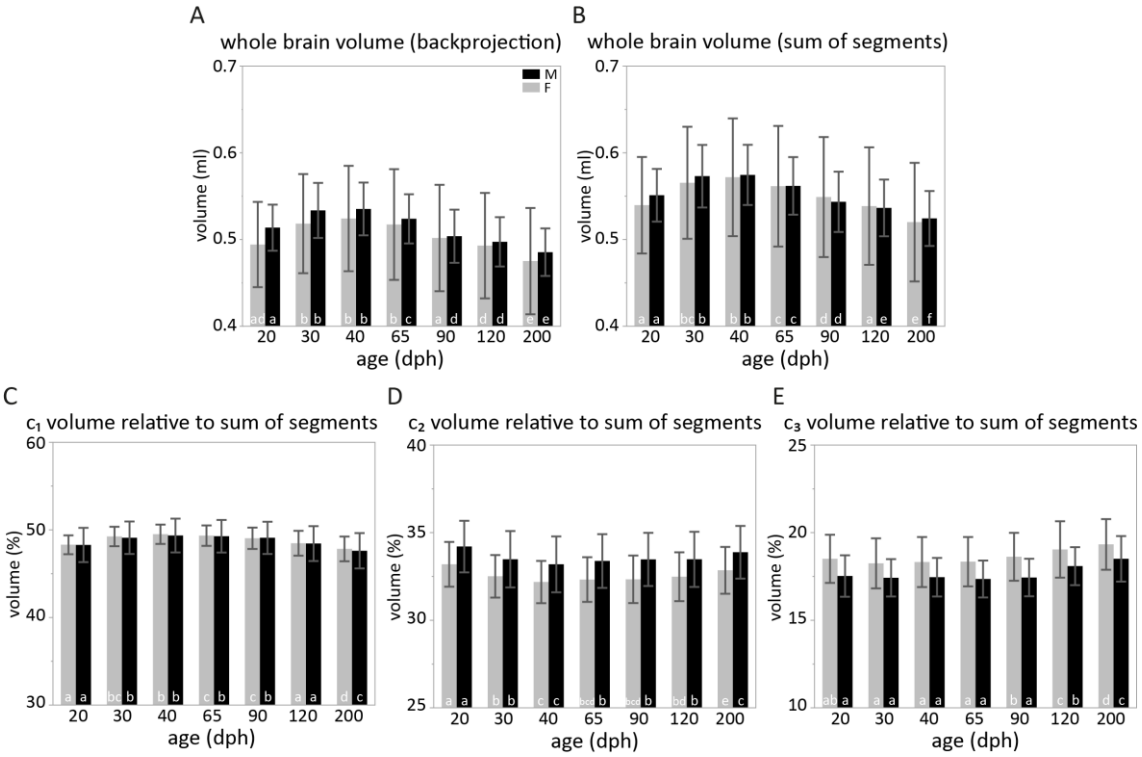

Figure 6-5: Whole brain and tissue compartment volume in function of age. The bar graphs illustrate the volume of the entire brain (A-B) and the volumes of the different segments, i.e. c_1 (C), c_2 (D) and c_3 (E), for male (black) and female (grey) zebra finches, in function of age. The bars indicate the mean ± standard deviation. The white letters at the base of each bar refer to the results of the post hoc test (Tukey HSD) to inform when in time volume changes occur, for each sex separately. If two time points share the same letter, then the volumes do not differ between both ages. Abbreviations: dph: days post hatching.

Both in males and females, the whole brain volume follows an 'inverted-U shape': it increases from 20 dph to 30 dph, peaks at 40 dph, after which it gradually decreases towards 200 dph. On average, male birds are characterised by larger brains, while the variability in brain size is higher in females. Surprisingly, no sex differences could be observed in the grey matter

compartment (c_1) which appears to follow a similar increasing and decreasing trend as the whole brain volume. The c_2 segment is bigger in males, whereas c_3 was found to be consistently larger in females. The white matter compartment (c_2) shows an initial drop in volume. However, this drop in inverted around 40 dph after which it gradually increases towards the end of the study. The CSF compartment (c_3) remains unchanged between 20 and 90 dph after which it consistently expands.

To obtain spatial information which brain areas primarily drive the initial increase and later decrease in total brain volume, we calculated for each time-point and sex separately an average divergence of velocity (dv) map (Figure 6-6 shows the average dv-maps of male birds; overall highly similar spatial pattern of coloured clusters was observed for both sexes (data of females is not shown); Appendix 6-A presents the sagittal slices with anatomical labels). The dv-maps outputted by the SLR encode for each voxel of the midpoint average whether the area should expand (dv>0) or contract (dv<0) to spatially match with the individual 3D scans in native space. Cold colours refer to negative divergence of velocity values which indicate that, on average, the midpoint average needs to contract to spatially match with the individual 3D scans, hence the native space tissue is smaller compared to the midpoint average. Warm colours cover brain area that display a larger volume in native space compared to the midpoint average. At 65 dph, the average dv of male birds appear to be situated between -0.05<dv<0.05 (arbitrary threshold), suggesting that the 65 dph time point most closely resembles the midpoint average (in terms of volume and spatial constitution). This is further corroborated by Figure 6-5-A-B which demonstrates that brain sizes measured at 65 dph lie most closely to the average brain size when considering all ages. At 20 dph, dv-maps reveal that mostly the rostral and lateral parts of the telencephalon are smaller in size, while parts of the cerebellum and mesencephalon (mainly the optic lobes, including MLd) appear to grow towards to midpoint average. Only minor changes, reflected in small, spatially confined suprathreshold voxels, are detected in the average dv-maps at 30, 40 and 90 dph. Towards 120 and 200 dph, the entire telencephalon and cerebellum appear to decrease in volume compared to the midpoint average. Interestingly, the volume of the thalamic zone appears to decrease consistently over the course of the study.

The average dv-images only provide descriptive or qualitative information. To enable more quantitative analyses, we performed voxel-wise statistical analyses on the modulated jacobian

determinant maps to establish a spatio-temporal map indicating when and where in the developing brain relative volume changes occur.

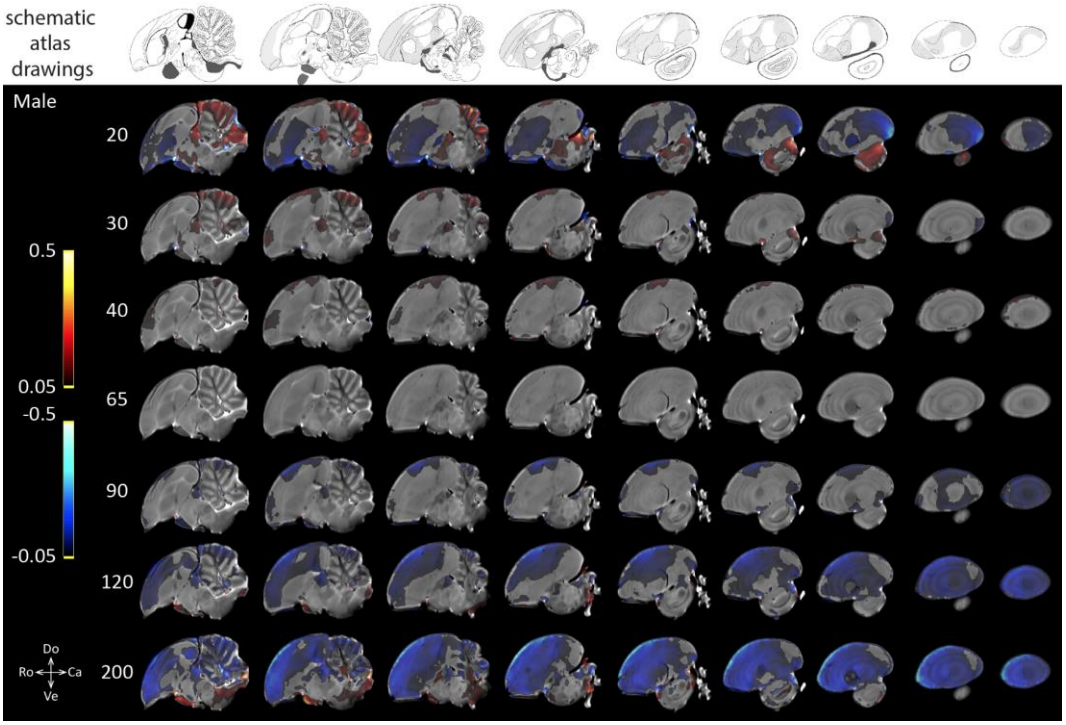

Figure 6-6: Origin of the inverted-U shape. Colour-coded representation of the average dv maps of all male zebra finches calculated for each time point separately. Volume increase relative to the 65 dph time point is indicated in red (dv > 0.05), while volume decreases relative to 65 dph is indicated in blue (dv < -0.05; colour-code according to the scale of the left). The schematic atlas drawings are obtained from [39]. Appendix 6-A contains an overview of the sagittal slices with anatomical labels. Abbreviations: Do: dorsal; Ve: ventral; Ro: rostral; Ca: caudal.

6.3.2.2 Brain-wide voxel-wise statistical analyses to explore localised volume changes over time

Similar to the dv-maps, the jacobian determinants are deduced from the deformation fields outputted by the SLR and encode relative volume changes between the midpoint average and the individual 3D scans (of the same bird) in native space. More specifically, jacobian determinants >1 indicate expansion of tissue (volume increase), while values <1 suggest contraction of tissue (volume decrease) from the mid-point average to spatially match the individual time-points (within-subject). Next, the jacobian determinant maps are warped to the population-based template to enable voxel-wise statistical testing. During this step, the jacobian determinant maps are modulated or 'rescaled', i.e. multiplied by the jacobian determinant extracted from the DARTEL flow field, hence, they incorporate relative volume

changes between the population-based template and the midpoint average (between-subject). As a result, the modulated jacobian determinant maps can be used to test for within-subject (interaction age and sex, main effect of age) as well as between-subject (main effect of sex) effects. To explore effects over time (within-subject comparisons) additional tests were performed on warped but non-modulated jacobian determinant maps. These tests resulted in similar statistical parametric maps and are therefore not included.

The main effect of age informs that almost the entire brain displays relative volume changes from 20 to 200 dph (Figure 6-7). This concurs with the backprojected whole brain delineations that present an initial increase and later decrease in volume. The peak change was localised near the thalamus. This appears consistent with the continual volume decline of the thalamic zone evident on the average dv-maps (Figure 6-6). The clusters cover similar brain areas in male and female birds. Next, we performed *post hoc* statistical tests to situate when in time relative volume changes occur. Two separate strategies were employed: (1) pair-wise comparison of subsequent sub-phases of vocal learning (Figure 6-8) and (2) a direct comparison of consecutive time points (Appendix 6-D Figure 6-19).

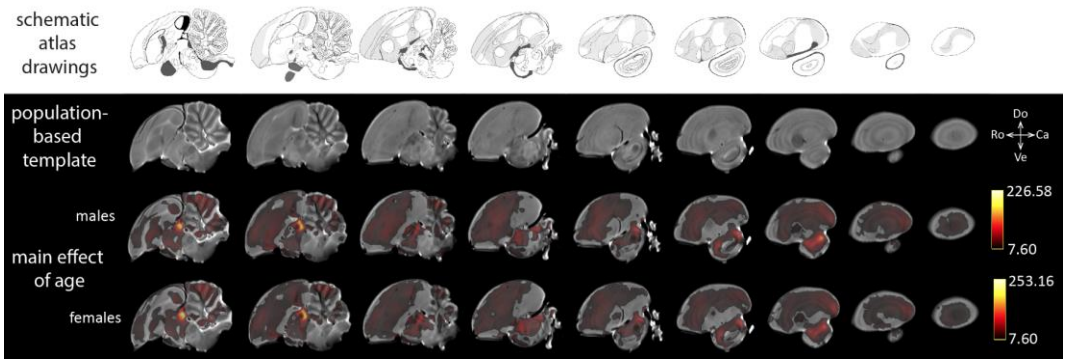

Figure 6-7: Statistical parametric maps displaying the main effect of age based on the modulated jacobian determinant maps. The spatial extent of the clusters covers similar areas in the male and female zebra finch brain. Almost the entire brain shows relative volume changes from 20 to 200 dph. The SPMs are displayed according to F>7.60 which corresponds to $p_{FWE}<0.05$ (colour-code on the right of each set of sagittal images), and overlaid on the population-based template. The schematic atlas drawings are obtained from [39]. Appendix 6-A presents the sagittal slices with anatomical labels. Abbreviations: Do: dorsal; Ve: ventral; Ro: rostral; Ca: caudal.

Next, hypothesis-driven tests comparing the different sub-phases of vocal learning indicated that when contrasting the sensory (20-30 dph) and the sensorimotor (40-65 dph) phase, several areas of the telencephalon, thalamic structures and the optical lobes display significant volume changes (Figure 6-8). The cluster in the telencephalon increases in volume towards the

sensorimotor phase and covers major parts of the striatum containing Area X, LMAN, and extends dorso-caudally and laterally towards areas in the nido- and mesopallium. Interestingly, the clusters covering the thalamus and the mesencephalon (optic lobes) and cerebellum appear to decrease in volume from the sensory to the sensorimotor phase. When comparing the sensorimotor (40-65 dph) and crystallisation phases (90-120 dph), again the thalamus (shrink) but also the lateral cerebellar nuclei (grow) and several clusters near the frontal parts of the telencephalon (i.e. apical and densocellular hyperpallium; shrink) including areas of the lateral, medial and caudal mesopallium (shrink) caudally demarcated by Field L could be observed. Furthermore, comparing the crystallisation phase (90-120 dph) to the last time point (200 dph) informs that still several frontal parts of the telencephalon decrease in volume over time. However, as opposed to the previous comparison, the clusters appear to be focussed in more ventral parts of the nido- and mesopallium lateral and frontal to the striatum extending to the ventral parts of the caudal mesopallium. Interestingly, LMAN is clearly excluded from this cluster. Furthermore, except for a cluster that covers the nidopallium and potentially includes the rostral portion of Field L2, no song control and/or auditory areas were found to display a change in relative volume, which clearly contrasts earlier comparisons. In addition, also more anatomically discrete clusters covering the posterior commissure, a ventro-rostral extension of the tOM and the TSM could be observed. All of which are characterised by a larger volume at 200 dph compared to 90 and 120 dph. Overall, the statistical maps of the male and female birds showed similar effects over time when comparing the subphases of vocal learning (Figure 6-8).

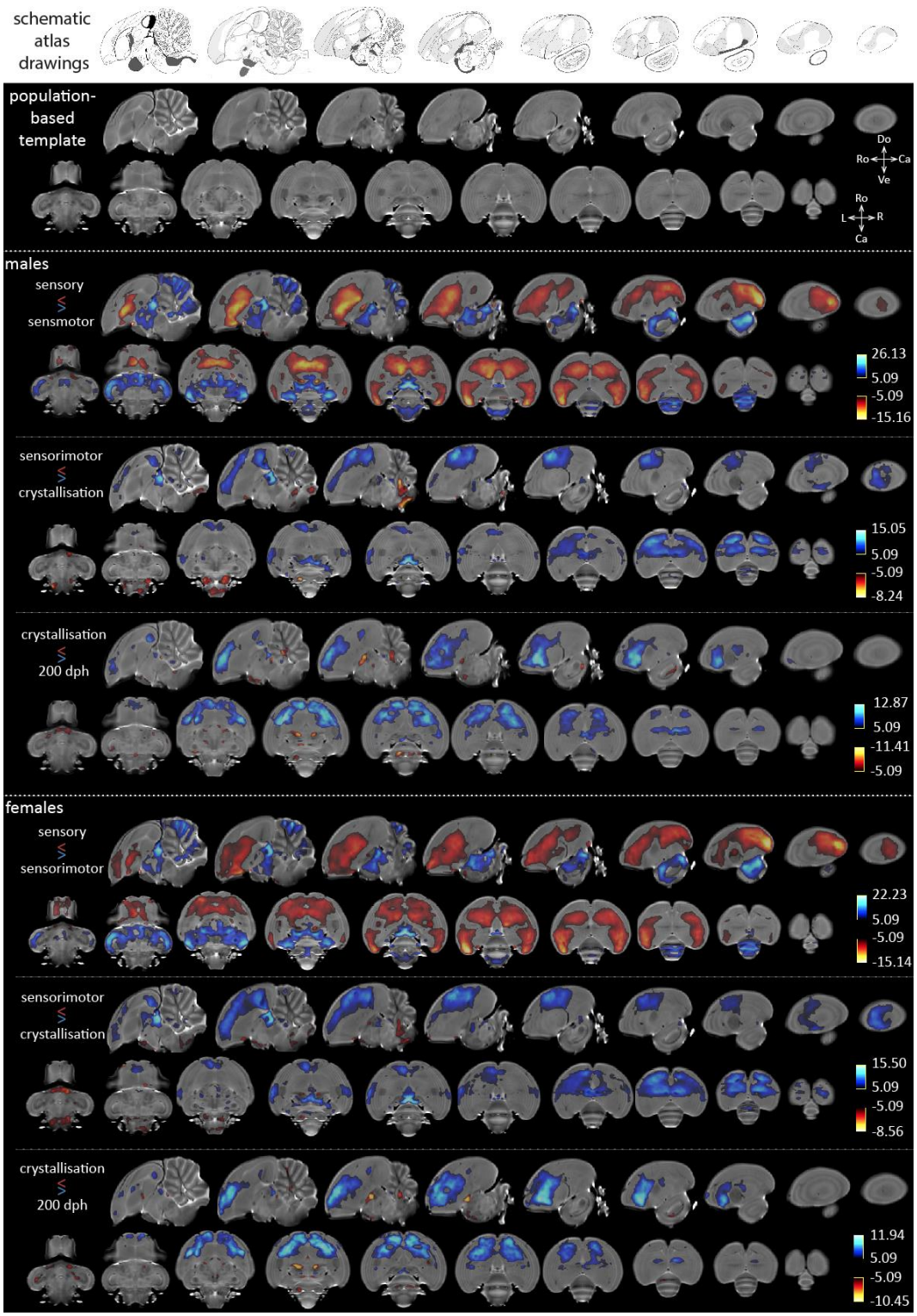

Figure 6-8: Statistical parametric maps highlighting relative volume changes between consecutive subphases of vocal learning in male and female zebra finches. The colours refer to voxels where modulated jacobian determinants are larger (blue: shrinkage from first to later phase) or smaller

(red; expansion from first to later phase) at the sensory phase compared to the sensorimotor phase, sensorimotor compared to the crystallisation phase, or around crystallisation compared to 200 dph. The sensory phase includes data obtained at 20-30 dph, the sensorimotor phase 40-65 dph, and the crystallisation phase 90-120 dph. The statistical maps are colour-coded according to the scale on the right (T-values; T=5.09 corresponds to $p_{FWE}<0.05$, no cluster extent threshold). The bottom row and Appendix 6-A present an anatomical overview of the slices underlying the statistical maps. The atlas drawings are obtained from [39]. Abbreviations: dph: days post hatching; Do: dorsal; Ve: ventral; Ro: rostral; Ca: caudal.

6.3.2.3 Diffusion properties of the maturing zebra finch brain

FA reflects maturation of fibre tracts and myelin-containing structures

Several brain areas displayed an interaction between age and sex over time, therefore, the main effects of age was explored in male and female birds separately. Figure 6-9 shows that most highly structured and/or myelin containing structures show significant changes in FA over time. In addition, several clusters identified by the (voxel-based) interaction were only found to be significantly changing over ontogeny in males (indicated by the white dotted boxes in Figure 6-9).

In general, FA values increase over ontogeny, except for structures such as HVC (Figure 6-18 in Appendix 6-C). The rate at which FA changes over time is strongly dependent on the brain region of interest. Many of the white matter structures highlighted by clusters in the main effect of time, are large tracts and/or lamina. Both carry diverse collections of axonal fibres connecting distinct brain areas. Due to the large anatomical heterogeneity, and the limited spatial resolution of the DTI scans (a combination which results in a low specificity), we did not convert this main effect into cluster-based ROIs for visualisation and further *post hoc* testing. Instead, to localise when in development most pronounced changes take place, we opted for hypothesis-driven comparison of consecutive sub-phases and time points. These tests inform that most striking differences occur when contrasting the sensory and sensorimotor phase. This relates especially to the tOM, both in male and female birds. When comparing 20 and 30 dph, the cluster displaying a significant difference in FA cover almost its entire path from the arcopallium passing the rostral border of the thalamus before traveling ventrally towards the diencephalon (where the FOV ends). Furthermore, parts of the LFS, the caudo-dorsal extension of the Area X surroundings, anterior commissure and a bilateral cluster medial to the entopallium at the level of the anterior and posterior commissure could be observed as well. Interestingly, in females (less in males) a small portion of Field L showed a change as well.

Comparing sensorimotor and crystallisation phase resulted in clusters coextensive with parts of the LaM, LFS, LFM and an area rostro-ventral to Field L.

In conclusion, most alterations in FA occur early, and it appears that first more caudally situated brain areas show alterations in FA, followed by more rostrally located areas in later stages.

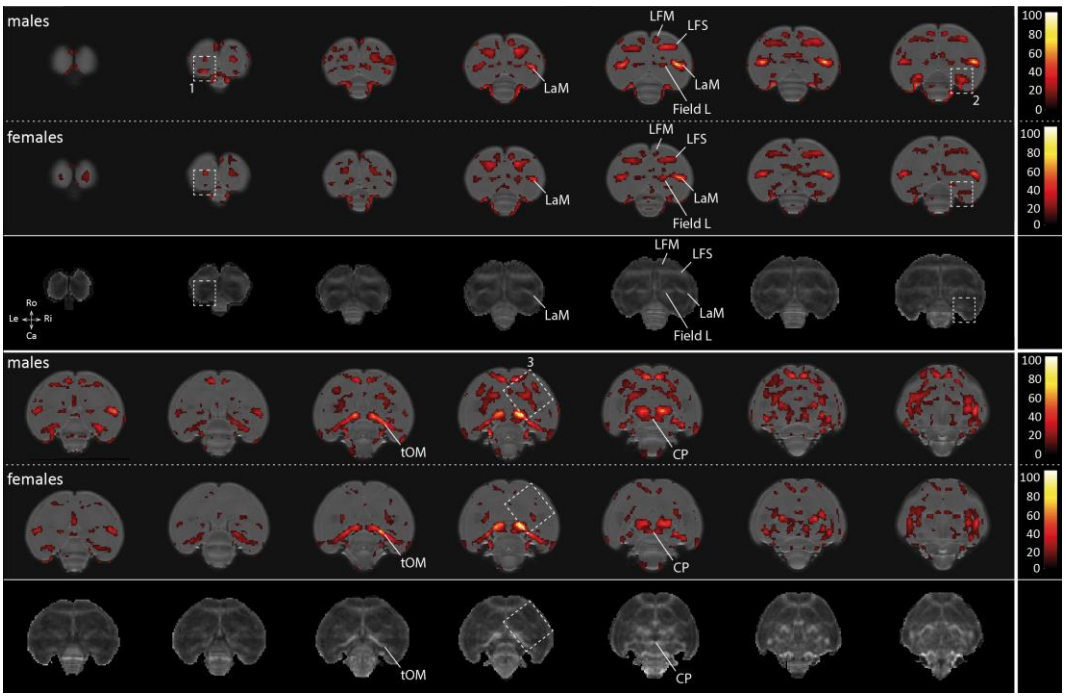

Figure 6-9: Statistical map illustrating the main effect of age of Fractional Anisotropy for male and female zebra finches. The results are displayed in accordance with $p_{FWE}<0.001$ $k_E \geq 5$ voxels, and overlaid the population-based template. The statistical maps are colour-coded according to the scales on the right. FA values range from 0 (black) to 1 (white). The areas demarcated by white-dotted lines refer to clusters identified in the interaction between age and sex as described in section 6.3.1.1. The third and sixth rows present an average FA map calculated from FA maps of male birds obtained at 200 dph and serves to identify the anatomical (mostly white matter) structures covered by a significant cluster. Abbreviations: LaM: mesopallial lamina; LFM: supreme frontal lamina; LFS: superior frontal lamina; tOM: occipitomesencephalic tract; CP: posterior commissure.

Changes in MD and the eigenvalues over time: MD points to two maturational waves covering major parts of the telencephalon

Mean diffusivity

Effects over time were assessed in males and females separately, however, overall, the spatial extents of the clusters appeared highly similar between both sexes. Both male and female birds show a major decrease in MD from 20 to 200 dph in the entire brain. The peak difference of the main effect of time is situated in the meso- and nidopallium rostral to Field L and caudal to

LMAN (indicated by the white crosshairs in Figure 6-10). When comparing MD between consecutive time points, it becomes clear that in addition to the first 'wave' of significant changes between 20 and 30 dph, a second drop in MD occurs between 40 and 65 dph, co-localised with the peak changes of the earlier cluster. In between the two 'waves' (30 vs 40 dph) or at later age comparisons (>65 dph), no clear clusters could be identified.

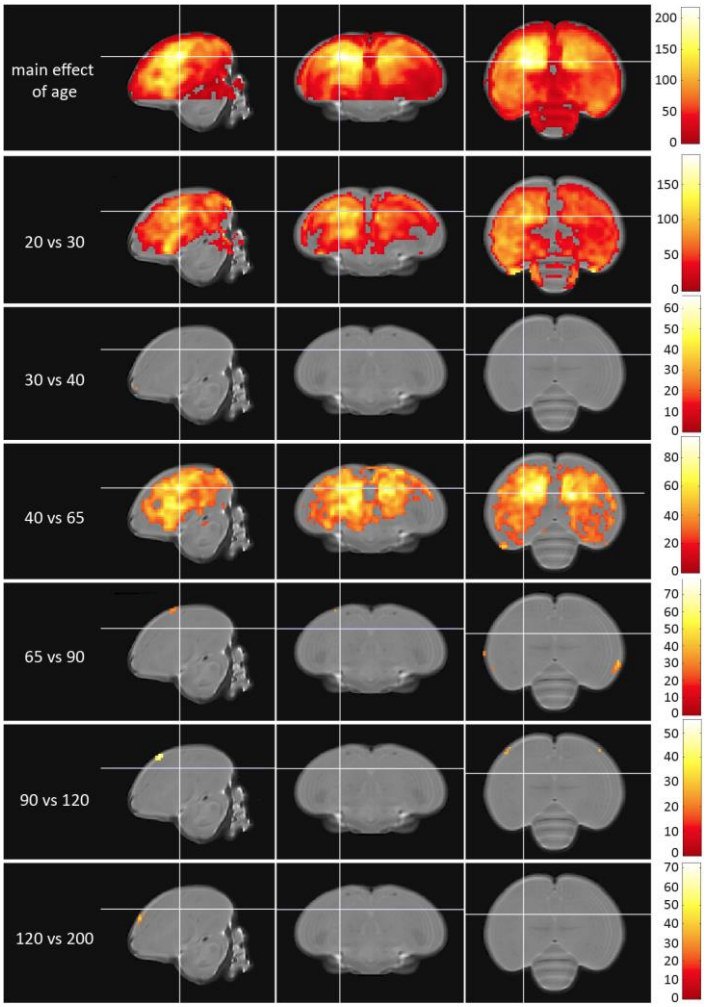

Figure 6-10: Two maturational waves coinciding with sensory and sensorimotor learning. The statistical parametric maps illustrate the main effect of time for MD for male zebra finches and post hoc F-tests comparing consecutive time points. The abrupt border of the cluster visible on the sagittal slices indicates the end of the FOV. The F-values are colour-coded according to the scale on the right. The results are displayed $p_{FWE}<0.05$ $k_E \geq 5$voxels and overlaid on the population-based template.

When testing for differences in MD between consecutive subphases of vocal learning ($p_{FWE}<0.001$; data not shown), a clearly distinct spatial profile of changes can be observed

between sensory-vs-sensorimotor phase and sensorimotor-vs-crystallisation phase. The first comparison shows brain-wide changes (FOV-wide), while the latter only appears to include more rostrally situated areas. Interestingly, the caudal border of the latter cluster is set at Field L, where it selectively excludes Field L, NCM and the caudal nidopallium immediately lateral to NCM. Furthermore, it omits lateral parts of the nidopallium, but incorporates the mesopallium, intermediate nidopallium and striatal areas. The spatial extent of the clusters is highly similar when testing in males and females suggesting that the differences in MD described here are likely reflecting general maturational processes rather than microstructural rearrangements specifically related to song learning. When comparing the crystallisation phase to datasets obtained at 200 dph, no bilateral clusters remain indicating that most changes in MD occur during the first 4 months of zebra finch *post* hatch life.

Eigenvalues

Similar to MD, the most extensive changes in λ_1, λ_2 and λ_3 occur when contrasting 20-30 and 40-65 dph (Figure 6-11), and no clear bilateral clusters can be observed when comparing 30 and 40 dph or later ages (>65 dph).

When comparing λ_1 and λ_2 at 20 and 30 dph in males at $p_{FWE}<0.001$ $k_E \geq 10$ voxels, then the cluster covers the entire brain (FOV), but excludes Field L, LMAN, the entopallium, tOM, arcopallium and many structures ventral to the thamalus. A similar trend is also observed in females (here also LMAN is excluded from the cluster, but Field L and the arcopallium are still partly included in the cluster, this however is highly dependent on the statistical threshold of visualisation of the SPMs). Most intense differences are situated in the meso- and nidopallium rostral to Field L and in the striatum. When comparing 40 to 65 dph, the cluster shifts rostrally focussing on the mesopallium and intermediate nidopallium. Also here, the spatial extent of the clusters is similar between male and female birds. No significant clusters were observed when opposing 65 to 90, 90 to 120 and 120 to 200 dph in both male and female birds.

Lastly, in contrast to λ_1 and λ_2, λ_3 clearly presents widespread differences when comparing 20 and 30 dph, both in male and female birds, including Field L and the arcopallium, but excluding the LFS (and lateral parts of the entopallium). Interestingly, between 40 and 65 dph, the cluster is focussed on the striatum and adjacent nidopallium, caudolateral to Area X and LMAN. Furthermore, bilateral clusters covering the LaM (departing from HVC), part of the LFS, caudal telencephalon close by HVC and RA are present as well. Remarkably, this spatial pattern is not

clearly visible in females (however, the apparent 'difference' does not reach satisfactory statistical power to be detected when testing for an interaction between age and sex).

To summarise, λ_1 and λ_2 follow a similar profile over time compared to MD, indicating that the effects in MD over time are mainly reflecting changes in λ_1-λ_2 and to a lesser extent in λ_3.

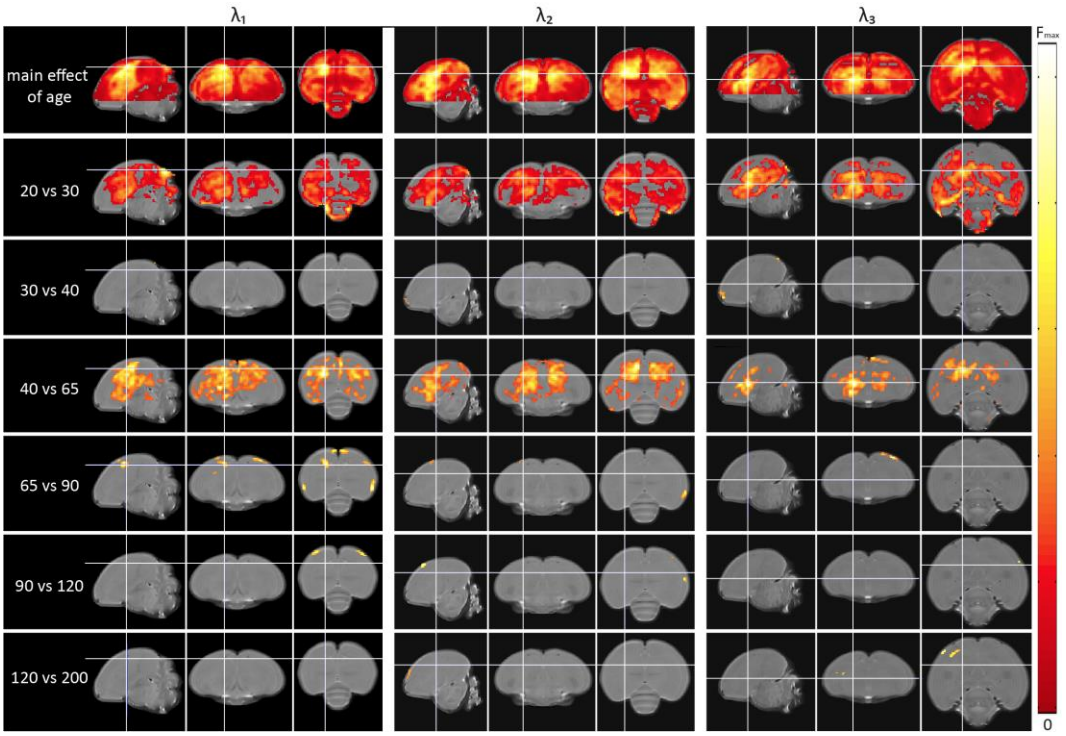

Figure 6-11: Main effect of age and comparisons of consecutive time points of the eigenvalues. The crosshairs converge in the peak voxel of the main effect of age, the spatial location of the crosshairs remains identical for the following comparisons. The SPMs of λ_1 and λ_2 appear similar, with the most significant main effect of age located in the meso- and nidopallium rostral to Field L. The area displaying the largest changes in λ_3 is situated near the striatum and nidopallium. The data are displayed $p_{FWE}<0.05$ $k_E \geq 5$ voxels, overlaid on the population-based template, and F-values are colour coded according to the scale on the right.

6.3.3 Quantification of song refinement from advanced plastic to fully mature song

To quantitatively evaluate the progression of sensorimotor learning and song refinement in male birds, we analysed the first 20 songs sung in the morning after 'lights on' in SAP [34]. First, the basic acoustical properties of the syllables were extracted to explore whether the spectral and temporal structure of individual syllables evolve from (advanced) plastic to fully mature, stereotyped song, and to probe when and to what extent the variability (standard deviation) of these features minimizes towards crystallisation. Next, several robust measures extracted from the song motifs were explored that inform how accurate the bird is able to produce an acoustic

copy of the tutor song (% similarity, accuracy and % sequential), how the syllable sequence stabilises towards song crystallisation (sequence stereotypy) and how song tempo or song 'density' maximise when juvenile birds achieve higher vocal (motor) proficiency. The latter measures are considered to be readouts for distinct aspects of vocal performance and were used to search for correlations with the structural properties of the zebra finch brain. These analyses could help understand if the neural substrate in control of song of birds that sing e.g. a better copy of the tutor song, would also display different macro- or micro-architectural tissue properties compared to less well performing birds.

6.3.3.1 Assessment of the acoustical properties of individual syllables

Because of technical issues with the song recording devices, we were not able to quantify the syllable features of one of the male zebra finches. This left us with respectively 16 and 15 adult male birds for motif and syllable feature tests. All voxel-wise correlation analyses were performed with 15 or 14 male zebra finches for respectively DBM and DTI analyses.

Inter-syllable intervals become shorter and Wiener entropy decreases

A significant main effect of age could be observed for the inter-syllable interval duration (p<0.0001 $F_{(3,38.2)}$=13.8789), but not for syllable duration (p=0.5534 $F_{(3,37.7)}$=0.7078). *Post hoc* tests inform that the inter-syllable intervals decrease most significantly form 65 and 90 to 200 dph. More specifically, the inter-syllable intervals gradually decrease from 65 to 120 dph and decline sharply between 120 and 200 dph, suggesting that song tempo increases from 65 to 200 dph (Figure 6-12-A-B). Furthermore, a significant main effect of age was detected for syllable Wiener entropy (p=0.0032 $F_{(3,37.8)}$=5.4803). Syllable Wiener entropy gradually becomes more negative (Figure 6-12-C), suggesting that syllables gain in tonal and harmonic structure (lower acoustic noisiness [41]) from the mid-sensorimotor phase to 200 dph. None of the pitch-related measures, or frequency and amplitude modulation display a significant main effect of age (syllable pitch: p=0.8897 $F_{(3,37.7)}$=0.2088; syllable mean frequency: p=0.1289 $F_{(3,38.6)}$=2.0078; syllable peak frequency: p=0.0649 $F_{(3,38.6)}$=2.6144; syllable goodness of pitch: p=0.2211 $F_{(3,38.1)}$=1.5348; syllable FM: p=0.3279 $F_{(3,37.4)}$=1.1867; syllable AM: p=0.5470 $F_{(3,37.4)}$=0.7189).

The acoustic variability of individual syllables decreases towards 200 dph

Next, the variability of the acoustic properties of different syllables was assessed. To this end, a mixed model was performed on the standard deviation of the different syllable feature scores. A main effect of age was observed for the standard deviation of syllable and inter-syllable

interval duration (respectively p=0.0064 $F_{(3,34.3)}$=4.8560 and p<0.0001 $F_{(3,25.4)}$= 20.8043), syllable mean and peak frequency (respectively p=0.0132 $F_{(3,37.5)}$=4.0891 and p=0.0280 $F_{(3,38.1)}$=3.3787), and syllable entropy (p=0.0021 $F_{(3,36.9)}$=5.9192). In all cases, the standard deviation decreased over time, indicating that the acoustic properties of the syllable features are sung less variable (more stereotyped) from the sensorimotor to the crystallisation phase. Interestingly, the standard deviation of the inter-syllable interval duration remains relatively constant between 65 and 90 dph. From 90 dph onwards, it decreases towards 200 dph. The standard deviation of the syllable duration, on the other hand, appears to decrease between 65-90 dph (relatively large inter-subject variation), after which it gradually declines towards 200 dph. The standard deviation of mean and peak frequency experiences a gradual reduction over time (65 vs 200 dph). The standard deviation of syllable entropy decreases significantly between 65 or 90 and 200 dph. The standard deviation of the other syllable features did not change significantly from 65 to 200 dph (syllable pitch: p=0.5824 $F_{(3,41.4)}$=0.6583; syllable goodness of pitch: p=0.0621 $F_{(3,33.1)}$=2.6910; syllable FM: p=0.0700 $F_{(3,33.2)}$=2.5803; syllable AM: p=0.0982 $F_{(3,41.5)}$=2.2367).

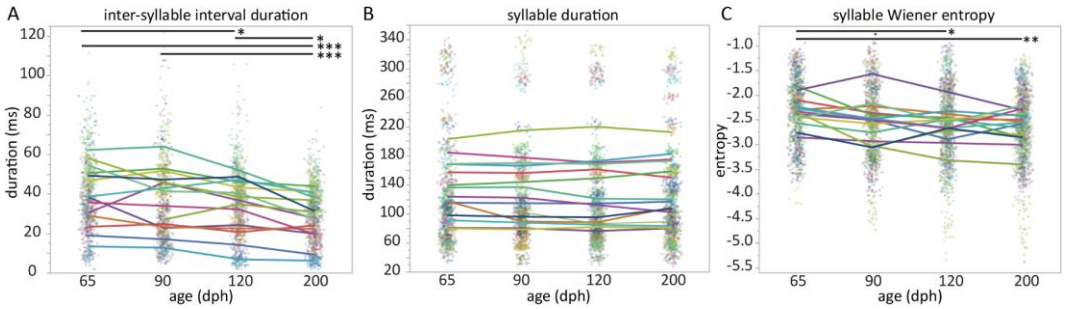

Figure 6-12: Syllable and inter-syllable interval duration and syllable entropy in function of time. The dots refer to individual raw syllable feature scores (A-C: 20 datapoints/bird/syllable/time point) or the standard deviation of the syllable feature scores (D-H: 1 datapoint/bird/syllable/timepoint). The lines connect the average performance of a particular bird between different time points. The asterisks indicate the results of Tukey's HSD post hoc tests: *: 0.05>p>0.01; **: 0.01>p>0.001; ***: 0.001>p. Wiener entropy does not have a unit. Abbreviations: dph: days post hatching.

6.3.3.2 Motif features as a proxy for song performance

Even though the inter-syllable interval duration decreases significantly over time while the syllable duration remains unchanged, motif length remains stable throughout the study (main effect of age: p=0.4681 $F_{(3,38.2)}$=0.8639). In contrast, song density –the relative duration (%) of syllables within an entire song motif– increases significantly over time (main effect of age: p=0.0011 $F_{(3,38.1)}$= 6.5560). Figure 6-13-C illustrates that song density increases sharply only after the crystallisation phase (song density at 200 dph differs significantly from all previous

time points). Furthermore, song sequence linearity and sequence stereotypy increased towards 200 dph (main effects of age, respectively, p=0.0034 $F_{(3,38.4)}$=5.3970; p=0.0052 $F_{(3,38.4)}$=4.7904, Figure 6-13-B; *post hoc* Tukey HSD: sequence linearity: 65-200 **; 90-200: *), indicating that syllable order became less variable towards the end of the study.

Song similarity to tutor song measures increased between 65 and 200 dph. More specifically, a main effect of age was detected for % similarity (p=0.0251 $F_{(3,37.0)}$=3.4890), accuracy (p=0.0061 $F_{(3,37.2)}$=4.8329) and % sequential (p=0.0389 $F_{(3,36.8)}$=3.0887). All three measures increased gradually displaying a significant difference when contrasting 65 and 200 dph (% similarity *; accuracy: **; % sequential: *). Song similarity provides an estimate of how much 'sound' of the tutor song can be found in the tutee song, while accuracy reflects the fine-grained similarity (acoustic similarity of small song intervals) and, % sequential is a measure of how well the order of the best matching section in the tutee song match the order in the tutor song (default settings use asymmetric comparisons [34]).

Lastly, we explored whether song performance would be affected by the tutoring bird, by testing for a main effect of tutor. Interestingly, % similarity (p=0.0159 $F_{(7,6.1)}$=6.7597) and song density (p=0.0153 $F_{(7,7.2)}$=5.8891), but not sequence stereotypy (p=0.1389 $F_{(7,7.3)}$=2.3350) appear to differ depending on the tutor. This is visualised in Figure 6-13, where each colour refers to a different tutor. For example, birds raised by the blue- and purple-coded tutors display a higher similarity to tutor song compared to the other birds. When assessing the similarity scores at 200 dph, no differences in the number of syllables for birds having a 'high' (>75%) or 'low' (<75%) similarity score could be observed (respectively on average 4.33 or 4.43 syllables per song motif; Appendix 6-E). This suggests that the number of syllables in the song did not affect song similarity scoring.

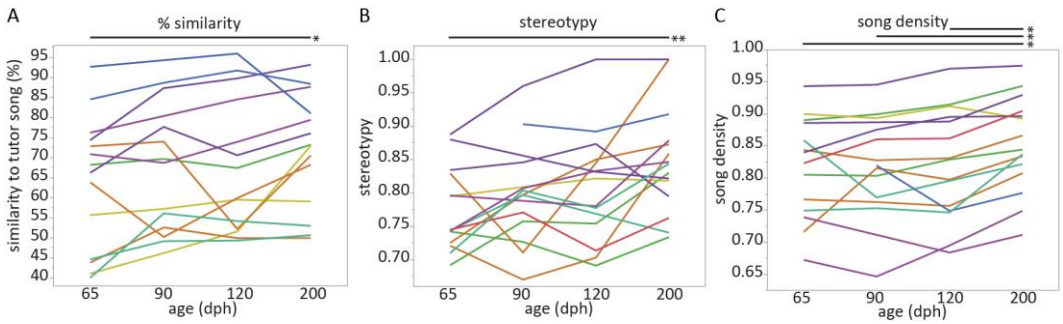

Figure 6-13: Song similarity, sequence stereotypy and density in function of age. Each line represents data obtained from an individual bird. The colour of the lines refers to a particular tutor. Panel A, B and C present the average % song similarity, stereotypy and song density for individual

juveniles over the different time points. The asterisks encode the results of the post hoc tests (Tukey HSD) assessing when in time differences occur, according to: *: 0.05>p>0.01; ** 0.01>p>0.001; ***: 0.001>p. Abbreviations: dph: days post hatching.

6.3.4 Brain-behaviour relationships: tracing the structural signature of vocal proficiency

Ample evidence describes relationships between skill proficiency and the structural properties of the brain [22]. Since birds seem to improve their vocal performance even beyond the crystallisation phase, we investigated the existence of similar relationships by executing a voxel-wise multiple regression for each smoothed DTI parameter or log-transformed modulated jacobian determinant maps and song density, song sequence stereotypy, accuracy or % similarity. No suprathreshold voxels (p_{FWE}<0.05 k_E≥5voxels) could be observed between any combination of smoothed MRI parameters and song density, accuracy or song sequence stereotypy. In contrast, % similarity correlated with the brain architecture at several locations.

6.3.4.1 Brain-wide voxel-wise multiple regression

A significant positive correlation was identified between FA and % similarity in a portion of the fronto-arcopallial tract (tFA; cluster: p_{FWE}=0.002 k_E=13 voxels; peak: p_{FWE}<0.001 T=6.81; Figure 6-14-A), a midsagittal region at the level of the mesopallium rostro-ventral to the anterior commissure and caudal to the TSM; dorsal to Area X (Figure 6-14-B), and in left NCM (rostral NCM; cluster: p_{FWE}=0.001 k_E=5 voxels; peak: p_{FWE}=0.019 T=5.69; Figure 6-14-C). Interestingly, when inspecting the statistical maps with an exploratory threshold ($p_{uncorrected}$<0.001 k_E≥40voxels), clusters could be observed at the right tFA (cluster: p_{FWE}=0.034; peak: p_{FWE}=0.001 T=6.42) and the right NCM (cluster: p_{FWE}=0.024 peak: p_{FWE}=0.032 T=5.55). Furthermore, at the exploratory threshold, the previously detected midsagittal cluster extends ventrally and follows (but does not overlap with) the TSM (sub-peak next to the TSM in the left hemisphere: p_{FWE}=0.159 T=5.08). Based on this spatial pattern and in accordance with the Karten-Mitra zebra finch brain atlas [39], we identify this area as the ventral pallidum (VP). The cluster covering the left NCM extends rostro-laterally towards the caudal mesopallium (sub-peak: p_{FWE}=0.194 T=5.01). When exploring the SPMs of the eigenvalues at an exploratory threshold, λ_3 shows a negative correlation with % similarity in left NCM and the left tFA. This suggests that mainly λ_3 (and not λ_1 or λ_2) is driving the correlation observed between FA and % similarity. Furthermore, a negative correlation was observed between the local volume and song similarity in (part of) the VP and, towards the midline, nucleus basalis of Meynert (cluster: p_{FWE}<0.001 k_E=2022

voxels; peak: p_{FWE}<0.001 T=8.06; Figure 6-15-A). In addition, another bilateral cluster displaying a negative correlation between local volume and % similarity was observed in the caudal mesopallium rostral to Field L, at the level of the CMM, possibly including the avalanche nucleus (Av), and CLM (left: cluster: p_{FWE}<0.001 k_E=1701 voxels; peak: p_{FWE}=0.001 T=7.10; right: cluster: p_{FWE}<0.001 k_E=3465 voxels; peak: p_{FWE}<0.001 T=7.42; Figure 6-15-B). Next, the clusters were converted to ROIs (at $p_{uncorrected}$<0.001 k_E≥40 voxels) and the average FA values or (log-transformed) modulated modulated jacobian determinants were extracted.

6.3.4.2 Region- and age-specific within- and between-subject correlations

The voxel-wise multiple regression function of SPM does not take subject-identity into account. To explore whether the voxel-wise correlations are mainly caused by within- or between-subject associations between the structural properties of the brain and song similarity, we performed a repeated-measures correlation analysis [38] on the cluster-based ROI data. Significant within-subject associations between the log-transformed jacobian determinants and song similarity were found in the CLM ('r' is the repeated-measures correlation coefficient; left: r=-0.391 p=0.0126 ; right: r=-0.416 p=0.0075) and the VP (VP: r=-0.429 p=0.0057), and between FA and song similarity in the VP (r=0.496 p=0.0010), right NCM (right: r=0.388 p=0.0121), the CM (left: r=0.348 p=0.0260; right: r=0.472 p=0.0019), but not in the tFA (left: r=0.129 p=0.4200; right: r=0.0215 p=0.8940) and left NCM (left: r=0.256 p=0.1060). These findings suggest that mainly between-subject variation rather than within-bird improvements in song performance drive the voxel-wise correlation observed in the tFA and left NCM, while 'personal' progression in producing a more accurate acoustic copy of the tutor song correlates with local tissue structure in the VP, caudal meso- and right nidopallium.

Next, we explored to what extent the cluster-based ROIs exhibit between-subject correlations by calculating Spearmans' ρ for individual time points in JMP. The results of the statistical tests are summarised in Table 6-3. No significant correlation can be found between relative volume and % similarity in the CM, both at 65 and 200 dph. In contrast, the tFA, NCM and VP display a significant between-subject correlation between % similarity and FA at 65 and 200 dph. Interestingly, the VP displays a significant correlation between % similarity and relative volume at 65 dph, but not at 200 dph. Lastly, the left, but not right CMM display a significant correlation between % similarity and FA at both ages, while FA of the right CMM is not correlated to % similarity at 65 dph.

Table 6-3: Summary time-point specific between-subject correlations of the cluster-based ROIs.

% similarity and …	Cluster-based ROI	Hemisphere	65 dph		200 dph	
			Spearmans' ρ	*p*	Spearmans' ρ	*p*
FA	tFA	Left	0.7846	0.0009	0.7714	0.0012
		Right	0.7099	0.0045	0.7143	0.0041
	NCM	Left	0.6747	0.0081	0.6835	0.0070
		Right	0.6396	0.0138	0.5692	0.0336
	CMM	Left	0.5648	0.0353	0.6176	0.0186
		Right	0.3978	0.1590	0.6571	0.0107
	VP		0.8154	0.0004	0.7890	0.0008
log mwj	VP		-0.7978	0.0006	-0.4418	0.1138
	CM	Left	-0.5297	0.0514	-0.3055	0.2882
		Right	-0.4769	0.0846	-0.1912	0.5126

'log mwj' refers to the log-transformed, modulated and warped jacobian determinants.
Abbreviations: dph: days post hatching.

6.3.4.3 No sex differences in brain architecture of areas that correlate with song performance

Only male zebra finches sing, consequently, no correlation analyses could be conducted in female birds. Despite this remarkable behavioural dimorphism, female zebra finches show preference for tutor-like song, indicating that females do memorise the tutor song to some extent [42]. To assess whether the brain regions identified by the voxel-wise multiple regression exhibit different structural properties in male and female zebra finches, we performed a linear mixed model analysis containing data obtained at 65, 90, 120 and 200 dph (bird-identity as random effect, age and sex as fixed effect). No significant interactions between age and sex or no significant main effect of sex was found for the modulated jacobian determinant in any of the ROIs (CM: left: interaction age*sex: p=0.1446 ($F_{(3,93.0)}$=1.8439), main effect of sex: p=0.9688 ($F_{(1,31.0)}$=0.0016); right: p=0.5797 ($F_{(3,93.0)}$=0.6583), main effect of sex: p=0.8547 ($F_{(1,31.0)}$=0.0341); VP: interaction age*sex: p=0.0734 ($F_{(3,93.0)}$=2.3938686); main effect of sex: p=0.2456 ($F_{(1,31.0)}$=1.4006)). Similarly, FA in the tFA or the VP did not show any difference between male and female birds (tFA: left: interaction age*sex: p=0.3418 ($F_{(3,93.0)}$=1.1282), main effect sex: p=0.4501 ($F_{(1,31.0)}$=0.5852); right: interaction age*sex: p=0.3861 ($F_{(3,93.0)}$=1.0233), main effect sex: p=0.2742 ($F_{(1,31.0)}$=1.2390); VP: interaction age*sex: p=0.2913 ($F_{(3,93.0)}$=1.2641); main effect of sex: p=0.2456 ($F_{(1,31.0)}$=1.4006)).The small cluster in the CM that shows a correlation between % similarity and FA in males, displayed a trend towards a significant interaction between age and sex in the left, but not the right hemisphere (CM: left: interaction age*sex: p=0.0432

($F_{(3,93.0)}$=2.8194); right: interaction age*sex: p=0.0731 ($F_{(3,93.0)}$=2.3962), main effect of sex: p=0.5994 ($F_{(1,31.0)}$=0.2817)). Lastly, NCM displayed a significant interaction between age and sex in the left, but not the right hemisphere (left: interaction age*sex: p=0.0165 ($F_{(3,93.0)}$=3.5935); right: interaction age*sex: p=0.6697 ($F_{(3,93.0)}$=0.5198), main effect sex: p=0.4446 ($F_{(1,31.0)}$=0.5995)). Important to note however, is that the correlation between FA and song similarity in NCM detected by the voxel-wise multiple regression appeared highly asymmetric: the cluster observed in the left hemisphere is much larger and spans more laterally compared its contralateral counterpart. This spatial asymmetry is likely to affect the sex difference in FA in NCM.

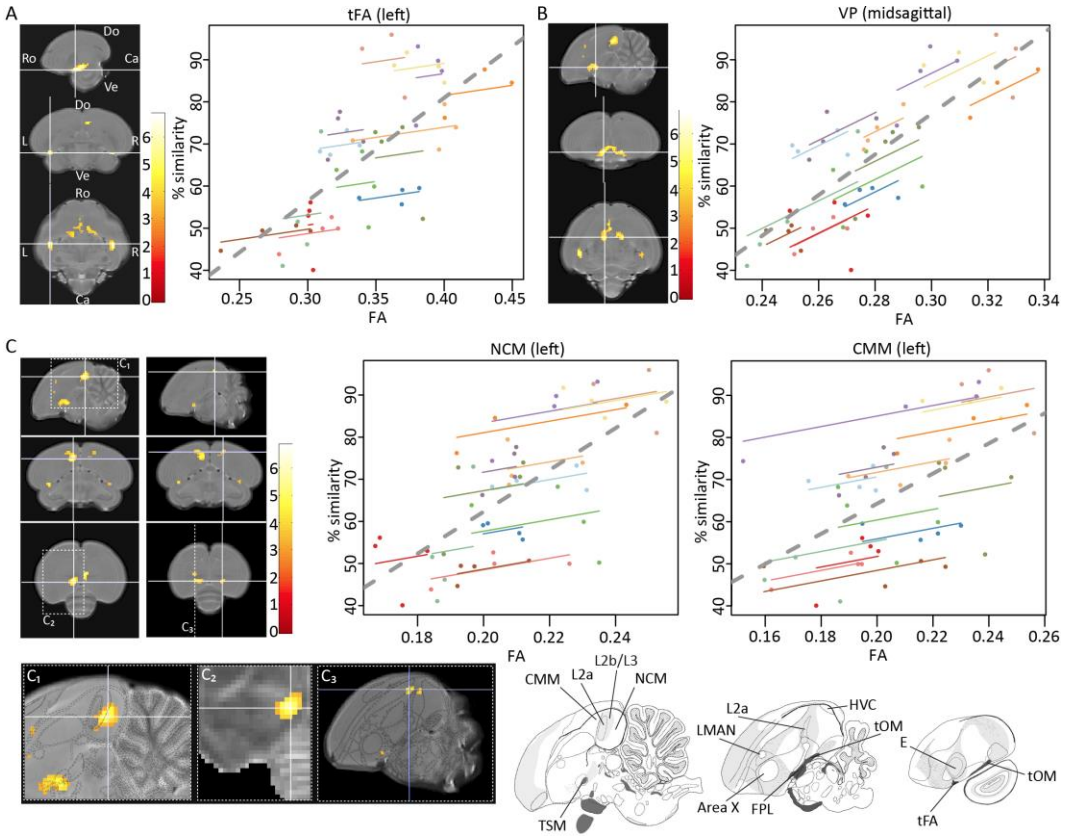

Figure 6-14: Song similarity correlates positively with FA in the tFA (A), VP (B), the NCM (C-C_{1-2}) and the CMM (C-C_3). All SPMs are displayed according to $p_{uncorrected}<0.001$; $k_E \geq 40$ voxels, colour-coded according to the scales on the right of the SPMs and all SPMs (except C_2) are overlaid onto the population-based template. The graphs visualise the nature of the correlation between song similarity (%) and FA where individual datapoints are colour-coded according to bird-identity (i.e. one colour = one bird). The average within-bird correlation is presented by the coloured lines, while the bold grey dotted line indicates the overall association between song similarity and FA, disregarding bird-identity or age. Even though most clusters were found bilateral, the graphs only present data obtained from the left hemisphere. The schematic atlas drawings approximate the anatomical level of the sagittal slices presented in A-C and are obtained from [39]. Panel B informs on the spatial extent of the cluster found midsagittal and extending (bi-)lateral in parts of the VP adjacent to the TSM. Panel C informs on the spatial extent of the clusters found in the NCM and CMM. NCM of the left (left panel) and right (right panel) hemisphere. Inset C_1 visualises the spatial extent of the cluster in left NCM with reference to Field L (L2a is visible on the T_2-weighted 3D RARE by a hypointense line-shaped area (indicated by white arrow). Based on the overlay of the schematic atlas drawings, the peak (indicated by crosshairs) is situated in (rostral) NCM, but potentially extends into caudal part of Field L2b or L3. The other cluster in the same inset (more ventrally situated), is localised near the TSM (presented in detail in panel B). Inset C_2 presents the NCM-cluster overlaid on an average FA map of male birds at 200 dph, and further corroborates that the NCM-cluster does not overlap with the highly myelinated, fiber-rich (hyperintense on FA) structure that can be identified as Field L(2a). Inset C_3 illustrates that a sub-peak of the NCM cluster extends to CMM, rostral to Field L. Abbreviations: TSM: septo-mesencephalic tract; tOM: occipitomesencephalic tract; L2a, L2b, L3: distinct parts of Field L; LMAN: lateral magnocellular nucleus of the anterior nidopallium; CMM: caudomedial mesopallium; NCM: caudomedial nidopallium; FPL: lateral prosencephalic fascicle; E: entopallium; tFA; fronto-arcopallial tract; HVC: high vocal centre (former abbreviation that is now used as a proper name).

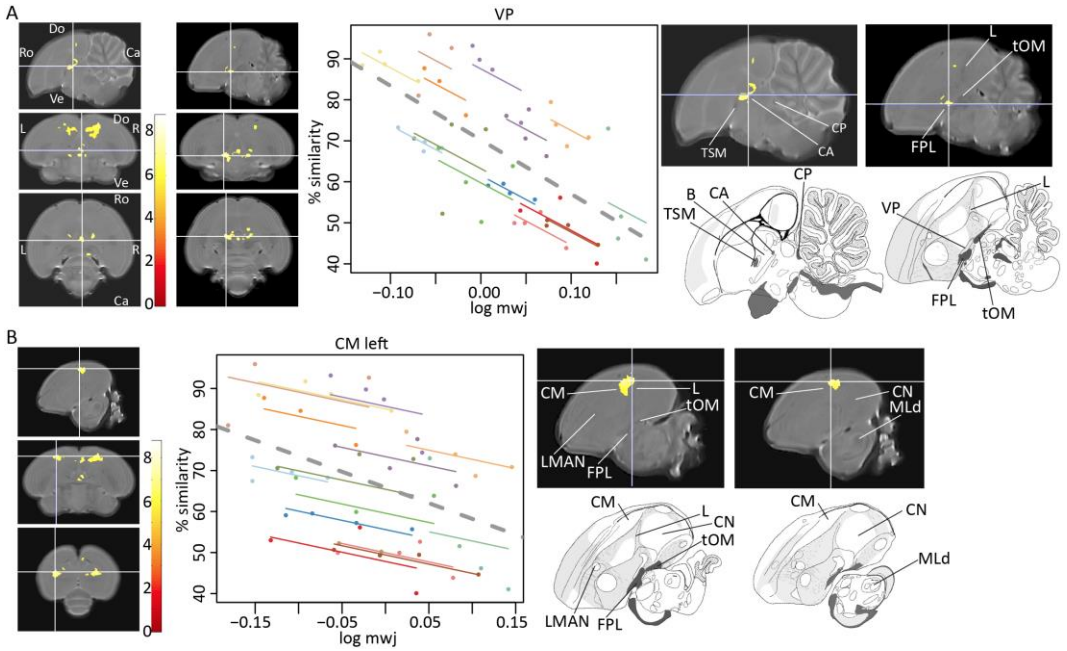

Figure 6-15: Song similarity correlates negatively with local relative volume in the VP (A) and the CM (B). Each panel presents the statistical maps visualised at $p_{FWE}<0.05$ and $k_E \geq 80$ voxels (T-values are colour-coded according to the scale immediately next to the SPMs) and overlaid to the population-based template, and graphs that inform on the nature of the association between song similarity (%) and log-transformed modulated jacobian determinant. The individual datapoints of the graphs are colour-coded according to bird-identity (i.e. one colour = one bird). The average within-bird correlation is presented by the coloured lines, while the bold grey dotted line indicates the overall association between song similarity and log mwj, disregarding bird-identity or age. The schematic atlas drawings approximate the anatomical level of the sagittal slices presented in A and B and are obtained from [39]. Abbreviations: TSM: septo-mesencephalic tract; B: nucleus basalis of Meynert; CA: anterior commissure; CP: posterior commissure; VP: ventral pallidum; FPL: lateral prosencephalic fascicle; tOM: occipitomesencephalic tract; L: Field L; LMAN: lateral magnocellular nucleus of the anterior nidopallium; CN: caudal mesopallium; CM: caudal mesopallium.

6.4 DISCUSSION

The first months of life are characterised by extensive neuroplastic adaptations to brain structure and function that parallel the acquisition of skills and abilities necessary for proper functioning in later life. A remarkable model in the study of developmental neuroplasticity related to learning a complex skill can be found in songbirds as convincing parallels have been described between human speech and zebra finch song learning [4]. As a result, most assessments of developmental neuroplasticity in zebra finches are almost exclusively focussed on areas implicated in vocal behaviour, i.e. brain regions linked to song control and audition, and relatively little is known about the structural development of other areas.

The present study aimed at composing a brain-wide comprehensive overview of the timing and spatial extent of alterations in tissue volume (3D anatomical scans) and micro-architecture (DTI) along the first 200 days of post-hatch life in male and female zebra finches. Complementary to the data presented in Chapter 5, we now determine when in ontogeny sex differences in microstructure become detectable and explore how the local volume of tissues differs between males and females. Furthermore, by measuring song similarity as a proxy for vocal proficiency, we found correlations between improvements in vocal performance and the architectural properties of the male zebra finch brain in the ventral pallidum, including nucleus basalis of Meynert, and several areas pertaining to the auditory system or related to motor aspects of song control.

6.4.1 Structural development of the zebra finch brain from 20 to 200 dph

6.4.1.1 Brain volume resembles an inverted U-shape

Both in males and females, whole brain volume increases between 20 and 30 dph, remained constant between 30 and 40 dph and progressively decreased from 40 dph towards the end of the study. This finding corroborates with and extends previous estimations of increasing telencephalon size between 12 and 53 dph in male and female zebra finches [43]. The temporal pattern, i.e. initial increase and later decrease, greatly resembles the curvilinear inverted U-shaped trajectory described in humans, e.g. [18, 19, 44, 45], for review [46-48], where the total brain volume initially increases, peaks somewhere in adolescence and gradually declines towards adulthood. In contrast, other small animal species displayed distinctly shaped brain volume trajectories e.g. mice [49-51], rats [52-54], ferrets [55] (used brain weight as metric), and cats [56]. Important to note is the age-range included in the study, as a potential volume decline might only affect older ages.

The inverted U-shaped temporal pattern was copied by the c_1 component, representing mainly grey matter structures. A study by Hammelrath et al (2016) in mice observed a continuing flattening of the cortex over time which occurred in a rostral-to-caudal direction, making that cortex volume gradually decreased relative to total brain volume [50]. In contrast, Zhang et al. (2016) did not observe any volume decline when assessing the normalised volume of the neocortex over time, in the same species [51]. Similar age-dependent increases in (absolute) cortical volume were obtained in rats [52, 53].

The white matter segment, i.e. c_2, first decreased in volume until 40 dph after which its volume consistently increased towards 200 dph. In most mammalian species, white matter volume appears to increase over time at a regionally-specific rate. Consequently, the initial dip in relative white matter volume observed in this study does not fully align with these descriptions. A potential reason for this early volume decline might be attributed to using relative instead of absolute volumes, i.e. expressing white matter volume proportional to total brain volume. For example, if the total brain volume increases at a faster pace than the white matter compartment, the latter might appear to decrease in volume. An alternative explanation for this effect might be found in the drastic changes in intrinsic tissue properties that occur in early postnatal life (developmental specificities of T1-and T2-weighted contrasts are demonstrated by [57] and reviewed by [58, 59]). Such changes in T1- and T2-relaxation times can significantly alter the MR image contrast and make that in early ages myelinated tissues appear less hypo-intense on T2-weighted images compared to later ages. These changes in image contrast might affect the accuracy of the spatial transformation and, since tissue segment volumes are in part based on the latter, might affect the volume determination.

6.4.1.2 DBM informs on regionally-specific developmental trajectories

Hypothesis-driven comparisons of the consecutive sub-phases of vocal learning uncovered clear regional differences in the timing of structural developmental plasticity. Effects of time were assessed in male and female finches separately, but resulted in highly similar overall maturational patterns. Males and females display early widespread changes covering the entire telencephalon and later neuroplastic alterations mainly affecting more rostral parts of the nido- and mesopallium. Similar regionally-specific developmental trajectories have been described in other species, for example in humans [18, 19, 21, 44, 60-62], Wistar rats [52, 53, 63], C57Bl/6J mice [50], and marmosets [64]. Based on a comprehensive overview of MR-based developmental studies in humans, brain maturation appears to evolve (1) from proximal to distal, (2) in sensory before motor pathways, (3) first in projection then in association pathways, (4) in central before polar cortices, (5) first in the occipital and then in the posterior parietal white matter and in temporal and frontal poles, and (6) phylogenetically older brain areas prior to 'younger' ones [18, 59]. These stereotyped patterns of brain maturation yield important functional implications reminiscent of critical and sensitive periods as cognitive milestones are reached in parallel with structural neuroplastic events [65].

A similar analytical approach can be applied to the current study. When contrasting the sensory and sensorimotor sub-phases, we observe a volume increase in parts of the striatum, meso- and nidopallium, and a volume decrease in the optic lobes, parts of the cerebellum and thalamic zone (Figure 6-8). More specifically, the optic tectum and the MLd located in the optic lobes decrease in volume between 20 and 30 dph (Appendix 6-D). The TeO receives direct input from both eyes, connects to various sensory and sensorimotor areas throughout the bird brain, and appears therefore most closely linked to the processing of visual information [66]. MLd is the songbird analogue of the mammalian inferior colliculus and the amphibian torus semicircularis, is an important 'early' auditory relay centre as several parallel auditory brainstem pathways converge in this nucleus [67], and it receives descending input from the HVC_{shelf} and RA_{cup} regions [68]. The latter pathway might serve to convey song-related feedback to the MLd. MLd is tonopically organised, displays selectivity for particular spectro-temporal features [69], with great sensitivity to temporal patterns characteristic to bird songs [70] and expresses the IEG 'zenk' following passive song playback [71]. The relative volume change in MLd occurs at the earliest stages of vocal learning when juvenile birds memorise the tutor song. Furthermore, the HVC-RA connection exhibits marked changes in both sexes taking place between 20 and 30 dph [72, 73], which potentially –via shelf and cup pathways– may affect the structure of MLd.

The volume increase that includes the striatum and the medial meso-and lateral nidopallium envelops Area X and LMAN (less so in female birds), two important components of the song control system. Despite the clear sex difference in volume of Area X [74], both males and females present a volume increase in the striatum from sensory to sensorimotor phase, suggesting that the observed volume increase might not relate to vocal-motor plasticity. The large subdivisions of the zebra finch brain likely contain distinct functional domains that present no clearly defined cytoarchitectonic borders and can only be properly identified based on tract tracing studies or, upon stimulation, by *in vivo* functional imaging. For example, specific parts of the dorsal NCL connect in a topographical manner to the dorsal intermediate arcopallium, as well as to the $LMAN_{shell}$ [75], and may serve in active song evaluation during vocal learning [76]. Further, Wild and Farabaugh showed structural connectivity between the specific parts of the NCL and the basorostral nucleus [77]. Important to note is that some of these topographical areas are too small to be accurately captured by *in vivo* MRI.

After the sensorimotor phase, only more rostrally situated brain structures appeared to change in volume. These include the caudal mesopallium (CM) and hyperpallium. Interestingly, both areas do not show volume differences in the early stages of vocal learning, instead a clear volume decrease is present from the sensorimotor to the crystallisation phase, and to a lesser extent towards 200 dph. The CM is involved in vocal learning and its structural properties correlate with how well the bird copies the tutor song (discussed in section 6.4.3.2). The hyperpallium apicale contains the Wulst which processes sensory information, including visual and somatosensory stimuli [78], and connects to nuclei related to song control and auditory system [79]. From crystallisation towards 200 dph, the most rostral parts of the hyperpallium, potentially including small parts of the rostral lateral nidopallium, decrease in volume.

6.4.1.3 Two maturational waves and development of white matter structures

Even though the localised relative volume differences described above clearly align with sensitive and critical period development, the diffusion metrics did not follow the same spatio-temporal trajectory. Voxel-wise analysis of the FA maps informed that most myelin-containing structures appeared to change over the course of the study. Many of the major fibre bundles identified by voxel-wise statistical testing contain heterogeneous collections of tracts connecting distinct brain areas that are involved in a variety of functions. This impedes strongly with assigning proper functions to the latter.

Mean Diffusivity (MD) decreases over the course of the entire study with most dramatic decline early, i.e. between 20 and 30 dph. The second drop was found to be less intense and occurred between 40 and 65 dph (Figure 6-10). Most developmental DTI studies in humans describe postnatal decreases in MD over time, ascribed to lowering of overall water content in tissues and closer interaction of water molecules with increasing amounts of macromolecules [62, 80-83], for review [59, 84, 85]. Similar observations have been obtained in other species, e.g. rats [52, 86], cats [87] and dogs [88].

6.4.2 Sex differences in volume and intrinsic tissue properties

Only male zebra finches sing. This behavioural contrast is mirrored in the neural substrate underlying singing behaviour as many brain areas directly in control of singing, i.e. HVC, RA and Area X, are enhanced in males compared to females [74, 89]. Most sex differences observed in this study corroborate with the data described in Chapter 5 and relate to areas in control of or tracts connecting different nuclei involved in song behaviour. More specifically, we observe

clear sex differences in local volume near HVC, Area X (left), RA (right), at two levels of the tOM (near the thalamus and near the ICo) and the ventral portion of Field L co-localising with the NIf. At a lower statistical threshold, we also observe a sex difference in volume at LMAN. Furthermore, sex-dependent differences in local tissue microarchitecture overlap with the arcopallium, rostro-lateral and caudal surroundings of Area X, HVC, LMAN, RA and Area X (left). The latter two were not observed in the proof-of-principle study described in Chapter 5. This might be explained as the sex difference in left Area X is only present from 20 to 40 dph after which it dissolves, and because the data of the proof-of-principle study only include adult animals (≥200 dph). The sex difference in RA did not reach statistical significance in the proof-of-principle study, which might be attributed to differences in sensitivity because of smaller group sizes (two groups versus longitudinal study design) or the quality of the 3D RARE scans used for spatial normalisation which we improved in between the two studies. Furthermore, the sex difference in RA-microstructure (MD) establishes late, i.e. at 120-200 dph. This microstructural difference might relate to findings by McDonald and Kirn (2012) who describe a decrease in soma size and increase in dendritic arbor in male birds between 3 and 12 months [90]. Further, RA is much smaller in females compared to males, consequently, the difference in microstructure might in part reflect sub-optimal image registration (more detailed explanation follows later in this section). However, the latter explanation seems questionable since we managed to detect a volume difference in (right) RA in the DBM analyses.

The white-matter structures that appear to surround RA (describes as ‘arcopallium’ in the results section) and surround Area X express a sex difference in FA early, at 30-40 dph, and this difference persists until the end of the study (Appendix 6-C). HVC presents sex differences from 65 dph towards adulthood. The sex-difference in MD in LMAN can be traced back to a sexual dimorphism in tissue microstructure explained in Chapter 5. Even though Nixdorf-Bergweiler (1996) did not report a sex difference in volume in LMAN throughout ontogeny [36], we observe a weak sex difference in local volume co-localised with LMAN.

To our knowledge, the sex-dependent volume difference near the ventral part of Field L, co-localising with the NIf, is a novel finding. The Nif receives auditory input from the CM which in turn gets input from Field L and is reciprocally connected to the NCM [91]. Other sources of sensory information may reach Nif via input from the rostral Wulst (visual; [79]) and the Uva (somatosensory; [92]). Besides the reciprocal connection with Av (discussed in section 6.4.3.2;

illustrated in the Pathway Scheme), the Nif is the main auditory afferent of HVC, the latter of which also receives input from Uva [93]. Based on these connectivity studies, the Nif is a likely candidate to integrate and relay multi-sensory stimuli to HVC. Furthermore, the Nif exhibits both auditory and vocal-motor activity [94] and drives sleep-related replay of premotor activity in HVC [95]. Lesion and inactivation studies provide evidence of the active involvement of Nif in sensorimotor learning and song production [96, 97]. In contrast, adult song production appears less impacted in case of bilateral lesioning of Nif [98]. Based on these and other findings (reviewed by [99]), one can conclude that the Nif plays an active role in song control. We conclude that our finding (volume of Nif M>F) adds to the generally accepted sex differences in volume described for areas pertaining to the song control system [89].

We did not expect to find unilateral sex differences in brain structure, since the previously mentioned studies did not report sex differences in brain structure to be confined to or more expressed in one hemisphere compared to the contralateral counterpart, e.g. small note regarding a pilot study in the left column of p447 of [36]. Studies assessing hemispheric asymmetry in brain structure have led to inconsistent reports [100, 101], and, in contrast to other songbird species, there is no strong dominance to either side of the zebra finch syrinx for song production [102]. We therefore argue that unilateral clusters might arise because of the method or stringent statistical thresholds applied in this study. The volumetric analyses fully rely on automated detection methods that use spatial registration methods –based on anatomical contrast present in the images– to estimate local relative volume differences [37]. Since most of the song control nuclei lack sufficient anatomical contrast on T1- or T2-weighted anatomical scans [40, 103], spatial registration and thus estimates of localised relative volumes, might be sub-accurate in some of these regions.

6.4.3 Practice makes perfect: song proficiency traces back to the structural properties of the male zebra finch brain

6.4.3.1 Song refinement continues beyond the critical period for song learning

Syllable features

We recorded and analysed song renditions from advanced plastic to fully stereotyped song. While most acoustical properties did not change throughout the study, a clear decrease of Wiener entropy could be observed, with most extensive changes situated within the critical

period for vocal learning, i.e. between 65 and 90-120 dph. Decreases in syllable Wiener entropy have been described to occur while syllables gain maturity during the sensorimotor phase of vocal learning [104]. Similar reductions in sound entropy have been described in juvenile marmosets over vocal refinement [105]. Furthermore, the acoustic variability of different renditions of the syllables became smaller (more stereotyped) towards 200 dph. Related observations have been reported by Ravbar et al. [106] who observed decreased variability of song features when syllables reach their target performance [107]. Taken together, the decrease in Wiener entropy and lower acoustic variability of individual syllables indicate that syllable renditions gain tonality, become more structured (less noisy) and less acoustically diverse along song maturation [5].

While the spectral content of syllables mainly forms during the sensorimotor phase, the temporal properties of the song motifs change beyond the crystallisation phase. These observations are in line with studies in zebra finches [108] and Bengalese finches [16]. Both studies reported adult song plasticity which selectively affected the temporal properties of song. Intriguingly, they observed an increase in song tempo caused exclusively by the shortening of the inter-syllable intervals (both the duration and variability) while leaving syllable duration unaffected. These changes continued up to approximately one year of age, well beyond the critical period of vocal learning. Others studies also noted non-significant tendencies of inter-syllable interval shortening in young adult birds, which lead to increased song tempo [15, 109] or increased song density as presented in Figure 6-13. Furthermore, the study in Bengalese finches also assessed the spectral content of song syllables, but did not report any significant changes after the critical period [16]. This observation aligns with historical reports (reviewed by e.g. [110, 111]) describing that even though the gross structure of adult song does not change, functional fine-tuning continues beyond crystallisation. A similar effect is observed for sequence stereotypy, a measure representing the fixed-ness of the order of syllables over different song renditions [11]. Sequence stereotypy gradually increases from 65-120 dph and, for the majority of birds, sharply increases from 120 to 200 dph. In conclusion, based on our and other findings, refinement of the temporal characteristics of song likely continues post song crystallisation and adult songs continue to include some form of ‘vocal motor practice’ [4].

Song similarity

Song similarity to tutor song, i.e. the percentage of tutors' song sounds that is found in the pupils' song, increased steadily from 65 to 200 dph, reaching similar levels as observed in other studies [34, 104, 112-114]. Consequently, besides speeding up the total performance (consistent shortening of the inter-syllable intervals) the continued 'vocal motor practice' includes further refinement of own vocalisations to acoustically match with the previously memorised tutor song. Post-critical period 'vocal motor practice' corroborates with the results obtained by studies using reinforcement learning paradigms to alter e.g. pitch [17, 115, 116], or real-time alterations to auditory feedback [10, 116-118]. These studies show that adult birds are capable of adapting the temporal and spectral features of their song, suggestive of some form of adult song plasticity. Furthermore, shortly after cessation of reinforcement training or restoration of auditory feedback, the birds will gradually return to their pre-reinforcement training song. Importantly, in case of bilateral NCM lesioning at the stage when e.g. pitch is altered, the song will not normalise to baseline performance when the reinforcement is withdrawn [119]. This implies that active processes focus on maintaining adult song closely matched to the initial pre-training song and point to a continual influence of the auditory system. Importantly however, the involvement of auditory feedback in maintaining song performance wanes with age, as deafening old zebra finches leads to a slower degeneration of the song compared to young birds, and overall song plasticity decreases with age [15, 120]. Moreover, song deterioration as a consequence of deafening could be prevented by concomitant lesioning of LMAN [15], which implies that the AFP is actively involved in song maintenance.

6.4.3.2 Neural correlates of vocal proficiency

Not all birds learn the song of their tutor equally well. This raised the question as to whether the brains of 'good' versus 'less good' learners could be distinguished by volume differences (3D) of specific brain structures or intrinsic neuronal tissue properties (DTI). The brain-wide voxel-wise analysis appointed four distinct areas –referred to as 'clusters' or 'cluster-based ROIs' of contiguous MRI voxels– where brain architecture appeared to correlate with song performance. These include medial and lateral parts of the caudal mesopallium (CM) and the caudo-medial nidopallium (NCM) which both pertain to the so-called 'auditory lobule', the ventral pallidum (VP) and a portion of the fronto-arcopallial tract (tFA). Surprisingly, we did not

observe any correlation co-localised with the traditional SCN. Throughout the discussion, we will mainly focus on the potential functional implications of these findings in the context of vocal learning. For elaborate discussions on potential biological phenomena underlying the MRI parameter readout we refer to Chapter 2, 3 and 4 of this thesis.

Two important notes should be made when considering the correlation analyses. First**,** given the relatively large difference between different birds in vocal proficiency (song similarity ranges from approximately 45% to 85%), the overall association between song performance and the structural properties of the songbird brain identified by the voxel-wise correlation analyses are mainly driven by between-subject variance. Intriguingly however, structural properties of the CM and the VP appear to correlate also at the within-subject level, indicating that while birds individually improve their song performance the local tissue properties will change in accordance with the overall trend between subjects (Figure 6-14 and Figure 6-15). Second, some of the localised clusters are embedded in larger brain regions –this relates especially to the CM– that appear to decrease in volume from the advanced sensorimotor stage (65 dph) to adulthood (200dph).

The auditory lobule: the caudo-medial nidopallium (NCM) and the caudal mesopallium (CM)

The 'auditory lobule' consists out of primary areas, i.e. (1) Field L, the homologue (similar ancestor) of the primary auditory cortex in the mammalian superior temporal gyrus, the (2) NCM and (3) the CM, which are analogues of the mammalian auditory associative cortices (analogy and homology proposed by [121, 122]). Field L, as primary thalamorecipient area [123], receives projections from the nucleus ovoidalis (Ov). In turn, Field L conveys auditory information directly towards portions of the NCM and the CLM, which both project to the CMM. Furthermore, the CLM connects to the interfacial nucleus (NIf) that is one of the principle inputs of HVC [91, 124, 125]. Lastly, the CLM and two distinct subdivisions of Field L (L1 and L3) send axons to the HVC_{shelf} and RA_{cup} regions [91, 126]. These connectivity patterns set the NCM and the CM as prime targets capable of conveying auditory information originating from the ascending auditory system to areas implicated in song control. A schematic overview of these brain regions and the connections to other auditory and song control areas can be found enclosed to this thesis (pathway scheme). In the following paragraphs, we will zoom in on the functional significance of each of these structures with regards to vocal learning.

The caudo-medial nidopallium (NCM)

We observe a clear correlation between song similarity and FA in the left NCM (Figure 6-14). Without multiple comparisons corrections, the NCM cluster extends towards a medial portion of the CM and additional clusters become visible that cover the right NCM and CMM. The overall association between tissue micro-architecture and song performance resides from between-subject variance, as the within-subject correlation did not reach significance. Consequently, individual improvements in song similarity do not immediately link to altered brain structure. Testing for sex-differences revealed a significant interaction between age and sex in the cluster covering the left NCM. In conclusion, between-subject variation in song similarity rather than personal (within-subject) improvements in song similarity drive the correlation detected by the voxel-based analysis in left NCM, and the local microstructural properties of NCM develop differently in males and females.

Since Mello et al. (1992) first described song selective responses in the NCM [127], ample evidence has been collected supporting the active involvement of the NCM in memorising tutor song during the sensory phase. In brief, NCM neurons appear to habituate after prolonged exposure to a particular song [128, 129], and the habituation rate measured in NCM correlates with song similarity to tutor song [8]. Pharmacological blockage of the ERK- (IEG expression) or mTOR signalling cascades in juvenile male zebra finches during exposure to tutor song prevented birds from memorising and producing a tutor-like song in adulthood [7, 130]. Furthermore, IEG expression in NCM correlates with how much of the tutor song has been learned in tape-tutored [131] and socially tutored zebra finches [132]. Interestingly, the positive correlation between song similarity and egr-1 expression was confirmed by a follow-up study of the same group, and was only observed in the NCM, not in HVC or the CM, and only after stimulation with tutor song, not with birds' own or novel song [133]. Furthermore, Van der Kant et al (2013) showed in adult male zebra finches that only in the (caudal portion of) left NCM BOLD activation was proportional to song similarity to tutor song [134]. Lesioning NCM in adult male zebra finches interferes with song discrimination as birds could not distinguish tutor song over conspecific songs [135], or with returning to baseline song performance after reinforcement training [119]. In sum, the NCM is necessary for tutor song memorisation during the sensorimotor phase, tutor song recognition and recall of recent song models or targets in adulthood, but has no apparent role in own song (vocal motor) production or in overall sound discrimination (including calls).

The voxel-wise correlation between song similarity and FA revealed a clear structural hemispheric asymmetry as only the cluster in the left hemisphere survived FWE multiple comparison correction. This finding corroborates with Moorman et al. (2012), who detected a higher overall egr-1 expression in juvenile male zebra finches in response to tutor song playback in the left compared to right NCM [6]. Moreover, song similarity appeared to correlate with the extent of lateralised egr-1 expression (not with absolute egr-1 expression levels within a hemisphere). This strikingly lateralised response was selective to tutor song stimulation (not in response to unfamiliar conspecific or silence), specific to NCM (not in HVC or the hippocampus) and was no longer observable in adult male birds [6]. In a follow-up study, Moorman et al. (2015) found good learners to have an overall left dominance of egr-1 expression in the left NCM while poor learners displayed the reverse [136].

Across species, IEG expression is induced by neural activity and is often associated with learning [137, 138]. Short-term functional network adaptations induced by learning can become consolidated into long-lasting memories by modifying the structural properties of these local circuitries [139]. Indeed, tutor song experience stimulates the enlargement, accumulation and stabilisation of dendritic spines in HVC of male birds [140]. These microstructural adaptations promote functional enhancement of synaptic transmission and –in case of sufficient number and spatial extent– can be detected by MRI methods sensitive to tissue microstructure such as DTI (see Chapter 2, 3 and 4 of this thesis). Since the spatial extent of the cluster observed in our DTI correlation study approximates the descriptions by Moorman and co-workers [6, 136], we hypothesise that the correlation between song similarity and FA in left NCM may be a readout of learning-driven microstructural tissue adaptations. An important difference, however, is that the DTI-FA-cluster also includes rostral parts of NCM, while most IEG studies exclusively sample caudal parts of NCM (summary of studies presented in Table 1 of [133]). Furthermore, the asymmetry towards left NCM detected in our study, continues into adulthood (between-subject correlation Spearmans' ρ of data obtained at 200 dph) and includes a correlation between song similarity and the structural microarchitectural properties of the brain. One could argue that when juvenile birds are still improving their song, functional lateralisation might be more pronounced compared to adult life stages, when the song is (actively) maintained but should no longer be further 'polished'. The structural correlates that result from tutor song memorisation, on the other hand, might persist.

The caudal mesopallium (CM) and the Avalanche nucleus (Av)

The voxel-wise analyses uncovered a bilateral cluster presenting a negative correlation between local tissue volume and song similarity coexisting with (medial and) lateral parts of the CM (CLM), including the Av. In contrast to the microstructural properties observed in left NCM, the overall correlation between song performance and local volume exists within birds. This suggests that improved performance might be directly related to the structural properties of the brain. Additionally, no significant interaction between age and sex or main effect of sex could be observed in this cluster-based ROI indicating that the local volume of this structure is not different between male and female birds.

The CM encompasses a large portion of the dorsal forebrain that lacks clear cyto-architectonic features which would enable demarcating distinct sub-regions based on Nissl stain or 'conventional' T2-weighted MRI scans. In contrast, tract tracing, IEG expression and electrophysiology studies have enabled the identification of functionally distinct domains that may subserve different aspects of sensorimotor integration [92, 141]. Its close proximity and inter-connectivity to the primary auditory centre Field L, HVC and NIf, presents it as a likely entry point for auditory information to the song control system [124, 142].

Keller and Hahnloser (2008) identified neuronal populations which respond to passive playback of own song or self-generated song in Field L and the CLM of juvenile male zebra finches aged 60-90 dph. Some cells selectively activate following real-time auditory perturbation of the birds' own song, suggestive of an internal error-detection system that helps to maintain the acoustic structure of the song towards a given song model [143]. In contrast to the clear birds' own selective responses in CLM detected in awake juvenile male birds [143], Shaevitz and Theunissen (2007) could not find similar song selective responses in the CLM of anaesthetised zebra finches [125]. This lack of song selective neuronal responses might be due to either the application of anaesthesia, or to anatomical differences as distinct subfields of the CM might respond differently to different stimuli.

An important sub-region of the lateral CM that is likely to be encapsulated by the voxel-wise analyses on the jacobian determinants, is the Avalanche nucleus (Av; or field Avalanche [144]), located dorsal to NIf, resting on the characteristic 'bend' of the LaM. The Av receives afferent input from Uva, contains reciprocal connections with Nif and HVC, and displays selective neural responses to the birds' own song, over reversed birds' own song and white noise [92]. Prior

studies have uncovered singing-driven IEG (egr-1 and c-fos) expression in Av which appears to correlate with the amount of singing in normally hearing and in deafened birds [145]. These findings indicate that IEG expression truly reflects singing-related neuronal activation rather than hearing own song. Moreover, Roberts et al. (2017) recently discovered that Av-projecting HVC neurons (HVC_{Av}) do not overlap with Area X- or RA projecting HVC neurons, convey motor-related signals based on input from RA-projecting HVC neurons, and take up an important role in auditory feedback-based timing of song elements. Additionally, genetic ablation of HVC_{Av} neurons in juvenile male zebra finches after sensory learning significantly impaired sensorimotor learning: song similarity to tutor song correlated with the number of HVC_{Av} neurons that survived genetic ablation [146].

The 3D volume data show that while birds improve their song, a large portion of the CM decrease in volume. *In vivo* MRI studies assessing the effects of training or skill acquisition on the structural properties of the brain show 'bidirectional' brain adaptations, that is, certain brain regions expand while others contract in response to training. For example, Sampaio-Baptista et al. (2014) assessed short- and long-term effects of intense or less intense training programs (learn to juggle) on the brain. They concluded that depending on the training intensity and the timing of investigation, distinct parameter readouts can be obtained as also different neuroplastic mechanisms might be at play [147]. Furthermore, Gryga et al. (2012) reported that between-subject variability in learning success could be explained by heterogeneous 'bidirectional' structural neuroplastic responses [148]. We argue that the decrease in brain volume observed in the CM might refer to a process related to pruning where redundant synapses are eliminated along the process of skill (and hence circuit) optimisation, leaving the best performing birds with the smallest local volume. Alternatively, continued improvements in song similarity as form of vocal motor practicing might evolve towards an optimised and 'automatic performance' requiring less intense neuroplastic adaptations, and where redundant circuitries are pruned to facilitate optimal performance.

The ventral pallidum (VP)

The voxel-based analyses show that song similarity correlates positively with FA and negatively with local volume of the VP. Intriguingly, both macro- (volume) and micro-structural (FA) measures present a significant within-subject correlation indicating that individual improvements of song performance actively sculpt the brain. Based on the MRI readout one

could argue that while birds improve their performance the VP scales down and becomes more orderly structured. The latter might include more accurate alignment of projection neurons. When assessing between-subject correlations at distinct time-points, i.e. advanced plastic (65 dph) versus mature (200 dph), significant correlations between song similarity and FA are observed at both ages, while local volume only correlates during sensorimotor song refinement, not when song is considered 'mature' and crystallised. Lastly, no sex difference in FA or modulated jacobian determinant in the VP could be found.

Besides the auditory lobule, other clusters displaying a negative or positive correlation between song similarity and local volume or DTI-FA values respectively, were also discerned immediately rostral and rostro-lateral to the anterior commissure, caudal to the TSM, dorsal and dorsomedial to the FPL. Based on zebra finch brain atlases and detailed description by Li and Sakaguchi, we believe this cluster co-localises with the VP, i.e. the avian homologue of the mammalian substantia innominata which includes the basal nucleus of Meynert [149]. In mammals, the substantia innominata and the basal nucleus of Meynert provide the predominant source of cholinergic input to the neocortex, hippocampus and amygdala, and are implicated in state-dependent regulation of cognitive processes including attention and memory. Indeed, loss of cholinergic signalling originating from the basal forebrain is inevitably linked with cognitive decline (review: [150]). Consequently, treatments aimed at re-boosting the cholinergic system, specifically targeting the basal nucleus of Meynert, are still being explored [151]. Likewise, in zebra finches, ChAT-immunopositive neurons of the VP send cholinergic projections to HVC and RA [149], and receive projections from nucleus ovoidalis (Ov), similar in function to the mammalian medial geniculate nucleus and an important relay centre of the ascending auditory pathway [152].

Combined usage of electrophysiology and pharmacological manipulations revealed that neural responses in HVC to birds' own song can be actively suppressed by pharmacological manipulation of the cholinergic projection neurons originating from the VP [153, 154]. Interestingly, the authors suggested that cholinergic modulation by HVC-projecting VP neurons might serve a similar function in the sleep-week transition of neural responsiveness. Sleep is generally acknowledged to be crucial in consolidating experiences into memories, by localised replay of neuronal firing patterns, affected by cholinergic and serotonergic signalling (for review: [155]). Likewise, several studies have explored to what extent sleep facilitates or

consolidates sensorimotor learning in the songbird brain (for review [156]) and how behavioural state and song-selective responses can be modulated by e.g. the cholinergic system [157].

The fronto-arcopallial tract (tFA)

Based on [39] and [158], we identified a third cluster presenting a positive correlation between FA and song similarity co-localised with the tFA. The correlation between song similarity and FA in the tFA is driven by between-subject variance, as no significant within-subject correlations could be traced. Further, FA values in the tFA of males and females are not statistically different. Parts of the cluster might also overlay with nearby white matter structures. More specifically, other close-by tracts include the tOM and the FPL, and myelin-containing structures such as the ventro-lateral portions of the avian analogue of the globus pallidus [39] and the lateral striatum [158]. When superimposed onto an FA map (data not shown), the cluster clearly coexists with a fibre structure. Based on its position ventral to the E, we believe this cluster reflects the tFA, rather than the FPL which –according to [158]– is situated more medial and frontal compared to the E and tFA. The tOM courses more medially (and caudally) compared to the location of the cluster we assign as tFA, however, the caudal extension of the latter might partly invade the tOM.

The tFA contains projections from the basorostral nucleus in the rostral forebrain ventral to the E, passing the frontal nidopallium, to the lateral arcopallium (and caudolateral nidopallium). The basorostral nucleus contains three major subparts (1) a rostral 'lingual' part, (2) a middle 'beak' part and (3) a caudal 'auditory' part, each of which receives ascending input from the principal sensory trigeminal nucleus (originating in the beak, tongue and oral cavity, and in an auditory lateral lemniscal nucleus which receives direct input from the cochlear nucleus) and several pontine nuclei [77] (reviewed by [159]). In budgerigars, the basorostral nucleus is crucial for vocal learning [160], however, no such direct link has so far been proven in the zebra finch. Nevertheless, several possible ways of involvement in vocal behaviour have been described. The basorostral nucleus sends somatosensory and auditory information to the lateral arcopallium [77], suggesting that the descending projections from the latter, which include the jaw and tongue premotor and trigeminal projections, might mediate auditory feedback during singing [161]. Also in humans, somatosensory information from facial skin and muscles of the vocal tract is vital for proper perception and production of speech [162]. Lastly, its potential

role in providing sensorimotor feedback from the beak and tongue up to the song control system during sensorimotor learning [163] has been suggested.

Alternatively, these somatosensory and auditory descending projections may serve to control beak movements that modulate gape size during singing, as gape size can affect the acoustic properties of individual syllables [164]. Furthermore, besides its potential implications in mediating acoustic properties, juveniles also copy beak movements characteristic to particular syllables, as beak movements appear to be an important component of courtship display [165]. Taken together, even though this tract is not considered part of the 'traditional' song control system, it might carry neuronal projections that are necessary for proper adjustment of vocalisations and be strengthened by vocal practicing. The association between FA and song similarity however, is less clear and might be attributed to factors related to song similarity that have not been quantified in this study e.g. better performing birds might perhaps have been singing more frequently, which could result in activity-induced alterations to FA. More details on mechanisms that underlie changes in FA can be found in Chapter 2, 3 and 4 of this thesis, and, in addition, [166] discusses how inter-subject differences in white matter might relate (or not) to altered behaviour or performance.

6.4.4 Methodological considerations

6.4.4.1 Processing pipeline

Voxel-based or deformation-based morphometry is very intensely used in MRI studies on human subjects. The technique, however, is less often employed in preclinical or fundamental research on small animals. In the methods section, we attempt to propose several additional steps that enable implementing deformation-based morphometry in non-mammalian or non-standard model species. Bird brains differ fundamentally from mammalian brains as cortical tissue is organised in nuclei instead of cortical layers. Consequently, generating tissue probability maps that grossly reflect grey matter, white matter or cerebrospinal fluid was a challenge. To facilitate automated image-based segmentation, we first created a population-based template using ANTs [167]. Next, the FAST tool of FSL was employed to enable unbiased determination of tissue classes based on our T2-weighted images [32]. This step produced tissue probability maps that could be readily inserted in the existing VBM pipelines that include tissue segmentation and inter-subject normalisation via DARTEL, in SPM [28, 31]. Both ANTs and DARTEL of SPM incorporate the most accurate intensity-based spatial registration

algorithms currently available [168] and have realised a highly accurate spatial correspondence between the images of this study. As such, they provided a solid basis for subsequent voxel-wise testing. The latter unveiled age-dependent relative volume changes that appeared spatially confined, bilateral symmetric and grossly aligned with (sub-parts of) established subdivisions of the brain e.g. [39]. A ROI-based analysis, which requires *a priori* ROI selection, would not have revealed similar information mainly because the areas detected by voxel-wise testing would be very difficult to delineate and prone to experimenter bias.

6.4.4.2 Longitudinal study design

The current study includes data points obtained at seven clearly defined time points which represent distinct stages of vocal learning. Alternatively, studies in humans report designing accelerated longitudinal studies where multiple cohorts of subjects are measured repeatedly, each starting at a different age [169]. Furthermore, over recent years, large multi-centre projects gathered extensive mixed cross-sectional and longitudinal datasets that constitute a rich database of brain imaging and behavioural data, e.g. [170]. Both strategies enable modelling of developmental patterns of MRI-based measures, e.g. [171], which give rise to more accurate hierarchical sequences of developmental trajectories across brain areas, groups, sexes etc. Furthermore, alternative strategies are being employed to estimate maturational trajectories according to which different brain structures mature based on multiparametric MRI data. This can be complemented with advanced modelling or data analyses approaches, for example Mahalanobis distances [172], Gompertz functions [53, 173], Legendre polynomials [174], graph-theory to trace the development of networks [175], and possibly many more. These integrative models might help to elucidate the biological nature that underlies these MRI-based findings.

APPENDICES

Appendix 6-A: Overview of zebra finch brain anatomy.

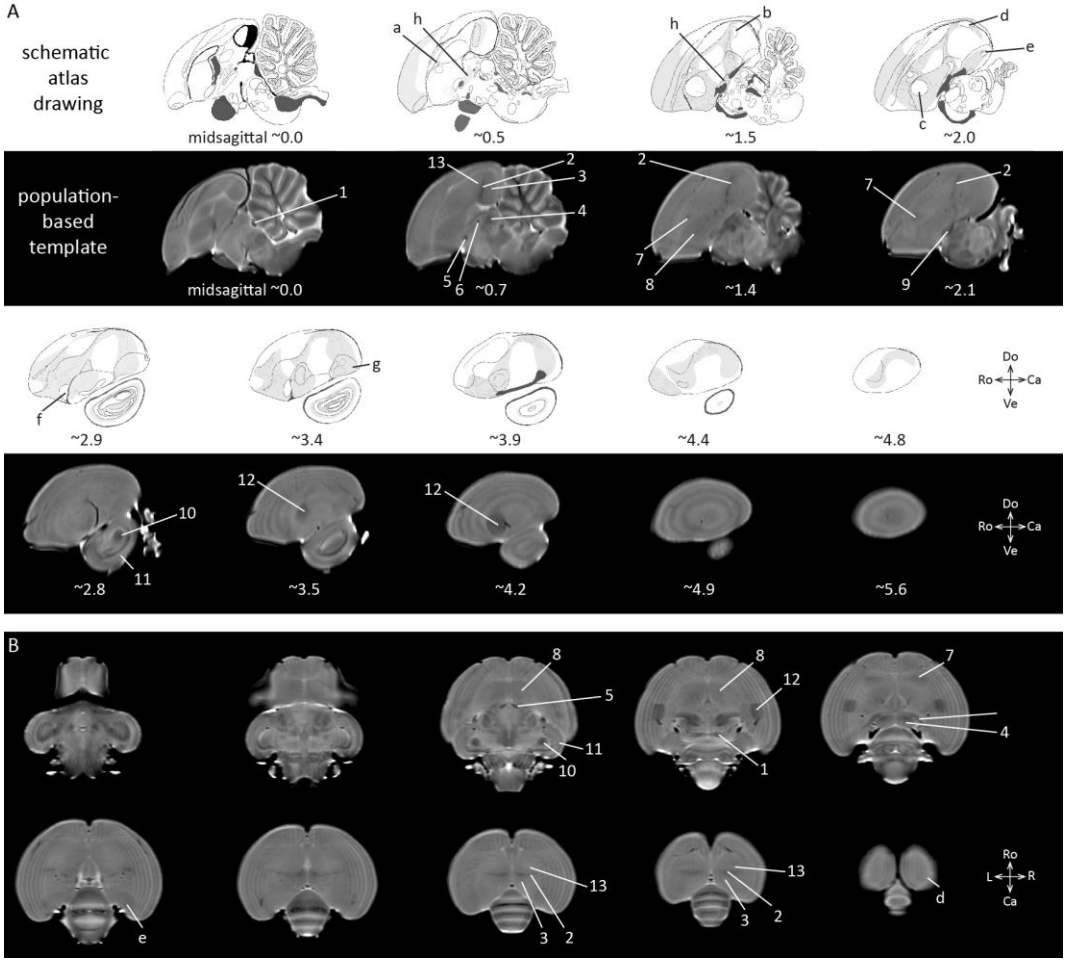

Figure 6-16: Bird brain anatomy. Panel (A) illustrates sagittal slices of the bird brain including schematic atlas drawings obtained from (Karten et al., 2013) and MR-images extracted from the population-based template. Anatomical areas visible on the T_2-weighted MRI slices are appointed by numbers, while the letters indicate regions that are only visible on the schematic atlas drawings. Panel (B) provides an overview of (the approximate position of) anatomical regions defined in (A) on horizontal slices derived from the population-based template. The numbers below the sagittal slices correspond to the approximate position (in 'mm' from the midline). Legend: a: MMAN; b: Field L2b; c: Area X; d: HVC; e: RA; f: basorostral nucleus; g: lateral arcopallium; h: basal nucleus of Meynert and ventral pallidum; 1: posterior commissure; 2: Field L; 3: NCM; 4: thalamic zone; 5: ; 6: anterior commissure; 7: LMAN; 8: striatum including Area X; 9: FPL (lateral prosencephalic fascicle); 10: MLd; 11: TeO or ventral part of the optical lobe; 12: entopallium; 13: medial and lateral portion of the caudal mesopallium (respectively CMM and CML).

Appendix 6-B: Sex difference in local volume.

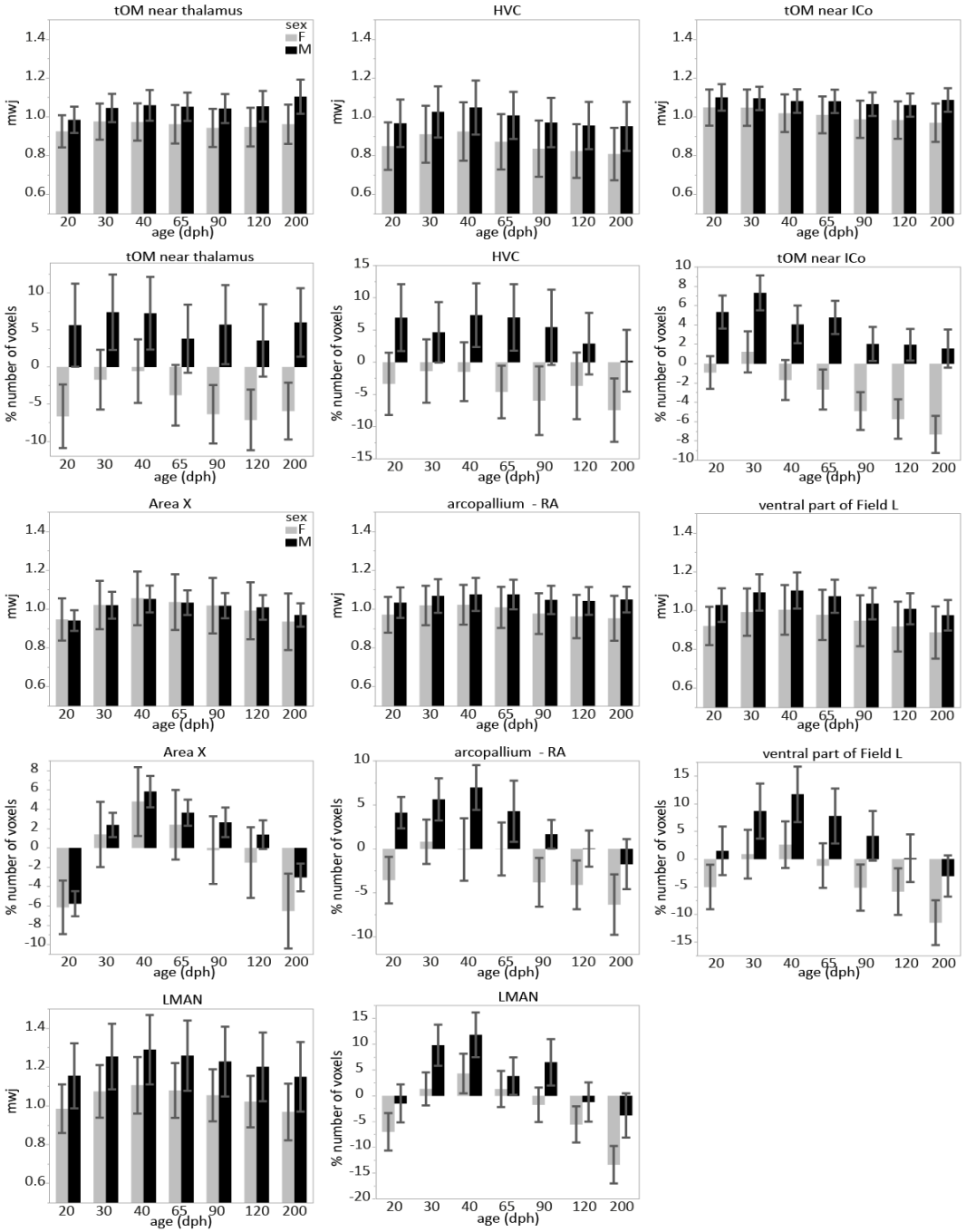

Figure 6-17: Bar graphs link sex differences detected in the modulated jacobian determinants to backprojected volumes. The graphs include the modulated jacobian determinant (mwj) or the relative number of voxels in the backprojected cluster-based ROIs (% relative to cluster-based ROI in reference space) that display a sex difference in local volume. The cluster-based ROIs are based on the statistical maps of the voxel-wise ANOVA's on the modulated jacobian determinant maps. The jacobian

determinants are plotted as mean ± standard deviation, while the graphs including relative volume measures are presented as mean ± standard error.

Appendix 6-C: Graphs displaying when in time sex difference in DTI parameters arise.

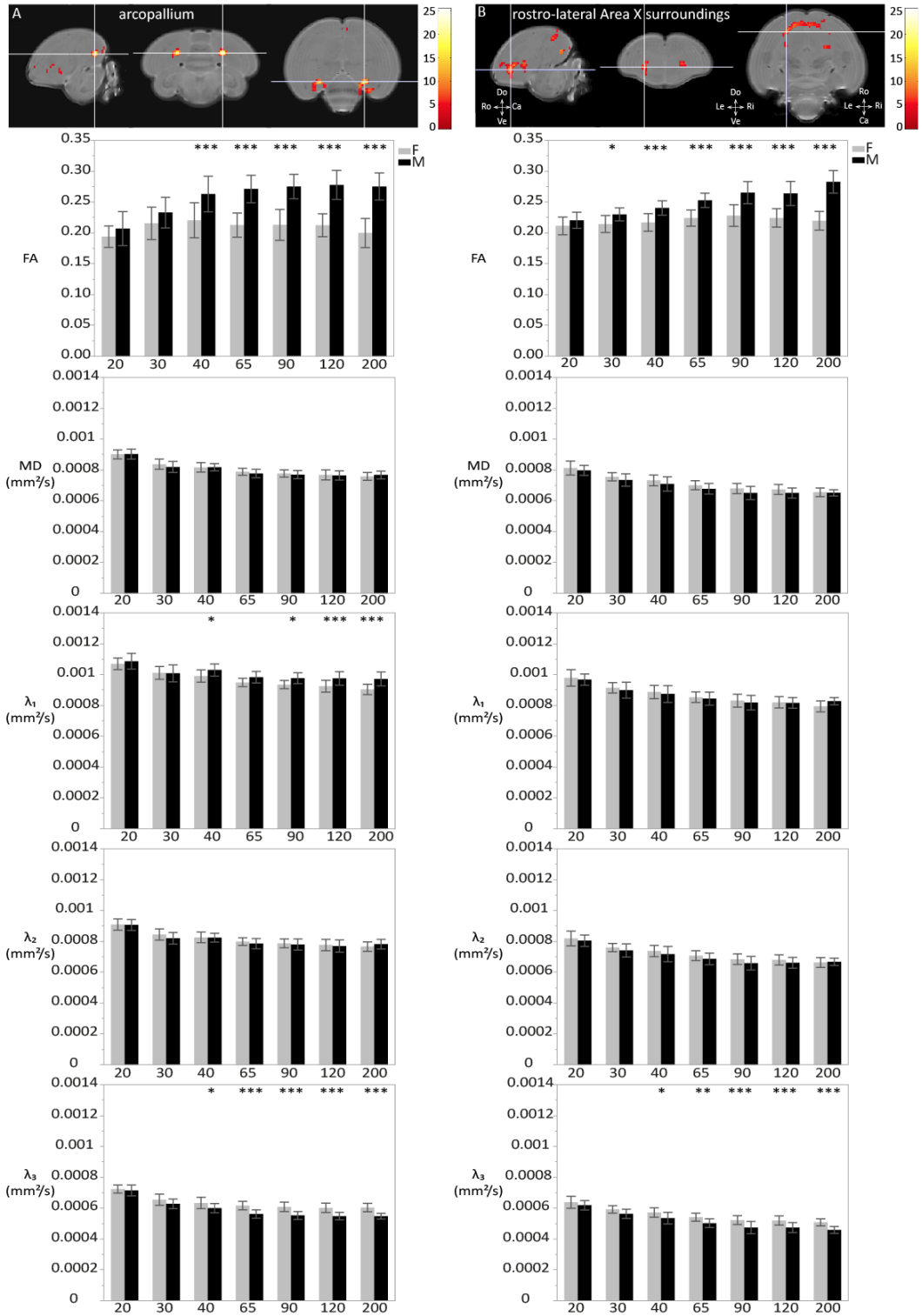

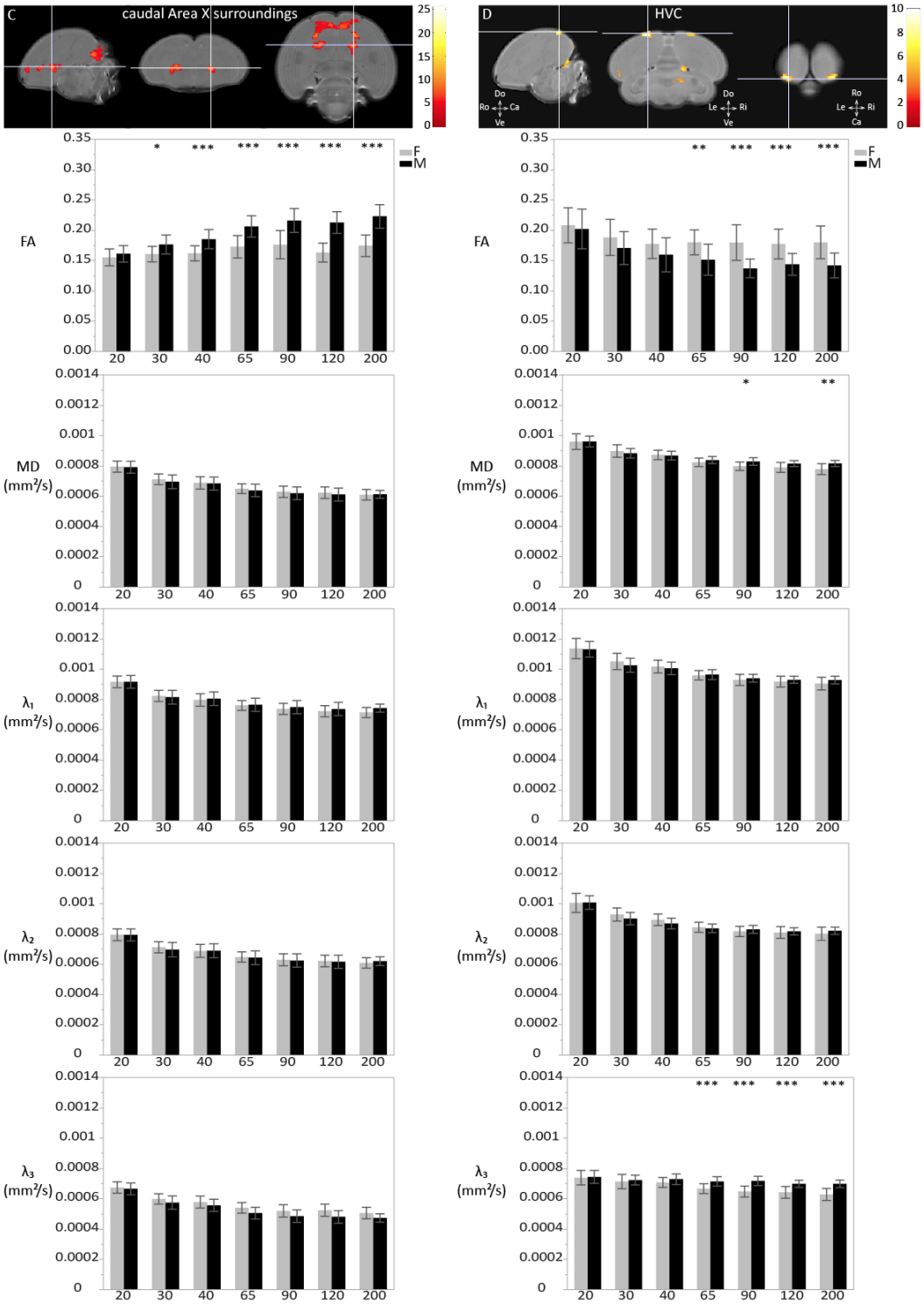
C
caudal Area X surroundings
D
HVC
Do
Ro
Ca
Ve
Le
Ri
F
M
FA
MD (mm²/s)
λ1 (mm²/s)
λ2 (mm²/s)
λ3 (mm²/s)
20
30
40
65
90
120
200

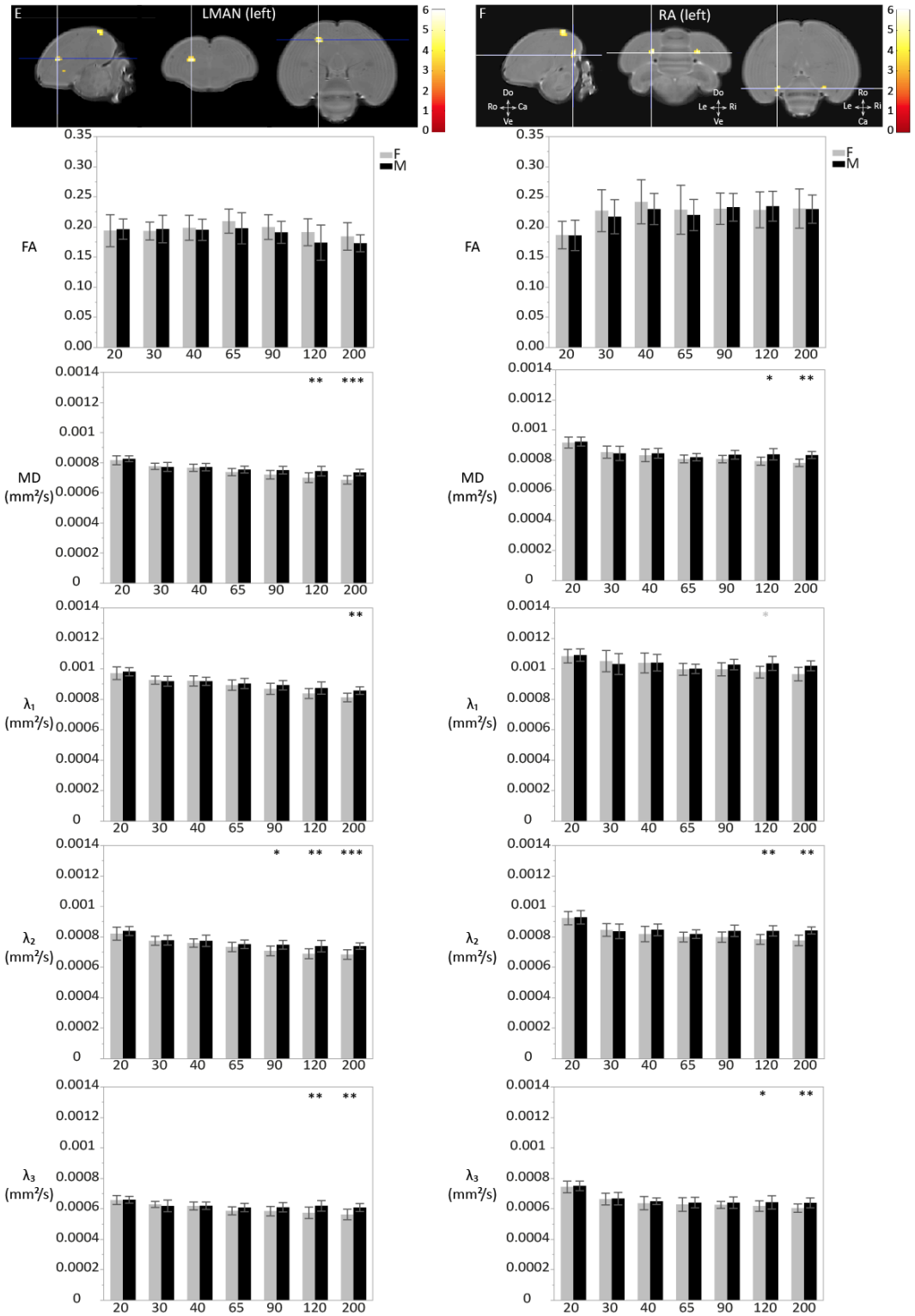
E
LMAN (left)
F
RA (left)
Do
Ro
Ca
Ve
Le
Ri
F
M
FA
MD (mm²/s)
λ1 (mm²/s)
λ2 (mm²/s)
λ3 (mm²/s)
20
30
40
65
90
120
200

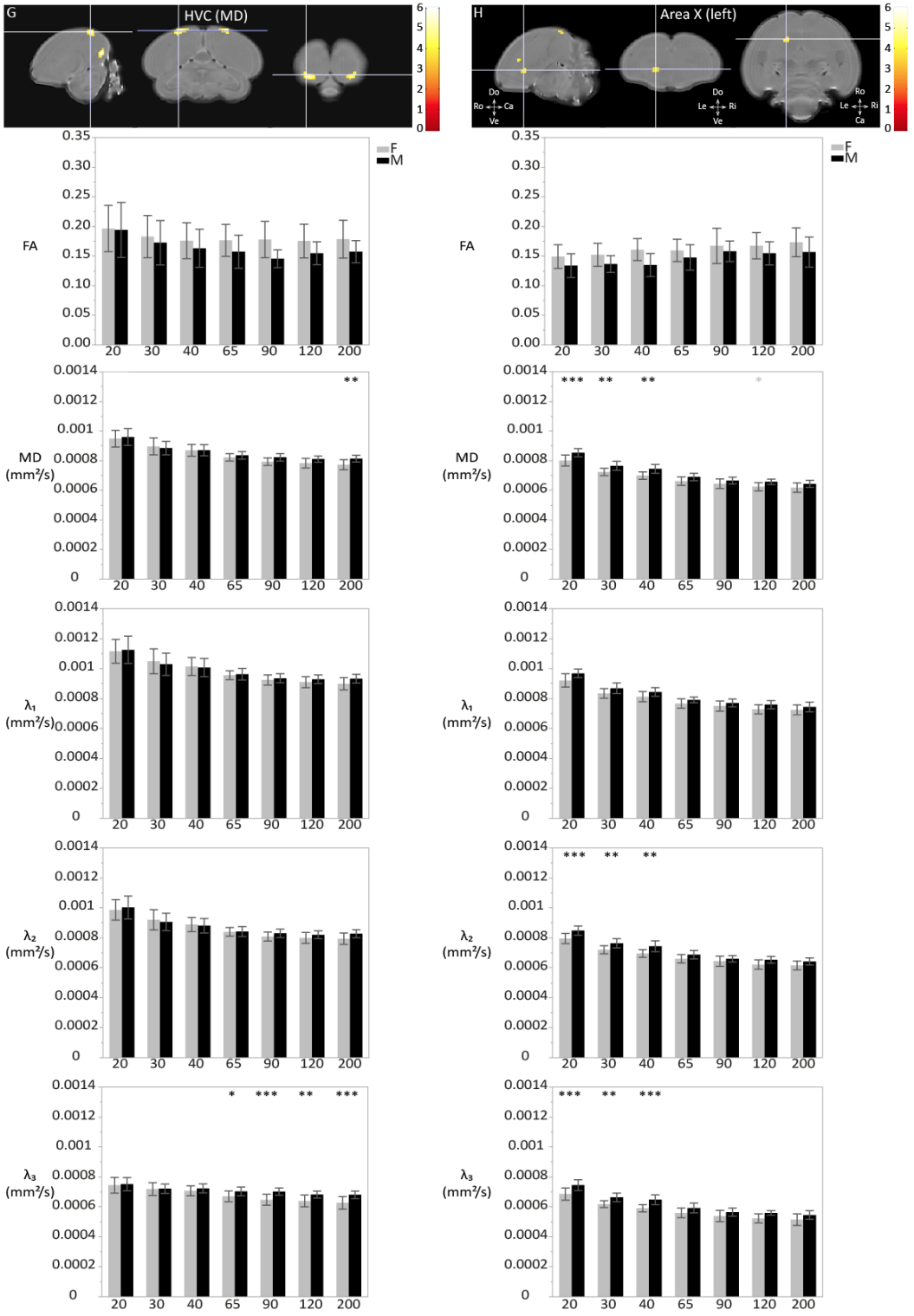

Figure 6-18: Graphs informing when in time sex differences in DTI parameters arise. The graphs include the average DTI metric of the cluster-based ROI extracted from the statistical parametric map displayed in the first row of the

column. The bar graphs are presented as mean ± standard deviation. A: arcopallium; B: rostro-lateral Area X surroundings; C: caudal Area X surroundings; D: HVC (λ_3); E: LMAN (left); F: RA (left); G: HVC (MD); H: Area X (left).

Appendix 6-D: Localised volume changes between consecutive time points in male and female zebra finches.

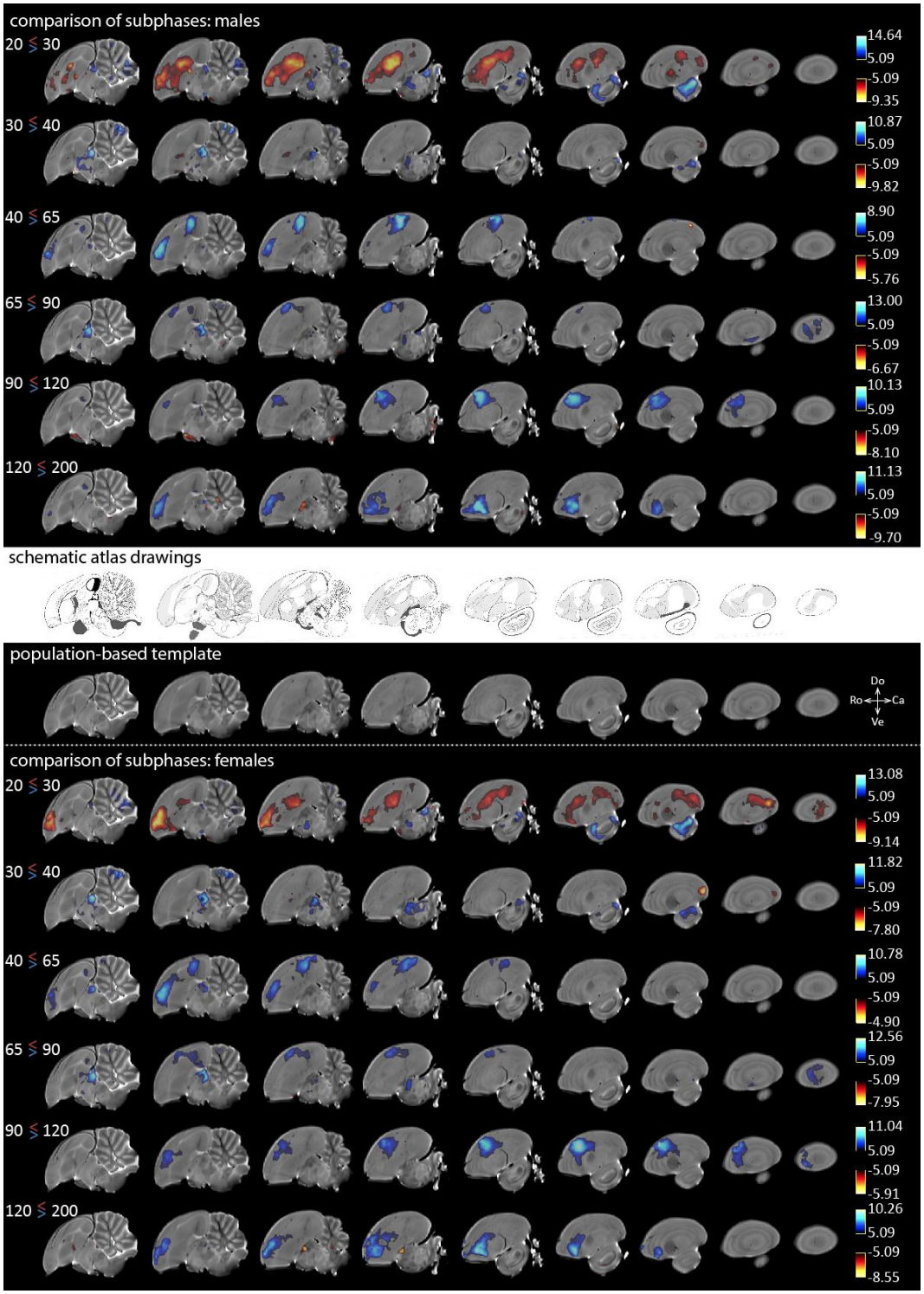

Figure 6-19: Localised volume changes between consecutive time points in male and female zebra finches. The colours refer to voxels where modulated jacobian determinants are larger (blue:

shrinkage from first to later time point) or smaller (red; expansion from first to later time point) at the first compared to the second time point in the comparison (indicated on the left side of each row). The statistical maps are colour-coded according to the scale on the right (T-values; T=5.09 corresponds to $p_{FWE}<0.05$, no cluster extent threshold). The atlas drawings are obtained from [39].

Appendix 6-E: Overview of the statistical results of the song analyses.

Table 6-4: Main effect of age of the syllable features

Main effect of age	*p*	*F*	
		(DFNum, DFDen)	*ratio*
Inter-syllable duration	**<0.0001**	**(3,38.2)**	**13.8789**
Syllable duration	0.5534	(3,37.7)	0.7078
Syllable pitch	0.8897	(3,37.7)	0.2088
Syllable mean frequency	0.1289	(3,38.6)	2.0078
Syllable peak frequency	0.0649	(3,38.6)	2.6144
Syllable goodness	0.2211	(3,38.1)	1.5348
Syllable FM	0.3279	(3,37.4)	1.1867
Syllable AM	0.5470	(3,37.4)	0.7189
Syllable entropy	**0.0032**	**(3,37.8)**	**5.4803**

Statistical analyses performed on the raw syllable feature scores.
Mixed model: Fixed factor: age; Random factor: subject; random slope: subject*age; syllable-identify nested within subject.

***Post hoc* tests to situate when in time inter-syllable interval duration (bottom left) and syllable entropy (top right) change significantly**

p	**65**	**90**	**120**	**200**
65		0.0773	0.0175*	0.0027**
90	0.5343		0.9469	0.6510
120	0.0370*	0.5143		0.9239
200	<.0001***	0.0003***	0.0120*	

Tukey HSD for all pairwise comparisons

Table 6-5: Main effect of age of the average and the standard deviation of the syllable features

Main effect of age	average			stdev		
	p	$F_{(DFNum, DFDen)}$	F_{ratio}	***p***	$F_{(DFNum, DFDen)}$	F_{ratio}
Intersyllable interval duration	**<0.0001**	(3,39.7)	11.6179	**<0.0001**	(3,25.4)	20.8043
Syllable duration	0.4400	(3,25.2)	0.9314	**0.0064**	(3,34.3)	4.8560
Syllable pitch	0.8558	(3,29.8)	0.2569	0.5824	(3,41.4)	0.6583
Syllable mean frequency	0.1351	(3,40.4)	1.9616	**0.0132**	(3,37.5)	4.0891
Syllable peak frequency	0.0700	(3,40.1)	2.5401	**0.0280**	(3,38.1)	3.3787
Syllable goodness of pitch	0.1935	(3.35.5)	1.6580	0.0621	(3,33.1)	2.6910
Syllable FM	0.2428	(3,28.2)	1.4742	0.0700	(3,33.2)	2.5803
Syllable AM	0.5030	(3,33.2)	0.7995	0.0982	(3,41.5)	2.2367
Syllable entropy	**0.0026**	(3,35.6)	5.7268	**0.0021**	(3,36.9)	5.9192

Statistical analyses on the average and the standard deviation of the syllable feature scores.
'stdev': standard deviation
Mixed model: Fixed factor: age; Random factor: subject; random slope: subject*age; subject nested within syllable-identity.

***Post hoc* tests to situate when in time the standard deviation of the inter-syllable interval (bottom left) or syllable duration (top right) changes significantly**

p	**65**	**90**	**120**	**200**
65		0.6338	0.0484*	0.0066**
90	0.1937		0.4705	0.1368
120	0.0001***	0.0259*		0.8767
200	<.0001***	0.0001***	0.1833	

Tukey HSD for all pairwise comparisons

***Post hoc* tests to situate when in time the standard deviation of syllable mean frequency (bottom left) or peak frequency (top right) changes significantly**

p	**65**	**90**	**120**	**200**
65		0.1644	0.1164	0.0211*
90	0.0378*		0.9994	0.8490
120	0.0752	0.9825		0.8936
200	0.0158*	0.9964	0.9285	

Tukey HSD for all pairwise comparisons

***Post hoc* tests to situate when in time the standard deviation of syllable entropy changes significantly**

p	**65**	**90**	**120**	**200**
65		0.9689	0.2697	0.0027**
90			0.5357	0.0114*
120				0.2212
200				

Tukey HSD for all pairwise comparisons

Table 6-6: Main effects of age of the motif features

Main effect of age	***p***	***F***	
		(DFNum, DFDen)	***ratio***
Motif length	0.4681	(3,38.2)	0.8639
Sequence linearity	**0.0034**	**(3,38.4)**	**5.3970**
Sequence consistency	0.0772	(3,38.8)	2.4594
Sequence stereotypy	**0.0052**	**(3,38.4)**	**4.9704**
% Similarity	**0.0251**	**(3,37.0)**	**3.4890**
Accuracy	**0.0061**	**(3,37.2)**	**4.8329**
% Sequential	**0.0389**	**(3,36.8)**	**3.0887**
Pitch diff	0.6448	(3,37.1)	0.5600
FM diff	**0.0009**	**(3,37.0)**	**6.7656**
Entropy diff	**0.0223**	**(3,37.0)**	**3.5988**
Goodness diff	**0.0170**	**(3,37.1)**	**3.8507**
AM diff	0.5525	(3,37.0)	0.7096
Song density	**0.0011**	**(3,38.1)**	**6.5560**

Mixed model: Fixed factor: age; Random factor: subject; random slope: subject*age

***Post hoc* tests to situate when in time sequence linearity (bottom left) and sequence stereotypy (top right) change significantly**

p	**65**	**90**	**120**	**200**
65		0.7348	0.4061	0.0033**
90	0.9830		0.9568	0.0615
120	0.2276	0.4304		0.1632
200	0.0047*	0.0163*	0.3818	

Tukey HSD for all pairwise comparisons

***Post hoc* tests to situate when in time % similarity (bottom left) and accuracy (top right) change significantly**

p	**65**	**90**	**120**	**200**
65		0.1401	0.0549	0.0039**
90	0.4525		0.9897	0.5738
120	0.3610	0.9998		0.7295
200	0.0131*	0.4034	0.4030	

Tukey HSD for all pairwise comparisons

***Post hoc* tests to situate when in time % sequential (bottom left) and song density (top right) change significantly**

p	**65**	**90**	**120**	**200**
65		0.9771	0.7835	0.0017**
90	0.7755		0.9560	0.0071**
120	0.1032	0.5757		0.0229*
200	0.0486*	0.3828	0.9858	

Tukey HSD for all pairwise comparisons

Table 6-7: Number of syllables in the songs of tutees that received a high or low similarity score.

>75% similarity		**<75% similarity**	
Bird ID	Motif structure	Bird ID	Motif structure
17	ABCDEF	03	ABCD
18	ABCDEF	05	ABCD
20	ABCD	07	ABCDE
21	ABC	08	ABCDE
23	ABCD	09	ABCDE
31	ABC	10	ABCDE
		35	ABC

REFERENCES

1. Petkov, C.I. and E. Jarvis, *Birds, Primates and Spoken Language Origins: Behavioral Phenotypes and Neurobiological Substrates.* Frontiers in Evolutionary Neuroscience, 2012. **4**.
2. Bolhuis, J.J., K. Okanoya, and C. Scharff, *Twitter evolution: converging mechanisms in birdsong and human speech.* Nat Rev Neurosci, 2010. **11**(11): p. 747-759.
3. Doupe, A.J. and P.K. Kuhl, *BIRDSONG AND HUMAN SPEECH: Common Themes and Mechanisms.* Annual Review of Neuroscience, 1999. **22**(1): p. 567-631.
4. Brainard, M.S. and A.J. Doupe, *Translating Birdsong: Songbirds as a Model for Basic and Applied Medical Research.* Annual Review of Neuroscience, 2013. **36**(1): p. 489-517.
5. Tchernichovski, O., et al., *Dynamics of the Vocal Imitation Process: How a Zebra Finch Learns Its Song.* Science, 2001. **291**(5513): p. 2564-2569.
6. Moorman, S., et al., *Human-like brain hemispheric dominance in birdsong learning.* Proceedings of the National Academy of Sciences, 2012. **109**(31): p. 12782-12787.
7. London, S.E. and D.F. Clayton, *Functional identification of sensory mechanisms required for developmental song learning.* Nat Neurosci, 2008. **11**(5): p. 579-586.
8. Phan, M.L., C.L. Pytte, and D.S. Vicario, *Early auditory experience generates long-lasting memories that may subserve vocal learning in songbirds.* Proceedings of the National Academy of Sciences of the United States of America, 2006. **103**(4): p. 1088-1093.
9. Konishi, M., *The Role of Auditory Feedback in Birdsong.* Annals of the New York Academy of Sciences, 2004. **1016**(1): p. 463-475.
10. Sakata, J.T. and M.S. Brainard, *Real-Time Contributions of Auditory Feedback to Avian Vocal Motor Control.* The Journal of Neuroscience, 2006. **26**(38): p. 9619-9628.
11. Scharff, C. and F. Nottebohm, *A comparative study of the behavioral deficits following lesions of various parts of the zebra finch song system: implications for vocal learning.* The Journal of Neuroscience, 1991. **11**(9): p. 2896-2913.
12. Wild, J.M., *Neural pathways for the control of birdsong production.* Journal of Neurobiology, 1997. **33**(5): p. 653-670.
13. Wild, J.M., M.N. Williams, and R.A. Suthers, *Neural pathways for bilateral vocal control in songbirds.* The Journal of Comparative Neurology, 2000. **423**(3): p. 413-426.
14. Williams, H., *Birdsong and Singing Behavior.* Annals of the New York Academy of Sciences, 2004. **1016**(1): p. 1-30.
15. Brainard, M.S. and A.J. Doupe, *Postlearning Consolidation of Birdsong: Stabilizing Effects of Age and Anterior Forebrain Lesions.* The Journal of Neuroscience, 2001. **21**(7): p. 2501-2517.
16. James, L.S. and J.T. Sakata, *Vocal motor changes beyond the sensitive period for song plasticity.* Journal of Neurophysiology, 2014. **112**(9): p. 2040-2052.
17. Tumer, E.C. and M.S. Brainard, *Performance variability enables adaptive plasticity of 'crystallized' adult birdsong.* Nature, 2007. **450**: p. 1240.
18. Gogtay, N., et al., *Dynamic mapping of human cortical development during childhood through early adulthood.* Proceedings of the National Academy of Sciences of the United States of America, 2004. **101**(21): p. 8174-8179.
19. Giedd, J.N., et al., *Brain development during childhood and adolescence: a longitudinal MRI study.* Nat Neurosci, 1999. **2**(10): p. 861-863.
20. Lebel, C., S. Treit, and C. Beaulieu, *A review of diffusion MRI of typical white matter development from early childhood to young adulthood.* NMR in Biomedicine: p. e3778-n/a.
21. Raznahan, A., et al., *Longitudinal four-dimensional mapping of subcortical anatomy in human development.* Proceedings of the National Academy of Sciences of the United States of America, 2014. **111**(4): p. 1592-1597.

22. Zatorre, R.J., R.D. Fields, and H. Johansen-Berg, *Plasticity in Gray and White: Neuroimaging changes in brain structure during learning.* Nature neuroscience, 2012. **15**(4): p. 528-536.
23. Dayan, E. and Leonardo G. Cohen, *Neuroplasticity Subserving Motor Skill Learning.* Neuron, 2011. **72**(3): p. 443-454.
24. Sagi, Y., et al., *Learning in the Fast Lane: New Insights into Neuroplasticity.* Neuron, 2012. **73**(6): p. 1195-1203.
25. De Groof, G. and A. Van der Linden, *Love songs, bird brains and diffusion tensor imaging.* NMR in Biomedicine, 2010. **23**(7): p. 873-883.
26. Bredenkotter, M., J. Engelage, and H.-J. Bischof, *Visual system alterations in white zebra finches.* BRAIN BEHAVIOR AND EVOLUTION. **47**(1).
27. Jones, D.K., M.A. Horsfield, and A. Simmons, *Optimal strategies for measuring diffusion in anisotropic systems by magnetic resonance imaging.* Magnetic Resonance in Medicine, 1999. **42**(3): p. 515-525.
28. Ashburner, J., *A fast diffeomorphic image registration algorithm.* NeuroImage, 2007. **38**(1): p. 95-113.
29. Avants, B.B., et al., *A reproducible evaluation of ANTs similarity metric performance in brain image registration.* NeuroImage, 2011. **54**(3): p. 2033-2044.
30. Jenkinson, M., et al., *FSL.* NeuroImage, 2012. **62**(2): p. 782-790.
31. Ashburner, J. and G.R. Ridgway, *Symmetric Diffeomorphic Modeling of Longitudinal Structural MRI.* Frontiers in Neuroscience, 2012. **6**: p. 197.
32. Zhang, Y., M. Brady, and S. Smith, *Segmentation of brain MR images through a hidden Markov random field model and the expectation-maximization algorithm.* IEEE Transactions on Medical Imaging, 2001. **20**(1): p. 45-57.
33. Ashburner, J. and K.J. Friston, *Computing average shaped tissue probability templates.* NeuroImage, 2009. **45**(2): p. 333-341.
34. Tchernichovski, O., et al., *A procedure for an automated measurement of song similarity.* Animal Behaviour, 2000. **59**(6): p. 1167-1176.
35. Mahalanobis, P.C. *On the generalised distance in statistics*. in *Proceedings National Institute of Science, India*. 1936.
36. Nixdorf-Bergweiler, B.E., *Divergent and parallel development in volume sizes of telencephalic song nuclei in and female zebra finches.* The Journal of Comparative Neurology, 1996. **375**(3): p. 445-456.
37. Ashburner, J. and G.R. Ridgway, *Tensor-Based Morphometry A2 - Toga, Arthur W*, in *Brain Mapping*. 2015, Academic Press: Waltham. p. 383-394.
38. Bakdash, J.Z. and L.R. Marusich, *Repeated Measures Correlation.* Frontiers in Psychology, 2017. **8**: p. 456.
39. Karten, H.J., et al., *Digital Atlas of the Zebra Finch (Taeniopygia guttata) Brain: a High Resolution Photo Atlas.* The Journal of comparative neurology, 2013. **521**(16): p. 3702-3715.
40. De Groof, G., et al., *In vivo diffusion tensor imaging (DTI) of brain subdivisions and vocal pathways in songbirds.* NeuroImage, 2006. **29**(3): p. 754-763.
41. Pytte, C., et al., *Adult neurogenesis is associated with the maintenance of a stereotyped, learned motor behavior.* The Journal of neuroscience : the official journal of the Society for Neuroscience, 2012. **32**(20): p. 7052-7057.
42. Riebel, K., et al., *Sexual equality in zebra finch song preference: evidence for a dissociation between song recognition and production learning.* Proceedings of the Royal Society of London. Series B: Biological Sciences, 2002. **269**(1492): p. 729-733.
43. Bottjer, S.W. and A.P. Arnold, *DEVELOPMENTAL PLASTICITY IN NEURAL CIRCUITS FOR A LEARNED BEHAVIOR.* Annual Review of Neuroscience, 1997. **20**(1): p. 459-481.
44. Lenroot, R.K., et al., *Sexual dimorphism of brain developmental trajectories during childhood and adolescence.* NeuroImage, 2007. **36**(4): p. 1065-1073.

45. Group., B.D.C., *Total and Regional Brain Volumes in a Population-Based Normative Sample from 4 to 18 Years: The NIH MRI Study of Normal Brain Development.* Cerebral Cortex, 2012. **22**(1): p. 1-12.
46. Giedd, J.N., et al., *Child Psychiatry Branch of the National Institute of Mental Health Longitudinal Structural Magnetic Resonance Imaging Study of Human Brain Development.* Neuropsychopharmacology, 2014. **40**: p. 43.
47. Mills, K.L. and C.K. Tamnes, *Methods and considerations for longitudinal structural brain imaging analysis across development.* Developmental Cognitive Neuroscience, 2014. **9**(0): p. 172-190.
48. Morita, T., M. Asada, and E. Naito, *Contribution of Neuroimaging Studies to Understanding Development of Human Cognitive Brain Functions.* Frontiers in Human Neuroscience, 2016. **10**(464).
49. Chuang, N., et al., *An MRI-based atlas and database of the developing mouse brain.* NeuroImage, 2011. **54**(1): p. 80-89.
50. Hammelrath, L., et al., *Morphological maturation of the mouse brain: An in vivo MRI and histology investigation.* NeuroImage, 2016. **125**: p. 144-152.
51. Zhang, J., et al., *Mapping postnatal mouse brain development with diffusion tensor microimaging.* NeuroImage, 2005. **26**(4): p. 1042-1051.
52. Mengler, L., et al., *Brain maturation of the adolescent rat cortex and striatum: Changes in volume and myelination.* NeuroImage, 2014. **84**: p. 35-44.
53. Calabrese, E., et al., *A quantitative magnetic resonance histology atlas of postnatal rat brain development with regional estimates of growth and variability.* NeuroImage, 2013. **71**: p. 196-206.
54. Calabrese, E., G.A. Johnson, and C. Watson, *An ontology-based segmentation scheme for tracking postnatal changes in the developing rodent brain with MRI.* NeuroImage, 2013. **67**: p. 375-384.
55. Barnette, A.R., et al., *Characterization of Brain Development in the Ferret via Magnetic Resonance Imaging.* Pediatric Research, 2009. **66**(1): p. 80-84.
56. Rathjen, S., et al., *The growth of cat cerebral cortex in postnatal life: a magnetic resonance imaging study.* European Journal of Neuroscience, 2003. **18**(7): p. 1797-1806.
57. Leppert, I.R., et al., *T2 relaxometry of normal pediatric brain development.* Journal of Magnetic Resonance Imaging, 2009. **29**(2): p. 258-267.
58. Deoni, S.C.L., *Quantitative Relaxometry of the Brain.* Topics in Magnetic Resonance Imaging, 2010. **21**(2): p. 101-113 10.1097/RMR.0b013e31821e56d8.
59. Dubois, J., et al., *The early development of brain white matter: A review of imaging studies in fetuses, newborns and infants.* Neuroscience, 2014. **276**: p. 48-71.
60. Sowell, E.R., et al., *Longitudinal Mapping of Cortical Thickness and Brain Growth in Normal Children.* The Journal of Neuroscience, 2004. **24**(38): p. 8223-8231.
61. Blakemore, S.-J. and S. Choudhury, *Development of the adolescent brain: implications for executive function and social cognition.* Journal of Child Psychology and Psychiatry, 2006. **47**(3-4): p. 296-312.
62. Dubois, J., et al., *Asynchrony of the early maturation of white matter bundles in healthy infants: Quantitative landmarks revealed noninvasively by diffusion tensor imaging.* Human Brain Mapping, 2008. **29**(1): p. 14-27.
63. Sumiyoshi, A., H. Nonaka, and R. Kawashima, *Sexual differentiation of the adolescent rat brain: A longitudinal voxel-based morphometry study.* Neuroscience Letters, 2017. **642**(Supplement C): p. 168-173.
64. Uematsu, A., et al., *Mapping orbitofrontal-limbic maturation in non-human primates: A longitudinal magnetic resonance imaging study.* NeuroImage, 2017. **163**(Supplement C): p. 55-67.

65. Knudsen, E.I., *Sensitive Periods in the Development of the Brain and Behavior.* Journal of Cognitive Neuroscience, 2004. **16**(8): p. 1412-1425.
66. Bischof, H.-J. and J. Niemann, *Contralateral projections of the optic tectum in the zebra finch (Taenopygia guttata castanotis).* Cell and Tissue Research, 1990. **262**(2): p. 307-313.
67. Wild, J.M., *Convergence of somatosensory and auditory projections in the avian torus semicircularis, including the central auditory nucleus.* The Journal of Comparative Neurology, 1995. **358**(4): p. 465-486.
68. Wild, M.J., H.J. Karten, and B.J. Frost, *Connections of the auditory forebrain in the pigeon (columba livia).* The Journal of Comparative Neurology, 1993. **337**(1): p. 32-62.
69. Woolley, S.M.N. and J.H. Casseday, *Processing of Modulated Sounds in the Zebra Finch Auditory Midbrain: Responses to Noise, Frequency Sweeps, and Sinusoidal Amplitude Modulations.* Journal of Neurophysiology, 2005. **94**(2): p. 1143-1157.
70. Woolley, S.M.N., P.R. Gill, and F.E. Theunissen, *Stimulus-Dependent Auditory Tuning Results in Synchronous Population Coding of Vocalizations in the Songbird Midbrain.* The Journal of Neuroscience, 2006. **26**(9): p. 2499-2512.
71. Mello, C.V. and S. Ribeiro, *ZENK protein regulation by song in the brain of songbirds.* The Journal of Comparative Neurology, 1998. **393**(4): p. 426-438.
72. Holloway, C.C. and D.F. Clayton, *Estrogen synthesis in the male brain triggers development of the avian song control pathway in vitro.* Nat Neurosci, 2001. **4**(2): p. 170-175.
73. Konishi, M. and E. Akutagawa, *Neuronal growth, atrophy and death in a sexually dimorphic song nucleus in the zebra finch brain.* Nature, 1985. **315**(6015): p. 145-147.
74. MacDougall-Shackleton, S.A. and G.F. Ball, *Comparative studies of sex differences in the song-control system of songbirds.* Trends in Neurosciences, 1999. **22**(10): p. 432-436.
75. Bottjer, S.W., J.D. Brady, and B. Cribbs, *Connections of a motor cortical region in zebra finches: Relation to pathways for vocal learning.* The Journal of Comparative Neurology, 2000. **420**(2): p. 244-260.
76. Mandelblat-Cerf, Y., et al., *A role for descending auditory cortical projections in songbird vocal learning.* eLife, 2014. **3**: p. e02152.
77. Wild, J.M. and S.M. Farabaugh, *Organization of afferent and efferent projections of the nucleus basalis prosencephali in a passerine, Taeniopygia guttata.* The Journal of Comparative Neurology, 1996. **365**(2): p. 306-328.
78. Wild, J.M. and M.N. Williams, *Rostral Wulst in passerine birds. I. Origin, course, and terminations of an avian pyramidal tract.* The Journal of Comparative Neurology, 2000. **416**(4): p. 429-450.
79. Wild, J.M. and M.N. Williams, *Rostral wulst of passerine birds: II. Intratelencephalic projections to nuclei associated with the auditory and song systems.* The Journal of Comparative Neurology, 1999. **413**(4): p. 520-534.
80. Gao, W., et al., *Temporal and Spatial Development of Axonal Maturation and Myelination of White Matter in the Developing Brain.* American Journal of Neuroradiology, 2009. **30**(2): p. 290-296.
81. Huppi, P.S., et al., *Microstructural Development of Human Newborn Cerebral White Matter Assessed in Vivo by Diffusion Tensor Magnetic Resonance Imaging.* Pediatr Res, 1998. **44**(4): p. 584-590.
82. Löbel, U., et al., *Diffusion tensor imaging: the normal evolution of ADC, RA, FA, and eigenvalues studied in multiple anatomical regions of the brain.* Neuroradiology, 2009. **51**(4): p. 253-263.
83. Provenzale, J.M., et al., *Diffusion Tensor Imaging Assessment of Brain White Matter Maturation During the First Postnatal Year.* American Journal of Roentgenology, 2007. **189**(2): p. 476-486.

84. Yoshida, S., et al., *Diffusion tensor imaging of normal brain development.* Pediatric Radiology, 2013. **43**(1): p. 15-27.
85. Cascio, C.J., G. Gerig, and J. Piven, *Diffusion Tensor Imaging.* Journal of the American Academy of Child & Adolescent Psychiatry, 2007. **46**(2): p. 213-223.
86. Calabrese, E. and G.A. Johnson, *Diffusion tensor magnetic resonance histology reveals microstructural changes in the developing rat brain.* NeuroImage, 2013. **79**(Supplement C): p. 329-339.
87. Baratti, C., A.S. Barnett, and C. Pierpaoli, *Comparative MR Imaging Study of Brain Maturation in Kittens with T1, T2, and the Trace of the Diffusion Tensor.* Radiology, 1999. **210**(1): p. 133-142.
88. Wu, Y.-C., et al., *High b-value and diffusion tensor imaging in a canine model of dysmyelination and brain maturation.* NeuroImage, 2011. **58**(3): p. 829-837.
89. Nottebohm, F. and A. Arnold, *Sexual dimorphism in vocal control areas of the songbird brain.* Science, 1976. **194**(4261): p. 211-213.
90. McDonald, K.S. and J.R. Kirn, *Anatomical plasticity in the adult Zebra Finch song system.* The Journal of comparative neurology, 2012. **520**(16): p. 3673-3686.
91. Vates, G.E., et al., *Auditory pathways of caudal telencephalon and their relation to the song system of adult male zebra finches (Taenopygia guttata).* The Journal of Comparative Neurology, 1996. **366**(4): p. 613-642.
92. Akutagawa, E. and M. Konishi, *New brain pathways found in the vocal control system of a songbird.* The Journal of Comparative Neurology, 2010. **518**(15): p. 3086-3100.
93. Coleman, M.J., et al., *Thalamic Gating of Auditory Responses in Telencephalic Song Control Nuclei.* The Journal of Neuroscience, 2007. **27**(37): p. 10024-10036.
94. Lewandowski, B.C. and M. Schmidt, *Short Bouts of Vocalization Induce Long-Lasting Fast Gamma Oscillations in a Sensorimotor Nucleus.* The Journal of Neuroscience, 2011. **31**(39): p. 13936-13948.
95. Hahnloser, R.H.R. and M.S. Fee, *Sleep-Related Spike Bursts in HVC Are Driven by the Nucleus Interface of the Nidopallium.* Journal of Neurophysiology, 2007. **97**(1): p. 423-435.
96. Roberts, T.F., et al., *Motor circuits are required to encode a sensory model for imitative learning.* Nature Neuroscience, 2012. **15**: p. 1454.
97. Naie, K. and R.H.R. Hahnloser, *Regulation of learned vocal behavior by an auditory motor cortical nucleus in juvenile zebra finches.* Journal of Neurophysiology, 2011. **106**(1): p. 291-300.
98. Cardin, J.A., J.N. Raksin, and M.F. Schmidt, *Sensorimotor Nucleus Nif Is Necessary for Auditory Processing But Not Vocal Motor Output in the Avian Song System.* Journal of Neurophysiology, 2005. **93**(4): p. 2157-2166.
99. Lewandowski, B., et al., *At the interface of the auditory and vocal motor systems: Nif and its role in vocal processing, production and learning.* Journal of Physiology-Paris, 2013. **107**(3): p. 178-192.
100. Williams, H., et al., *Right-side dominance for song control in the zebra finch.* Journal of Neurobiology, 1992. **23**(8): p. 1006-1020.
101. Floody, O.R. and A.P. Arnold, *Song Lateralization in the Zebra Finch.* Hormones and Behavior, 1997. **31**(1): p. 25-34.
102. Goller, F. and B.G. Cooper, *Peripheral Motor Dynamics of Song Production in the Zebra Finch.* Annals of the New York Academy of Sciences, 2004. **1016**(1): p. 130-152.
103. Van der Linden, A., et al., *Non invasive in vivo anatomical studies of the oscine brain by high resolution MRI microscopy.* Journal of Neuroscience Methods, 1998. **81**(1–2): p. 45-52.
104. Saar, S., et al., *Developmental song learning in the zebra finch*, in *Neuroscience of birdsong.* 2008, Cambridge University Press: New York, NY, US. p. 217-227.

105. Takahashi, D.Y., et al., *The developmental dynamics of marmoset monkey vocal production.* Science, 2015. **349**(6249): p. 734-738.
106. Ravbar, P., et al., *Vocal Exploration Is Locally Regulated during Song Learning.* The Journal of Neuroscience, 2012. **32**(10): p. 3422-3432.
107. Tchernichovski, O., et al., *Studying the Song Development Process: Rationale and Methods.* Annals of the New York Academy of Sciences, 2004. **1016**(1): p. 348-363.
108. Glaze, C.M. and T.W. Troyer, *Development of temporal structure in zebra finch song.* Journal of Neurophysiology, 2013. **109**(4): p. 1025-1035.
109. Pytte, C.L., et al., *Increasing stereotypy in adult zebra finch song correlates with a declining rate of adult neurogenesis.* Developmental Neurobiology, 2007. **67**(13): p. 1699-1720.
110. Brainard, M.S. and A.J. Doupe, *What songbirds teach us about learning.* Nature, 2002. **417**(6886): p. 351-358.
111. Konishi, M., *Birdsong: From Behavior to Neuron.* Annual Review of Neuroscience, 1985. **8**(1): p. 125-170.
112. Derégnaucourt, S. and M. Gahr, *Horizontal transmission of the father's song in the zebra finch (Taeniopygia guttata).* Biology Letters, 2013. **9**(4): p. 20130247.
113. Derégnaucourt, S., et al., *How sleep affects the developmental learning of bird song.* Nature, 2005. **433**: p. 710.
114. Funabiki, Y. and M. Konishi, *Long Memory in Song Learning by Zebra Finches.* The Journal of Neuroscience, 2003. **23**(17): p. 6928-6935.
115. Ali, F., et al., *The basal ganglia is necessary for learning spectral, but not temporal features of birdsong.* Neuron, 2013. **80**(2): p. 494-506.
116. Andalman, A.S. and M.S. Fee, *A basal ganglia-forebrain circuit in the songbird biases motor output to avoid vocal errors.* Proceedings of the National Academy of Sciences, 2009. **106**(30): p. 12518-12523.
117. Sober, S.J. and M.S. Brainard, *Adult birdsong is actively maintained by error correction.* Nature Neuroscience, 2009. **12**: p. 927.
118. Cynx, J. and U. von Rad, *Immediate and transitory effects of delayed auditory feedback on bird song production.* Animal Behaviour, 2001. **62**(2): p. 305-312.
119. Canopoli, A., J.A. Herbst, and R.H.R. Hahnloser, *A Higher Sensory Brain Region Is Involved in Reversing Reinforcement-Induced Vocal Changes in a Songbird.* The Journal of Neuroscience, 2014. **34**(20): p. 7018-7026.
120. Lombardino, A.J. and F. Nottebohm, *Age at Deafening Affects the Stability of Learned Song in Adult Male Zebra Finches.* The Journal of Neuroscience, 2000. **20**(13): p. 5054-5064.
121. Bolhuis, J.J. and M. Gahr, *Neural mechanisms of birdsong memory.* Nature Reviews Neuroscience, 2006. **7**: p. 347.
122. The Avian Brain Nomenclature, C., *Avian brains and a new understanding of vertebrate brain evolution.* Nature reviews. Neuroscience, 2005. **6**(2): p. 151-159.
123. Fortune, E.S. and D. Margoliash, *Cytoarchitectonic organization and morphology of cells of the field L complex in male zebra finches (taenopygia guttata).* The Journal of Comparative Neurology, 1992. **325**(3): p. 388-404.
124. Bauer, E.E., et al., *A Synaptic Basis for Auditory–Vocal Integration in the Songbird.* The Journal of Neuroscience, 2008. **28**(6): p. 1509-1522.
125. Shaevitz, S.S. and F.E. Theunissen, *Functional Connectivity Between Auditory Areas Field L and CLM and Song System Nucleus HVC in Anesthetized Zebra Finches.* Journal of Neurophysiology, 2007. **98**(5): p. 2747-2764.
126. Fortune, E.S. and D. Margoliash, *Parallel pathways and convergence onto HVc and adjacent neostriatum of adult zebra finches (Taeniopygia guttata).* The Journal of Comparative Neurology, 1995. **360**(3): p. 413-441.

127. Mello, C.V., D.S. Vicario, and D.F. Clayton, *Song presentation induces gene expression in the songbird forebrain.* Proceedings of the National Academy of Sciences of the United States of America, 1992. **89**(15): p. 6818-6822.
128. Mello, C., F. Nottebohm, and D. Clayton, *Repeated exposure to one song leads to a rapid and persistent decline in an immediate early gene's response to that song in zebra finch telencephalon.* The Journal of Neuroscience, 1995. **15**(10): p. 6919-6925.
129. Chew, S.J., et al., *Decrements in auditory responses to a repeated conspecific song are long-lasting and require two periods of protein synthesis in the songbird forebrain.* Proceedings of the National Academy of Sciences of the United States of America, 1995. **92**(8): p. 3406-3410.
130. Ahmadiantehrani, S. and S.E. London, *Bidirectional manipulation of mTOR signaling disrupts socially mediated vocal learning in juvenile songbirds.* Proceedings of the National Academy of Sciences, 2017. **114**(35): p. 9463-9468.
131. Bolhuis, J.J., et al., *Localized neuronal activation in the zebra finch brain is related to the strength of song learning.* Proceedings of the National Academy of Sciences of the United States of America, 2000. **97**(5): p. 2282-2285.
132. Bolhuis, J.J., et al., *Localized immediate early gene expression related to the strength of song learning in socially reared zebra finches.* European Journal of Neuroscience, 2001. **13**(11): p. 2165-2170.
133. Terpstra, N.J., J.J. Bolhuis, and A.M. den Boer-Visser, *An Analysis of the Neural Representation of Birdsong Memory.* The Journal of Neuroscience, 2004. **24**(21): p. 4971-4977.
134. van der Kant, A., et al., *Representation of Early Sensory Experience in the Adult Auditory Midbrain: Implications for Vocal Learning.* PLoS ONE, 2013. **8**(4): p. e61764.
135. Gobes, S.M.H. and J.J. Bolhuis, *Birdsong Memory: A Neural Dissociation between Song Recognition and Production.* Current Biology, 2007. **17**(9): p. 789-793.
136. Moorman, S., et al., *Learning-related brain hemispheric dominance in sleeping songbirds.* Scientific Reports, 2015. **5**: p. 9041.
137. Guzowski, J.F., *Insights into immediate-early gene function in hippocampal memory consolidation using antisense oligonucleotide and fluorescent imaging approaches.* Hippocampus, 2002. **12**(1): p. 86-104.
138. Guzowski, J.F., et al., *Mapping behaviorally relevant neural circuits with immediate-early gene expression.* Current Opinion in Neurobiology, 2005. **15**(5): p. 599-606.
139. Yang, G., F. Pan, and W.-B. Gan, *Stably maintained dendritic spines are associated with lifelong memories.* Nature, 2009. **462**: p. 920.
140. Roberts, T.F., et al., *Rapid spine stabilization and synaptic enhancement at the onset of behavioural learning.* Nature, 2010. **463**: p. 948.
141. Feenders, G., et al., *Molecular Mapping of Movement-Associated Areas in the Avian Brain: A Motor Theory for Vocal Learning Origin.* PLOS ONE, 2008. **3**(3): p. e1768.
142. Amin, N., J.A. Grace, and F.E. Theunissen, *Neural response to bird's own song and tutor song in the zebra finch field L and caudal mesopallium.* Journal of Comparative Physiology A, 2004. **190**(6): p. 469-489.
143. Keller, G.B. and R.H.R. Hahnloser, *Neural processing of auditory feedback during vocal practice in a songbird.* Nature, 2008. **457**: p. 187.
144. Nottebohm, F., J.A. Paton, and D.B. Kelley, *Connections of vocal control nuclei in the canary telencephalon.* The Journal of Comparative Neurology, 1982. **207**(4): p. 344-357.
145. Jarvis, E.D. and F. Nottebohm, *Motor-driven gene expression.* Proceedings of the National Academy of Sciences, 1997. **94**(8): p. 4097-4102.
146. Roberts, T.F., et al., *Identification of a motor-to-auditory pathway important for vocal learning.* Nature Neuroscience, 2017. **20**: p. 978.

147. Sampaio-Baptista, C., et al., *Gray matter volume is associated with rate of subsequent skill learning after a long term training intervention.* NeuroImage, 2014. **96**(0): p. 158-166.
148. Gryga, M., et al., *Bidirectional gray matter changes after complex motor skill learning.* Frontiers in Systems Neuroscience, 2012. **6**: p. 37.
149. Li, R. and H. Sakaguchi, *Cholinergic innervation of the song control nuclei by the ventral paleostriatum in the zebra finch: a double-labeling study with retrograde fluorescent tracers and choline acetyltransferase immunohistochemistry.* Brain Research, 1997. **763**(2): p. 239-246.
150. Ballinger, Elizabeth C., et al., *Basal Forebrain Cholinergic Circuits and Signaling in Cognition and Cognitive Decline.* Neuron, 2016. **91**(6): p. 1199-1218.
151. Liu, R., et al., *Intermittent Stimulation of the Nucleus Basalis of Meynert Improves Working Memory in Adult Monkeys.* Current Biology, 2017. **27**(17): p. 2640-2646.e4.
152. Li, R., M.-X. Zuo, and H. Sakaguchi, *Auditory-vocal cholinergic pathway in zebra finch brain.* NeuroReport, 1999. **10**(1): p. 165-169.
153. Shea, S.D. and D. Margoliash, *Basal Forebrain Cholinergic Modulation of Auditory Activity in the Zebra Finch Song System.* Neuron, 2003. **40**(6): p. 1213-1226.
154. Rauske, P.L., S.D. Shea, and D. Margoliash, *State and Neuronal Class-Dependent Reconfiguration in the Avian Song System.* Journal of Neurophysiology, 2003. **89**(3): p. 1688-1701.
155. Atherton, L.A., D. Dupret, and J.R. Mellor, *Memory trace replay: the shaping of memory consolidation by neuromodulation.* Trends in Neurosciences, 2015. **38**(9): p. 560-570.
156. Brawn, T.P. and D. Margoliash, *A Bird's Eye View of Sleep-Dependent Memory Consolidation*, in *Sleep, Neuronal Plasticity and Brain Function*, P. Meerlo, R.M. Benca, and T. Abel, Editors. 2015, Springer Berlin Heidelberg: Berlin, Heidelberg. p. 207-237.
157. Shea, S.D. and D. Margoliash, *Behavioral state-dependent reconfiguration of song-related network activity and cholinergic systems.* Journal of Chemical Neuroanatomy, 2010. **39**(2): p. 132-140.
158. Nixdorf-Bergweiler, B. and H.-J. Bischof, *Atlas Of The Brain Of The Zebra Finch, Taeniopygia Guttata: With Special Emphasis On Telencephalic Visual And Song System Nuclei in Transverse and Sagittal Sections*, ed. N.C.f.B.I. (US). 2007.
159. Wild, J.M., *Functional Neuroanatomy of the Sensorimotor Control of Singing.* Annals of the New York Academy of Sciences, 2004. **1016**(1): p. 438-462.
160. Striedter, G.F., *The vocal control pathways in budgerigars differ from those in songbirds.* The Journal of Comparative Neurology, 1994. **343**(1): p. 35-56.
161. Wild, J.M. and N.E.O. Krützfeldt, *Trigeminal and Telencephalic Projections to Jaw and Other Upper Vocal Tract Premotor Neurons in Songbirds: Sensorimotor Circuitry for Beak Movements During Singing.* The Journal of comparative neurology, 2012. **520**(3): p. 590-605.
162. Ito, T., M. Tiede, and D.J. Ostry, *Somatosensory function in speech perception.* Proceedings of the National Academy of Sciences, 2009. **106**(4): p. 1245-1248.
163. Bottjer, S.W. and M. To, *Afferents from Vocal Motor and Respiratory Effectors Are Recruited during Vocal Production in Juvenile Songbirds.* The Journal of Neuroscience, 2012. **32**(32): p. 10895-10906.
164. Hoese, W.J., et al., *Vocal tract function in birdsong production: experimental manipulation of beak movements.* Journal of Experimental Biology, 2000. **203**(12): p. 1845-1855.
165. Williams, H., *Choreography of song, dance and beak movements in the zebra finch (Taeniopygia guttata).* Journal of Experimental Biology, 2001. **204**(20): p. 3497-3506.
166. Johansen-Berg, H., *Behavioural relevance of variation in white matter microstructure.* Current Opinion in Neurology, 2010. **23**(4): p. 351-358.

167. Avants, B.B., et al., *Symmetric diffeomorphic image registration with cross-correlation: Evaluating automated labeling of elderly and neurodegenerative brain.* Medical Image Analysis, 2008. **12**(1): p. 26-41.
168. Klein, A., et al., *Evaluation of 14 nonlinear deformation algorithms applied to human brain MRI registration.* NeuroImage, 2009. **46**(3): p. 786-802.
169. Galbraith, S., J. Bowden, and A. Mander, *Accelerated longitudinal designs: An overview of modelling, power, costs and handling missing data.* Statistical Methods in Medical Research, 2017. **26**(1): p. 374-398.
170. Evans, A.C., *The NIH MRI study of normal brain development.* NeuroImage, 2006. **30**(1): p. 184-202.
171. Ziegler, G., et al., *Multivariate dynamical modelling of structural change during development.* NeuroImage, 2017. **147**: p. 746-762.
172. Kulikova, S., et al., *Multi-parametric evaluation of the white matter maturation.* Brain Structure and Function, 2015. **220**(6): p. 3657-3672.
173. Sadeghi, N., et al., *Regional characterization of longitudinal DT-MRI to study white matter maturation of the early developing brain.* NeuroImage, 2013. **68**: p. 236-247.
174. Prastawa, M., et al., *A NEW FRAMEWORK FOR ANALYZING WHITE MATTER MATURATION IN EARLY BRAIN DEVELOPMENT.* Proceedings / IEEE International Symposium on Biomedical Imaging: from nano to macro. IEEE International Symposium on Biomedical Imaging, 2010: p. 97-100.
175. Khundrakpam, B.S., et al., *Developmental Changes in Organization of Structural Brain Networks.* Cerebral Cortex (New York, NY), 2013. **23**(9): p. 2072-2085.

Chapter 7

Image-guided discoveries of cerebellar remodelling upon lesioning the cortico-basal ganglia-thalamo-cortical loop in control of learned vocal communication

This study was performed in collaboration with Dr Kristina Lukacova and Dr Lubica Kubikova from the Centre of Biosciences, Institute of Animal Biochemistry and Genetics, Slovak Academy of Sciences. This chapter is based on:

Hamaide J*, Lukacova K*, Van Audekerke J, Verhoye M, Kubikova L, Van der Linden A. *Neuroplasticity in the cerebello-thalamo-basal ganglia pathway: a longitudinal* in vivo *MRI study in male songbirds*. Under review at NeuroImage. (* equal contribution)

ABSTRACT

Like humans, new neurons are continuously added to the avian striatum, including Area X, even in adulthood. Furthermore, compelling evidence points towards upregulated rates of migration of progenitor cells upon neurotoxic lesioning to Area X, and, in the longer term, these progenitor cells differentiate into neurons that become functionally active while singing undirected song. This underscores the extraordinary capacity of the songbird brain to recuperate from brain injury. The timing by which these new neurons re-establish the connection to its efferent target, i.e. the medial part of the dorsolateral nucleus of the anterior thalamus (DLM), and whether other components of the song control circuitry are affected by structural neuroplastic adaptations, remains unknown. Consequently, this study sought to clarify the re-establishment of the pathway connecting Area X and DLM upon neurotoxic lesioning, and explore whether alterations of the song can be linked to the occurrence of structural neuroplastic events. We observed relative volume changes in the medial striatum adjacent to the lesion site. Interestingly, the timing of the relative volume changes coincided with previously reported increases in the migration of neural progenitor cells. Furthermore, voxel-wise statistical analyses showed structural alterations in the dorsal thalamic zone, including DLM, and in the deep cerebellar nuclei occurring within the first two months after lesioning. Correlating song performance with the diffusion metrics revealed relationships with motif length in several brain regions previously linked to song control.

7.1 INTRODUCTION

While nearly all vertebrate species are able to vocalize, only few species, including humans and songbirds, communicate through acoustically complex socially-learned vocalizations [1, 2]. Both speech and song are highly complex and rapid motor behaviours, driven by a sharply tuned vocal motor apparatus that enables adaptation of the temporal and spectral content of sounds to result in complex communication signals. Based on molecular genetics, neurophysiology and behavioural studies, songbirds –especially zebra finches– are currently regarded as a valuable model to study aspects of human speech learning in a laboratory setting [3, 4]. Opposed to humans, zebra finches learn to produce only one song which –in normal circumstances– will remain unchanged throughout their life.

Despite fundamental differences in the overall organization of the songbird brain, convincing parallels exist in the brain networks supporting acquired vocal behaviour [5]. Like human speech, bird song production relies on cortical areas [6] and on a cortico-basal ganglia-thalamic-cortical (C-BG-T-C) loop (Figure 7-2-A) that enables trial-and-error vocal exploration during vocal learning and contributes to song maintenance in adulthood [7-9]. In songbirds, the cortical pathway directly responsible for the motor aspect of song production is termed the posterior motor pathway (PMP) and consists of a direct connection between premotor nucleus HVC (abbreviation used as a proper name; [10]; Figure 7-2-A) and the robust nucleus of the arcopallium (RA), avian analogue of the mammalian (laryngeal) motor cortex [11]. RA ultimately connects to brain stem nuclei that innervate the vocal motor neurons [12] and respiratory centres [13]. The C-BG-T-C loop or anterior forebrain pathway (AFP) originates in HVC from where it projects to Area X, a large brain region that is functionally and structurally similar to the mammalian basal ganglia and contains striatal- and pallidal-like neurons [14, 15]. The pallidal neurons of Area X course to the dorsolateral nucleus of the medial part of the anterior thalamus (DLM), which in turn sends projections to the lateral magnocellular nucleus of the anterior nidopallium (LMAN), a frontal cortical nucleus. Lastly, LMAN sends recurrent projections directly to Area X and an axon collateral to the final target of the AFP, nucleus RA [16, 17]. Compelling evidence suggests similarity between the cortical areas HVC and LMAN and Broca's area in humans [2, 11, 18]. In humans, a second subcortical pathway has been identified that supports an important role in vocal learning and vocal motor control, i.e. cerebro-

cerebellar motor loop [19]. To date, only limited evidence points towards a functionally similar avian counterpart [14, 20].

Both in humans and songbirds, new-born neurons migrate to the striatum in normal circumstances [21-24]. Disruption of the C-BG-T-C loop in adult songbirds, by neurotoxic or electrolytic lesioning of Area X, does not affect the overall structure of their song [9], but is capable of inducing alterations to song tempo or transient stuttering-like song [25]. The change in behaviour is mirrored by a massive upregulation of proliferation and migration of progenitor cells in and near the lesioned area [25]. Structural and functional neuroplastic changes have been described along the C-BG-T-C loop, including the loss of Area X-originating DLM axonal terminal fields throughout the first 3-4 days after neurotoxic lesion [26, 27], and altered singing-induced gene expression in the downstream motor cortex region RA, the final target of the AFP [25]. Together, these data suggest that neurotoxic disengagement of one song control system component affects the other constituents of the same circuitry and results in aberrant vocal motor performance. However, several questions still remain unanswered. Do structural alterations induced by the neurotoxic lesion extend beyond DLM, the first downstream target of Area X, propagate upstream to the cortical premotor area HVC or maybe even affect remote areas that are not part of the song control system? Can we establish links between song performance and the structural micro-architecture of specific anatomical areas?

We sought to address these questions by designing a longitudinal study using *in vivo* imaging tools. We first explored the use of Manganese-enhanced MRI (MEMRI) to map the re-establishment of the Area X-DLM connection *in vivo*. The results are outlined in the first subsection immediately following this Introduction. As we could not detect any difference in manganese (Mn^{2+}) accumulation in DLM between control and Area X-lesioned birds, we opted to discontinue the MEMRI and continued exploring structural neuroplasticity following neurotoxic lesioning of Area X using two complementary *in vivo* Magnetic Resonance-based imaging tools i.e. 3D anatomical scans and Diffusion Tensor Imaging (DTI), similar to Chapter 5. Even though DTI is less sensitive compared to MEMRI to detect alterations in brain connectivity, DTI and 3D anatomical scans present an advantage over MEMRI as they allow to assess structural brain changes without administration of contrast agents. This enabled us to extend the initial hypothesis by also exploring structural neuroplastic events taking place remote to Area X and DLM. MRI data were acquired before and at five time points after introducing a

neurotoxic lesion in Area X, i.e. 2 weeks, 1 month, 2 months, 3 months and 4 months after surgery. Following each MR experiment, the songs of the birds were recorded to evaluate possible changes in song features over time and to explore possible correlations with microstructural tissue properties. The 3D anatomical scans were processed for Deformation-based Morphometry (DBM) that provides a quantitative readout for localised relative volume changes (based on the jacobian determinants), while the DTI data informs on possible changes in microstructural tissue properties deduced from alterations in the local diffusion profiles of water molecules within a voxel. Both MR modalities were prepared for voxel-wise statistical testing which enables exploring the entire brain without *a priori* selection of Regions-of-Interest (ROIs). The results of the longitudinal follow-up are described in subsection 2 of this chapter.

SUBSECTION 1: PILOT STUDY: Manganese-enhanced MRI to trace the re-establishment of the Area X-DLM connection

One of the principle aims of this study was to evaluate the de- and regeneration of the Area X-DLM connection that occurs during the first months following a neurotoxic lesion to Area X. To this end, we designed a longitudinal MRI experiment using Manganese-enhanced MRI (MEMRI). Chapter 2 of this thesis covers the theoretical background of this MRI technique. In brief, manganese dichloride ($MnCl_2$) is an MR contrast agent that holds two very important characteristics: (1) it is a Ca^{2+} analogue and (2) it is paramagnetic. The first makes that Mn^{2+} can make use of Ca^{2+} transport mechanisms including Ca^{2+} channels. Consequently, Mn^{2+} can travel within cells but can also pass synapses and proceed to and within neighbouring neurons. The second property implies that Mn^{2+} markedly shortens the T_1 relaxation time resulting in local image hyper- or hypo-intensities (depending on the MR image contrast settings). In conclusion, $MnCl_2$ can serve as an MR contrast agent that can be employed for *in vivo* tract tracing experiments.

We hypothesised that upon neurotoxic lesioning, the Area X-DLM connection would first degenerate [26] after which over the course of several months the connection would re-establish. To trace these processes, we planned to acquire MEMRI data at baseline and at several time points up to 4 months after neurotoxic lesioning. In addition, by analysing the songs of the birds, we would be able to link the re-establishment of the connection with

changes in song performance. Even though MEMRI had been used very extensively by the Bio-Imaging lab in the past (examples in Chapter 4), the protocol had to be optimized for this new application.

7.1.1 Optimisation: in vivo visualisation of the Area X-DLM connection

To enable detecting subtle differences that might characterise the process of re-generation, we opted for dynamic MEMRI measurements, i.e. at least one scan every 15 minutes. These dynamic measurements would allow to map the arrival and rate of uptake of Mn^{2+} in the target area (DLM) after injection into Area X. We opted for an inversion recovery (IR) sequence as Tindemans et al. (2006) stated that IR is more sensitive compared to more conventional T_1-weighted pulse sequences, which makes that lower doses of $MnCl_2$ result in sufficient image contrast [28]. This is important as high levels of $MnCl_2$ are neurotoxic, which might interfere with the regeneration process (considering the repeated administration of $MnCl_2$ in a longitudinal study).

Besides the pulse sequence, the route of administration, the dose (volume and concentration) of $MnCl_2$ had to be optimised. The first tests were based on previous descriptions [28-31] and included unilateral injections of $MnCl_2$ in Area X. The injection procedure was based on the expertise of Dr Lukacova and Dr Kubikova in performing stereotactic injections in Area X [25, 27, 32, 33]. We tested different volumes (13.8 nl, 23 nl and 46 nl) and concentrations (10, 50, 100 mM) of $MnCl_2$. The optimal dosage had to meet the following criteria: (i) as low as possible to avoid neurotoxicity which was evaluated by closely monitoring the animals' behaviour the first days following the imaging session, and to avoid excessive shortening of T_2-relaxation in the surroundings of the injection site ('blooming effect'), (ii) limited diffusion of $MnCl_2$ to neighbouring tissue, and (iii) successful visualisation of the efferent (downstream) nuclei. An example of MEMRI images obtained after unilateral injection of $MnCl_2$ in Area X can be found in Figure 7-1.

The final protocol consisted of injecting 23 nl of 50 mM $MnCl_2$ in Area X, which resulted in optimal image contrast differences in DLM 3 h after injection, using inversion times (TI): 500 ms and 1000 ms.

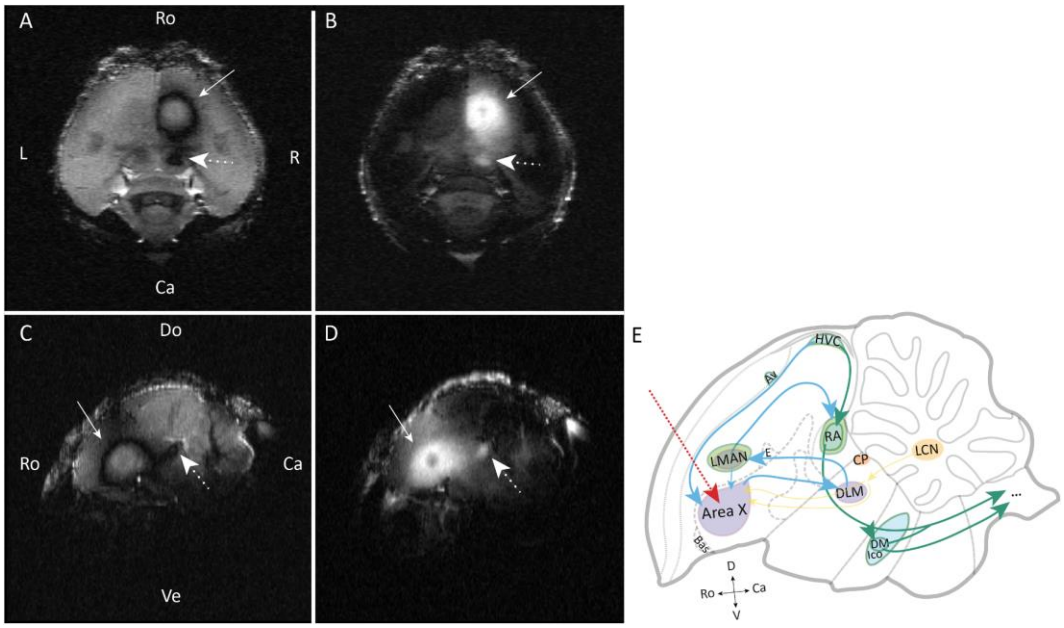

Figure 7-1: Overview of MEMRI images obtained in an adult male zebra finch 24 hours after a unilateral injection of $MnCl_2$ (23nl 100mM) into Area X. Panel **A-C** and **B-D** include IR MR-images obtained with TI = 500 ms and TI = 1000 ms, respectively, panel E provides a schematic view of the song control circuitry in an adult male zebra finch brain where the red arrow indicates the path taken by the needle to inject $MnCl_2$ or ibotenic acid. In panel A-D, Area X is indicated by the white (solid) arrow, its downstream target DLM by the white dotted arrow. The bird received a unilateral injection of $MnCl_2$, the contralateral hemisphere is a control as no interhemispheric projections from Area X to DLM have been described. The hyper-intense (bright) signal on the right and the hypo-intense (dark) signal on the left panels are induced by the presence of Mn^{2+}. Abbreviations: Ro: rostral; Ca: caudal; L: left; R: right; Do: dorsal; Ve: ventral.

7.1.2 Proof-of-principle test

We tested the optimised protocol 5 days after inducing a bilateral neurotoxic lesion in Area X. Unexpectedly, we observed a change in signal intensity in DLM over time, indicating that $MnCl_2$ was still transported from Area X or the damaged medial striatum, to DLM. These observations suggest that $MnCl_2$ (i) might be transported by a few neurons that survived the ibotenic acid treatment, or alternatively, (ii) might be picked up by the Area X surrounding tissue (medial striatum) and carried to the DLM area via either direct or indirect projections [14, 34]. In an attempt to prevent possible contamination of $MnCl_2$ to the Area X surrounding medial striatum, we tried to inject $MnCl_2$ into HVC, upstream to Area X, and follow its dynamic transport to DLM. HVC is smaller than Area X, therefore, after determination of the proper dosage of $MnCl_2$ (13.8 nl at 100 mM), we injected the contrast agent one and two month(s) after unilateral lesioning

of Area X. In both cases, we observed the accumulation of $MnCl_2$ in the ipsilateral DLM 9 h after injection of $MnCl_2$.

Based on these findings, we concluded that targeted MEMRI is not a suitable technique as it lacks the required specificity to trace structural neuroplastic events affecting exclusively the Area X-DLM pathway upon neurotoxic injury to Area X.

SUBSECTION 2: LONGITUDINAL STUDY: Brain-wide mapping of structural neuroplasticity following brain lesion using DTI and 3D anatomical scans

7.2 MATERIALS AND METHODS

7.2.1 Animals and Ethical statement

Adult male zebra finches (*Taeniopygia guttata*; n=14; age > 200 days post hatching (dph)) bred in the animal facility of the Slovak Academy of Sciences or the University of Antwerp, participated to the study. Except during the song recordings, the birds were group-housed in large indoor aviaries, on a 12h/12h light/dark cycle with food and water available *ad libitum* at all times. All experimental procedures were reviewed and approved by the State Veterinary and Food Administration of the Slovak Republic (permit number: 3569/16-221) and the Committee of Animal Care and Use at the University of Antwerp, Belgium (permit number: 2015-03).

7.2.2 Study design

A detailed overview of the study design can be found in Figure 7-2-B. The neurotoxic lesion consisted of a stereotaxic injection of ibotenic acid in Area X of both hemispheres. This neurotoxic compound causes neural cell death by over-excitation, while keeping the surrounding tissue –extracellular matrix and passing nerve terminals from extrinsic origin– unaffected [35]. Since T2-weighted MRI images are used to locate oedema in the brain, we verified the location of the lesion based on a hyper-intense (bright) signal indicative of oedema, 2 days after surgery. Following each MR experiment, the songs of the birds were recorded and analysed.

MRI data, i.e. DTI and 3D scans, were acquired before and at five time points after introducing a neurotoxic lesion in Area X, i.e. 2 weeks, 1 month, 2 months, 3 months and 4 months after

surgery. All MRI data were prepared for voxel-wise statistical testing which enables unbiased data-based detection of areas that display structural changes in the entire brain without *a priori* selection of Regions-of-Interest (ROIs). We designed voxel-wise statistical tests that inform on potential changes in tissue volume (3D) or intrinsic properties (DTI) over time or that explore potential correlations between song performance and the structural properties of the zebra finch brain.

7.2.3 Stereotactic surgery

The induction of the bilateral neurotoxic lesion was performed similar to previously described protocols [25, 32, 33]. In brief, the birds were anaesthetized by inhalation of isoflurane in a mixture of oxygen and nitrogen (induction: 2.5 %; maintenance: 1.5-2.5 %; IsoFlo®, Abbott, Illinois, USA). After localizing the zero-point, i.e. a midsagittal landmark that defines the transition between the cerebrum and the cerebellum, we navigated a glass micropipette to the centre of Area X at the following coordinates: 4.5-5 mm rostral, 1.3 mm lateral (to both left and right hemisphere) and 3.5 mm ventral. The injector was placed at a 20° angle so as to prevent traversing LMAN while inserting the needle. Each Area X received three injections of 46 µl ibotenic acid (total volume 138 µl per hemisphere; 1%; pH 7.3-7.6; Tocris Bioscience UK), administered approximately 2 minutes apart using the Nanoject II injector (Drummond Scientific, USA). After the last injection, the needle was left in place for approximately 5 min to minimize possible back-flow along the path of the needle, after which the injector was retracted gently. When all injections were successfully performed, the skin was glued together and mesocaine gel was applied. All birds were monitored until full recovery.

7.2.4 Song recordings and analyses

The songs of the birds were recorded in sound attenuating chambers via the automated song detection setup implemented in Sound Analysis Pro (SAP) software version 2011.104 ([36]; http://soundanalysispro.com/). Only during song recordings, the birds were housed solitary and all recordings contain exclusively undirected songs (not directed to a female zebra finch). As song tempo changes over the course of a day [37], we examined the first 25 song motifs sung after initiation of the photophase. To be able to compare the song tempo, only the same sequence of syllables within a motif in the same bird were selected for the analyses, i.e. only motifs containing the same number of syllables (ABCD) were measured even if the bird sometimes sang a syllable more (ABCDE) or less (ABC; Figure 7-2-C). Introductory notes and

calls were omitted from all analyses. First, motif duration was quantified, defined by respectively the duration of one song motif visible on the sound spectrogram. Next, individual syllables were segmented based on sharp changes in amplitude and Wiener entropy visible on the sound spectrogram and the duration of the syllables and inter-syllable intervals, i.e. time period in between two consecutive syllables, was measured.

To investigate whether certain syllable types respond differently after surgery, two independent researchers categorized each syllable based on visual inspection of the sound spectrograms obtained at baseline. Syllable categorisation was performed in accordance with criteria defined by Sturdy et al. [38], and include short slide notes, high notes, flat notes, slide notes, combination notes, unclassified notes and unreadable notes.

7.2.5 MRI data acquisition

All MRI experiments were executed on a 7T horizontal small animal scanner (PharmaScan 70/16 US, Bruker BioSpin GmbH, Germany), equipped with the standard setup including a quadrature transmit volume coil, a linear array coil designed for mice and a 400 mT/m gradient insert (Bruker BioSpin, Germany). To minimize stress and movement during acquisition, the birds were anaesthetized with isoflurane in a mixture of oxygen and nitrogen (induction: 2.5%; maintenance: 1.3-1.7%; IsoFlo®, Abbott, Illinois, USA). Throughout the entire imaging session, the bird's breathing rate was monitored using a pressure-sensitive pad positioned under the chest of the animals, and body temperature was maintained within narrow physiological levels (40.0 ± 0.2°C) by means of a cloacal thermistor probe connected to a warm-air feedback system (SA instruments, Inc.). To enable consistent head positioning over different imaging sessions, the birds were placed in an MR-compatible, custom-build stereotactic scanner bed.

After obtaining piloting scans, a field map was acquired to measure local inhomogeneities in the magnetic field which aided subsequent local shimming procedures. Next, the DTI data were collected using a diffusion-weighted spin echo (SE) echo planar imaging (EPI) pulse sequence with the following imaging parameters: TE 22 ms, TR 7000 ms, FOV (20x15) mm^2, acquisition matrix (105x79), in-plane resolution (0.19x0.19) mm^2, slice thickness 0.24 mm, 28 horizontal slices, b-value 670 s/mm^2, diffusion gradient duration (δ) 4 ms, diffusion gradient separation (Δ) 12 ms. A total of 21 b_0 images and 60 unique diffusion gradient directions were sampled in three scans of 12 min each (7 b_0 and 20 diffusion-weighted volumes). This entire DTI protocol was repeated twice (total DTI acquisition duration: approximately 72 min).

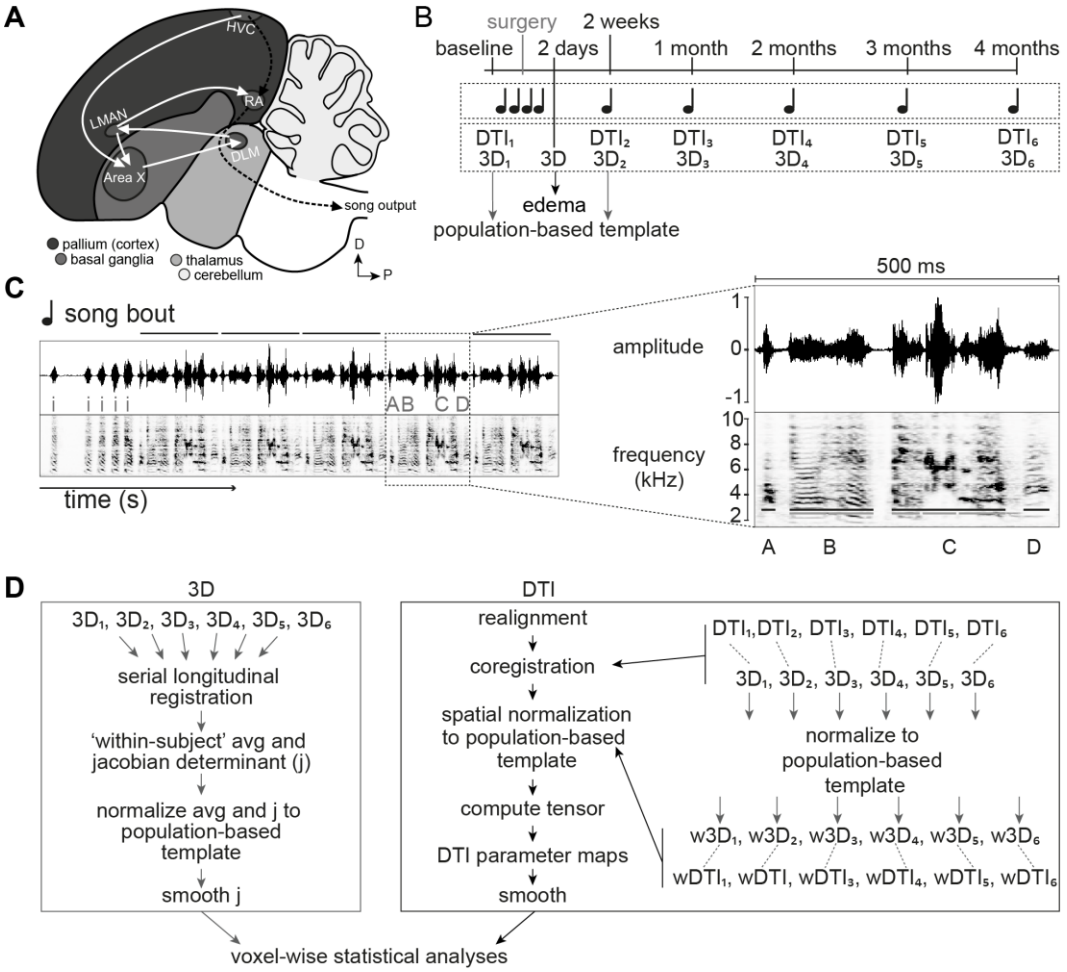

Figure 7-2: Schematic view of the song control system in songbirds (A), the study design (B) and the processing of the song (C) and MRI (D) data. The schematic songbird brain (**A**) presents two main pathways in control of song, i.e. cortical pathway that directly connects HVC and RA (grey dashed arrows), and an indirect C-BG-T-C loop that sequentially connects HVC-Area X-DLM-LMAN-RA (solid white arrows). The black area refers to the avian pallium, similar to the mammalian cortex. Dark grey covers the avian striatum and pallidum, similar to the mammalian basal ganglia. Light grey areas refer to the thalamic zone and cerebellum. More details on the study design (**B**) and MRI data processing (**D**) can be found in the text. Male zebra finches usually sing song bouts (**C**) consisting of introductory notes (i) followed by several renditions of the song motif (indicated by horizontal lines above the song bout). Each motif consists, on average, of 3-5 syllables (indicated by the black lines and letters below the inset, e.g. A-B-C-D) that can be further subdivided into notes (indicated by grey lines)), e.g. syllable C consists of 3 notes. All song analyses have been performed on sound spectrograms (frequency) and included measurements of the motif, syllable and inter-syllable interval duration.

Immediately after the DTI scan, a T_2-weighted 3D Rapid Acquisition with Relaxation Enhancement (RARE) scan was acquired with the following characteristics: TE 11 ms (TE_{eff} 55 ms), TR 2500 ms, RARE factor 8, FOV (18x16x10) mm^3, matrix (256x92x64) zero-filled to

(256x228x142), spatial resolution (0.07x0.17x0.16) mm^3 zero-filled to (0.07x0.07x0.07) mm^3, scan duration 29 min. The FOV of the 3D RARE scans covered the entire birdbrain.

7.2.6 MRI data processing

All MRI data was prepared for voxel-wise statistical analyses using SPM12 (Statistical Parametric Mapping, version 6225, http://www.fil.ion.ucl.ac.uk/spm/) complemented with the Diffusion II and Dartel [39, 40] toolboxes, and the Advanced Normalization Tools (ANTs; http://stnava.github.io/ANTs/; [41]). An overview of the different steps of the DBM and DTI processing pipelines is included in Figure 7-2-D.

7.2.6.1 Population-based template

First, we created a population-based template based on all 3D anatomical scans acquired at baseline and at 2 weeks *post*-surgery using the 'atlasbuildtemplate' function in ANTs [41-43]. The resulting inter-subject template was used as reference space for the voxel-wise DBM and DTI analyses. Important to note is that no visible traces of oedema could be observed in the 3D RARE scans obtained 2 weeks *post*-surgery, in contrast, only very small hypo-intensities covering the path taken by the needle and the core of the lesion were discernible.

7.2.6.2 Deformation-Based Morphometry

For each animal, an average 3D RARE ('within-subject template' or 'midpoint average') was estimated based on the 3D RARE images acquired before and at five time points after introducing a neurotoxic lesion in Area X, i.e. 2 weeks, 1 month, 2 months, 3 months and 4 months after surgery using the serial longitudinal registration tool (SLR; [44]) embedded in SPM12. This step includes an intensity inhomogeneity (bias field) correction followed by a rigid-body transformation combined with symmetric non-linear diffeomorphic mapping. Next, the resulting midpoint average was masked to exclude non-brain tissue and spatially normalized to the population-based template built in ANTs using the 'oldNormalise' function in SPM. The latter incorporates a global affine transformation followed by nonlinear deformations. The transformation matrix estimated by this step was applied to the jacobian determinant maps – without modulation, which would account for between-subject volume differences– outputted by the SLR step. For multiple regression analyses, the normalized jacobian determinant maps were log-transformed. Lastly, all normalized jacobian determinant maps were smoothed in plane using a Gaussian filter with FWHM set at (0.28x0.28) mm^2.

7.2.6.3 Diffusion Tensor Imaging

After assigning the b-value and diffusion gradient directions pertaining to each volume, the DTI scans were realigned to the first volume by a two-step procedure. Firstly, an initial estimation of movement was performed on the b_0 images, after which a second movement estimate included all data i.e. b_0 and diffusion weighted scans. Next, the realigned diffusion time series were co-registered, using normalized mutual information as objective function, to the 3D RARE scan acquired at the same time-point. In parallel, the masks delineated on the midpoint average produced by the SLR step, were back-projected to the native space of the individual datasets using the inverse of the deformation fields computed by the SLR. Next, the masked individual 3D RAREs acquired at each time point were bias corrected and spatially normalized to the population-based template using the oldNormalise function in SPM12. Then, the spatial normalization parameters estimated on the masked, bias corrected 3D RARE scans were applied to the diffusion time series and the diffusion time series was up-sampled to an isotropic resolution of 0.19 mm. The normalized diffusion data were used to estimate the tensor, which was used to compute the diffusion parameters, i.e. the Eigenvalues (λ_1, λ_2, λ_3), Fractional Anisotropy (FA), and Mean Diffusivity (MD) for each voxel in the image. Finally, the DTI parameter maps were smoothed in plane with a Gaussian kernel of (0.38x0.38) mm^2.

7.2.7 Statistical analyses

All voxel-wise statistical tests were performed in SPM12, while statistical analyses on the song data and cluster-based region-of-interest (ROI) data were executed in JMP® (Version 13, SAS Institute Inc., Cary, NC, 1989-2007) and rmcorr [45] software.

7.2.7.1 Song analyses

We tested whether the motif, syllable or inter-syllable duration changed significantly over time using linear mixed models ('time point' as fixed effect, 'subject' as random effect, 'subject*timepoint' as random slope, and syllable-identity was nested within subject for analyses on the syllable and inter-syllable intervals) and selected Tukey's Honest Significant Difference (HSD) for *post hoc* testing. Statistical analyses were performed on absolute (averaged) song scores, but presented as data normalized to the baseline level.

7.2.7.2 Voxel-based analyses

Time-dependent changes of the structural properties of the brain were evaluated by setting up a voxel-wise repeated-measures ANOVA in a flexible factorial design for each smoothed MRI parameter map separately, with 'time point' as fixed factor and 'subject' as random factor. Next, clusters covering a similar anatomical area in both hemispheres were converted to ROIs of which the average MRI parameters were extracted and used for *post hoc* statistical testing in JMP. If significant main effects of time were found, then Tukey's HSD (Honest Significant Difference) was used for *post hoc* statistical testing. In addition, voxel-wise multiple regressions tested for potential positive or negative correlations between each set of MRI parameters and motif score, including datasets obtained at all 6 time points. Only clusters surviving a Family-Wise-Error (FWE) correction for multiple comparisons set at $p<0.05$, and containing at least (k_E) 80 voxels or 10 voxels for respectively the DBM and DTI analyses, were considered significant.

7.2.7.3 Cluster-based ROI analyses

Clusters that displayed a significant correlation between a particular MRI parameter and song feature were converted to ROIs of which the average MRI parameter was extracted and Spearmans' ρ was selected to explore the nature and strength of the overall association between the MRI parameters and song feature scores. To discriminate whether the correlation was mainly due to within-bird variance, we performed a repeated-measures correlation using the custom-build R-script 'rmcorr' developed by [45].

7.3 RESULTS

7.3.1 In vivo assessment of the spatial extent of the lesion

Two days after neurotoxic injury, we acquired T2-weighted 3D anatomical scans to assess the spatial extent of the lesion based on hyper-intense voxels indicative of oedema. The oedema might either be induced by mechanical damage, e.g. along the path of the needle, or by neurotoxic injury at the injection site. Based on these scans, we concluded that 12 out of 14 birds displayed a hyper-intense signal co-localized with major parts of Area X (Figure 7-3-A). The 2 birds that did not show a lesion in the right anatomical area were excluded from further analyses. Furthermore, besides the target area, hyper-intense voxels were observed near the rostral border of the most medial part of $LMAN_{core/shell}$ (Figure 7-3-B). MMAN, situated closer to the midline, was not covered by hyper-intense signals and thus not likely to be affected by the surgical procedure.

Next, the scans obtained two days after surgery were spatially normalized to the population-based template and averaged into one 3D image. This dataset was used to delineate the 'average' region affected by oedema. The delineation was projected onto the population-based template and indicated by means of a black area (Figure 7-3, bottom rows). This dataset serves as an anatomical reference underlying all statistical parametric maps.

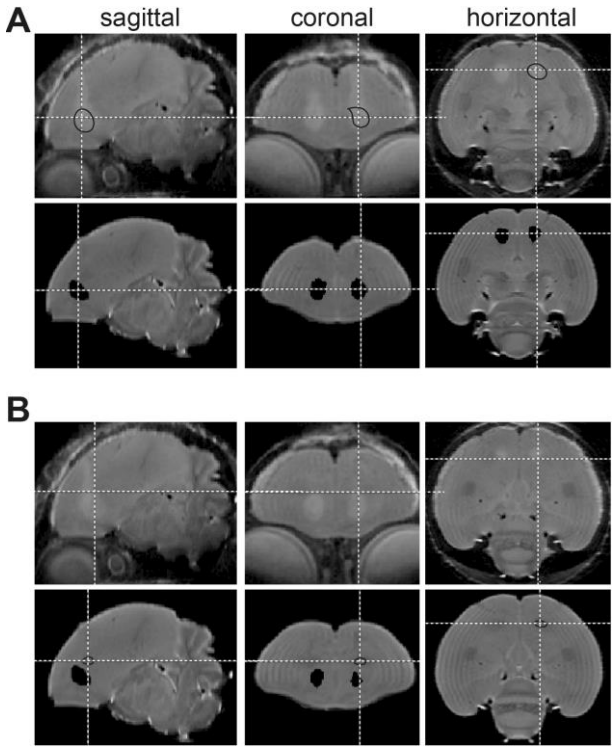

Figure 7-3: T2-weigthed 3D RARE scans obtained two days after surgery inform on the spatial extent of the lesion. The crosshairs point to Area X (**A**) or LMAN (**B**), both are delineated by a black line in one hemisphere and visible as respectively hyper- (oedema) or hypo-intense (intrinsic MRI contrast) area on the contralateral side. The top row of (A) and (B) display the average 3D based on all 3D RARE scans obtained 2 days after surgery (n=12). Areas affected by oedema induced by either neurochemical (ibotenic acid) or mechanical (needle) damage are represented by hyper-intense (bright) voxels. The bottom rows of (A) and (B) illustrate the population-based template where the manually delineated black coloured regions refer to the parts of the striatum (Area X) affected by oedema. The delineation is based on the hyper-intense area visible in the top row and only contains voxels above a manually defined voxel-intensity threshold (retain only brightest voxels).

7.3.2 DBM exposes relative volume changes in the striatum

The voxel-wise repeated measures ANOVA (n=12) of the smoothed non-modulated jacobian determinant maps identified a main effect of time in a large bilateral cluster covering the caudal, medial, and lateral surroundings of the lesion (Figure 7-4-A, cluster (a); the cluster (p_{FWE}<0.001 k_E=25359) includes 3 main peaks: peak 1 p_{FWE}<0.001 F=24.82; peak 2: p_{FWE}<0.001

F=6.84; peak 3: p_{FWE}<0.001 *F*=18.96). Interestingly, the cluster did not co-localize with the dark area that reflects the lesioned region. It appears to be situated mainly in the striatum and exceeds partially to the nidopallium. Furthermore, several smaller clusters were found where the needle entered the brain, dorsal to Area X, (Figure 7-4-A, clusters (b) and (c); left: cluster level p_{FWE}<0.001 k_E=307; peak level p_{FWE}<0.001 *F*=18.83; right cluster$_1$: cluster level p_{FWE}<0.001 k_E=350; peak level p_{FWE}<0.001 *F*=20.10; right cluster$_2$: cluster level p_{FWE}<0.001 k_E=671; peak level p_{FWE}<0.001 *F*=16.00).

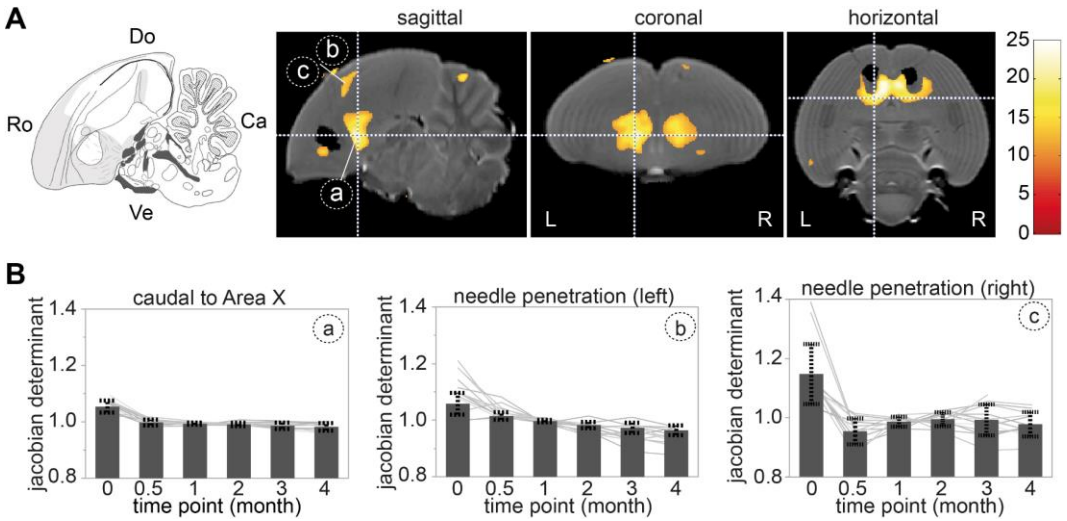

Figure 7-4: DBM analysis reveals relative volume changes in the striatum. A: The statistical parametric maps represent the results of a main effect of time derived from a repeated-measures ANOVA (n=12) on the jacobian determinant maps. The atlas drawing on the left –obtained from the zebra finch histological atlas browser (Oregon Health & Science University, Portland, OR 97239; http://www.zebrafinchatlas.org [46]– was taken at approximately the same lateral position as the sagittal MR image immediately adjacent to it. The crosshairs in the sagittal slice indicate the relative location of the coronal and horizontal MR slices displayed on the right. Results are overlaid on the population-based template and scaled according to the colour-code on the right (F values). Only voxels that reached p_{FWE}<0.05 and took part of a cluster of k_E≥80 contiguous voxels are displayed. The black area reflects the area affected by the surgery (ibotenic acid) and was drawn based on the 3D RARE scans acquired two days after surgery. **B**: The bar graphs illustrate the mean ± standard deviation of the mean jacobian determinant of the clusters identified in A (denoted with encircled letter). The grey lines refer to the evolution of the average jacobian determinant in a specific cluster-based ROI for each individual animal. The different cluster-based ROIs overlay with (**a**) the medial striatum caudal to the lesion site, and (**b-c**) the needle penetration areas in respectively the left and right hemispheres. Time point '0' refers to the baseline, before neurotoxic lesioning. Abbreviations: Do: dorsal; Ve: ventral; Ro: rostral; Ca: caudal; L: left; R: right.

Voxel-wise tests assessing differences between consecutive time points (data not shown) informed that the main effect of time is caused by differences between baseline and 2 weeks *post*-surgery. This trend is visualized in Figure 7-4-B which plots the average jacobian determinant for the cluster-based ROIs at each individual time point (relative volume of the cluster is larger at baseline (j>1), compared to at 2 weeks *post*-surgery (j≈1)).

7.3.3 DTI uncovers lesion-induced structural remodelling of the cerebello-thalamo-striatal pathway within the first two months after a neurotoxic lesion

The voxel-wise repeated-measures ANOVA (n=12) identified large widespread bilateral clusters displaying a main effect of time in FA, MD and λ_1 (Figure 7-5-A). In contrast, clusters found in the smoothed λ_2 and λ_3 maps did not appear bilateral and were therefore not further explored. When inspecting differences in FA over time, a very clear bilateral cluster was observed near the striatum and Area X, partly invading the lesion (Figure 7-5-A, cluster (a); left: cluster level: $p_{FWE}<0.001$ $k_E = 97$; peak voxel: $p_{FWE}<0.001$; F=32.54; right: cluster level: $p_{FWE}<0.001$ $k_E=40$; peak voxel: $p_{FWE}<0.001$; F=19.84). Another cluster was found dorsal to Area X, spatially corresponding with the entrance of the needle in the brain (Figure 7-5-A, cluster (b); left: cluster level: p_{FWE} $k_E=80$; peak level: $p_{FWE}<0.001$; F=22.50; right: cluster level $p_{FWE}<0.001$ $k_E=51$; peak level: $p_{FWE}<0.001$ F=16.62). No further changes in FA were found. A similar cluster covering Area X was present when testing λ_1 over time (not shown; left: cluster level: $p_{FWE}<0.001$ $k_E=29$; peak level: $p_{FWE}<0.001$ F=17.96; right: cluster level $p_{FWE}<0.001$ $k_E=78$; peak level: $p_{FWE}<0.001$; F=20.44). Furthermore, a widespread cluster covering caudal subpallial (i.e. subcortical) parts of the telencephalon and extending ventrally towards the mesencephalon and cerebellum was also found to display changes in λ_1 and MD over time. Several sub-peaks of this large cluster could be anatomically identified, including the dorsal thalamic zone (including DLM; Figure 7-5-A cluster (c)), an anatomically discrete bilateral cluster in the lateral cerebellar nuclei (Figure 7-5-A cluster (d)), the medial parts of the tractus occipitomesencephalicus (tOM: Figure 7-5-A cluster (e)), and the commissura posterior (Figure 7-5-A cluster (f)).

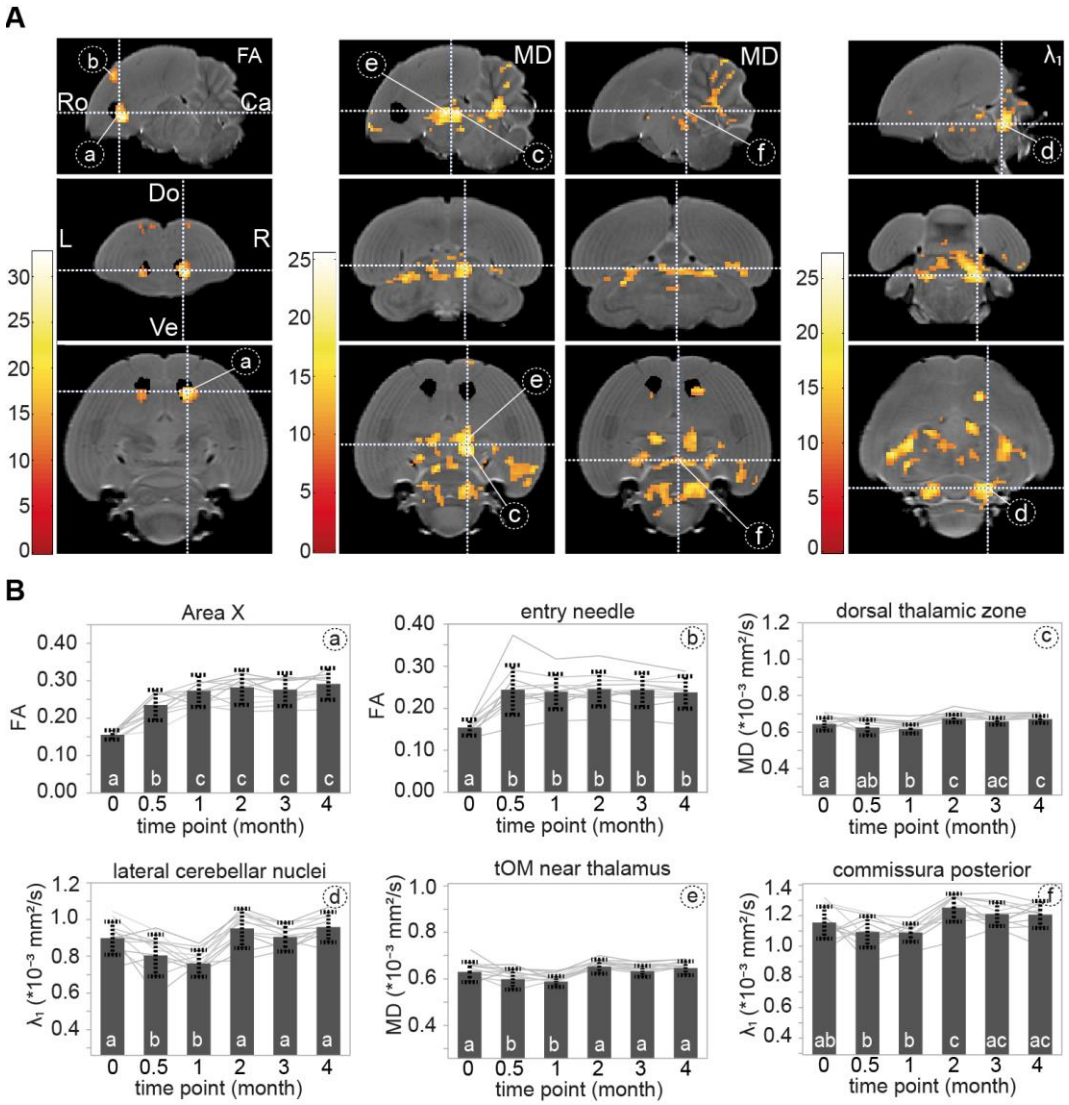

Figure 7-5: DTI detects microstructural remodelling in the cerebellar-thalamic-basal ganglia pathway. A: The statistical parametric maps display the main effect of time derived from a repeated-measures ANOVA (n=12), for FA, MD (at two different locations) and λ_1. The maps are thresholded at $p_{FWE}<0.05$ and $k_E \geq 10$ voxels (F-values are color-coded according to the scales left to the SPMs), and overlaid on the population-based template. The black area reflects the lesioned area. The white-dotted crosshairs converge in local maxima (F-test), the latter of which have been the basis for drawing the cluster-based ROIs, appointed by (encircled) letters, i.e. (**a**): Area X (lesion); (**b**): entry of the needle; (**c**): dorsal thalamic zone; (**d**): lateral cerebellar nuclei; (**e**): tOM near the thalamus; and (**f**): commissura posterior. **B**: The bar graphs that illustrate the mean FA, MD and λ_1 for several cluster-based ROIs identified in the voxel-wise statistical maps. The white letters at the base of the bars represent the results of the post hoc tests (Tukey HSD); if two time points share the same letter, then no significant difference exists between both. Each grey line presents the average DTI metric of the cluster for each individual bird over time. Time point '0' refers to the baseline, before neurotoxic lesioning. Abbreviations: Ro: rostral; Ca: caudal; Ve: ventral; Do: dorsal; L: left; R: right.

Next, the clusters were converted to ROIs of which the average DTI parameter was extracted. The cluster-to-ROI conversion was done either directly if the cluster appeared well-delineated and confined to an anatomically discrete region e.g. Area X lesion detected by FA; or indirectly based on thresholded statistical maps (*F*-values) and anatomically recognizable areas e.g. the dorsal thalamic zone was extracted from peak *F*-values in the large cluster found in the SPM based on λ_1. The average DTI parameters were extracted for each individual cluster-based ROI and used for post hoc statistical testing to test when in time the differences occurred (Figure 7-5-B).

Fractional anisotropy and λ_1 showed an immediate increase in Area X (lesion site and caudal to lesion) at 2 weeks and further at 1 month post-surgery, after which they remained stable (Figure 7-5-B, FA for cluster (a)). At the needle penetration area, FA and λ_1 values increased acutely at 2 weeks post-surgery due to the penetration and remained stable from 2 weeks onwards (Figure 7-5-B, FA for cluster (b)). The changes in MD and λ_1 observed in the dorsal thalamic zone (including DLM) occurred more gradually. From baseline towards 1 month after surgery, MD and λ_1 decreased slowly, yet, from 1 to 2 months post-surgery both DTI metrics increased significantly and remained relatively constant thereafter (Figure 7-5-B, MD for cluster (c)). The lateral cerebellar nuclei (Figure 7-5-B, λ_1 for cluster (d)), tOM (Figure 7-5-B, MD for cluster (e)), and the commissura posterior (Figure 7-5-B, λ_1 for cluster (f)) follow similar trends over time, i.e. a decrease at 2 weeks and 1 month after which they return to baseline levels at 2 months post-surgery and remain stable until the end of the study.

7.3.4 Song tempo acutely increases and later decreases following neurotoxic lesioning of Area X

Due to technical limitations we were not able to obtain song data of the baseline measurement for two out of 12 birds. Consequently, all song analyses were performed on 10 birds. Motif duration changed significantly over the course of the study (mixed model main effect of time: $p<0.0001$ $F_{(10.86.0)}=13.0585$; Figure 7-6-A). From 3 months post lesioning onwards, motif duration was significantly shorter compared to baseline performance. The long-term decrease in motif duration can be ascribed to a progressive shortening of the syllable duration (mixed model main effect of time: $p=0.0110$ $F_{(11,98.8)}=2.4019$; Figure 7-6-B), while the inter-syllable interval duration did not change significantly over time (mixed model main effect of time: $p=0.9823$ $F_{(11,97.9)}=0.3098$; Figure 7-6-C). The latter exhibited a slight non-significant increase in

duration immediately following surgery which persisted over the entire course of the study. Although the relative changes in syllable duration were smaller than those of inter-syllable duration, the absolute change in the durations of the syllables were bigger than the absolute change in the durations of inter-syllable intervals (respectively 111.35 ± 5.82 ms vs. 35.07 ± 1.92 ms, mean ± SEM; baseline data).

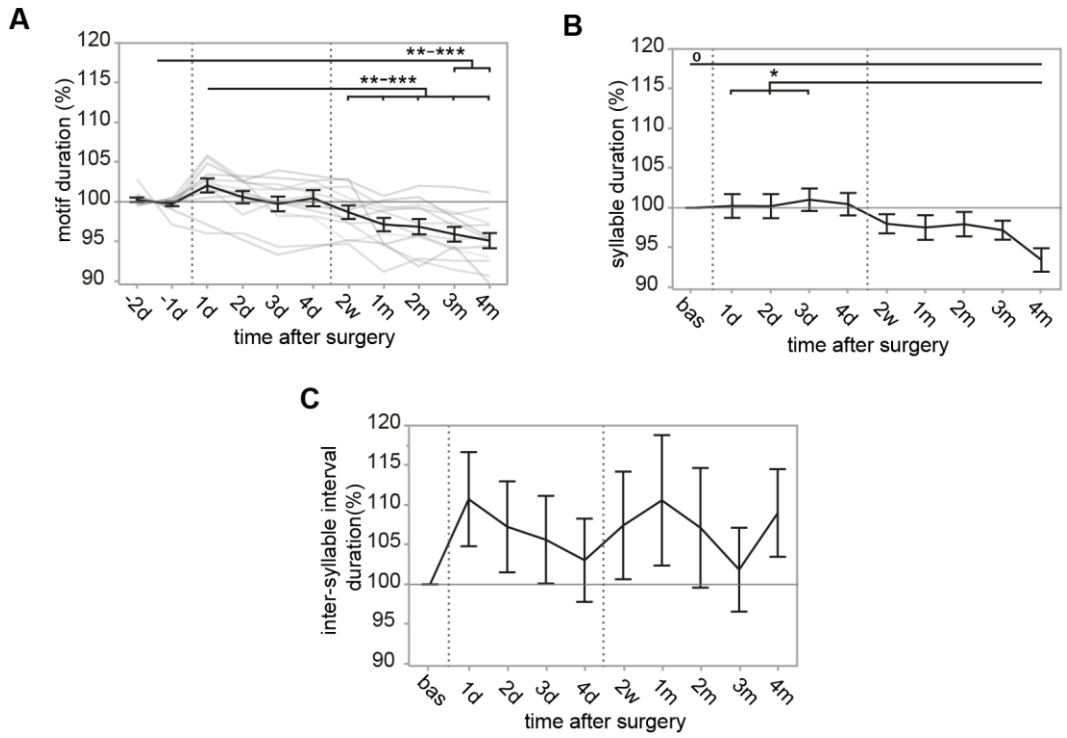

Figure 7-6: Motif length acutely increases and later decreases following neurotoxic lesioning of Area X. Motif length (**A**), the syllable (**B**) and inter-syllable intervals (**C**) duration are expressed relative (%) to the average baseline performance. The data is presented as mean ± standard error of the mean (n=10). Each grey line in (A) refers to the evolution of the average relative motif length for an individual bird over time, while the black line presents that average across all animals. The dotted lines subdivide the graph into three distinct phases relative to the surgery: baseline (bas or -2 and -1 days), acute (1-4 days after surgery) and chronic (2 weeks and 1-4 months after surgery) phases. The horizontal grey area covers an arbitrarily chosen 5% range between 97.5-102.5%. Asterisks indicate the results of the mixed model with post hoc Tukey HSD, i.e. o: p=0.06; *: 0.05>p>0.01; ** 0.01>p>0.001; *** p<0.001. Note that all statistical analyses have been performed on the absolute averaged data. Abbreviations: d: day; w: week; m: month.

On average, syllables decrease in duration several months after lesioning. However, not all syllables present a similar trajectory over time, as reflected in the relatively large variation (error bars) observed after lesioning. To test whether different syllable types would be affected in a specific way after lesioning, we categorised all syllables in accordance with criteria published by Sturdy et al. (1999). An overview of the syllable categorisation can be found in 'Appendix B – Syllable categorisation'. We did not observe any unreadable or high note

syllables. Next, we tested for significant changes in syllable duration for each category and observed a main effect of time for slide notes (p=0.0092 $F_{(11,21.4)}$=3.2649), combination notes (p=0.0017 $F_{(11,47.2)}$=3.3786) and unclassifiable syllables (p<0.0001 $F_{(11,75.3)}$=5.4896). In contrast, short slide or flat note syllables did not present a significant main effect of time (respectively p=0.0562 $F_{(11,78.8)}$=1.8695 or p=0.4462 $F_{(11,44.0)}$=1.0193).

7.3.5 Song performance correlates with the microstructural properties of distinct areas in the songbird brain

Besides testing for effects of Area X lesioning on motif duration over time, we performed additional tests to investigate possible relationships between the birds' motif duration and microstructural tissue properties characterizing particular brain regions (n=10). No significant clusters could be observed in the voxel-wise multiple regression between smoothed (log-transformed) jacobian determinant maps and motif duration, or for searching correlations between the jacobian determinant or the DTI parameter maps and motif duration expressed relative to baseline. In contrast, several clusters displayed a correlation between motif duration and the smoothed DTI parameter maps. These clusters were converted to ROIs (cluster-based ROIs). Important to note is that the voxel-wise multiple regression does not take bird-identity into account, it describes the overall association between the song performance and a specific MRI parameter. Consequently, to find out whether the correlations detected by voxel-wise statistical testing were mainly driven by within- or between-bird variance, we performed a repeated-measures correlation analysis on the cluster-based ROI data [45]. Figure 7-7 informs on the spatial location of the observed clusters (voxel-wise multiple regression) and the adjacent graphs illustrate the nature of the within- and between-subject correlation [45]. Table 7-1 summarizes the cluster size, peak and cluster p-values, overall data association (Spearmans' ρ) and within-subject correlation (rmcorr) and corresponding p-value of the repeated-measures correlation analyses of the cluster-based ROIs.

A negative correlation between FA and motif duration was found near the ventro-rostral border of HVC and/or HVC_{shelf} (Figure 7-7-A) and was mirrored by a positive correlation between motif duration and λ_2 (data not shown) and λ_3 (Figure 7-7-B). Furthermore, a positive correlation between motif duration and λ_1, and motif duration and MD was identified in the caudal parts of the striatum immediately adjacent to (but not co-localizing with) the lesion (Figure 7-7-C). At a milder statistical threshold ($p_{uncorrected}$<0.0001 k_E≥20 voxels), the cluster extends more laterally

and appears more symmetric and comparable in size between both hemispheres (Figure 7-7-C, horizontal right). In addition, λ_1 (and MD) correlated positively with motif duration in the anterior nidopallium dorsal to and potentially including parts of LMAN (Figure 7-7-D).

Lastly, a negative correlation between FA and motif duration was found near a white matter structure which was identified as the fasciculus prosencephalis lateralis (FPL; according to [46]) or a white matter structure containing both the FPL and the tractus thalamo-frontalis et frontalis thalamicus medialis (TFM; based on [47]; Figure 7-7-E). Interestingly, a similar cluster was found to display a positive correlation between λ_3 and motif duration (data not shown). MD resulted in a similar statistical parametric map as λ_1 when correlating with motif duration (results not shown).

7.4 DISCUSSION

The present study explored neuroplastic events, i.e. relative volume changes and alterations in microstructural tissue properties, that characterize both short- and long-term effects of neurotoxic lesioning of the striatal component of the song control circuitry in adult male zebra finches. We identified relative volume changes in an area immediately adjacent to the lesion site, and detected altered microstructural tissue properties in the lesion, the efferent dorsal thalamic zone (including DLM) and surprisingly also in the lateral cerebellar nuclei. Furthermore, as the neurotoxic injury was previously found to induce particular changes in vocal behaviour [25, 33], we tested whether relationships could be established between motif duration and the structural properties of specific brain areas. This analysis revealed correlations between the DTI metrics and motif duration in several areas of which most could be linked to the C-BG-T-C loop involved in song maintenance.

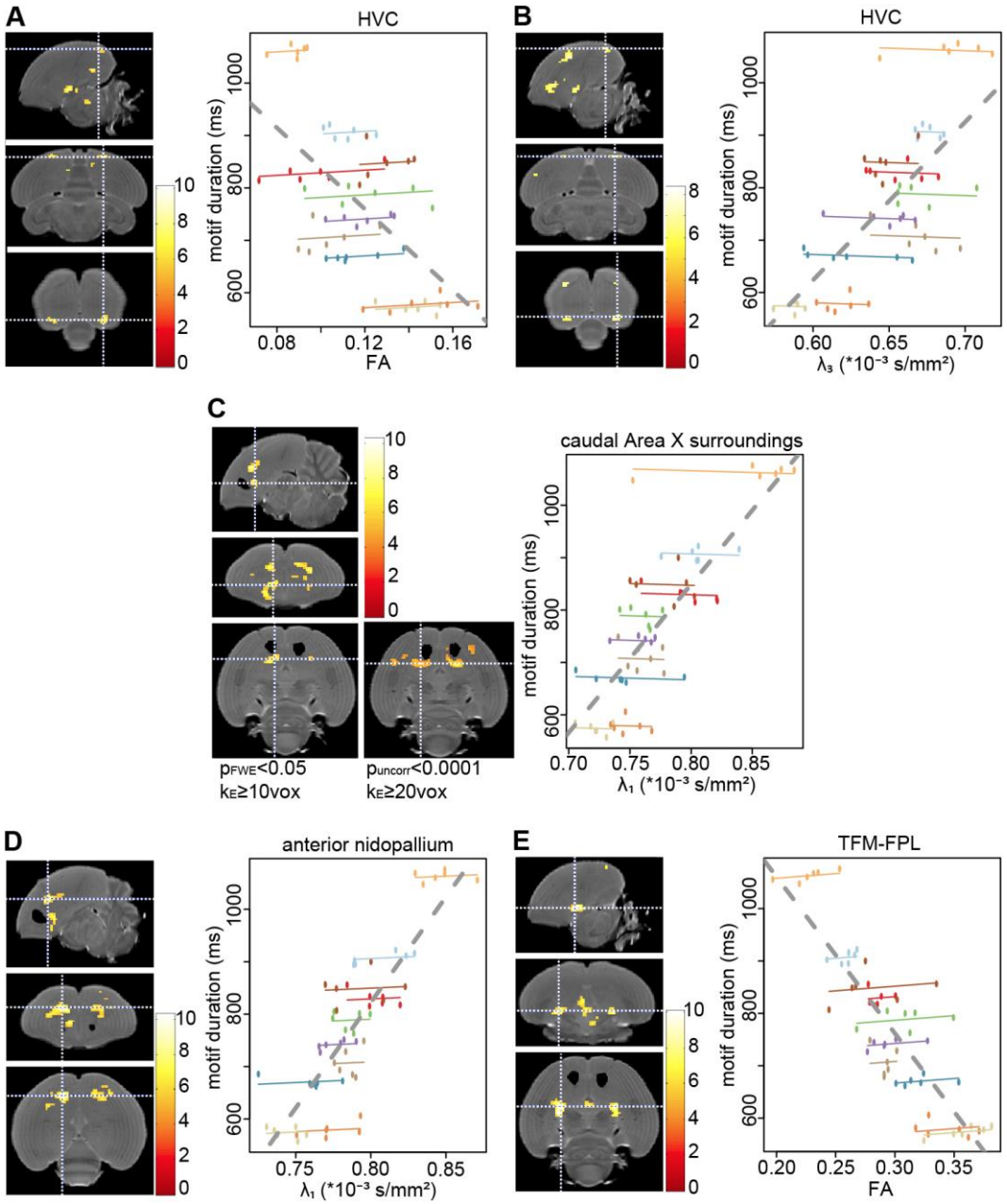

Figure 7-7: Voxel-wise correlations between motif length and DTI metrics. The crosshairs (white dotted lines) converge in (**A-B**) HVC and/or HVC_{shelf}, (**C**) medial striatum caudal to the lesion, (**D**) anterior nidopallium dorsal to LMAN, and (**E**) parts of the FPL and/or TFM. The statistical maps present the voxel-wise multiple regression (n=10) between motif length (y-axis) and the DTI parameters (x-axis) on the graph immediately right to the SPMs. The statistical maps are displayed corrected for multiple comparisons using $p_{FWE}<0.05$, and $k_E \geq 10$ voxels and T-values are color-coded according to the scales immediately right to the statistical maps. The black area reflects the lesioned area. The graphs are generated using 'rmcorr' [45] and visualize the common within-subject regression slope shared among individuals (coloured lines) and overall relationship between motif length and the DTI parameter of the cluster-based ROIs (grey dashed line, all time points included). Each colour refers to an individual bird and each dot is an individual data point (6 times points per bird, presenting data of the cluster-based ROI of one hemisphere indicated in the adjacent SPM). Abbreviations: Do: dorsal; Ve: ventral; Ro: rostral; Ca: caudal; L: left; R: right.

7.4.1 Striatal regeneration

We observed relative volume changes taking place within the first two weeks after surgery including exclusively the medial and caudal striatal surroundings of the lesion site. The cluster co-localizes with parts of the ventral pallidum which receives direct projections from Area X [14, 48]. Ibotenic acid causes neuronal cell death by over-excitation, while keeping the surrounding tissue –extracellular matrix and passing nerve terminals from extrinsic origin– unaffected [35]. Its neurotoxic effect is fully exerted within 48h [35] and leads to massive apoptosis in the lesioned area [25]. Likewise, 2 weeks after surgery, we did not observe any traces of altered image intensities remote to the path of the needle and Area X lesion site that might affect the spatial registration procedure. It suggests that the observed cluster is not a processing-related artefact.

The timing of the observed relative volume changes clearly aligns with our previous studies that described drastic neuroplastic processes occurring in the striatum within the first months after lesioning. More specifically, based on T2-weighted scans, [32] describe that the relative portion of Area X affected by the lesion decreased from 87% to 35% within the first month, to 20% at 3 months and 12% at 6 months after lesioning . Similarly, based on histology (Hu stain for neurons), [25] describe a drastic reduction in the lesion size after 2 weeks and 1 month post neurotoxic lesioning accompanied with an increased number of proliferated cells ($BrdU^+$) in the lesion and in the medial and lateral striatal lesion-surroundings. Moreover, this was paralleled by increasing numbers of undirected singing-induced immediate early gene (IEG) egr-1 expressing, and thus functionally active, cells dispersed throughout the previously damaged Area X. Many of the $BrdU^+$ cells also stained positive for DARPP-32, a marker for medium spiny neurons [25]. In addition, several studies in adult zebra finches provide evidence that neural progenitor cells reach the striatum from the ventricular zone at its caudal and medial border, migrate to Area X, and are able to differentiate into medium spiny neurons [23, 49]. All this indicates that new cells migrate from the ventricular zone adjacent to the striatum to the damaged area and transform into functionally-active medium spiny neurons. We argue that the relative volume changes that exclusively affect the caudo-medio-lateral lesion-surroundings might arise from massive regenerative neuroplastic processes taking place most extensively in the first month after neurotoxic lesioning.

7.4.2 Microstructural remodelling in the C-BG-T-C loop and cerebello-thalamic-striatal pathway

One of the major aims of this experiment was to uncover possible remote brain regions displaying disparate microstructural tissue properties at different stages following neurotoxic injury. We observed subtle changes in diffusion properties in the dorsal thalamic zone (containing DLM). Structural alterations to the thalamus agree with data obtained by [26] who discovered a marked reduction of GABAergic nerve terminals of projection neurons originating from Area X in DLM 3-4 days after injecting ibotenic acid unilaterally in Area X of adult male zebra finches. Interestingly, our data suggest that the structural properties of the dorsal thalamic zone appear to normalize to baseline levels by 2 months *post*-surgery and remain constant thereafter. This might imply a reinstatement of previously lost connectivity.

Within the first month after surgery, we observed significantly deviating λ_1 in a bilateral cluster in the cerebellum covering the lateral portion of the deep nuclei. Tract tracing experiments in zebra finches [14], canaries [50] and pigeons [51] describe a di-synaptic connection between the cerebellum and the contralateral medial striatum and Area X. More specifically, they observed a coextensive stain within the dorsal thalamic zone when injecting retrograde tracers in Area X and the medial striatum and anterograde tracer in the contralateral cerebellum. Positively stained nerve terminals in the dorsal thalamic zone included the dorsomedial anterior and posterior nucleus of the thalamus (respectively DMA and DMP), but merely surrounded DLM [50], suggesting that cerebellar input to the contralateral Area X is indirect and relayed via the thalamus. In humans, it is well known that the cerebellum connects to the basal ganglia and takes an important part in both speech acquisition in early childhood and feedforward motor input in adulthood [19]. As such, the basal ganglia serve as a 'platform' where the cerebro-striatal and cerebellar pathways converge [19]. Our findings clearly point to a potential avian analogue of the feedforward cerebellar connection observed in humans. Further research is required to unravel the distinct functional roles of each pathway in vocal motor control and to explore potential parallels between songbirds and humans.

7.4.3 Striatal lesion affects motif duration

Area X lesioning after song crystallization has little effect on the overall structure of the song [9]. More recent research [25, 33] as well as this study showed a gradual decrease in motif duration reaching approximately 95% relative to baseline duration at 4 months after surgery

(Figure 7-6). Interestingly, reduced syllable duration with intact song structure points to alterations in song tempo: birds progressively appeared to sing faster compared to baseline performance. Similarly, patient studies have reported that even though the sound structure of vocal utterances remains unaffected, dysarthric patients with striatal disorders or cerebellar abnormalities exhibited normal, slowed or accelerated speech rates [52, 53]. The relatively divergent disease phenotypes underlying basal ganglia dysfunctioning underscore that more research is needed to unravel the pathophysiological role of each component in vocal motor output.

We observed several correlations between local diffusion properties and motif duration, including clusters in/near HVC, the caudo-medio-lateral striatal surroundings of the lesion site, the TFM/LFP, and the anterior nidopallium (cortical) dorsal to $LMAN_{core/shell}$. These are brain areas linked to the C-BG-T-C pathways in control of song behaviour. Important to note is that most of the areas identified by the voxel-based analysis (Figure 7-7) are driven by variability in motif duration present between birds, rather than variation in motif duration as a consequence of the striatal injury (visible in correlation graphs in Figure 7-7).

7.4.3.1 Motif duration & HVC

HVC sends direct projections to Area X [54]. Even though no direct microstructural changes in HVC could be observed along the course of the study, it might be plausible that the correlation between FA or λ_3 with motif duration might in part be driven by direct lesion-induced structural remodelling propagating upstream, to HVC.

Across songbird species, brain-behaviour relationships have been observed between the volume or cell number of song control system components and song performance. Indeed, HVC volume correlates positively with the number of syllables in the song of male canaries [55] or with song repertoire size in Marsh wrens [56], song sparrows [57], and in warblers [58, 59]. In male zebra finches, HVC volume and neuron number correlates positively with the number of tutor syllables that are accurately copied [60, 61]. Likewise, the correlation observed between FA or λ_3 and motif length might in part rely on a potential volume difference between HVC of birds singing short compared to longer song motifs, that potentially still remains present after the spatial normalization procedure (since on T2-weighted datasets HVC cannot be distinguished from the surrounding tissue and therefore lead to sub-accurate spatial corresponding between subtle differences in HVC volume between subjects).

Alternatively, substantial evidence has appointed HVC as time keeper of song, i.e. in control of the temporal characteristics of the motor program underlying a particular song [62, 63]. For example, both in humans and songbirds, localized cooling of respectively Broca's area or HVC affects speech rate or slows down song speed by stretching the motif sequence [64, 65]. Even though the lesion-induced alterations in motif duration (song tempo) are not sufficient to result in clear within-subject correlations, part of the correlation might build on subtle differences in song tempo controlled by HVC.

7.4.3.2 Motif duration & TFM/LFP & caudal surroundings of the lesion

The voxel-based multiple regression demonstrated clear bilateral clusters in a part of the TFM/FPL (motif duration correlated negatively with FA and positively with λ_3) and the caudal surroundings of the lesion (motif duration correlated positively with λ_1 and MD). The latter one was found to display relative volume changes within 1 month *post*-surgery.

The TFM/FPL is a white matter tract that accommodates fibres pertaining to the striato-thalamic part of the AFP. More specifically, after exciting Area X from its caudo-ventral end, Area X projection neurons course to the region of the FPL and TFM, infiltrate DLM via its anterior part where the axon terminals form a basket-like lattice surrounding DLM cells [14, 26, 34].

Previous studies have shown that undirected singing-driven IEG egr-1 expression levels in RA are dependent on Area X and a functioning AFP [27]. Intriguingly, upon neurotoxic lesioning of Area X, undirected singing-driven egr-1 expression levels drop and only recover between 1-3 months after Area X lesioning [25]. Consequently, the lack of expression of IEG egr-1 in RA suggests that the AFP is not yet fully functional before 1 month after neurotoxic damage to Area X. Similarly, partial lesioning of Area X lowers the undirected singing-driven IEG expression in the intact Area X [27]. This might be due to altered local interconnectivity within the striatum as, in normal circumstances, striatal neurons are tightly interconnected [15]. Together with the previously reported massive regenerative processes [25] that coincide and co-localize with the relative volume differences observed in this study, the voxel-wise correlations between the DTI metrics and motif length might connect tissue remodelling aimed at recovering local connectivity within Area X with the neighbouring striatum and downstream AFP to alterations in vocal performance. Therefore, our findings align with [25] who hypothesized that behavioural changes might be a direct result of new neurons being integrated to re-establish connectivity locally and within the AFP after Area X lesioning.

7.4.3.3 Motif duration & anterior nidopallium and/or LMANshell/core

When searching for possible correlations between DTI metrics and motif duration, we discovered a clear bilateral cluster near the anterior nidopallium dorsal to (and potentially including parts of) $LMAN_{core/shell}$. We propose two explanations underlying this observation: (1) this region might be directly affected by the surgical procedure and/or back flow of ibotenic acid, or directly by lesioning of Area X, or (2) this finding might point to involvement of the parallel AFP.

Surgical procedure or direct effect by neurotoxic lesioning

Based on the T_2-weighted scans acquired 2 days after the surgery, we concluded that the anterior nidopallium possibly including a small rostral portion of the $LMAN_{core/shell}$ might be covered by oedema (Figure 7-3) and thus affected by either mechanical or neurotoxic damage. The latter is not very likely, as based on effects over time, we did not observe clear clusters co-localized with the caudal nidopallium nor LMAN that could indicate microstructural remodelling due to a lesion. The only cluster covering the anterior nidopallium possibly involving parts of $LMAN_{core/shell}$ was found when testing for a correlation with motif duration, the latter of which appeared to change over time. Alternatively, LMAN sends a direct projection back to Area X [16, 17]. Consequently, the cluster that partly overlaps with LMAN might suggest direct lesion-induced structural alterations affecting one of its immediate up-stream areas.

Parallel pathways

When mapping the thalamo-cortical part of the AFP, i.e. DLM-LMAN-RA pathway, in adult male zebra finches, Johnson and co-workers provided evidence for two parallel pathways originating in different sub-regions of DLM [66]. One set emerged from the dorsolateral portion of DLM, connected with the $LMAN_{core}$ and ended in RA. The other pathway included axonal projections stemming from the medioventral portion of DLM, projected to the $LMAN_{shell}$ region and travelled further to the dorsal arcopallium (arc-like structure within the arcopallium lateral to RA). Follow-up studies showed that the $LMAN_{shell}$ also projects to ventral parts of the arcopallium and the dorsal caudo-lateral nidopallium, and receives connections from the contralateral ventral arcopallium, recently summarized by [67]. Moreover, disruption of the $LMAN_{shell}$ circuitry (by lesioning the dorsal arcopallium) during the critical period of vocal learning prevents birds from imitating an accurate copy of the tutor song [68]. Based on these and other findings, the $LMAN_{shell}$ region might serve as entry site for multimodal sensory

information (inputted via the dorsal caudo-lateral nidopallium) in the song control system and might be implicated in the bilateral coordination of the song control circuitries situated in the left and right hemispheres [67]. Yet, the exact role of the parallel pathway on vocal behaviour requires further investigation.

7.5 CONCLUSION

In conclusion, using whole-brain *in vivo* structural MRI, this study complements previous reports on the detection of neuroplastic microstructural remodelling in brain sites reaching as far as the cerebellum following neurotoxic lesioning of Area X. This finding calls out the need for in-depth studies focused on the role of the lateral cerebellar nuclei in song learning in ontogeny, and extends existing parallels between bird song and human speech [3, 19]. As such, songbirds might help resolve the open questions concerning the physiological workings and interplay of the cortical and subcortical neural network architecture that underlies speech motor production which is of vital importance to understand how proper speech control is altered in various disorders of the human brain.

FUNDING

This work was supported by grants from the Research Foundation—Flanders (FWO, Project No. G030213N, G044311N and G037813N), the Hercules Foundation (Grant No. AUHA0012), Interuniversity Attraction Poles (IAP) initiated by the Belgian Science Policy Office ('PLASTOSCINE': P7/17 and P7/11) to AVdL, and a grant from the Slovak Research and Development Agency (APVV-15-0077) to LK. JH is a PhD student supported by the University of Antwerp.

ACKNOWLEDGEMENTS

The computational resources and services used in this work to build the population-based template were provided by the HPC core facility CalcUA of the Universiteit Antwerpen, the VSC (Flemish Supercomputer Center), funded by the Hercules Foundation and the Flemish Government – department EWI. We thank prof. Dr. E. Fransen (StatUa Center for Statistics) for a critical revision of the statistical methodology (mixed models).

APPENDIX A – Voxel-wise multiple regressions: motif length versus DTI

Table 7-1: Summary of the correlation analyses (n=10).

Cluster-based ROI	DTI parameter	Hemis-phere	Cluster level		Peak level		Overall association	rmcorr	
			p_{FWE}	k_E	p_{FWE}	*T*	Spearman's ρ	*p*	r
TFM / LFP	FA	left	<0.001	78	<0.001	10.06	-0.8265	0.156	0.202
		right	<0.001	44	<0.001	9.09	-0.7497	0.684	-0.058
	λ_3	left	<0.001	510	<0.001	8.10*	0.7440	.	.
		right	<0.001	32	0.001	6.45	0.6427	.	.
HVC (and HVC_{shelf})	FA	left	<0.001	46	<0.001	7.05	-0.7828	0.698	-0.056
		right	<0.001	10	<0.001	6.61	-0.5266	0.145	0.207
	λ_3	left	<0.001	12	<0.001	7.74	0.5507	0.782	0.044
		right	<0.001	24	<0.001	6.95	0.6691	0.450	-0.108
Caudal surroundings of lesion	λ_1	left	<0.001	87	<0.001	8.66	0.7546	0.517	-0.093
		right	<0.001	10	0.008	5.78	0.6078	0.009	0.361
Anterior nidopallium dorsal to LMAN	MD	left	<0.001	601	<0.001	9.81*	0.7383	.	.
		right	<0.001	447	<0.001	7.40*	0.6836	.	.
	λ_1	left	<0.001	141	<0.001	10.28	0.7859	0.443	0.110
		right	<0.001	160	<0.001	8.10	0.7245	0.952	0.009

*This is the T-max of a sub-peak co-localized with the anatomical area delineated by the cluster-based ROI. The spatial extent of the cluster is not necessarily constricted to the anatomical area, but can be co-localized with the brain region to which the cluster-based ROI refers. Several subpeaks within the same cluster can be assigned to different cluster-based ROIs e.g. caudal surroundings of the lesion and anterior nidopallium dorsal to LMAN. Spearman's ρ is calculated based on all data of all time points and describes the overall association between the DTI parameter and motif duration, without taking bird-identity into account.
'rmcorr' refers to the outcome of the repeated-measures correlation with the average within-subject correlation coefficient 'r' and the corresponding *p*-value '*p*' [45].

APPENDIX B – Syllable categorisation

Table 7-2: Overview of the results of the syllable classification performed on baseline scores.

bird-ID	motif structure	syllable	Sturdy syllable category
Bird_1	ABCDE	A	7
		B	4
		C	5
		D	7
		E	4
Bird_2	ABCD	A	4
		B	2
		C	6
		D	6
Bird_3	ABCDE	A	2
		B	2
		C	7
		D	2
		E	4
Bird_4	ABCDEF	A	7
		B	2
		C	5
		D	5
		E	7
		F	7
Bird_5	ABCDE	A	7
		B	2
		C	5
		D	5
		E	7
Bird_7	ABCDE	A	4
		B	7
		C	7
		D	2
		E	6
Bird_8	ABCDE	A	2
		B	6
		C	6
		D	4
		E	6
Bird_10	ABC	A	7
		B	7
		C	7
Bird_11	ABCDE	A	2
		B	7
		C	6
		D	2
		E	7
Bird_12	ABCDE	A	6
		B	7
		C	7
		D	2
		E	7

REFERENCES

1. Petkov, C.I. and E. Jarvis, *Birds, Primates and Spoken Language Origins: Behavioral Phenotypes and Neurobiological Substrates.* Frontiers in Evolutionary Neuroscience, 2012. **4**.
2. Jarvis, E.D., *Learned Birdsong and the Neurobiology of Human Language.* Annals of the New York Academy of Sciences, 2004. **1016**(1): p. 749-777.
3. Brainard, M.S. and A.J. Doupe, *Translating Birdsong: Songbirds as a Model for Basic and Applied Medical Research.* Annual Review of Neuroscience, 2013. **36**(1): p. 489-517.
4. Bolhuis, J.J., K. Okanoya, and C. Scharff, *Twitter evolution: converging mechanisms in birdsong and human speech.* Nat Rev Neurosci, 2010. **11**(11): p. 747-759.
5. Jarvis, E.D., et al., *Avian brains and a new understanding of vertebrate brain evolution.* Nat Rev Neurosci, 2005. **6**(2): p. 151-159.
6. Wild, J.M., *Neural pathways for the control of birdsong production.* Journal of Neurobiology, 1997. **33**(5): p. 653-670.
7. Nordeen, K.W. and E.J. Nordeen, *Deafening-Induced Vocal Deterioration in Adult Songbirds Is Reversed by Disrupting a Basal Ganglia-Forebrain Circuit.* The Journal of Neuroscience, 2010. **30**(21): p. 7392-7400.
8. Brainard, M.S., *Contributions of the Anterior Forebrain Pathway to Vocal Plasticity.* Annals of the New York Academy of Sciences, 2004. **1016**(1): p. 377-394.
9. Scharff, C. and F. Nottebohm, *A comparative study of the behavioral deficits following lesions of various parts of the zebra finch song system: implications for vocal learning.* The Journal of Neuroscience, 1991. **11**(9): p. 2896-2913.
10. Reiner, A., et al., *Songbirds and the Revised Avian Brain Nomenclature.* Annals of the New York Academy of Sciences, 2004. **1016**(1): p. 77-108.
11. Pfenning, A.R., et al., *Convergent transcriptional specializations in the brains of humans and song-learning birds.* Science (New York, N.Y.), 2014. **346**(6215): p. 1256846-1256846.
12. Vicario, D.S., *Organization of the zebra finch song control system: Functional organization of outputs from nucleus robustus archistriatalis.* The Journal of Comparative Neurology, 1991. **309**(4): p. 486-494.
13. Wild, J.M., *Descending projections of the songbird nucleus robustus archistriatalis.* The Journal of Comparative Neurology, 1993. **338**(2): p. 225-241.
14. Person, A.L., et al., *Organization of the songbird basal ganglia, including area X.* The Journal of Comparative Neurology, 2008. **508**(5): p. 840-866.
15. Reiner, A., et al., *An immunohistochemical and pathway tracing study of the striatopallidal organization of area X in the male zebra finch.* The Journal of Comparative Neurology, 2004. **469**(2): p. 239-261.
16. Nixdorf-Bergweiler, B.E., M.B. Lips, and U. Heinemann, *Electrophysiological and morphological evidence for a new projection of LMAN-neurones towards area X.* NeuroReport, 1995. **6**(13): p. 1729-1732.
17. Vates, G.E. and F. Nottebohm, *Feedback circuitry within a song-learning pathway.* Proceedings of the National Academy of Sciences, 1995. **92**(11): p. 5139-5143.
18. Moorman, S., et al., *Human-like brain hemispheric dominance in birdsong learning.* Proceedings of the National Academy of Sciences, 2012. **109**(31): p. 12782-12787.
19. Ziegler, W. and H. Ackermann, *Subcortical Contributions to Motor Speech: Phylogenetic, Developmental, Clinical.* Trends in Neurosciences, 2017. **40**(8): p. 458-468.
20. Doupe, A.J., et al., *Birdbrains could teach basal ganglia research a new song.* Trends in Neurosciences, 2005. **28**(7): p. 353-363.

21. Goldman, S.A. and F. Nottebohm, *Neuronal production, migration, and differentiation in a vocal control nucleus of the adult female canary brain.* Proceedings of the National Academy of Sciences, 1983. **80**(8): p. 2390-2394.
22. Doetsch, F. and C. Scharff, *Challenges for Brain Repair: Insights from Adult Neurogenesis in Birds and Mammals.* Brain, Behavior and Evolution, 2001. **58**(5): p. 306-322.
23. Kosubek-Langer, J., L. Schulze, and C. Scharff, *Maturation, Behavioral Activation, and Connectivity of Adult-Born Medium Spiny Neurons in a Striatal Song Nucleus.* Frontiers in Neuroscience, 2017. **11**(323).
24. Ernst, A., et al., *Neurogenesis in the Striatum of the Adult Human Brain.* Cell. **156**(5): p. 1072-1083.
25. Kubikova, L., et al., *Basal ganglia function, stuttering, sequencing, and repair in adult songbirds.* Scientific Reports, 2014. **4**: p. 6590.
26. Luo, M. and D.J. Perkel, *Long-range GABAergic projection in a circuit essential for vocal learning.* The Journal of Comparative Neurology, 1999. **403**(1): p. 68-84.
27. Kubikova, L., E.A. Turner, and E.D. Jarvis, *The pallial basal ganglia pathway modulates the behaviorally driven gene expression of the motor pathway.* The European journal of neuroscience, 2007. **25**(7): p. 2145-2160.
28. Tindemans, I., et al., *IR-SE and IR-MEMRI allow in vivo visualization of oscine neuroarchitecture including the main forebrain regions of the song control system.* NMR in Biomedicine, 2006. **19**(1): p. 18-29.
29. Tindemans, I., et al., *In vivo dynamic ME-MRI reveals differential functional responses of RA- and area X-projecting neurons in the HVC of canaries exposed to conspecific song.* European Journal of Neuroscience, 2003. **18**(12): p. 3352-3360.
30. Van der Linden, A., et al., *In vivo manganese-enhanced magnetic resonance imaging reveals connections and functional properties of the songbird vocal control system.* Neuroscience, 2002. **112**(2): p. 467-474.
31. Van Meir, V., et al., *In vivo MR imaging of the seasonal volumetric and functional plasticity of song control nuclei in relation to song output in a female songbird.* NeuroImage, 2006. **31**(3): p. 981-992.
32. Lukacova, K., et al., *Imaging of striatal injury in a songbird brain.* General Physiology and Biophysics, 2017. **36**(1): p. 5.
33. Lukacova, K., et al., *Dopamine D3 receptors modulate the rate of neuronal recovery, cell recruitment in Area X, and song tempo after neurotoxic damage in songbirds.* Neuroscience, 2016. **331**: p. 158-168.
34. Bottjer, S.W., et al., *Axonal connections of a forebrain nucleus involved with vocal learning in zebra finches.* The Journal of Comparative Neurology, 1989. **279**(2): p. 312-326.
35. Schwarcz, R., et al., *Ibotenic acid-induced neuronal degeneration: A morphological and neurochemical study.* Experimental Brain Research, 1979. **37**(2): p. 199-216.
36. Tchernichovski, O., et al., *A procedure for an automated measurement of song similarity.* Animal Behaviour, 2000. **59**(6): p. 1167-1176.
37. Glaze, C.M. and T.W. Troyer, *Temporal Structure in Zebra Finch Song: Implications for Motor Coding.* The Journal of Neuroscience, 2006. **26**(3): p. 991-1005.
38. Sturdy, C.B., L.S. Phillmore, and R.G. Weisman, *Note types, harmonic structure, and note order in the songs of zebra finches (Taeniopygia guttata).* Journal of Comparative Psychology, 1999. **113**(2): p. 194-203.
39. Ashburner, J., *A fast diffeomorphic image registration algorithm.* NeuroImage, 2007. **38**(1): p. 95-113.
40. Ashburner, J. and K.J. Friston, *Computing average shaped tissue probability templates.* NeuroImage, 2009. **45**(2): p. 333-341.

41. Avants, B.B., et al., *A reproducible evaluation of ANTs similarity metric performance in brain image registration.* NeuroImage, 2011. **54**(3): p. 2033-2044.
42. Avants, B.B., et al., *The optimal template effect in hippocampus studies of diseased populations.* NeuroImage, 2010. **49**(3): p. 2457-2466.
43. Avants, B.B., et al., *Symmetric diffeomorphic image registration with cross-correlation: Evaluating automated labeling of elderly and neurodegenerative brain.* Medical Image Analysis, 2008. **12**(1): p. 26-41.
44. Ashburner, J. and G.R. Ridgway, *Symmetric Diffeomorphic Modeling of Longitudinal Structural MRI.* Frontiers in Neuroscience, 2012. **6**: p. 197.
45. Bakdash, J.Z. and L.R. Marusich, *Repeated Measures Correlation.* Frontiers in Psychology, 2017. **8**: p. 456.
46. Karten, H.J., et al., *Digital Atlas of the Zebra Finch (Taeniopygia guttata) Brain: a High Resolution Photo Atlas.* The Journal of comparative neurology, 2013. **521**(16): p. 3702-3715.
47. Nixdorf-Bergweiler, B. and H.-J. Bischof, *Atlas Of The Brain Of The Zebra Finch, Taeniopygia Guttata: With Special Emphasis On Telencephalic Visual And Song System Nuclei in Transverse and Sagittal Sections*, ed. N.C.f.B.I. (US). 2007.
48. Gale, S.D., A.L. Person, and D.J. Perkel, *A novel basal ganglia pathway forms a loop linking a vocal learning circuit with its dopaminergic input.* The Journal of Comparative Neurology, 2008. **508**(5): p. 824-839.
49. Scott, B.B. and C. Lois, *Developmental origin and identity of song system neurons born during vocal learning in songbirds.* The Journal of Comparative Neurology, 2007. **502**(2): p. 202-214.
50. Vates, G.E., D.S. Vicario, and F. Nottebohm, *Reafferent thalamo-"cortical" loops in the song system of oscine songbirds.* The Journal of Comparative Neurology, 1997. **380**(2): p. 275-290.
51. Arends, J.J.A. and H.P. Zeigler, *Organization of the cerebellum in the pigeon (Columba livia): II. Projections of the cerebellar nuclei.* The Journal of Comparative Neurology, 1991. **306**(2): p. 245-272.
52. Bodranghien, F., et al., *Consensus Paper: Revisiting the Symptoms and Signs of Cerebellar Syndrome.* The Cerebellum, 2016. **15**(3): p. 369-391.
53. Riecker, A., et al., *The cerebral control of speech tempo: Opposite relationship between speaking rate and BOLD signal changes at striatal and cerebellar structures.* NeuroImage, 2006. **29**(1): p. 46-53.
54. Nottebohm, F., T.M. Stokes, and C.M. Leonard, *Central control of song in the canary, Serinus canarius.* The Journal of Comparative Neurology, 1976. **165**(4): p. 457-486.
55. Nottebohm, F., S. Kasparian, and C. Pandazis, *Brain space for a learned task.* Brain Research, 1981. **213**(1): p. 99-109.
56. Canady, R.A., D.E. Kroodsma, and F. Nottebohm, *Population differences in complexity of a learned skill are correlated with the brain space involved.* Proceedings of the National Academy of Sciences, 1984. **81**(19): p. 6232-6234.
57. Pfaff, J.A., et al., *Song repertoire size varies with HVC volume and is indicative of male quality in song sparrows (Melospiza melodia).* Proceedings of the Royal Society B: Biological Sciences, 2007. **274**(1621): p. 2035-2040.
58. Székely, T., et al., *Evolutionary changes in a song control area of the brain (HVC) are associated with evolutionary changes in song repertoire among European warblers (Sylviidae).* Proceedings of the Royal Society of London. Series B: Biological Sciences, 1996. **263**(1370): p. 607.
59. Airey, D.C., et al., *Song, sexual selection, and a song control nucleus (HVc) in the brains of European sedge warblers.* Journal of Neurobiology, 2000. **44**(1): p. 1-6.
60. Ward, B.C., E.J. Nordeen, and K.W. Nordeen, *Individual variation in neuron number predicts differences in the propensity for avian vocal imitation.* Proceedings of the National Academy of Sciences, 1998. **95**(3): p. 1277-1282.

61. Airey, D.C. and T.J. DeVoogd, *Greater song complexity is associated with augmented song system anatomy in zebra finches.* NeuroReport, 2000. **11**(10): p. 2339-2344.
62. Hahnloser, R.H.R., A.A. Kozhevnikov, and M.S. Fee, *An ultra-sparse code underliesthe generation of neural sequences in a songbird.* Nature, 2002. **419**(6902): p. 65-70.
63. Ali, F., et al., *The basal ganglia is necessary for learning spectral, but not temporal features of birdsong.* Neuron, 2013. **80**(2): p. 494-506.
64. Long, M.A. and M.S. Fee, *Using temperature to analyse temporal dynamics in the songbird motor pathway.* Nature, 2008. **456**(7219): p. 189-194.
65. Long, Michael A., et al., *Functional Segregation of Cortical Regions Underlying Speech Timing and Articulation.* Neuron, 2016. **89**(6): p. 1187-1193.
66. Johnson, F., M.M. Sablan, and S.W. Bottjer, *Topographic organization of a forebrain pathway involved with vocal learning in zebra finches.* The Journal of Comparative Neurology, 1995. **358**(2): p. 260-278.
67. Paterson, A.K. and S.W. Bottjer, *Cortical inter-hemispheric circuits for multimodal vocal learning in songbirds.* Journal of Comparative Neurology, 2017. **525**(15): p. 3312-3340.
68. Bottjer, S.W. and B. Altenau, *Parallel pathways for vocal learning in basal ganglia of songbirds.* Nat Neurosci, 2010. **13**(2): p. 153-155.

Chapter 8

General discussion

8.1 Short recapitulation of the goals

Vocal behaviour in songbirds –especially zebra finches– has come to serve as an indispensable model to trace brain-behaviour relationships that arise along the acquisition and maintenance of bird song, a complex sensorimotor skill that relies on experience, includes learning and memorisation processes that are confined to a sensitive period early in life, and is significantly influenced by social context. Decades of research provide a wealth of information available on the songbird brain and ongoing implementation and refinement of experimental techniques bring previously un-addressable biological phenomena within the grasp of experimentation. Notwithstanding the rich set of research tools and methods available at the start of this thesis, only few methods were capable of assessing the structural properties of the zebra finch brain, and none of them were non-invasive. Consequently, the major aim of this thesis was focussed on exploring the structural architecture of the zebra finch brain *in vivo* using MR-based imaging tools. Using such methods, we set out to explore brain-behaviour changes that occur during vocal learning in ontogeny or upon neurotoxic lesioning of the striatal component of the song control circuitry in adulthood. As such, we observed structural neuroplastic events that align with established findings in songbird literature which we used to validate our newly implemented MRI acquisition and processing protocols. Besides this, our findings also appear to shed new light and, hence, open up new exciting research questions. Therefore, this final chapter will briefly summarise the main findings obtained in this PhD project, and address new and enticing research questions that arose from the experimental findings.

8.2 Sharpen the tools: How to characterise the structural properties of the zebra finch brain *in vivo*?

Over the last few decades, MRI has propelled to the forefront of neuroscience as an indispensable translational research tool to study soft tissues such as the brain. Its biological versatility combined with its non-invasive character, described in Chapter 2, enable measuring the functional, structural and biochemical properties of the brain at different stages of learning, disease or development. Inspired by the extensive literature review focused on optimal strategies to capture neuroplastic adaptations in living brains outlined in Chapter 3 and previous MRI experiments conducted in songbirds summarised in Chapter 4, we decided to quantify structural neuroplastic events at two levels: (1) measure overall macro-structural brain anatomy by acquiring T2-weighted 3-dimensional anatomical scans (3D); and (2) gauge the

micro-architectural tissue properties using Diffusion Tensor Imaging (DTI). Further, we complemented the newly implemented data acquisition protocols with voxel-wise statistical analyses that can be performed on processed 'derivatives' of the initially acquired images.

To test whether the optimised protocols were sensitive enough, we performed a proof-of-principle study to detect known and well-documented structural sex-differences in the adult – but still tiny– zebra finch brain. The results are presented in Chapter 5, and are in line with established findings [1]. To better understand some of the results obtained *in vivo*, especially relating to the structural difference observed *surrounding* but not including Area X, we acquired additional high-resolution *ex vivo* DTI combined with brain-wide Track Density Imaging (TDI). This enabled a 3-dimensional view of the white matter architecture of the songbird brain in both sexes. Instead of focussing on the song control nuclei, the TDI maps present a complementary view by highlighting white matter structures that encapsulate and inter-connect the individual nuclei of the songbird brain. Similar 3-dimensional observations would be challenging to obtain with histological methods. In conclusion, the optimised protocols appeared sensitive enough and this set the stage to address more challenging research questions such as tracing the timing and spatial extent of structural neuroplasticity of the developing brain or along the process of recovery.

8.3 Structural development of the zebra finch brain

Knowing the spatiotemporal characteristics of normal brain development is vital to understand what goes wrong in neurodevelopmental disorders. Since the 1990's, several MR research centres have started collecting brain imaging and 'meta'-data so as to establish a complete spatiotemporal map of human brain development, e.g. The NIH BRAIN Initiative, Allen Brain Atlases, etc. More recently, the developmental trajectory of the brains of the most extensively studied animal model species has been characterised, for example in rats [2-5] and mice [6]. Encouraged by these studies, we set out to explore the structural development of the zebra finch brain to further understanding of (1) general brain maturational trajectories outside of the traditionally studied song control and auditory system, and (2) explore whether certain improvements in vocal proficiency can be traced back to particular structural features in the male zebra finch brain. Doing so, we created a brain-wide spatiotemporal map displaying when particular areas expand or contract (Figure 6-8), reminiscent of waves of brain maturation

reflected in altered cortical thickness in mammals e.g. [3, 6, 7]. Further, brain-wide voxel-wise data analyses have revealed two additional previously unidentified sex differences in brain structure, both of which have a clear role in vocal behaviour. Last (but definitely not least), we found that, as evidenced in mammalian species, skill performance correlates to the structural properties of the zebra finch brain (Figure 6-14 and Figure 6-15). More specifically, the correlation includes both tissue micro- (DTI) and macro-architecture (3D) and affects areas involved in tutor song memorisation, sensorimotor integration necessary for trial-and-error song learning, and neuromodulation. We will discuss each of these novel insights in more detail in the following sections.

8.3.1 Distinct brain areas exhibit different maturational patterns

Based on the DTI data, we observed widespread decreases in Mean Diffusivity (MD) that occur between 20-30 dph and 40-65 dph and describe those as 'maturational waves' (Figure 6-10). Decreases in MD along the first months of life align with observations in other animal species [8]. Even though it is tempting to speculate that the two 'maturational waves' accidently coincide with the initiation of the sensory and sensorimotor sub-phases of vocal learning, several other developmental milestones exist in parallel with the early stages of vocal learning. For example, juvenile zebra finches fledge around 18-20 dph [9]. Consequently, at 20 dph they are mastering this complex motor skill that relies on tightly coordinated action of sensory and motor systems. Up to around 30-35 dph, juvenile zebra finches depend on their parents to obtain food.

In humans, several studies outlined the developmental or maturational trajectory of distinct brain areas based on changes in volume or thickness (summarised in the discussion of Chapter 6). We implemented a similar processing method, termed voxel-based, deformation-based or tensor-based morphometry [10], to explore whether similar regionally-specific brain maturation patterns could be observed in the developing zebra finch brain. The resulting statistical maps clearly show that distinct brain subdivisions expand or contract at a specific time in ontogeny (Figure 6-8). For example, comparing sensory and sensorimotor ages informs that the striatum, including Area X, and parts of the meso- and nidopallium, including LMAN, increase in volume, while the optic lobes, including the TeO and MLd, and several parts of the cerebellum decrease in volume. These spatio-temporal patterns appeared highly similar in males and females.

Only few sex differences in local tissue volume could be detected in the voxel-based analyses, of which most aligned with established findings [1]. Importantly however, we observed additional sex differences at two levels in the tOM, i.e. near the thalamus, which is in line with the sex difference in DTI-FA near the tOM observed in the proof-of-principle study, and near the Ico complex, and Nif. In general, studies concerning sex differences in brain structure have mainly focussed on the song control system, as these structures underlie the sexually dimorphic behavioural difference (only males sing). In contrast, the tOM is a white matter tract and therefore difficult to delineate or quantify based on histological measures. Nif is more closely related to the auditory system, even though it might be regarded as intermediate relay nucleus [11]. Taken together, the observation of previously unknown sex-differences in the specific structures outside of the traditionally assessed song control system clearly illustrates the advantage of brain-wide voxel-based research strategies that do not rely on *a priori* definition of brain regions-of-interest.

8.3.2 Post-critical period song refinement

Vocal refinement continues well beyond the typically defined temporal boundaries of the 'critical' period of vocal learning. Only few studies that focuss on developmental song learning investigate age ranges beyond the traditionally defined crystallisation phase between 90 and 120 dph. Most extensive post-critical period changes included increased song tempo, caused by selective shortening of the inter-syllable intervals, while leaving syllable duration unaffected. The results presented in Chapter 6 (Figure 6-12 and Figure 6-13) clearly align with those. Spontaneous age-related adapations to song performance appear to stagnate around 1 year of age, both in zebra [12] and Bengalese finches [13]. Interesting parallels can be drawn to motor learning of complex skills observed in mammalian species (including humans), such as dancing, piano playing etc. First, separate segments of the routine or detailed gestures of movements are accurately mastered before speeding up the entire performance (segmental motor learning [14].

Complex motor skill learning was and still is an active field of research. Consequently, functional and structural neuroplastic events that characterise the different types and stages of motor learning of complex skills have been explored thoroughly with various methods, including *in vivo* MRI. Using the same translational imaging tools, we aimed to explore the existance of similar brain-behaviour relationships. If succesful, this would enable gaining insights into brain

areas involved in song refinement and enable drawing potential parallels with previous reports of complex motor skill.

8.3.3 Vocal performance relates to the structural properties of the zebra finch brain

According to Paus (2005), exploring brain-behaviour relationships can be realised by two strategies: perturbation or correlation [15]. Perturbation relates to brain lesion studies, which can be accidently incurred or experimentally induced, and which often include a well-controlled spatially defined trauma of a particular brain area and strictly controlled environment along recovery. This strategy and was employed in Chapter 7. Correlation studies benefit from being non-invasive and, as such, avoid deleterious confounders such as inflammation. We chose to perform correlation analyses in both ontogeny and upon neurotoxic lesioning in adulthood, to assess whether structural properties of brain areas could be linked to song performance. Importantly however, correlation analyses are no proof for causality. Consequently, a full distinction between time- or age-dependent effects and changes in a particular performance are not possible as both are inherently linked, e.g. older birds will normally sing a better song copy. We tried to gain deeper insights into the nature of the overall correlation by performing within- and between subject correlation analyses. The first informs whether specific improvements in song scores result in similar structural readout among different animals [16]. The second included Spearmans' ρ and indicates whether the variance between subjects drives the overall association between behaviour and structure. A clear example of the first can be found in the areas that display a negative correlation between local volume and song similarity (Chapter 6), while the correlations of the lesion study e.g. HVC and motif length (Chapter 7), mainly exist due to between-subject variability.

We observed correlations between song performance –based on song similarity to tutor song measurements– and tissue structure in four distinct brain areas, i.e. the NCM, CM, VP and tFA. An elaborate overview of the functional implications for each of these structures in song learning is outlined in the discussion of Chapter 6. The following paragraphs will briefly recapitulate some important links to literature and add additional studies that contribute to a more general understanding of e.g. lateralisation or functional specialisation of these auditory or neuromodulatory areas. Lastly, the correlation between song similarity and FA in the tFA sheds new light on the role of the basorostral nucleus in song behaviour, and given the limited information available on this nucleus, necessitates further investigation.

8.3.3.1 Song performance and the Auditory Lobule

Our findings confirm and present additional support for an active role of the caudo-medial nidopallium (NCM) and the caudal mesopallium (CM) in song learning including sensorimotor and post critical period song refinement.

The caudal medial nidopallium and the tutor song memory

Substantial evidence implicates that the tutor song memory is stored in the NCM (outlined in the discussion of Chapter 6). Moreover, several studies point to intriguing hemispheric specialisation or lateralised brain function towards the left hemisphere, e.g. [17]. The correlation analyses present in Chapter 6 concur with these observations as they suggest a relationship between song similarity and the microstructural tissue characteristics of left NCM (Figure 6-14). Hemispheric specialisation in brain function (and structure) is an often-observed phenomenon in neurosciences, e.g. for review [18], also in vocal learning-related contexts, e.g. left-ward lateralisation of speech and language processing in humans [19]. Despite being omnipresent in neuroscience literature, it is still not entirely clear how the brain benefits from lateralised processing and what processes might steer hemispheric specialisation.

Even though adult male birds retain the ability to adapt the spectral and temporal characteristics of specific syllables [20], in normal rearing conditions, sensory learning appears to be limited to the first 2 months of post-hatch life [21]. Most information relating to sensitive and critical period neuroplasticity stems from studies that assess sensory skill acquisition in early development, including ocular dominance, whisker-barrel and absolute pitch (described in Chapter 3). In these sensory systems, GABAergic inhibition is regarded as an important critical period delineator, as it gates the malleability of circuits and is necessary to enable (and stop) experience-dependent plasticity [22]. A recent review by Dr. Sarah E. London summarises parallels observed between critical period delineators in mammals and mechanisms implicated in song learning in birds, to further understanding about the factors that prevent close-ended learners to change their song beyond the critical period [23].

Having a closer look at the cells presenting song-stimulus driven Immediate Early Gene (IEG) expression, Pinaud and co-workers (2004) revealed that a large proportion of song-induced egr-1 cells in NCM (42.2%) and CMM (33.8%) were GABAergic [24]. Electrophysiological measures obtained from inhibitory neurons located in HVC [25], RA [26] and (dorsal) NCM [27] have been linked to change upon learning, as it appears that "*inhibition protects learned song elements*"

[25]. Furthermore, in a follow-up study Pinaud et al. (2006) described another set of GABAergic neurons in caudal NCM that did not display song-driven IEG expression, but that expressed high levels of aromatase [28], the enzyme that converts testosterone into oestrogen. These data might connect to a more recent study that revealed an age-dependent lateralisation of hormone selectivity that affects auditory processing. More specifically, while both hemispheres appeared equally responsive to estradiol during the sensory phase, a clear divergent response to estradiol depending on hemisphere was observed in sensorimotor aged male zebra finches [29]. Previous studies showed that in adult birds, inhibition of oestrogen production in the left NCM actively suppressed burst firing of auditory neurons and hence interfered with proper song discrimination in NCM, i.e. preference of BOS versus CON [30] and further downstream in HVC [31]. It might be interesting to assess potential lateralised hormone sensitivity and/or the distribution of GABAergic cells in the NCM of tutor-deprived birds, to evaluate whether this might affect the hormone sensitive responses or IEG patterns.

The caudal mesopallium and the avalanche nucleus

A specific, bilateral portion of the caudal mesopallium displayed a negative correlation between local volume and song performance (Chapter 6). This area co-localises with the CLM including the avalanche nucleus (Av).

Keller and Hahnloser (2009) discovered that Field L and the lateral caudal mesopallium (CLM) contain cells that exhibit selective responses during perturbed auditory feedback in zebra finches [32]. They conclude that these cells might play a role in error-detection necessary for trial-and-error sensorimotor learning. Very recently, Roberts et al. (2017) discovered a third type of projection neurons that project from HVC to the Av. Targeted ablation of these Av-projecting cells interfered with proper song learning and highlighted a role for these cells in the adaptive modification of the temporal features of song [33]. Fascinatingly, perhaps the negative correlation between local volume and song similarity in the CLM including Av observed in Chapter 6 might agree with these observations. More specifically, the advanced sensorimotor and post-critical period refinement of song tempo, i.e. inter-syllable intervals become shorter while syllable duration remains constant, might contribute to increased tutor song similarity and, hence, improve song similarity scores which gave rise to the observed voxel-wise correlations. Previously, in adult birds, Ali et al. (2013) found evidence that while the anterior forebrain pathway including basal ganglia was necessary for birds to change the spectral

content of syllables during reinforcement learning, distinct pathways appeared responsible to alter the temporal features of syllables [20]. Taken together, the data of both Ali et al. and Roberts et al. point to a mechanistic dissociation between altering the temporal or the spectral features of song, both during sensorimotor as well as adult song adaptation.

In a recent review, Prather et al. (2017) discuss these findings, and the importance of HVC and the CM in the context of auditory-to-vocal sensorimotor integration necessary for trial-and-error learning to succeed [34]. Importantly however, also alternative sites of 'self-evaluation' of song performance have been considered. For example, Mandelblat-Cerf et al. (2014) propose a descending auditory cortical projection that links the auditory system to the dopaminergic midbrain areas which connect to Area X in the Anterior Forebrain Pathway (AFP) [35]. More specifically, they focus on the ventral portion of the intermediate arcopallium (AIV) as it receives direct input from the NC, Field L, HVC_{shelf} and the CM (including the Av). The latter connection potentially links to the study by Keller and Hahnloser (CLM) and Roberts et al. (Av), which might steer error-related activity in the AIV. The AIV connects to the VTA and SNc which in turn send dopaminergic input to the anterior forebrain pathway (Area X) which might elicit vocal exploration [35].

In sum, we uncovered two regions apparently involved in distinct facets of vocal learning. While the NCM has been identified as (tentative) site of tutor song memory storage during the sensory phase, the CM likely functions as sensorimotor integration centre, implicated in error-detection and fine-tuner of the temporal aspects of song during vocal learning. The age-range we assessed in this study does not allow us to tease apart structural neuroplastic characteristics that arise due to sensory or sensorimotor learning. Further, by only including ages at which birds progressed to advanced plastic songs, we only found minor changes in syllable entropy, all other song features were already mastered by 65 dph. Therefore, finding out which neural circuitries or brain areas present structural correlates with learning of the acoustic structure of song syllables requires studying song development in earlier ages (early plastic song). In conclusion, more detailed understanding of the pathways involved in these different aspects of song learning warrants further investigation.

8.3.3.2 Song performance and the Ventral Pallidum

The ventral pallidum (VP) displayed a positive and negative correlation between song similarity and respectively FA and local volume. According to Li and Sakaguchi, the VP can be considered

as being similar to the mammalian substantia innominata which includes the basal nucleus of Meynert [36]. In mammals, both structures provide the predominant source of cholinergic input to the neocortex, hippocampus and amygdala, and are implicated in state-dependent regulation of cognitive processes including attention and memory. Indeed, loss of cholinergic signalling originating from the basal forebrain is inevitably linked with cognitive decline [37]. Section 6.4.3.2 of the discussion of Chapter 6 briefly reviews studies in songbirds that have shown that cholinergic projection neurons originating from the VP directly synapse on HVC where they are capable of gating auditory responses. Important to note is that not all projection neurons residing in the VP are cholinergic, as for example the VP might also relay fibres of passage, and Gale et al. describe that the dopaminergic projection neurons that project from the VTA and SNc to Area X course through the VP [38]. Our findings make it relevant to further investigate the role of the ventral pallidum in song learning and adult song behaviour.

8.4 Targeted lesioning highlights a link between the cerebellum and the song control system

Besides vocal learning in ontogeny, songbirds have been studied extensively to understand the mechanisms underlying adult neurogenesis for regeneration purposes, both in close-ended learning and open-ended seasonal songbirds [39]. Adult neurogenesis occurs in normal conditions and becomes upregulated following lesioning [40]. Lesion studies have helped identifying the contribution of different components of the song control and auditory system in song behaviour and perceptual discrimination between distinct songs.

In Chapter 7, we again employed 3D anatomical scans and DTI data combined with unbiased brain-wide voxel-wise data processing strategies to uncover the timing and spatial extent of neuroplastic changes as a (in)direct result of neurotoxic lesioning. We observed clear, bilateral, widespread alterations to brain micro- and macro-architecture. We observe that, among others, far beyond the lesion site, the lateral cerebellar nuclei appear structurally affected by neurotoxic lesioning of Area X. Evidence of indirect connections between the cerebellum and the song control system exists in avian literature [41, 42]. Unfortunately however, descriptions in zebra finches are relatively vague in specifying exactly which anatomical parts of the cerebellum project to the thalamic zone and thence to Area X [43]. Recently, not-yet-published findings provide a more complete picture of the structural connection between the cerebellum and Area X and appoint that the lateral cerebellar nuclei are necessary for succesful vocal

learning (bioRχiv database reference: [44]). Further, in humans, clear evidence supports the active role of the cerebellum in several aspects of speech, such as sensorimotor integration, or in speech-related conditions such as autism spectrum disorders (reviews on the role of the cerebellum in language, which includes speech, [45], or speech and autism spectrum disorders [46]). Moreover, a recent review that aims at drawing parallels between human speech and birdsong learning literally states the following "*…the role of the cerebellum in birdsong learning and song motor control in underexplored and a research area requiring more attention…*" [47].

A first step towards understanding how and to what extent the cerebellum affects vocal behaviour might be to further uncover connectivity between the cerebellum and the telencephalon, as, in line with findings in humans, the cerebellum might be connected to more cortical-like structures. Additionally, continuing on (currently unpublished) findings of Pidoux et al., explore the role of distinct components of the cerebellum in song learning in ontogeny and song maintenance in adulthood. This might be achieved by targeted lesioning, or by selective inactivation of specific cell types by e.g. optogenetic techniques [33].

Lastly, previous analyses that assessed the effects of neurotoxic lesioning of Area X in adult male zebra finches focus on birds that have an innate predisposition to repeat the last syllable of the motif [48]. Overall, approximately 7% of zebra finches present this predisposition for stuttering [49], and along the process of recovery after neurotoxic lesioning, they will transiently produce stuttering-like songs [48]. Zooming in on possible structural differences that exist between the brains of this small percentage of birds compared to normally singing birds might shed further light onto this peculiar predisposition, and perhaps also inform on possible mechanisms that allow or facilitate stuttering-like behaviour.

8.5 Impact of this thesis to songbird neurosciences and beyond

The MRI data obtained during this thesis project laid the basis to what might become an open access database for the zebra finch model, creating a hub for 3D spatial co-registration of additional *ex vivo* imaging data and combined re-analyses. One such project already exists and includes spatial expression profiles of numerous genes in the brains of adult male zebra finches (ZEBrA project Mello and Lovell; in situ hybridisation; http://www.zebrafinchatlas.org/). Extending this database with information obtained from female and juvenile birds, and adding multiple modalities, including tract tracing, brain imaging (including functional and structural

imaging data), histological and molecular data will result in a comprehensive data repository. Combined analysis of multi-modal input has great potential to uncover the factors that control windows of neuroplasticity by identification of the mechanisms that up- and down-regulate neuroplasticity, and will be a major asset to the songbird-science community.

We believe MRI is a highly translational imaging tool that can form a solid bridge between preclinical and clinical research. Our findings have uncovered clear similarities between avian and mammalian brain in terms of regionally-specific maturational trajectories during brain development, clear hemispheric asymmetry related to vocal learning, structural tissue properties that correlate with skill proficiency, and a structural link between the cerebellum and areas in control of vocal behaviour. These parallels provide further support to songbirds – zebra finches– as being a valid and valuable model to study (aspects of) speech learning or speech-related disorders in humans.

Even though this work is performed in zebra finches, its relevance lies in the substantial impact it could have on human health. This PhD project is situated within a broader research context that aims to discover mechanisms and pathways that allow heightened levels of neuroplasticity. Not only would this benefit educational programs ('when are children most susceptible to learn particular skills?'), it can aid in understanding developmental disorders as well as what factors might facilitate or even improve neural recovery.

REFERENCES

1. MacDougall-Shackleton, S.A. and G.F. Ball, *Comparative studies of sex differences in the song-control system of songbirds.* Trends in Neurosciences, 1999. **22**(10): p. 432-436.
2. Mengler, L., et al., *Brain maturation of the adolescent rat cortex and striatum: Changes in volume and myelination.* NeuroImage, 2014. **84**: p. 35-44.
3. Calabrese, E., et al., *A quantitative magnetic resonance histology atlas of postnatal rat brain development with regional estimates of growth and variability.* NeuroImage, 2013. **71**: p. 196-206.
4. Calabrese, E. and G.A. Johnson, *Diffusion tensor magnetic resonance histology reveals microstructural changes in the developing rat brain.* NeuroImage, 2013. **79**(Supplement C): p. 329-339.
5. Calabrese, E., G.A. Johnson, and C. Watson, *An ontology-based segmentation scheme for tracking postnatal changes in the developing rodent brain with MRI.* NeuroImage, 2013. **67**: p. 375-384.
6. Hammelrath, L., et al., *Morphological maturation of the mouse brain: An in vivo MRI and histology investigation.* NeuroImage, 2016. **125**: p. 144-152.

7. Gogtay, N., et al., *Dynamic mapping of human cortical development during childhood through early adulthood.* Proceedings of the National Academy of Sciences of the United States of America, 2004. **101**(21): p. 8174-8179.
8. Yoshida, S., et al., *Diffusion tensor imaging of normal brain development.* Pediatric Radiology, 2013. **43**(1): p. 15-27.
9. Trillmich, F., et al., *Patient Parents: Do Offspring Decide on the Timing of Fledging in Zebra Finches?* Ethology, 2016. **122**(5): p. 411-418.
10. Ashburner, J. and G.R. Ridgway, *Tensor-Based Morphometry A2 - Toga, Arthur W*, in *Brain Mapping*. 2015, Academic Press: Waltham. p. 383-394.
11. Lewandowski, B., et al., *At the interface of the auditory and vocal motor systems: Nif and its role in vocal processing, production and learning.* Journal of Physiology-Paris, 2013. **107**(3): p. 178-192.
12. Glaze, C.M. and T.W. Troyer, *Development of temporal structure in zebra finch song.* Journal of Neurophysiology, 2013. **109**(4): p. 1025-1035.
13. James, L.S. and J.T. Sakata, *Vocal motor changes beyond the sensitive period for song plasticity.* Journal of Neurophysiology, 2014. **112**(9): p. 2040-2052.
14. Asanuma, H. and C. Pavlides, *Neurobiological basis of motor learning in mammals.* Neuroreport: An International Journal for the Rapid Communication of Research in Neuroscience, 1997. **8**(4): p. i-vi.
15. Paus, T., *Mapping brain maturation and cognitive development during adolescence.* Trends in Cognitive Sciences, 2005. **9**(2): p. 60-68.
16. Bakdash, J.Z. and L.R. Marusich, *Repeated Measures Correlation.* Frontiers in Psychology, 2017. **8**: p. 456.
17. Moorman, S., et al., *Human-like brain hemispheric dominance in birdsong learning.* Proceedings of the National Academy of Sciences, 2012. **109**(31): p. 12782-12787.
18. Güntürkün, O. and S. Ocklenburg, *Ontogenesis of Lateralization.* Neuron, 2017. **94**(2): p. 249-263.
19. Bishop, D.V.M., *Cerebral Asymmetry and Language Development: Cause, Correlate, or Consequence?* Science, 2013. **340**(6138).
20. Ali, F., et al., *The basal ganglia is necessary for learning spectral, but not temporal features of birdsong.* Neuron, 2013. **80**(2): p. 494-506.
21. Gobes, S.M.H., R.B. Jennings, and R.K. Maeda, *The sensitive period for auditory-vocal learning in the zebra finch: Consequences of limited-model availability and multiple-tutor paradigms on song imitation.* Behavioural Processes, 2017.
22. Takesian, A.E. and T.K. Hensch, *Chapter 1 - Balancing Plasticity/Stability Across Brain Development*, in *Progress in Brain Research*, M.N. Michael M. Merzenich and M.V.V. Thomas, Editors. 2013, Elsevier. p. 3-34.
23. London, S.E., *Developmental song learning as a model to understand neural mechanisms that limit and promote the ability to learn.* Behavioural Processes, 2017.
24. Pinaud, R., et al., *GABAergic neurons participate in the brain's response to birdsong auditory stimulation.* European Journal of Neuroscience, 2004. **20**(5): p. 1318-1330.
25. Vallentin, D., et al., *Inhibition protects acquired song segments during vocal learning in zebra finches.* Science (New York, N.Y.), 2016. **351**(6270): p. 267-271.
26. Miller, M.N., C.Y.J. Cheung, and M.S. Brainard, *Vocal learning promotes patterned inhibitory connectivity.* Nature Communications, 2017. **8**(1): p. 2105.
27. Yanagihara, S. and Y. Yazaki-Sugiyama, *Auditory experience-dependent cortical circuit shaping for memory formation in bird song learning.* Nature Communications, 2016. **7**: p. 11946.

28. Pinaud, R., et al., *Calbindin-positive neurons reveal a sexual dimorphism within the songbird analogue of the mammalian auditory cortex.* Journal of Neurobiology, 2006. **66**(2): p. 182-195.
29. Vahaba, D.M., M. Macedo-Lima, and L. Remage-Healey, *Sensory Coding and Sensitivity to Local Estrogens Shift during Critical Period Milestones in the Auditory Cortex of Male Songbirds.* eneuro, 2017. **4**(6).
30. Remage-Healey, L., et al., *Brain estrogens rapidly strengthen auditory encoding and guide song preference in a songbird.* Proceedings of the National Academy of Sciences of the United States of America, 2010. **107**(8): p. 3852-3857.
31. Remage-Healey, L. and N.R. Joshi, *Changing Neuroestrogens Within the Auditory Forebrain Rapidly Transform Stimulus Selectivity in a Downstream Sensorimotor Nucleus.* The Journal of Neuroscience, 2012. **32**(24): p. 8231-8241.
32. Keller, G.B. and R.H.R. Hahnloser, *Neural processing of auditory feedback during vocal practice in a songbird.* Nature, 2008. **457**: p. 187.
33. Roberts, T.F., et al., *Identification of a motor-to-auditory pathway important for vocal learning.* Nature Neuroscience, 2017. **20**: p. 978.
34. Prather, J.F., K. Okanoya, and J.J. Bolhuis, *Brains for birds and babies: Neural parallels between birdsong and speech acquisition.* Neuroscience & Biobehavioral Reviews, 2017. **81**(Part B): p. 225-237.
35. Mandelblat-Cerf, Y., et al., *A role for descending auditory cortical projections in songbird vocal learning.* eLife, 2014. **3**: p. e02152.
36. Li, R. and H. Sakaguchi, *Cholinergic innervation of the song control nuclei by the ventral paleostriatum in the zebra finch: a double-labeling study with retrograde fluorescent tracers and choline acetyltransferase immunohistochemistry.* Brain Research, 1997. **763**(2): p. 239-246.
37. Ballinger, Elizabeth C., et al., *Basal Forebrain Cholinergic Circuits and Signaling in Cognition and Cognitive Decline.* Neuron, 2016. **91**(6): p. 1199-1218.
38. Gale, S.D., A.L. Person, and D.J. Perkel, *A novel basal ganglia pathway forms a loop linking a vocal learning circuit with its dopaminergic input.* The Journal of Comparative Neurology, 2008. **508**(5): p. 824-839.
39. Balthazart, J. and G.F. Ball, *Endocrine and social regulation of adult neurogenesis in songbirds.* Frontiers in Neuroendocrinology, 2016. **41**: p. 3-22.
40. Doetsch, F. and C. Scharff, *Challenges for Brain Repair: Insights from Adult Neurogenesis in Birds and Mammals.* Brain, Behavior and Evolution, 2001. **58**(5): p. 306-322.
41. Vates, G.E., D.S. Vicario, and F. Nottebohm, *Reafferent thalamo-"cortical" loops in the song system of oscine songbirds.* The Journal of Comparative Neurology, 1997. **380**(2): p. 275-290.
42. Arends, J.J.A. and H.P. Zeigler, *Organization of the cerebellum in the pigeon (Columba livia): II. Projections of the cerebellar nuclei.* The Journal of Comparative Neurology, 1991. **306**(2): p. 245-272.
43. Person, A.L., et al., *Organization of the songbird basal ganglia, including area X.* The Journal of Comparative Neurology, 2008. **508**(5): p. 840-866.
44. Pidoux, L., P. Leblanc, and A. Leblois, *A subcortical circuit linking the cerebellum to the basal ganglia engaged in vocal learning.* bioRxiv, 2017.
45. Mariën, P., et al., *Consensus Paper: Language and the Cerebellum: an Ongoing Enigma.* Cerebellum (London, England), 2014. **13**(3): p. 386-410.
46. Hampson, D.R. and G.J. Blatt, *Autism spectrum disorders and neuropathology of the cerebellum.* Frontiers in Neuroscience, 2015. **9**(420).
47. Konopka, G. and Todd F. Roberts, *Insights into the Neural and Genetic Basis of Vocal Communication.* Cell, 2016. **164**(6): p. 1269-1276.

48. Kubikova, L., et al., *Basal ganglia function, stuttering, sequencing, and repair in adult songbirds.* Scientific Reports, 2014. **4**: p. 6590.
49. Helekar, S.A., et al., *Development and adult phase plasticity of syllable repetitions in the birdsong of captive zebra finches (Taeniopygia guttata).* BEHAVIORAL NEUROSCIENCE, 2003. **117**(5): p. 939-951.

Acknowledgements - Dankwoord

Curriculum vitae

EDUCATION

2012-present: PhD

Bio-Imaging Lab, University of Antwerp

Supported by a PhD grant by the University of Antwerp (1/10/2012 – 30/09/2016) and a project grant awarded to Prof Dr Annemie Van der Linden (1/10/2016-present).

This PhD project is part of a BELSPO 'Interuniversity Attraction Poles' collaboration between four different Belgian universities (UGent, KULeuven, ULiège and UA) and three international partners (Germany, USA, UK).

PhD-related courses, trainings and workshops

- '***Writing Academic Papers***': January 2013, Linguapolis and Antwerp Doctoral School
- '***How to communicate effectively in an academic context***': March 2013, Linguapolis and Antwerp Doctoral School.
- '***Imaging the brain at different scales: how to integrate multi-scale structural information?***': 2-6/09/2013, organized by the Belgian node of the International Neuroinformatics Coordinating Facility (INCF), https://www.frontiersin.org/events/Imaging_the_brain_at_different_scales_How_to_integrate_multi-scale_structural_information_/1907/abstracts.
- '***SPM for fMRI course***': 14-16/05/2015 London, United Kingdom, organized by the Methods group of the Wellcome Trust Center for NeuroImaging part of the University College of London (developers of the SPM software: http://www.fil.ion.ucl.ac.uk/spm/).
- '***From molecules to networks***' ESMI TOPIM winterschool: February 19th to 24th 2017, Les Houches, France, organized by the European Society for Molecular Imaging, http://www.e-smi.eu/index.php?id=topim-201700.
- '***BIG DATA – machine learning, algorithms, relevance for imaging science***': pre-symposium organized by the European Society for Molecular Imaging (EMIM), http://www.e-smi.eu/index.php?id=big-data-symposium-2017.
- '***Biomolecular data mining: a hands-on training***': September 11-13 2017, organized by the Biomina research group at the University of Antwerp (Prof Dr Kris Laukens), http://www.biomina.be/BioMolDM2017.

2010-2012: Master

Biomedical Sciences: Neurosciences

Graduated in June 2012: *Magna Cum Laude* / great distinction

Obtained a FELASA C certificate

Masterthesis: Cross-sectional study to evaluate the role of neuro-inflammation during epileptogenesis in an animal model of temporal lobe epilepsy

Promotor: Prof. Dr. S. Dedeurwaerdere,
Lab of Translational Neurosciences,
Faculty of Medicine - University of Antwerp

2007-2010: Bachelor

Biomedical sciences

Graduated in June 2010: distinction

Bachelorthesis: Microtomographic analysis of changes in bone tissue due to osteoporosis
Promotor: Prof. Dr. N. De Clerck, Research group of Microtomography, University of Antwerp

INTERNATIONAL PEER-REVIEWED PUBLICATIONS

(*equal contribution)

1. **Hamaide J**, De Groof G, Van Steenkiste G, Jeurissen B, Van Audekerke J, Naeyaert M, Van Ruijssevelt L, Cornil C, Sijbers J, Verhoye M, Van der Linden A. *Exploring sex differences in the adult zebra finch brain:* In vivo *diffusion tensor imaging and* ex vivo *super-resolution track density imaging*. NeuroImage. 2017 Feb 1;146:789-803. doi: 10.1016/j.neuroimage.2016.09.067. Epub 2016 Sep 30. (data described in Chapter 5)
2. **Hamaide J**, De Groof G, Van der Linden A. *Neuroplasticity and MRI: A perfect match.* NeuroImage. 2016 May 1;131:13-28. doi: 10.1016/j.neuroimage.2015.08.005. Epub 2015 Aug 7. Review.
3. Van Ruijssevelt L, Chen Y, von Eugen K, De Groof G, **Hamaide J**, Verhoye M, Güntürkün O, Woolley SC*, and Van der Linden A*. *fMRI reveals a novel region for evaluating courtship signals in a female songbird*. Current Biology, In press.
4. Van Ruijssevelt L, **Hamaide J**, van Gurp MT, Verhoye M, and Van der Linden A. *Auditory evoked BOLD responses in awake compared to lightly anaesthetised zebra finches*. Sci Rep. 2017 Oct 19. 7(1):13563. doi: 10.1038/s41598-017-13014-x.
5. Van Ruijssevelt L*, Washington SD*, **Hamaide J**, Verhoye M, Keliris GA, Van der Linden A. *Song Processing in the Zebra Finch Auditory Forebrain Reflects Asymmetric Sensitivity to Temporal and Spectral Structure*. Front Neurosci. 2017 Oct 5;11:549. doi: 10.3389/fnins.2017.00549. eCollection 2017.
6. Ellis SR, Cappell J, Potočnik NO, Balluff B, **Hamaide J**, Van der Linden A, Heeren RM. *More from less: high-throughput dual polarity lipid imaging of biological tissues*. Analyst. 2016 Jun 21;141(12):3832-41. doi: 10.1039/c6an00169f. Epub 2016 Apr 4.
7. Jonckers E, Shah D, **Hamaide J**, Verhoye M, Van der Linden A. *The power of using functional fMRI on small rodents to study brain pharmacology and disease*. Front Pharmacol. 2015 Oct 21;6:231. doi: 10.3389/fphar.2015.00231. eCollection 2015. Review.

MANUSCRIPTS IN PREPARATION

(*equal contribution)

1. Washington SD, **Hamaide J**, Van Steenkiste G, Jeurissen B, Sijbers J, Deleye S, De Groof G, Liang S, Van Audekerke J, Wenstrup JJ, Van der Linden A, Radtke-Schuller S, Verhoye M. *A three-dimensional digital atlas of the mustached bat brain*. In preparation for re-submission.
2. **Hamaide J**, Bigler A, Van der Linden A. *MRI: an ideal tool to explore the neural substrate of vocal communication in songbirds*. Chapter in the 'Handbook of In Vivo Neural Plasticity Techniques: A Systems Neuroscience Approach to the Neural Basis of Memory and Cognition'. Editor: D Manahan-Vaughan, Elsevier. Awaiting proofs (submitted revision in September 2017).
3. **J Hamaide***, K Lukacova*, J Van Audekerke, M Verhoye, L Kubikova, A Van der Linden. *Image-guided discoveries of cerebellar remodelling upon lesioning the cortico-basal*

ganglia-thalamo-cortical circuitry in control of learned vocal communication. Submitted to 'NeuroImage'. (data described in Chapter 7)

4. **J Hamaide**, G De Groof, L Van Ruijssevelt, J Van Auderkerke, M Verhoye, A Van der Linden. *Longitudinal* in vivo *MRI study maps structural plasticity in the brain of juvenile zebra finches during the first 200 days of post-hatch life*. Submitted to 'NeuroImage'. (data described in Chapter 6, part I)
5. **J Hamaide**, K Lukacova, M Verhoye, A Van der Linden. *Practice makes perfect:* in vivo *detection of structural neuroplasticity related to vocal imitation*. (data described in Chapter 6, part II)
6. C Anckaerts, I Blockx, S Priska, M Johanna, **J Hamaide**, C Kreutzer, H Boutin, S Couillard-Despres, M Verhoye, A Van der Linden. *Reduced functional connectivity and progressive microstructural alterations in the female TgF344-AD rat model of Alzheimer's Disease*. Submitted to 'Neurobiology of Disease'.

BOOK CHAPTER

1. **Hamaide J**, Van Ruijssevelt L, Kara F, De Groof G and Van der Linden A. *Imaging in Neurology Research II: Exploring Plasticity and Cognitive Networks by In Vivo MRI*. Small Animal Imaging: Basics and Practical Guide. 2017 Editors: F. Kiessling, B. J. Pichler and P. Hauff. Cham, Springer International Publishing: 727-760. doi: https://doi.org/10.1007/978-3-319-42202-2_29.

ABSTRACTS AND CONFERENCE PRESENTATIONS

(presenting author; *equal contribution)

Oral presentations at international conferences

1. **J Hamaide**, G. De Groof , J. Van Audekerke, L. Van Ruijssevelt, Z. Mai, F. Kara, M. Verhoye, A. Van Der Linden, In vivo detection of sexual dimorphisms in the brain of a Passerine songbird, a proof-of-principle study. Oral Presentation, 9th annual meeting of the European Society for Molecular Imaging, Antwerp, Belgium, June 4-6,2014.
2. **J Hamaide**, G. De Groof, J. Van Audekerke, M. Verhoye, A. Van der Linden, Structural development of the zebra finch brain: *in vivo* Diffusion Tensor Imaging to explore the critical period of vocal learning in juvenile birds. Power poster (oral & poster presentation), ISMRM Benelux (2016), Eindhoven, The Netherlands, January 22nd, 2016.
3. **J Hamaide**, K. Lukacova, L. Kubikova, M. Verhoye, A. Van der Linden, Correlation of striatal remodeling with changes in song performance: a longitudinal diffusion tensor imaging study of adult male zebra finches. Oral presentation, ISMRM Benelux, Tilburg, The Netherlands, January 20th 2017.
4. N. Orginc Potocnik*, **J Hamaide***, G. Yadav, A. Van der Linden, R.M.A. Heeren, A molecular insight of the song learning behaviour of Zebra Finch (Taeniopygia guttata) songbirds during ontogeny with mass spectrometry imaging. Oral presentation, Study group on Imaging Mass Spectrometry at the European Molecular Imaging Society Meeting (EMIM) in Cologne, Germany, April 4th 2017.
5. **J Hamaide**, K. Lukacova, L. Kubikova, A. Van der Linden, Lesion-induced remodeling of a circuitry: uncovering links between aberrant singing behavior and structural neuroplasticity in

adult male zebra finches. Oral presentation, Belgian Molecular Imaging Meeting in Brussels, Belgium, May 16th 2017.

6. **J Hamaide**, L. Van Ruijssevelt, M. Verhoye, A. Van der Linden, Tracing structural neuroplasticity in the developing zebra finch brain during the critical period for vocal learning by in vivo Magnetic Resonance Imaging. Oral presentation, European Birdsong Meeting in Bordeaux, France, May 22-23th 2017.

Poster presentations (traditional or electronic) at (inter)national conferences

7. **J Hamaide**, G. De Groof, J. Van Audekerke, F. Kara, A. Van Der Linden, *In vivo* detection of the sexual dimorphism in the caudal motor pathway of a Passerine songbird, a preliminary study, Poster Frontiers in Neuroinformatics, 5-days course, Conference Abstract: Imaging the brain at different scales: How to integrate multi-scale structural information? doi: 10.3389/conf.fninf.2013.10.00025; epub 31 Aug 2013. **=> 'best poster' award**
8. **J Hamaide**, G. De Groof, J. Van Audekerke, L. Van Ruijssevelt, Z. Mai, F. Kara, M. Verhoye, A. Van der Linden. *In vivo* detection of sexual dimorphisms in the brain of a Passerine songbird, a proof-of-principle study. E-Poster, Joint Annual Meeting ISMRM-ESMRMB, May 10-16, 2014, Milan, Italy.
9. **J Hamaide**, G. De Groof, J. Van Audekerke, L. Van Ruijssevelt, Z. Mai, F. Kara, C. Cornil, M. Verhoye, A. Van der Linden A. In vivo non-invasive structural imaging tools to investigate sex- and ontogeny-related differences in zebra finch brain. Poster presentation, 8th International Conference on Hormones, Brain and Behavior (ICHBB) in Liège, June 24-27, 2014.
10. G. Van Steenkiste*, **J Hamaide***, B. Jeurissen, D.H.J. Poot, J. Van Audekerke, J. Sijbers, M. Verhoye, Combination of super-resolution reconstruction diffusion tensor imaging and track density imaging reveals song control system connectivity in zebra finches, Poster Presentation, ISMRM Toronto, May 30-June 5 2015.
11. **J Hamaide**, G. De Groof, A. Van der Linden, Longitudinal in vivo Diffusion Tensor Imaging study maps structural plasticity in the brain of juvenile male zebra finches throughout the critical period for vocal learning. Poster presentation, Society for Neuroscience, Chicago, IL, USA, October 17-21, 2015.
12. **J Hamaide**, G. De Groof, J. Van Audekerke, M. Verhoye, A. Van der Linden, Diffusion Tensor Imaging sheds light on microstructural brain changes related to the process of vocal learning in juvenile zebra finches. E-Poster presentation, ISMRM, Singapore, May 7-13, 2016.
13. **J Hamaide**, E. Jonckers, J. Diddens, L. Van Ruijssevelt, G. De Groof, A. Van der Linden, In vivo magnetic resonance imaging explores the establishment of sex differences in the zebra finch brain during the critical period for vocal learning. Poster presentation, International Symposium on Avian Endocrinology, Niagara-on-the-Lake, Canada, October 11-14, 2016.
14. **J Hamaide**, K. Lukacova, L. Kubikova, M. Verhoye, A. Van der Linden, Tracing neuroplasticity after neurotoxic injury tot he song control circuitry, a longitudinal diffusion tensor imaging study in zebra finches. Poster presentation, TOPIM ESMI, Les Houches, France, February 19-24th 2017.
15. **J Hamaide**, K. Lukacova, L Kubikova, M. Verhoye, A. Van der Linden, Correlation of striatal remodeling with changes in song performance: a longitudinal diffusion tensor imaging study of adult male zebra finches. Electronic Poster presentation, ISMRM 25th Annual Meeting & Exhibition in Honolulu, Hawaii, April 22-27 2017.
16. **J Hamaide**, K Lukacova, G De Groof, J Van Audekerke, M Verhoye, A Van der Linden, *In vivo* voxel-based morphometry study during the critical period of song learning in juvenile zebra finches. Poster presentation, ISMRM Benelux, Antwerp, January 26th 2018.

ACADEMIC ASSIGNMENTS

- Assistant supervisor for practical sessions:
  - Laboratory animal sciences (FELASA): Master (2nd) and PhD students
    - September-October 2012
    - September-October 2013
    - September-October 2014
    - September-October 2015
    - September-October 2016

    Prof Dr P.P. De Deyn, Prof Dr C. Van Ginneken, Dr D. Van Dam
  - Algemene celfysiologie (General cell physiology): Bachelor (2nd) students
    - November 2012
    - November 2013

    Prof Dr N. De Clerck

- Supervision Internships and theses
  - Bachelor internship
    - 1 student 2012-2013: Biology, BA1
      Name student: Sezer Koyuncu
      Subject: habituation training birds for awake functional MRI (rsfMRI and auditory fMRI)
  - Bachelor papers
    - 1 student 2012-2013: Biomedical Sciences, BA3
      Name student: Dieter Van de Sande
      Subject: *Hersenplasticiteit en GABAergische inhibitie*
    - 1 student 2015-2016: Biomedical Sciences, BA3
      Name student: Lotte Van Den Bosch
      Subject: *Neuroplasticiteit en kritische perioden*
  - Master Internships
    - 2 students 2012-2013: Biomedical Sciences – Neurosciences & Imaging, MA1
      Name students: and Ruben Houbrechts and Cedric Theuns
      Subject: *habituation training birds for awake functional MRI (rsfMRI and auditory fMRI)*
  - Master theses
    - 1 student 2013-2014: Biomedical Sciences -Neurosciences, MA2
      Name student: Ward Eertmans
      Subject: *Follow up of morphological neuroplastic changes in early zebra finch ontogeny*
    - 1 student 2015-2016: Biomedical engineering, MA2
      Name student: Matthijs Van Gurp
      Subject: *Spatiotemporal effects of anesthesia during functional imaging experiments in zebra finches: approaches with BOLD-weighted imaging and MR spectroscopy*

- Representative of 'UA-alumni' in the Educational committee of the Department of Pharmaceutical, Veterinary and Biomedical Sciences at the University of Antwerp ('Onderwijscommissie Biomedische Wetenschappen')
  - January 2013 - October 2013
  - October 2015 - present